

KALUZA-KLEIN FRW RENYI HOLOGRAPHIC DARK ENERGY MODEL IN SCALAR-TENSOR THEORY OF GRAVITATION

Y. Sobhanbabu^{a*}, M. Vijaya Santhi^b, A. Srinivasa Rao^b, M. Praveen Kumar^a

^aSagi Rama Krishnam Raju Engineering College (A), Bhimavaram, 534204, India

^bAndhra University, Visakhapatnam, 530003, India

*Corresponding Author e-mail: sobhan.maths@gmail.com

Received May 22, 2024; revised July 6, 2024; accepted July 12, 2024

This work examines the dark energy phenomenon by studying the Renyi Holographic Dark Energy (RHDE) and pressure-less Dark Matter (DM) within the frame-work of Saez-Ballester (SB) scalar-tensor theory of gravitation (Phys. Lett. A113, 467:1986). To achieve a solution, we consider the viable deceleration parameter (DP), which contributes to the average scale factor $a = e^{\frac{1}{\gamma}\sqrt{2\gamma t+c_1}}$, where γ , and c_1 are respectively arbitrary, and integration constants. We have derived the field equations of SB scalar-tensor theory of gravity with the help of Kaluza-Klein FRW Universe. We have investigated cosmological parameters namely, DP (q), energy densities (ρ_M) and (ρ_R) of DM and RHDE, scalar field (ϕ), and equation of state parameter (ω_R). The physical debate of these cosmological parameters are investigated through graphical presentation. Moreover, the stability of the model are studied through squared sound speed (v_s^2) and the well-known cosmological plane $\omega_R - \omega'_R$ and all energy conditions and also, density parameters are analyzed through graphical representation for our model.

Keywords: Kaluza-Klein FRW Universe; RHDE; Energy Conditions; Saez-Ballester theory

PACS: 04; 98.80cq; 04.5-h; 98.80.-k; 04.50.Kd; 04.20.Jb

1. INTRODUCTION

The cosmological observations like, type Ia Supernovae [1, 2] have provided the convincing evidence that our Universe is dominated by two dark sectors containing dark matter and dark energy. The behavior of Dark Matter (DM) and Dark Energy (DE) is one of the most important issues today in modern cosmology. The present Planck data says that there is 68.3% DE of the total energy contents of the Universe. The approaches to answer this DE problems and cosmic acceleration issues fall into two categories: (i) To introduce dynamical DE models in the RHS of Einstein's field equations in the background of general relativity, (ii) Modify the LHS of Einstein's field equations, it leads to modified theories of gravity. We refer [3, 4, 5] for the detail investigation of DE models and modified theories of gravity.

The holographic DE model (HDE) suggests, this model is originated from holographic principle and its energy density can be expressed by $\rho_{de} = \frac{3C^2 M_p^2}{L^2}$, here C^2 is a numerical constant, M_p^2 is the reduced Planck mass and L denotes the size of the current Universe such as the Hubble scale [6, 7]. In addition, the holographic DE has some problems and cannot explain the time line of a flat FRW Universe [8, 9]. One of the proposed solutions for the HDE problems is the consideration of various entropies. One of the considered entropy is Tsallis entropy which has been used in many papers [10, 11, 12, 13]. In recent years, various entropy formalism have been used to discuss the gravitational and cosmological setups. Also, some new holographic DE models are constructed such as Tsallis HDE [14]. In literature [15, 16, 17] ADE models are available which deal with various aspects of the evolution of the Universe. Wei and Cai [18] have proposed a new version of this model referred as New Agegraphic Dark Energy (NADE) model, by replacing the cosmic age T with the cosmic conformal age η for the time scale. Hence, in this model, the dark energy density is of the form $\rho_a = 3n^2 m_p^2 \eta^{-2}$, where the conformal time η is defined as $\eta = \int_0^t \frac{1}{a} dt = \int_0^a \frac{1}{a^2 H} da$ here a is the average scale factor of the Universe and Hubble parameter $H = \frac{\dot{a}}{a}$, and overdot ($\dot{}$) represents derivative with respect to the cosmic time (t) only. Sheykhi and Setare [19] have explore NADE model with viable gravitational constant G in a non-flat Universe. And also, they have generalized to viscous the NADE model in the presence of interacting term between dark sectors.

A new DE model based on the holographic hypothesis, inspired by a Q generalized entropy, suggested by Renyi [20], called RHDE [21], has proposed with IR cutoff as the Hubble radius. Maradpour et al. [22] have investigated thermodynamic approach to HDE and the Renyi entropy. Some other researchers [23, 24, 25] have analyzed based on Renyi entropy to investigate various cosmological phenomena. Dixit [26] have investigated RHDE models in FRW Universe with two IR cutoffs with redshift parametrization. Chunlen and Rangdeey [27] have discussed exploring the RHDE model with the future and the particle Horizons as IR cutoff. Sharma and Dubey [28] have discussed cosmological behavior of interacting RHDE models. Sarfraz et al. [29] have analyzed the Study of RHDE model in framework of Chern Simons Modified Gravity.

Sharma and Dubey [30] have discussed statefinder diagnostic for the RHDE. Saha et al. [31] have investigated RHDE in higher dimension cosmology. Sharma and Dubey [32] have studied RHDE model in the framework of Brans-Dicke (BD) scalar tensor theory of gravity. Divya and Aditya [33] have investigated anisotropic RHDE models in background of general relativity. Recently, Bhattacharjee [34] has investigated interacting Tsallis and Renyi HDE with hybrid expansion law. Santhi and Sobhanbabu [35] have studied Bianchi type-III Tsallis holographic dark energy model in Saez–Ballester theory of gravitation. Sobhanbabu and Santhi [36] have investigated Kantowski–Sachs Tsallis holographic dark energy model with sign-changeable interaction. Divya and Aditya [37] have studied observational constraints on RHDE model in anisotropic Kantowski Sachs Universe. recently, Sobhanbabu and Santhi [38] have studied Bianchi type-III RHDE models a in scalar tensor theory. Very recently, Sobhanbabu et al. [39] have analyzed Kantowski–Sachs Barrow holographic dark energy model in the frame-work of SB theory of gravitation.

In this paper, inspired by the above investigations, we have considered the KK FRW Universe for the RHDE model with the frame-work of scalar-tensor theory of gravity. This model also, provides the DE model for clear and easy cosmological evolution. The paper is organized as follows: In the next Section, we present the field equations and obtained their solution of RHDE model in the frame-work of SB theory. In Section. 3, we study the solution of the field equations and cosmological parameters are investigated to RHDE model. In the last Section, we have presented some conclusions.

2. METRIC AND FIELD EQUATIONS OF RHDE IN SB THEORY

We consider the non-Ricci, non-compact five-dimensional FRW type KK Universe in the form

$$ds^2 = dt^2 - R^2(t) \left[\frac{dr^2}{1 - kr^2} + r^2 \left(d\theta^2 + \sin^2\theta d\phi^2 \right) + (1 - kr^2) d\xi^2 \right], \tag{1}$$

where $R(t)$ is the five-dimensional scale factor of the model and $k = 0, 1, -1$ represents the curvature parameter for flat, closed and open Universe. We define the following physical parameters for KK FRW Universe: Volume $V = R^3$, Hubble parameter $H = \frac{\dot{R}}{R}$, scalar expansion $\theta = 3\frac{\dot{R}}{R}$, and DP $q = -\frac{R\ddot{R}}{\dot{R}^2}$, here R is average scale factor.

The SB field equations for matter and RHDE distribution are given by [40]

$$G_{\mu\nu} - w\phi^n \left(\phi_{,\mu}\phi_{,\nu} - \frac{1}{2}g_{\mu\nu}\phi_{,\lambda}\phi^{,\lambda} \right) = -(T_{\mu\nu} + \bar{T}_{\mu\nu}), \tag{2}$$

and the scalar field ϕ satisfies the following equation

$$2\phi^n \phi_{,\mu}^{;\mu} + n\phi^{n-1} \phi_{,\lambda}\phi^{,\lambda} = 0, \tag{3}$$

where $G_{\mu\nu}$ represents the Einstein tensor and $T_{\mu\nu}$ & $\bar{T}_{\mu\nu}$ are energy momentum tensors for pressure-less dark matter and RHDE respectively. For physical interpretation, the energy momentum tensors for matter and RHDE can be written as

$$T_{\mu\nu} = \text{diag}[1, 0, 0, 0]\rho_M, \tag{4}$$

and

$$\bar{T}_{\mu\nu} = \text{diag}[1, -\omega_R, -\omega_R, -\omega_R]\rho_R, \tag{5}$$

where ρ_R, ρ_M are energy densities of RHDE and matter and p_R is the pressure of RHDE. $\omega_R = \frac{p_R}{\rho_R}$ is an equation of state (EoS) parameter. So, the field equations for the discussed metric can be written as SB field Eq.(2), for KK FRW Universe Eq.(1) with the help of Eq.(4), and (5) can be written as

$$6\frac{\dot{R}^2}{R^2} + 6\frac{k}{R^2} + \frac{w\phi^n \dot{\phi}^2}{2} = \rho_M + \rho_R, \tag{6}$$

$$3\left(\frac{\ddot{R}}{R} + \frac{\dot{R}^2}{R^2} + \frac{k}{a^2} \right) - \frac{w\phi^n \dot{\phi}^2}{2} = -\omega_R \rho_R, \tag{7}$$

$$\ddot{\phi} + 4\frac{\dot{R}\dot{\phi}}{R\phi} + \frac{n\dot{\phi}^2}{2\phi^2} = 0, \tag{8}$$

From Eq.(6), we get the continuity equation is

$$\dot{\rho}_R + \dot{\rho}_M + 4\left((1 + \omega_R)\rho_R + \rho_M \right) \frac{\dot{R}}{R} = 0, \tag{9}$$

where the overhead dot indicates differentiation with respect to time t .

3. SOLUTION AND THE MODEL

The field Eqs.(6)-(8) form a system of three highly non-linear equations with $R, \phi, \rho_M, \rho_R,$ and ω_R five (5) unknowns. So, we need three more physical conditions to get consistency solution. For this reason we take the following conditions: The DP is taking as linear function of the average scale factor as [41, 42]

$$q = -\frac{R\ddot{R}}{\dot{R}^2} = k_2 + \gamma\frac{\dot{R}}{R}, \tag{10}$$

where k_2 and γ is an arbitrary constants. For $k_2 = -1$, we get the solution of Eq.(10),

$$R = e^{\frac{1}{\gamma}\sqrt{2\gamma t+c_1}}, \tag{11}$$

where c_1 is an integrating constant. Hence, KK FRW Universe Eq.(1), can be written as

$$ds^2 = dt^2 - e^{\frac{2}{\gamma}\sqrt{2\gamma t+c_1}} \left[\frac{dr^2}{1-kr^2} + r^2 \left(d\theta^2 + \sin^2\theta d\phi^2 \right) + (1-kr^2)d\xi^2 \right] \tag{12}$$

The Volume V , Hubble parameter H for our model found to be

$$V = e^{\frac{3}{\gamma}\sqrt{2\gamma t+c_1}}, \tag{13}$$

$$H = (2\gamma t + c_1)^{-\frac{1}{2}}, \tag{14}$$

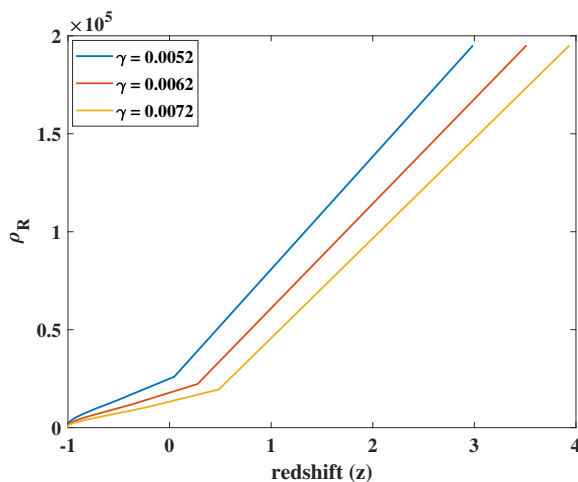


Figure 1. The behavior of energy density (ρ_R) of RHDE versus redshift (z) for $\gamma = 0.0052, \gamma = 0.0062, \gamma = 0.0072$ and $c_1 = 0.000016$.

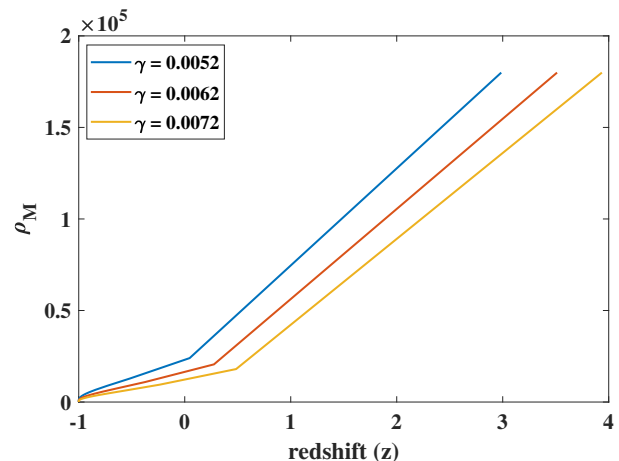


Figure 2. The behavior of energy density (ρ_R) of BHDE versus redshift (z) for $\gamma = 0.0052, \gamma = 0.0062, \gamma = 0.0072$ and $c_1 = 0.000016$.

In Figures 1 & 2, corresponding equations (15) & (16), we show the variation of the energy density (ρ_R) of RHDE & matter (ρ_M) with the Hubble’s horizon cut-off with respect to the redshift (z) for the appropriate values of the model parameter respectively. It is observed that the both ρ_R & ρ_M are positive throughout evolution of the Universe and decreasing function of redshift and finally it reached to zero.

We consider Hubble horizon as a candidate for IR cutoff [43] i.e., $L = H^{-1}$ and $8\pi = 1$, we obtain energy density of RHDE as

$$\rho_R = \frac{3d^2H^2}{1 + \pi\nu H^{-2}} = \frac{3d^2(2\gamma t + c_1)^{-1}}{1 + \pi\delta(2\gamma t + c_1)} \tag{15}$$

From equations (6) & (15), we have the energy density of DM is

$$\rho_M = \frac{6}{2\gamma t + c_1} + 6ke^{-\frac{2\sqrt{2\gamma t+c_1}}{\gamma}} + \frac{w}{2}e^{-\frac{8}{\gamma}\sqrt{2\gamma t+c_1}} - \frac{3d^2}{(2\gamma t + c_1) + \pi\delta(2\gamma t + c_1)} \tag{16}$$

From equations (7), (11), (14) & (15), we have EoS parameter is

$$\omega_R = \left[\frac{w}{2H^2} e^{-\frac{8}{\gamma H}} - 3(1 - \gamma H)H^{-\frac{3}{2}} - 3kH^{-2} e^{-\frac{2}{\gamma H}} \right] \left[\frac{1 + \pi\delta H^{-2}}{3d^2} \right], \tag{17}$$

$$H = (2\gamma t + c_1)^{-\frac{1}{2}}, \text{ and } \dot{H} = -\frac{\gamma}{\sqrt{(2\gamma t + c_1)^3}}$$

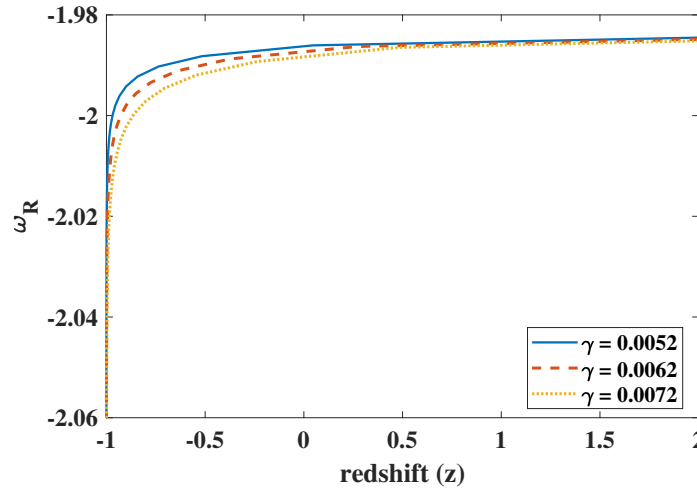


Figure 3. The behavior of equation of state parameter (ω_R) of BHDE versus redshift (z) for $\gamma = 0.0052$, $\gamma = 0.0062$, $\gamma = 0.0072$ and $c_1 = 0.000016$.

Variation of equation of state parameter (ω_R) against redshift (z) in Figure 3,, corresponding to Eq. (17) for the values of $\gamma = 0.0052, 0.0062, 0.0072$. It can be observed that the ω_R completely varies in aggressive phantom region ($\omega_R < -1$) only. If the value of γ increases the phantom region increases.

$\omega_R - \omega'_R$ plane:

In this section, ω'_R is found

$$\omega'_R = \frac{2\pi\delta\dot{H}}{3d^2} \left[3kH^{-2} e^{-\frac{2}{\gamma H}} + 3(1 - \gamma H)H^{-\frac{3}{2}} - \frac{w}{2} H^{-2} e^{-\frac{8}{\gamma H}} \right] + \left(\frac{1 + \pi\delta H^{-2}}{3d^2 H} \right) \left[w \left(\frac{4}{\gamma} - H \right) e^{-\frac{8}{\gamma H}} \frac{\dot{H}}{H^4} + \frac{9}{2} (1 - \gamma H) H^{-\frac{5}{2}} \dot{H} + 3\gamma H^{-\frac{3}{2}} \dot{H} - \frac{3k\dot{H}}{2\gamma H^4} (1 - \gamma H^5) e^{-\frac{2}{\gamma H}} \right] \tag{18}$$

The evolution of the $\omega_R - \omega'_R$ plane is shown in Figure 4 for different values of γ . We observe that the $\omega_R - \omega'_R$ plane for our model is in the thawing region throughout evolution of the Universe ($\omega_R < 0$, and $\omega'_R > 0$).

Stability Analysis

We consider an important parameter to verify the stability of the RHDE model. If squared speed sound v_s^2 is ($v_s^2 > 0$) positive then the model is stable whereas v_s^2 is ($v_s^2 < 0$) negative the model is unstable. For our RHDE model v_s^2 is given by

$$v_s^2 = \left[\frac{w}{2H^2} e^{-\frac{8}{\gamma H}} - 3(1 - \gamma H)H^{-\frac{3}{2}} - 3kH^{-2} e^{-\frac{2}{\gamma H}} \right] \left[\frac{1 + \pi\delta H^{-2}}{3d^2} \right] + \frac{1 + \pi\delta H^{-2}}{2\dot{H}(1 + \pi\delta H^{-2} + \pi\delta H^2)} \left[\frac{2\pi\delta\dot{H}}{3d^2} \left[3kH^{-2} e^{-\frac{2}{\gamma H}} + 3(1 - \gamma H)H^{-\frac{3}{2}} - \frac{w}{2} H^{-2} e^{-\frac{8}{\gamma H}} \right] + \left(\frac{1 + \pi\delta H^{-2}}{3d^2 H} \right) \left[w \left(\frac{4}{\gamma} - H \right) e^{-\frac{8}{\gamma H}} \frac{\dot{H}}{H^4} + \frac{9}{2} (1 - \gamma H) H^{-\frac{5}{2}} \dot{H} + 3\gamma H^{-\frac{3}{2}} \dot{H} - \frac{3k\dot{H}}{2\gamma H^4} (1 - \gamma H^5) e^{-\frac{2}{\gamma H}} \right] \right] \tag{19}$$

Figure 5 shows that the sound speed c_s^2 is decreasing function of redshift (z) and it is negative ($c_s^2 < 0$) throughout history of the Universe for the various values of γ , and $c_1 = 0.000016$ which describes our RHDE model is unstable.

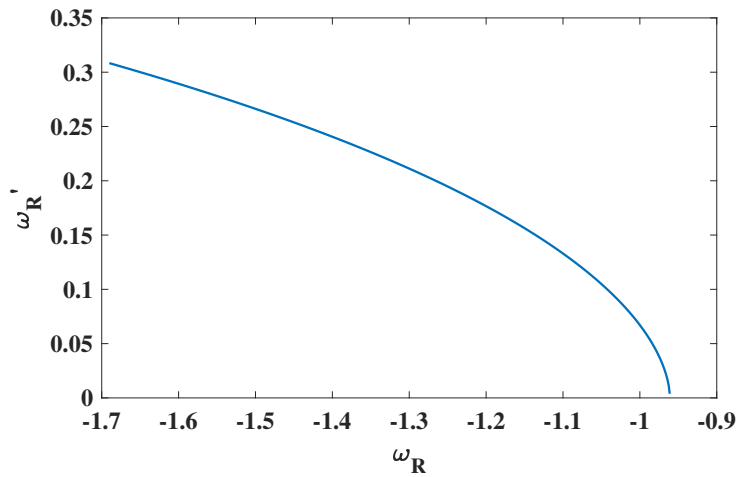


Figure 4. The behavior of ω_R versus ω'_R for $\gamma = 0.0052$ and $c_1 = 0.000016$.

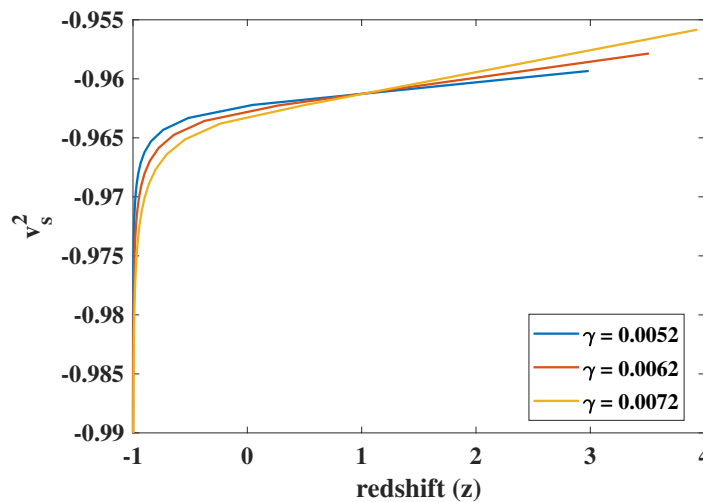


Figure 5. The behavior of squared speed of sound v_s^2 (km/h) versus redshift (z) for $\gamma = 0.0052$, $\gamma = 0.0062$, $\gamma = 0.0072$ and $c_1 = 0.000016$.

Density Parameters

Now we define dimensionless density parameters of dark energy as

$$\Omega_M = \frac{\rho_M}{3H^2}, \quad \text{and} \quad \Omega_R = \frac{\rho_R}{3H^2} \tag{20}$$

By substituting the expressions of ρ_M and ρ_R and Hubble parameter H in the above equations, we get the density parameter of dark matter (ρ_M) and dark energy (ρ_R) for our RHDE model and analyzed its behavior through graphical representation for the various values of γ . Figure 6 & 7 shows the behavior of Ω_M and Ω_R versus redshift (z). The density parameter of DM observed that it increases as the universe evolves. The density parameter of RHDE observed that it decreases as the universe evolves. Also, we have observed that the RHDE density parameter Ω_R meets the [44] values which exhibits consistent results with the recent observations for different values of γ .

Energy Conditions

The study of the energy conditions came into existence from the Raychaudhuri equations which play significant role in any discussion of the congruence of null and time like geodesics. The bounce behavior of cosmological model is also realized using these conditions (energy conditions) as mentioned in references [45, 46, 47, 48, 49, 50, 51].

Null Energy Condition (NEC): $\rho_R(1 + \omega_R) \geq 0$,

Weak Energy Condition (WEC): $\rho_R \geq 0, \rho_R(1 + \omega_R)$,

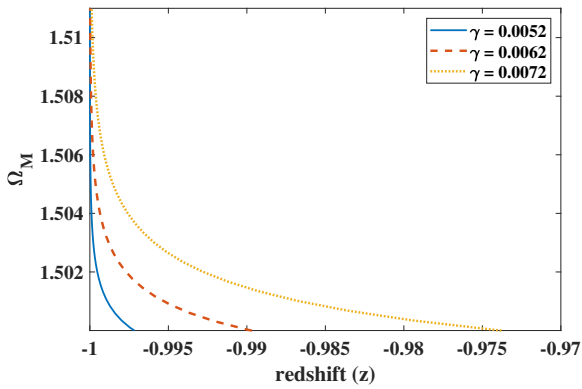


Figure 6. The behavior of matter density parameter (Ω_M) versus redshift (z) for $\gamma = 0.0052$, $\gamma = 0.0062$, $\gamma = 0.0072$ and $c_1 = 0.000016$.

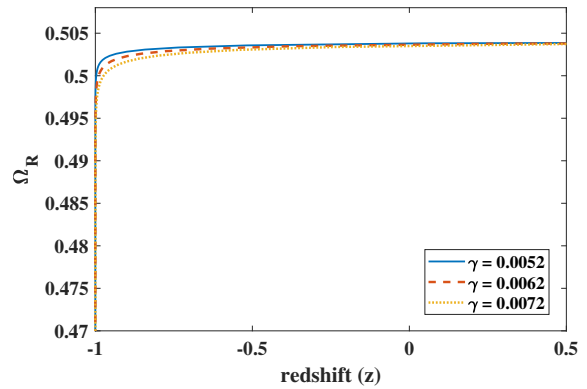


Figure 7. The behavior of density parameter (Ω_R) of RHDE versus redshift (z) for $\gamma = 0.0052$, $\gamma = 0.0062$, $\gamma = 0.0072$ and $c_1 = 0.000016$.

Strong Energy Condition (SEC): $\rho_R(1 + \omega_R) \geq 0$, $\rho_R(1 \pm 3p) \geq 0$,
Dominant Energy Conditions (DEC): $\rho_R \geq 0$, $\rho(1 \pm \omega_R) \geq 0$.

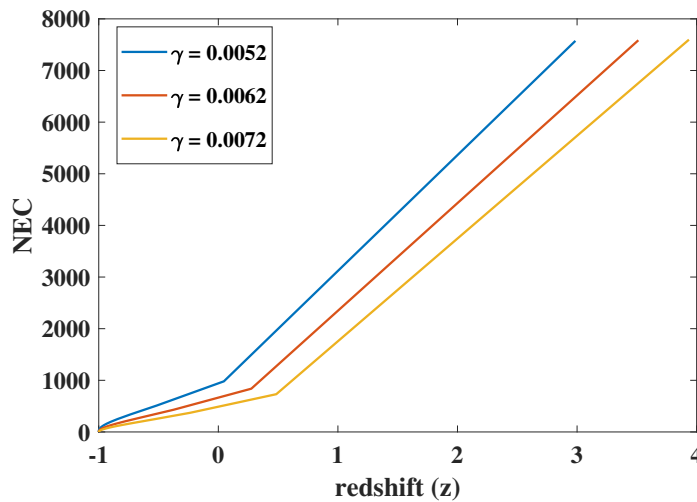


Figure 8. The behavior of NEC of RHDE versus redshift (z) for $\gamma = 0.0052$, $\gamma = 0.0062$, $\gamma = 0.0072$ and $c_1 = 0.000016$.

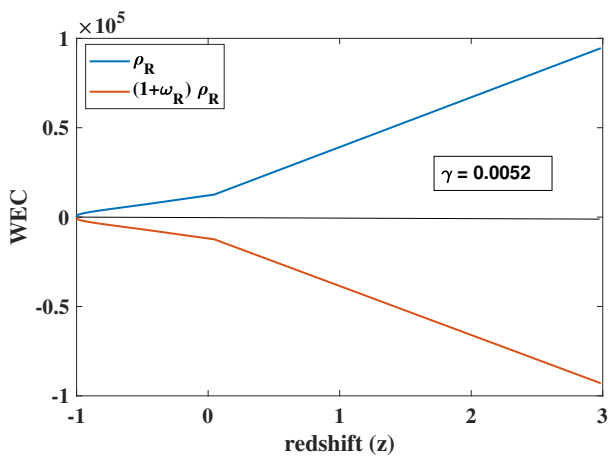


Figure 9. The behavior of WEC of RHDE versus redshift (z) for $\gamma = 0.0052$, and $c_1 = 0.000016$.

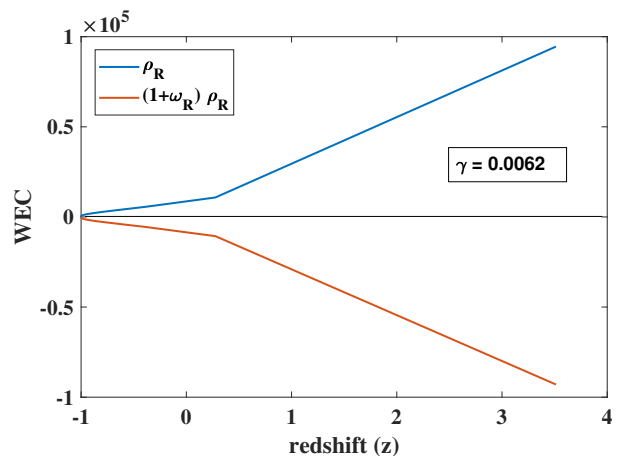


Figure 10. The behavior of WEC of RHDE versus redshift (z) for $\gamma = 0.0062$, and $c_1 = 0.000016$.

From Figure 8, we observe that the NEC $((1 + \omega_R)\rho_R \geq 0)$ are satisfied throughout evolution of the Universe for different values of $\gamma = 0.0052, 0.0062, 0.0072$.

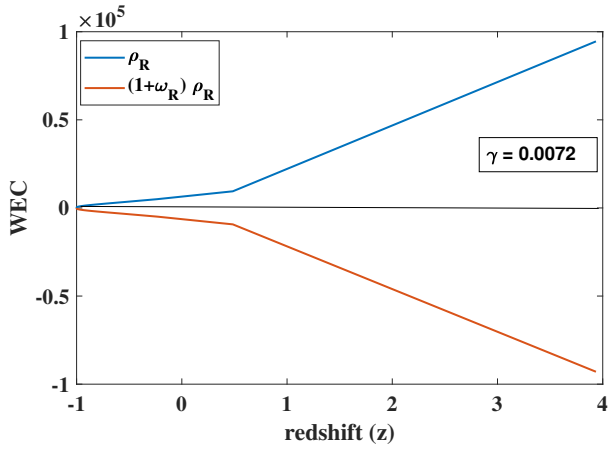


Figure 11. The behavior of WEC of RHDE versus redshift (z) for $\gamma = 0.0072$, and $c_1 = 0.000016$.

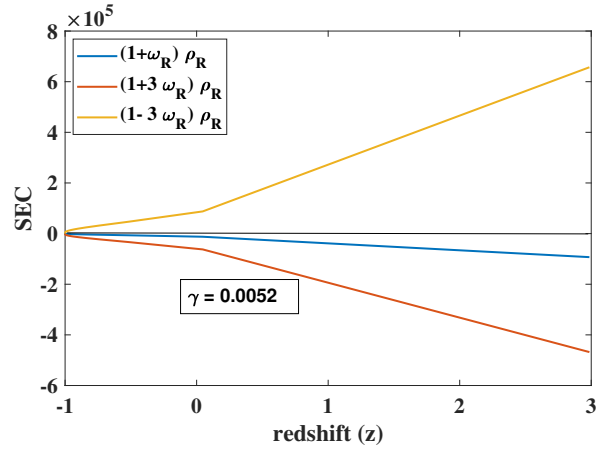


Figure 12. The behavior of SEC of RHDE versus redshift (z) for $\gamma = 0.0052$, and $c_1 = 0.000016$.

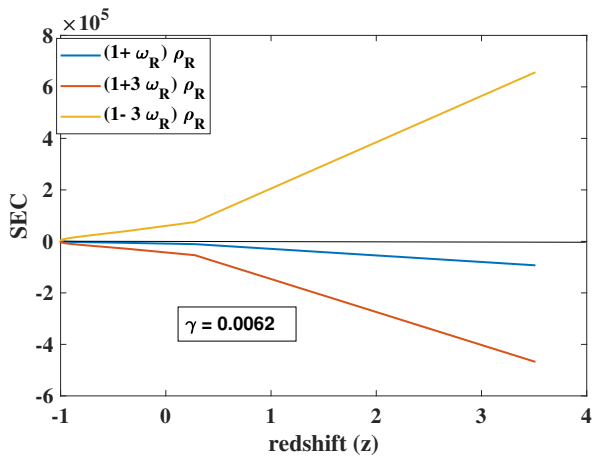


Figure 13. The behavior of SEC of RHDE versus redshift (z) for $\gamma = 0.0062$, and $c_1 = 0.000016$.

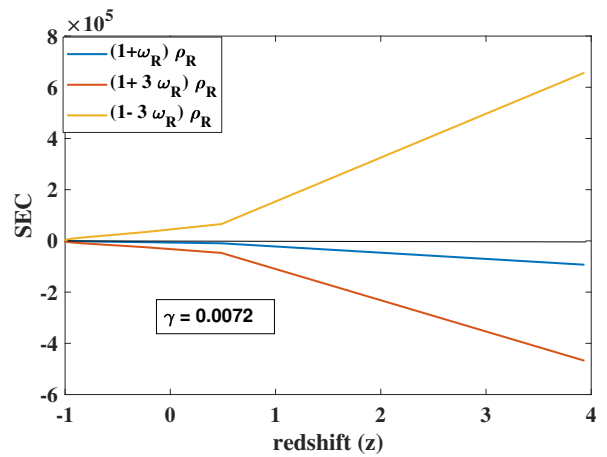


Figure 14. The behavior of SEC of RHDE versus redshift (z) for $\gamma = 0.0072$, and $c_1 = 0.000016$.

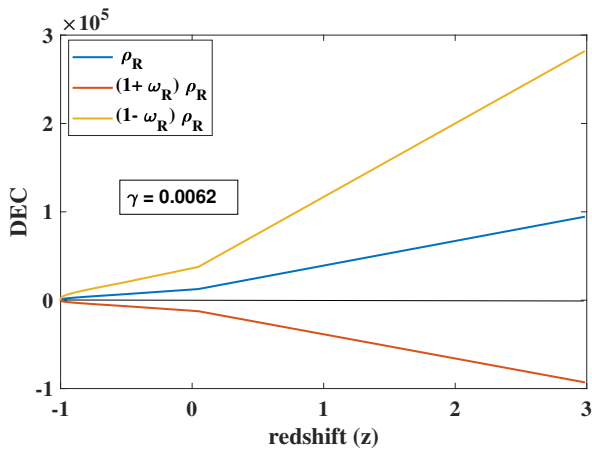


Figure 15. The behavior of DEC of RHDE versus redshift (z) for $\gamma = 0.0052$, and $c_1 = 0.000016$.

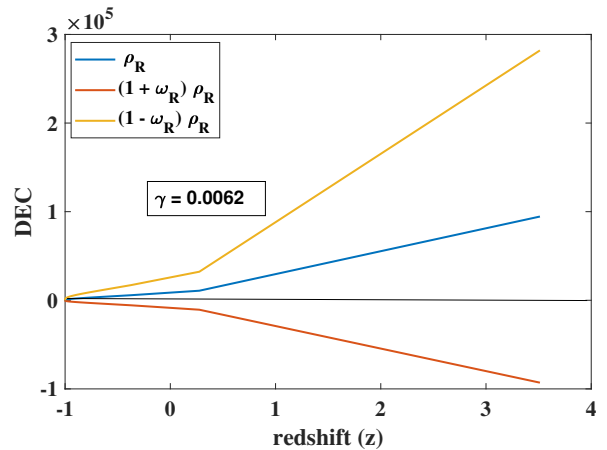


Figure 16. The behavior of DEC of RHDE versus redshift (z) for $\gamma = 0.0062$, and $c_1 = 0.000016$.

Figures 9, 10, 11, 12, 13, 14, 15, 16, 17 describes variation of WEC, DEC and SEC versus redshift (z) for the various

values of γ . We observe that energy conditions WEC ($\rho_R \geq 0, \rho_R(1 + \omega_R)$), DEC ($\rho_R(1 + \omega_R) \geq 0, \rho_R(1 \pm 3p) \geq 0$) and SEC ($\rho_R \geq 0, \rho(1 \pm \omega_R) \geq 0$) are not satisfied for the various values of $\gamma = 0.0052, 0.0062, 0.0072$. The violation of the SEC condition represents the accelerated expansion of the Universe.

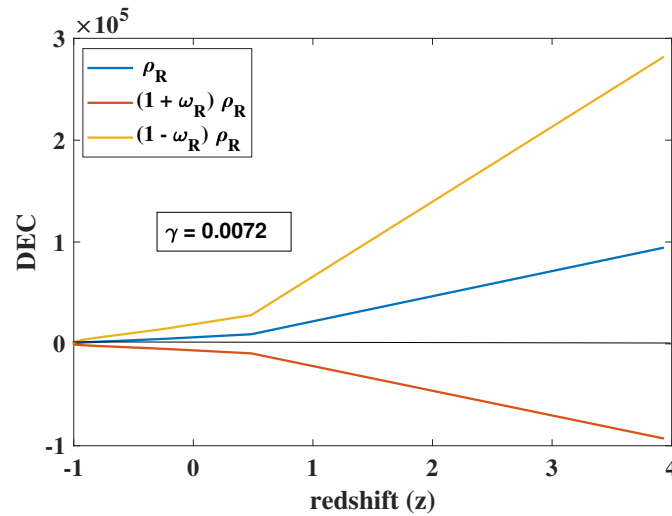


Figure 17. The behavior of DEC of RHDE versus redshift (z) for the values $\gamma = 0.0072$ and $c_1 = 0.000016$.

Deceleration Parameter

The signature of deceleration parameter (q) shows whether the model either accelerates or decelerates. If $q > 0$, the model exhibits decelerating expansion, the Universe exhibits accelerating expansion, for $q < 0$. The DP for our models, is given by

$$q = \frac{a\ddot{a}}{\dot{a}^2} = -1 + \gamma(2\gamma t + c_1)^{-\frac{1}{2}} \tag{21}$$

The evolution of the deceleration parameter (q) with redshift z is shown in Fig. 6. The DP q is observe that there is a

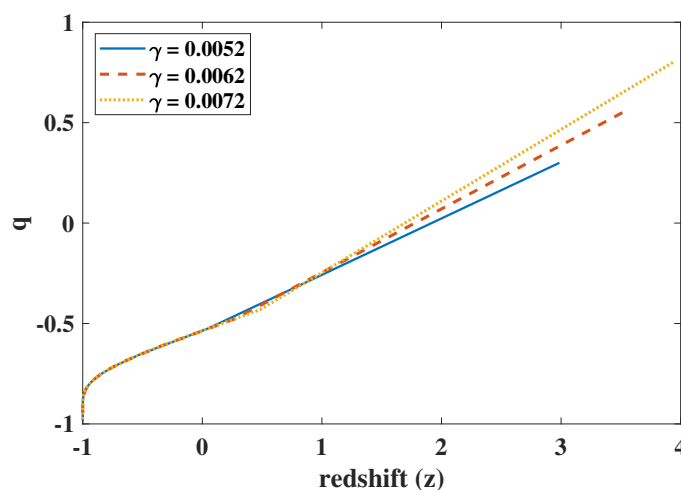


Figure 18. The behavior of deceleration parameter (q) versus redshift (z) for $\gamma = 0.0052, \gamma = 0.0062, \gamma = 0.0072$ and $c_1 = 0.000016$.

sign change in the trajectory of q from positive ($q > 0$) to negative value ($q < 0$). It represents that the Universe smooth transition from early decelerating region ($q > 0$) to accelerating region ($q < 0$) at late epochs. The present value of DP is consistent with the recent observational data [58].

Statefinder Parameters

The DE models have been proposed for explaining the accelerated expansion phenomenon of the universe. In order to check the viability of these models, statefinder parameters are widely used [52, 53, 54, 55, 56, 57]

$$r = \frac{\ddot{a}}{aH^3}, \quad s = \frac{r - 1}{3(q - \frac{1}{2})} \tag{22}$$

The important model described by the parameters ($r = 1, s = 1$) shows CDM model, ($r = 1, s = 0$) represents ΛCDM model, while $r < 1, s > 0$ indicate quintessence and phantom DE models.

In the present work, the trajectory statefinder $r - s$ plane for different values of γ is shown in Figure 20. It can be observed that the trajectory $r - s$ plane approaches ΛCDM ($r = 1, s = 0$) model for the value of $\gamma = 0.0052$. We also, observed that the trajectory of $r - s$ plane is initially lies in quintessence region $r < 1$, crosses the with quintessence and phantom regions and finally reached to ΛCDM in late times for the values of $\gamma = 0.0062$ and 0.0072 . We have also

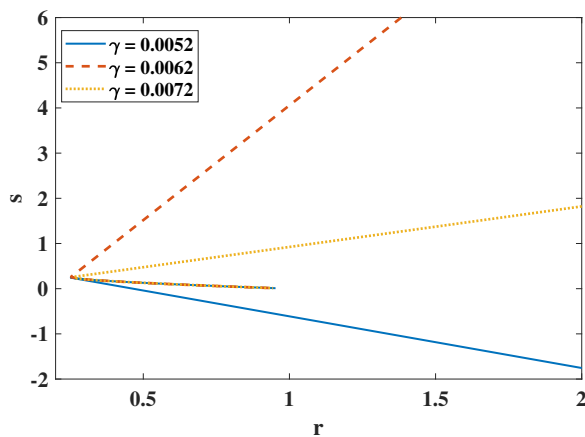


Figure 19. The behavior of statefinder $r - q$ plane for $\gamma = 0.0052, \gamma = 0.0062, \gamma = 0.0072$ and $c_1 = 0.000016$.

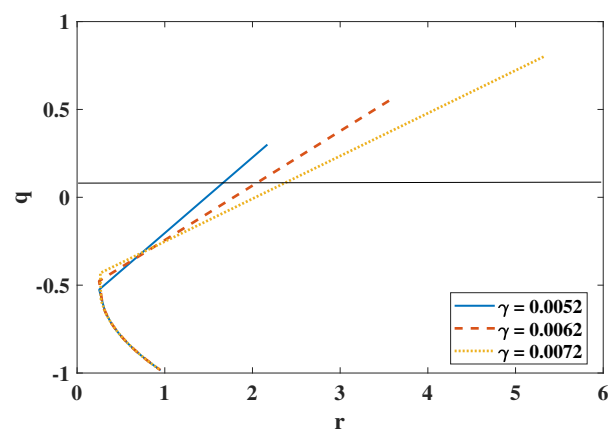


Figure 20. The behavior of Statefinder $r - q$ plane for $\gamma = 0.0052, \gamma = 0.0062, \gamma = 0.0072$ and $c_1 = 0.000016$.

shown the evolutionary trajectories of another statefinder $r - q$ plane for the RHDE model in Figure 20 for the best-fit values of γ . The evolutionary curve of the $r - q$ plane of RHDE model starts from the SCDM in the past and reaches above the de-Sitter expansion in the future, and it also shows the Chaplygin gas behavior throughout the evaluation. Since q changes its sign from positive to negative, it also represents the recent phase transition of the Universe.

4. CONCLUSIONS





In this work, we have studied the Kaluza-Klein FRW RHDE model in SB scalar-tensor theory of gravitation. To obtain the deterministic model of the Universe we consider some physical plausible conditions, these conditions leads to a varying DP, which represents transition from the past decelerating Universe to the current accelerating Universe. The main conclusions of these two models are summarized as follows:

- The variation of the energy density (ρ_R) of RHDE & matter (ρ_M) with the Hubble's horizon cut-off observed that the both ρ_R & ρ_M are positive throughout evolution of the Universe and decreasing function of redshift and finally it reached to zero.
- Behavior of equation of state parameter (ω_R) completely varies in aggressive phantom region ($\omega_R < -1$) only for the different values of $\gamma = 0.0052, 0.0062, 0.0072$. If the value of γ increases the phantom region increases.
- The evolution of the $\omega_R - \omega'_R$ plane for our model is in the thawing region throughout evolution of the Universe.
- The sound speed c_s^2 is decreasing function of redshift (z) and it is negative ($c_s^2 < 0$) throughout history of the Universe for the various values of γ , and $c_1 = 0.000016$ which describes our RHDE model is unstable.
- The density parameter of DM observed that it increases as the universe evolves. The density parameter of RHDE observed that it decreases as the universe evolves. Also, we have observed that the RHDE density parameter Ω_R meets the [44] values which exhibits consistent results with the recent observations for different values of γ .
- We observe that energy conditions WEC, DEC and SEC are not satisfied for the various values of $\gamma = 0.0052, 0.0062, 0.0072$. The violation of the SEC condition represents the accelerated expansion of the Universe.

- The evolution of the deceleration parameter (q) is observe that there is a sign change in the trajectory of q from positive ($q > 0$) to negative value ($q < 0$). It represents that the Universe smooth transition from early decelerating region ($q > 0$) to accelerating region ($q < 0$) at late epochs. The present value of DP is consistent with the recent observational data [58].
- The trajectory $r-s$ plane approaches to Λ CDM ($r = 1, s = 0$) model for the value of $\gamma = 0.0052$. We also, observed that the trajectory of $r-s$ plane is initially lies in quintessence region $r < 1$, crosses the with DE (quintessence and phantom) regions and finally reached to Λ CDM in late times for the values of $\gamma = 0.0062$ and 0.0072 . The evolutionary curve of the $r-q$ plane of RHDE model starts from the SCDM in the past and reaches above the de-Sitter expansion in the future, and it also shows the Chaplygin gas behavior throughout the evaluation. Since q changes its sign from positive to negative, it also represents the recent phase transition of the Universe.

Data Availability Statement: This manuscript has no associated data or the data will not be deposited. **Acknowledgments:** The authors are very much grateful to the honorable referees and to the editor for the illuminating suggestions that have significantly improved our work in terms of research quality, and presentation.

ORCID

 **Y. Sobhanbabu**, <https://orcid.org/0000-0003-0717-1323>;  **M. Vijaya Santhi**, <https://orcid.org/0000-0002-0050-3033>;
 **A. Srinivasa Rao**, <https://orcid.org/0009-0004-1689-9759>;  **M. Praveen Kumar**, <https://orcid.org/0000-0002-4209-037X>

REFERENCES

- [1] A.G. Riess, *et al.*: *Astron. J.* **116**, 1009 (1998). <https://doi.org/10.1086/300499>
- [2] S. Perlmutter, *et al.*, *Astrophys. J.* **517**, 565 (1999). <https://doi.org/10.1086/307221>
- [3] M. Padmanabhan, *Phys. Rep.* **380**, 235 (2003). [https://doi.org/10.1016/S0370-1573\(03\)00120-0](https://doi.org/10.1016/S0370-1573(03)00120-0)
- [4] E.J. Copeland, M. Sami, and S. Tsujikawa, *Int. J. Mod. Phys. D*, **15**, 1753 (2006). <https://doi.org/10.1142/S021827180600942X>
- [5] K. Bamba, *et al.*, *Astrophys. Space Sci.* **342**, 155 (2012). <https://doi.org/10.1007/s10509-012-1181-8>
- [6] P. Horava, and M. Djordje, *Phys. Rev. Lett* **85**, 1610 (2000). <https://doi.org/10.1103/PhysRevLett.85.1610>
- [7] S. Thomas. *Phys. Rev. Lett.* **89**, 081301 (2002). <https://doi.org/10.1103/PhysRevLett.89.081301>
- [8] S.D.H. Hsu, *Phys. Lett. B*, **594**, 13 (2004). <https://doi.org/10.1016/j.physletb.2004.05.020>
- [9] M. Li, *Phys. Lett. B*, **603**, 1 (2004). <http://dx.doi.org/10.1016/j.physletb.2004.10.014>
- [10] R. D'Agostino, *Phys. Rev. D*, **99**, 103524 (2019). <https://doi.org/10.1103/PhysRevD.99.103524>
- [11] A. Majhi, *Phys. Lett. B*, **775**, 32 (2017). <https://doi.org/10.1016/j.physletb.2017.10.043>
- [12] S. Abe, *Phys. Rev. E*, **63**, 061105 (2001). <https://doi.org/10.1103/PhysRevE.63.061105>
- [13] T.S. Biró, and P. Ván, *Phys. Rev. E*, **83**, 061147 (2011). <https://doi.org/10.1103/PhysRevE.83.061147>
- [14] M. Tavayef, A. Sheykhi, *et al.*, *Phys. Lett. B*, **781**, 195 (2018). <https://doi.org/10.1016/j.physletb.2018.04.001>
- [15] K.Y. Kim, H.W. Lee, and Y.S. Myung, *Phys. Lett. B*, **660**, 118 (2008). <https://doi.org/10.1016/j.physletb.2007.12.045>
- [16] I.P. Neupane, *Phys. Lett. B*, **673**, 111 (2009). <https://doi.org/10.1016/j.physletb.2009.02.012>
- [17] O.A. Lemets, D.A. Yerokhin, and L.G. Zazunov, *J. Cosmol. Astropart. Phys.* **01**, 007 (2011). <https://doi.org/10.1088/1475-7516/2011/01/007>
- [18] H. Wei, and R.G. Cai, *Phys. Lett. B*, **665**, 1 (2007). <https://doi.org/10.1016/j.physletb.2007.08.066>
- [19] A. Sheykhi, and M.R. Setare, *Int. J. Theor. Phys.* **49**, 2777 (2010). <https://doi.org/10.1007/s10773-010-0469-0>
- [20] A. Rényi, *Prob. theory.* (North-Holland, Amsterdam). 540-616 (1970).
- [21] H. Moradpour, A. Sheykhi, *et al.*, *Phys. Lett. B*, **783**, 82 (2018). <https://doi.org/10.1016/j.physletb.2018.06.040>
- [22] H. Moradpour, S. A. Moosavi, *et al.*, *Eur. Phys. J. C*, **78**, 829 (2018). <https://doi.org/10.1140/epjc/s10052-018-6309-8>
- [23] A. Jawad, K. Bamba, *et al.*, *Symmetry*, **10**, 635 (2018). <https://doi.org/10.3390/sym10110635>
- [24] A. Iqbal, and A. Jawad, *Phys. Dark Univ.* **26**, 100349 (2019). <https://doi.org/10.1016/j.dark.2019.100349>
- [25] M. Younas, *et al.*, *Adv. High Energy Phys.* 1287932, (2019). <https://doi.org/10.1155/2019/1287932>
- [26] A. Dixit, V.K. Bhardwaj, and A. Pradhan, (2020). <https://doi.org/10.48550/arXiv.2010.10847>
- [27] S. Chunlen, and P. Rangdeey, (2020). <https://doi.org/10.48550/arXiv.2008.13730>
- [28] U.K. Sharma and V.C. Dubey, (2020). <https://doi.org/10.48550/arXiv.2001.02368>
- [29] A. Sarfraz, S. Khan, and S. Sattar, (2020). <https://arxiv.org/abs/2011.10046v1>
- [30] U.K. Sharma, and V.C. Dubey, *New Astronomy*, **80**, 101419 (2020). <https://doi.org/10.1016/j.newast.2020.101419>
- [31] A. Saha, *et al.*, (2021). <https://arxiv.org/abs/2101.04060v1>

- [32] U.K. Sharma, and V.C. Dubey, *Mod. Phys. Lett. A*, **35**(34), 2050281 (2021). <https://doi.org/10.1142/S0217732320502818>
- [33] U.Y.D. Prasanthi, and Y. Aditya, *Results in Phys.* **17**, 103101 (2020). <https://doi.org/10.1016/j.rinp.2020.103101>
- [34] S. Bhattacharjee, *Astrophys. and Space Sci.* **365**, 103 (2020). <https://doi.org/10.1007/s10509-020-03820-7>
- [35] M.V. Santhi, and Y. Sobhanbabu, *Eur. Phys. J. C*, **80**, 1198, (2020). <https://doi.org/10.1140/epjc/s10052-020-08743-9>
- [36] Y. Sobhanbabu, and M.V. Santhi, *Eur. Phys. J. C*, **81**, 1040 (2021). <https://doi.org/10.1140/epjc/s10052-021-09815-0>
- [37] U.Y.D. Prasanthi, and Y. Aditya, *Phys. Dark Univ.* **31**, 100782 (2021). <https://doi.org/10.1016/j.dark.2021.100782>
- [38] Y. Sobhanbabu, and M.V. Santhi, *Gen. Relativ. Gravit.* **54**, 95 (2022).
- [39] Y. Sobhanbabu, et al., *New Astronomy*, **104**, 102066, (2023). <https://doi.org/10.1016/j.newast.2023.102066>
- [40] D. Saez, and V.J. Ballester, *J. Phys. Lett.* **113**, 467 (1986). [https://doi.org/10.1016/0375-9601\(86\)90121-0](https://doi.org/10.1016/0375-9601(86)90121-0)
- [41] R. Tiwari, R. Singh, and Shukla, *Afric. Rev. Phys. B*, **10**, 0048 (2015). <http://aphysrev.ictp.it/index.php/aphysrev/article/download/1137/460>
- [42] U.K. Sharma, et al., *Res. Astron. Astrophys.* **19**, 055 (2019). <https://doi.org/10.1088/1674-4527/19/4/55>
- [43] L.N. Granda, and A. Oliveros, *Phys. Lett. B*, 671, 199 (2009). <https://doi.org/10.1016/j.physletb.2008.12.025>
- [44] G. Hinshaw, et al., *Astrophys. J. Suppl.* **208**, 19 (2013). <https://doi.org/10.1088/0067-0049/208/2/19>
- [45] S.W. Hawking, and G.F.R. Ellis, *The Large-Scale Structure of Space Time*, (Cambridge Univ. Press, Cambridge, 1973).
- [46] R.M. Wald, *Generality*, (University of Chicago Press, Chicago) (1984).
- [47] M. Visser, *Science*, **276**, 88 (1997). <https://doi.org/10.1126/science.276.5309.88>
- [48] C. Molina-Paris, and M. Visser, *Phys. Lett. B*, **455**, 90 (2013). [https://doi.org/10.1016/S0370-2693\(99\)00469-4](https://doi.org/10.1016/S0370-2693(99)00469-4)
- [49] T. Singh, et al., *Astro. Space Sci.* **361**, 106 (2016). <https://doi.org/10.1007/s10509-016-2696-1>
- [50] J. Santos, J.S. Alcaniz, et al., *Phys. Rev. D*, **76**, 083513 (2007). <https://doi.org/10.1103/PhysRevD.76.083513>
- [51] E.-A. Kontou, and K. Sanders, (2020). <https://arxiv.org/abs/2003.01815v2>
- [52] U. Alam, et al. *Mon. Not. R. Astron. Soc.* **344**, 1057 (2003). <https://doi.org/10.1046/j.1365-8711.2003.06871.x>
- [53] V. Sahni, et al., *JETP Lett.* **77**, 201 (2003). <https://doi.org/10.1134/1.1574831>
- [54] M. Sharif, and A. Jawad, *Eur. Phys. J. C*, **73**, 2600 (2013). <https://doi.org/10.1140/epjc/s10052-013-2600-x>
- [55] A. Al Mamon, et al., *Universe*, **7**, 362 (2021). <https://doi.org/10.3390/universe7100362>
- [56] R.R. Caldwell, and E.V. Linder, *Phys. Rev. Lett.* **95**, 141301 (2005). <https://doi.org/10.1103/PhysRevLett.95.141301>
- [57] R. Giotri, M. Vargas dos Santos, I. Waga, et al., *J. Cosmol. Astropart. Phys.* **3**, 027 (2012). <https://doi.org/10.1088/1475-7516/2012/03/027>
- [58] N. Aghanim, et al., [Plancks Collaboration], (2018). <https://arxiv.org/abs/1807.06209v2>

ГОЛОГРАФІЧНА МОДЕЛЬ ТЕМНОЇ ЕНЕРГІЇ КАЛУЗА-КЛЕЙНА FRW РЕНЬЇ В СКАЛЯРНО-ТЕНЗОРНІЙ ТЕОРІЇ ГРАВІТАЦІЇ

Ю. Собханбабу^a, М. Віджая Санті^b, А. Шрініваса Рао^b, М. Правін Кумар^a

^aІнженерний коледж Сагі Рама Кришнам Раджу (А), Бхімаварам, 534204, Індія

^bУніверситет Андхра, Вішакхапатнам, 530003, Індія

У цій роботі розглядається явище темної енергії шляхом вивчення голографічної темної енергії Реньї (RHDE) і темної матерії без тиску (DM) у рамках скалярно-тензорної теорії гравітації Саеза-Баллестера (SB) (Phys. Lett. A113), 467:1986). Щоб знайти рішення, ми розглядаємо життєздатний параметр уповільнення (DP), який вносить внесок у середній масштабний коефіцієнт $a = e^{\frac{1}{\gamma} \sqrt{2\gamma t + c_1}}$, де γ і c_1 відповідно довільні та константи інтегрування. Ми вивели польові рівняння скалярно-тензорної теорії гравітації SB за допомогою Всесвіту Калузи-Клейна FRW. Ми досліджували космологічні параметри, а саме DP (q), густину енергії (ρ_M) і (ρ_R) DM і RHDE, скалярне поле (ϕ) і рівняння параметра стану (ω_R). Фізичні дебати цих космологічних параметрів досліджуються за допомогою графічного представлення. Крім того, стабільність моделі досліджується через квадрат швидкості звуку (v_s^2) і добре відому космологічну площину $\omega_R - \omega'_R$ і всі енергетичні умови а також параметри щільності аналізуються за допомогою графічного представлення нашої моделі.

Ключові слова: Калуза-Клейн FRW Всесвіт; RHDE; енергетичні умови; теорія Саеза-Баллестера

CONSTRAINING LOGARITHMIC $f(R, T)$ MODEL USING DARK ENERGY DENSITY PARAMETER Ω_Λ AND HUBBLE PARAMETER H_0

 Biswajit Deb,  Atri Deshamukhya*

Department of Physics, Assam University, Silchar, India

*Corresponding Author e-mail: atri.deshamukhya@aus.ac.in

Received May 5, 2024; revised July 10, 2024; accepted July 26, 2024

Of many extended theories of gravity, $f(R, T)$ gravity has gained reasonable interest in recent times as it provides interesting results in cosmology. Logarithmic corrections in modified theories of gravity has been studied extensively. In this work, we considered logarithmic correction to the trace term T and take the functional form as $f(R, T) = R + 16\pi G\alpha \ln T$ where α is a free parameter. The free parameter is constrained using dark energy density parameter Ω_Λ and Hubble parameter H_0 . The lower bound is found to be $\alpha \geq -9.85 \times 10^{-29}$. The cosmological implications are also studied.

Keywords: $f(R, T)$ Gravity, Dark Energy

PACS: 04.50kd, 95.36+X

1. INTRODUCTION

The remarkable discovery in 1998 by Riess et. al and Perlmutter et. al paused a fundamental question on the classical General Relativity (GR) [1, 2]. The standard GR predicts that the expansion of the Universe should be decelerating with time. Instead, it is observed that the current Universe has entered a second phase of accelerated expansion which started around $z = 1$ [1, 2]. Besides this, it is observed that nearly 70% of the total energy density of the Universe is in some mysterious form called Dark Energy [1, 2]. Whether this Dark Energy is driving the present expansion of the Universe is a matter of investigation.

Einstein field equations, in their original form can't explain this late time acceleration because it gives an equation of state (EoS) parameter $w = 0$ [3]. Whereas, the present late time acceleration demands EoS parameter to be $w < -\frac{1}{3}$. Now, this can be explained if one considers the Universe filled with some exotic form of fluid with EoS parameter $w < -\frac{1}{3}$ [3]. That means the dominant Dark Energy constituent is driving the expansion. Apart from this, cosmological constant with EoS parameter $w = -1$ is a viable alternative explanation for Dark Energy as well as late time expansion of the Universe [3]. In fact the Λ CDM model gives the best fit results to the present observed Universe [4]. But the Cosmological constant Λ is into fine tuning problem [5].

$f(R)$ theory, a class of modified gravity, emerged in 1980's and gained popularity as it can explain the early inflationary Universe without considering the scalar fields in the theory [6]. Since then different modifications of gravity viz. $f(G)$, $f(R, G)$, $f(G, T)$, $f(R, T)$, $f(Q)$, $f(Q, T)$ etc. have been proposed and studied in literature where R , Q , G and T are the Ricci scalar, non-metricity, Gauss-Bonnet scalar and Trace of the Energy momentum tensor respectively [7, 8, 9, 10, 11, 12]. After the discovery of late time acceleration, studies of modified theories of gravity gained even more interest as it has the potential to explain late time acceleration of the Universe without invoking Dark Energy in the theory [13].

$f(R, T)$ theory of gravity, proposed by Harko et. al is found to be extremely sound in explaining cosmological phenomena. It has been studied with reference to inflation [14, 15, 16, 17], dark energy [18, 19, 20, 21, 22], dark matter [23], wormhole [24, 25, 26, 27, 28, 29, 30], pulsar [31, 32], white dwarfs [33], gravitational waves [34, 35], scalar field models [36, 37], anisotropic models [38, 39], bouncing cosmology [40, 41], big-bang nucleosynthesis [42], baryogenesis [43], brane world [44, 45] etc. Further, the energy conditions and junction conditions in $f(R, T)$ gravity have also been studied [46, 47, 48, 49]. Snehasish et. al developed a novel way to impose lower bound on the model parameter λ of the simplest $f(R, T) = R + 2\lambda T$ model through the equation relating the cosmological constant and critical density of the universe [18]. This method can be applied to other complex forms of $f(R, T)$ to constrain the model parameter(s). This might reveal interesting result.

Logarithmic correction in modified gravity theories has been studied extensively. The first Logarithmic correction to trace term T in $f(R, T)$ theory has been proposed by Elizalde et. al where they have studied the stability conditions & energy conditions of the model [50]. In this work, we have considered the simplest $f(R, T)$ model with logarithmic correction to trace term T as $f(R, T) = R + 16\pi G\alpha \ln T$, where α is the model parameter and will constrain the model parameter α using equation relating to the cosmological constant Λ and critical density of the universe ρ_{cr} . Recently Maurya et. al have studied similar model and found that it shows a quintessence dark energy model and late time universe approaches to Λ CDM model [56].

The paper has been organised as follows: In section 2, we present a brief review of $f(R, T)$ gravity. In section 3, we present mathematical framework to impose bound on the model parameter. In section 3, we present our conclusion. Here, we will use (+,-,-,-) sign convention for the metric tensor.

2. A BRIEF NOTE ON $f(R, T)$ GRAVITY

In $f(R, T)$ gravity, the gravitational Lagrangian depends on a general function of Ricci scalar R as well as of the trace of energy momentum tensor T . The action in $f(R, T)$ gravity reads as,

$$S = \int \left[\frac{f(R, T)}{16\pi G} + L_m \right] \sqrt{-g} d^4x \tag{1}$$

where L_m is the matter Lagrangian, g is the metric determinant and G is the Newtonian gravitational constant. On variation of the action with respect to the metric, we obtain the modified field equations as,

$$f_R(R, T)R_{\mu\nu} - \frac{1}{2}g_{\mu\nu}f(R, T) + [g_{\mu\nu}\nabla_\sigma\nabla^\sigma - \nabla_\mu\nabla_\nu]f_R(R, T) = 8\pi GT_{\mu\nu} - f_T(R, T)(T_{\mu\nu} + \Theta_{\mu\nu}) \tag{2}$$

where we have denoted $f_R(R, T) = \frac{\partial f(R, T)}{\partial R}$, $f_T(R, T) = \frac{\partial f(R, T)}{\partial T}$ and defined $T_{\mu\nu}$ and $\Theta_{\mu\nu}$ as,

$$T_{\mu\nu} = g_{\mu\nu}L_m - 2\frac{\delta L_m}{\delta g^{\mu\nu}} \tag{3}$$

$$\Theta_{\mu\nu} = g^{\beta\gamma}\frac{\delta T_{\beta\gamma}}{\delta g^{\mu\nu}} = -2T_{\mu\nu} + g_{\mu\nu}L_m - 2\frac{\delta^2 L_m}{\delta g^{\mu\nu}\delta g^{\beta\gamma}} \tag{4}$$

The term $\Theta_{\mu\nu}$ plays a significant role in $f(R, T)$ gravity. Since it contains matter Lagrangian L_m , depending on the nature of the matter field, the field equation for $f(R, T)$ gravity will vary. Besides this the functional form of $f(R, T)$ will also change the field equation. Thus, the field equations in $f(R, T)$ gravity depend both on the nature of matter field and choice of the functional form of $f(R, T)$.

Harko proposed four different forms of the function $f(R, T)$ in his paper[10], viz.:

- $f(R, T) = R + 2f(T)$
- $f(R, T) = f_1(R) + f_2(T)$
- $f(R, T) = f_1(R) + f_2(R)f_3(T)$
- $f(R, T^\phi) = R + f(T^\phi)$, where ϕ is a self interacting scalar field.

Beside these forms, various other forms have been proposed in literature [15, 54, 55] which are as follows:

- $f(R, T) = R + \phi f(T)$, ϕ is scalar field.
- $f(R, T) = R + \alpha e^{RT}$, α is a constant.
- $f(R, T) = R + \alpha e^{\beta T} + \gamma T^n$, α, β, γ are constant.

3. CONSTRAINING MODEL PARAMETER

Considering $f(R, T) = R + 16\pi G\alpha \ln T$, the Einstein-Hilbert action becomes,

$$S = \int \sqrt{-g} \left[\frac{R}{16\pi G} + \alpha \ln T + L_m \right] d^4x \tag{5}$$

This leads to field equations,

$$R_{\mu\nu} - \frac{1}{2}g_{\mu\nu}R = 8\pi GT_{\mu\nu}^{(eff)} \tag{6}$$

where $T_{\mu\nu}^{(eff)}$ is the effective stress-energy tensor given by,

$$T_{\mu\nu}^{(eff)} = T_{\mu\nu} - \frac{2\alpha}{T} \left(T_{\mu\nu} - \frac{T}{2}g_{\mu\nu} \ln T + \Theta_{\mu\nu} \right) \tag{7}$$

Clearly, depending on the nature of the matter field, the field equation for $f(R, T)$ gravity will be different. Now, assuming the Universe is dominated by perfect fluid, the energy-momentum tensor is

$$T_{\mu\nu} = (\rho + p)u_\mu u_\nu - pg_{\mu\nu} \tag{8}$$

and hence the matter Lagrangian density can be assumed as $L_m = -p$. Now, let us assume the Friedmann-Lemaitre-Robertson-Walkar (FLRW) metric in spherical coordinate for flat Universe,

$$ds^2 = dt^2 - a(t)^2 [dr^2 + r^2(d\theta^2 + \sin^2 \theta d\phi^2)] \tag{9}$$

where $a(t)$ denotes scale factor of the Universe. Now, considering the FLRW metric, the 00 component of field Eq. 6 yields first modified Friedmann equation as,

$$3H^2 = 8\pi G \left[\rho + \frac{2\alpha}{\rho - 3p} \left(\rho + p + \frac{\rho - 3p}{2} \ln(\rho - 3p) \right) \right] \tag{10}$$

where H is Hubble parameter, ρ is energy density and p is pressure of the Universe. Further, $T = \rho - 3p$ is the trace of the EM tensor. Now using equation of state parameter $w = p/\rho$, the above Friedmann equation can be rearranged as

$$3H^2 = 8\pi G \left[\rho + \frac{2\alpha}{(1 - 3w)\rho} \left((1 + w)\rho + \frac{(1 - 3w)\rho}{2} \ln(1 - 3w)\rho \right) \right] \tag{11}$$

Current observation [4] suggest that $w = -1$ and hence substituting this value in Friedmann Eq. yields,

$$3H^2 = 8\pi G(\rho + \alpha \ln 4\rho) \tag{12}$$

Now, Friedmann equation in GR with Cosmological Constant Λ is given by [51],

$$3H^2 = 8\pi G\rho + \Lambda c^2 \tag{13}$$

Equating Eq.12 and Eq.13 yields,

$$\Lambda c^2 = 8\pi G\alpha \ln 4\rho \tag{14}$$

Now, Cosmological Constant Λ can be defined in terms of present value of Hubble parameter H_0 and dark energy density parameter Ω_Λ as [52],

$$\Lambda = 3 \left(\frac{H_0}{c} \right)^2 \Omega_\Lambda \tag{15}$$

Substituting Eq.15 in Eq.14 we get,

$$\Omega_\Lambda = \frac{8\pi G\alpha}{3H_0^2} \ln 4\rho \tag{16}$$

The present Universe is spatially flat. As a result the total density parameter is $\Omega_0 = \rho/\rho_{cr} = 1$ [4]. Hence we can replace ρ by ρ_{cr} in the previous equation.

$$\Omega_\Lambda = \frac{8\pi G\alpha}{3H_0^2} \ln 4\rho_{cr} \tag{17}$$

Now the critical density of the Universe is defined as [53]

$$\rho_{cr} = \frac{3H_0^2}{8\pi G} \tag{18}$$

From Eq.17 and Eq.18 we get the final expression of the model parameter α in terms of Hubble parameter and dark energy density parameter as

$$\Omega_\Lambda = \frac{8\pi G\alpha}{3H_0^2} \ln \frac{3H_0^2}{2\pi G} \tag{19}$$

From Planck 2018 data [4], we have $H_0 = 67.4 \pm 0.5 Kms^{-1} Mpc^{-1}$ and $\Omega_\Lambda = 0.6889 \pm 0.0056$. Substituting $H_0 = 2.17 \times 10^{-18} s^{-1}$ (in SI unit) and $\Omega_\Lambda = 0.6833$ in Eq.19, we obtain the lower bound on the model parameter

$$\alpha \geq -9.85 \times 10^{-29}$$

4. CONCLUSION

Free parameters in modified gravity theories are trivial and hold significant role. It allows a particular gravity model to be consistent with observational results. In this work we tried to constrain the simplest $f(R, T)$ model with logarithmic correction, using Hubble parameter and dark energy density parameter. The analysis reveals that the model parameter α can assume any non negative value.

This method of imposing lower bound on the model parameter by relating equation to the cosmological constant and critical density of the Universe developed by Snehasish et. al is exclusively model dependent. For more complex forms of $f(R, T)$, more input parameters are required to constraint the model. Further, this method can be applied to constrain other modified gravity models but it may require more constraining parameters beside dark energy density parameter.

Snehasish et. al obtained the lower bound for $f(R, T) = R + 2\lambda T$ model which is of the order of 10^{-8} . In case $f(R, T) = R + 16\pi G\alpha \ln T$, the lower bound obtained is of the order of 10^{-29} . In both the cases, the lower bound on the model parameter is quite small. As a result, these bounds need to be validated from other sources like spectral indices, tensor-to-scalar ratio etc which is beyond the scope of this work.

As a possible extension of this work, one can apply this methodology to other $f(R, T)$ models, specially non-minimally coupled ones. Further, this method can also be applied to other modified gravity theories like $f(R, G)$, $f(G, T)$ etc. which may generate interesting results.

ORCID

 Biswajit Deb, <https://orcid.org/0000-0001-8992-7600>;  Atri Deshamukhya, <https://orcid.org/0000-0003-4350-6645>

REFERENCES

- [1] A.G. Riess, A.V. Filippenko, P. Challis, A. Clocchiatti, A. Diercks, P.M. Garnavich, R.L. Gilliland, et al., "Observational evidence from supernovae for an accelerating universe and a cosmological constant," *The Astronomical Journal*, **116**, 1009 (1998). <https://doi.org/10.1086/300499>
- [2] S. Perlmutter, G. Aldering, G. Goldhaber, R. Knop, P. Nugent, P.G. Castro, S. Deustua, et al., "Measurements of Ω and Λ from 42 high-redshift supernovae," *The Astrophysical Journal*, **517**, 565 (1999). <https://doi.org/10.1086/307221>
- [3] E.J. Copeland, M. Sami, and S. Tsujikawa, "Dynamics of dark energy," *International Journal of Modern Physics D*, **15**, 1753 (2006). <https://doi.org/10.1142/S021827180600942X>
- [4] N. Aghanim, Y. Akrami, M. Ashdown, J. Aumont, C. Baccigalupi, M. Ballardini, A. Banday, et al., "Planck 2018 results-vi. cosmological parameters," *Astronomy and Astrophysics* **641**, A6 (2020). <https://doi.org/10.1051/0004-6361/201833910>
- [5] S. Weinberg, "The cosmological constant problem," *Reviews of modern physics*, **61**, 1 (1989). <https://doi.org/10.1103/RevModPhys.61.1>
- [6] A.A. Starobinsky, "Dynamics of phase transition in the new inflationary universe scenario and generation of perturbations," *Physics Letters B*, **117**, 175-178 (1982). [https://doi.org/10.1016/0370-2693\(82\)90541-X](https://doi.org/10.1016/0370-2693(82)90541-X)
- [7] S. Nojiri, and S.D. Odintsov, "Modified gauss-bonnet theory as gravitational alternative for dark energy," *Physics Letters B*, **631**, 1-6 (2005). <https://doi.org/10.1016/j.physletb.2005.10.010>
- [8] S. Nojiri, and S.D. Odintsov, "Modified gravity and its reconstruction from the universe expansion history," *Journal of Physics: Conference Series*, **66**, 012005 (2007). <https://doi.org/10.1088/1742-6596/66/1/012005>
- [9] M. Sharif, and A. Ikram, "Energy conditions in $f(G, T)$ gravity," *The European Physical Journal C*, **76**, 640 (2016). <https://doi.org/10.1140/epjc/s10052-016-4502-1>
- [10] T. Harko, F.S. Lobo, S. Nojiri, and S.D. Odintsov, " $f(R, T)$ gravity," *Physical Review D*, **84**, 024020 (2011). <https://doi.org/10.1103/PhysRevD.84.024020>
- [11] J.B. Jimenez, L. Heisenberg, and T. Koivisto, "Coincident general relativity," *Physical Review D*, **98**, 044048 (2018). <https://doi.org/10.1103/PhysRevD.98.044048>
- [12] Y. Xu, G. Li, T. Harko, and S.-D. Liang, "f (q,t) gravity," *The European Physical Journal C*, **79**, 708 (2019). <https://doi.org/10.1140/epjc/s10052-019-7207-4>
- [13] S. Nojiri, S. Odintsov, and V. Oikonomou, "Modified gravity theories on a nutshell: inflation, bounce and late-time evolution," *Physics Reports*, **692**, 1-104 (2017). <https://doi.org/10.1016/j.physrep.2017.06.001>
- [14] S. Bhattacharjee, J. Santos, P. Moraes, and P. Sahoo, "Inflation in $f(R, T)$ gravity," *The European Physical Journal Plus*, **135**, 576 (2020). <https://doi.org/10.1140/epjp/s13360-020-00583-6>
- [15] M. Gamonal, "Slow-roll inflation in $f(R, T)$ gravity and a modified Starobinsky-like inflationary model," *Physics of the Dark Universe*, **31**, 100768 (2021). <https://doi.org/10.1016/j.dark.2020.100768>
- [16] B. Deb, and A. Deshamukhya, "Inflation in $f(R, T)$ gravity with double-well potential," *International Journal of Modern Physics A*, **37**, 2250127 (2022). <https://doi.org/10.1142/S0217751X22501275>
- [17] C.-Y. Chen, Y. Reymuaji, and X. Zhang, "Slow-roll inflation in $f(R, T)$ gravity with a RT mixing term," *Physics of the Dark Universe*, **38**, 101130 (2022). <https://doi.org/10.1016/j.dark.2022.101130>
- [18] S. Bhattacharjee, and P. Sahoo, "Constraining $f(R, T)$ gravity from the dark energy density parameter Ω_Λ ," *Gravitation and Cosmology*, **26**, 281-284 (2020). <https://doi.org/10.1134/S0202289320030032>

- [19] M. Houndjo, and O.F. Piattella, "Reconstructing $f(R, T)$ gravity from holographic dark energy," International Journal of Modern Physics D, **21**, 1250024 (2012). <https://doi.org/10.1142/S0218271812500241>
- [20] A. Pasqua, S. Chattopadhyay, and I. Khomenko, "A reconstruction of modified holographic ricci dark energy in $f(R, T)$ gravity," Canadian Journal of Physics, **91**, 632 (2013). <https://doi.org/10.1139/cjpp-2013-0016>
- [21] J. Singh, and N. Sharma, "Bianchi type-ii dark energy model in $f(R, T)$ gravity," International Journal of Theoretical Physics, **53**, 1424-1433 (2014). <https://doi.org/10.1007/s10773-013-1939-y>
- [22] D. Reddy, R.S. Kumar, and T.P. Kumar, "Bianchi type-III dark energy model in $f(R, T)$ gravity," International Journal of Theoretical Physics, **52**, 239-245 (2013). <https://doi.org/10.1007/s10773-012-1325-1>
- [23] R. Zaregonbadi, M. Farhoudi, and N. Riazi, "Dark matter from $f(R, T)$ gravity," Physical Review D, **94**, 084052 (2016). <https://doi.org/10.1103/PhysRevD.94.084052>
- [24] N. Godani, and G.C. Samanta, "Wormhole modeling in $f(R, T)$ gravity with minimally-coupled massless scalar field," International Journal of Modern Physics A, **35**, 2050186 (2020). <https://doi.org/10.1142/S0217751X20501869>
- [25] A.K.M. Shweta, and U.K. Sharma, "Traversable wormhole modelling with exponential and hyperbolic shape functions in I framework," International Journal of Modern Physics A, **35**(25), 2050149 (2020). <https://doi.org/10.1142/S0217751X20501493>
- [26] E. Elizalde, and M. Khurshudyan, "Wormholes with $\rho(R, R')$ matter in $f(R, T)$ gravity," Physical Review D, **99**, 024051 (2019). <https://doi.org/10.1103/PhysRevD.99.024051>
- [27] P. Moraes, W. De Paula, and R. Correa, "Charged wormholes in $f(R, T)$ -extended theory of gravity," International Journal of Modern Physics D, **28**, 1950098 (2019). <https://doi.org/10.1142/S0218271819500986>
- [28] E. Elizalde, and M. Khurshudyan, "Wormhole formation in $f(R, T)$ gravity: Varying Chaplygin gas and barotropic fluid," Physical Review D, **98**, 123525 (2018). <https://doi.org/10.1103/PhysRevD.98.123525>
- [29] P. Moraes, and P. Sahoo, "Nonexotic matter wormholes in a trace of the energy-momentum tensor squared gravity," Physical Review D, **97**, 024007 (2018). <https://doi.org/10.1103/PhysRevD.97.024007>
- [30] Z. Yousaf, "Construction of charged cylindrical gravastarlike structures," Physics of the Dark Universe, **28**, 100509 (2020). <https://doi.org/10.1016/j.dark.2020.100509>
- [31] S. dos Santos, G. Carvalho, P. Moraes, C. Lenzi, and M. Malheiro, "A conservative energy-momentum tensor in the $f(R, T)$ gravity and its implications for the phenomenology of neutron stars," The European Physical Journal Plus, **134**, 398 (2019). <https://doi.org/10.1140/epjp/i2019-12830-8>
- [32] P. Moraes, J.D. Arbanil, and M. Malheiro, "Stellar equilibrium configurations of compact stars in $f(R, T)$ theory of gravity," Journal of Cosmology and Astroparticle Physics, **2016**, 005 (2016). <https://doi.org/10.1088/1475-7516/2016/06/005>
- [33] F. Rocha, G. Carvalho, D. Deb, and M. Malheiro, "Study of the charged super-chandrasekhar limiting mass white dwarfs in the $f(r, t)$ gravity," Physical Review D, **101**, 104008 (2020). <https://doi.org/10.1103/PhysRevD.101.104008>
- [34] M. Sharif and A. Siddiqua, "Propagation of polar gravitational waves in $f(R, T)$ scenario," General Relativity and Gravitation, **51**, 75 (2019). <https://doi.org/10.1007/s10714-019-2558-6>
- [35] M. Bhatti, Z. Yousaf, and M. Yousaf, "Stability of selfgravitating anisotropic fluids in $f(R, T)$ gravity," Physics of the Dark Universe, **28**, 100501 (2020). <https://doi.org/10.1016/j.dark.2020.100501>
- [36] V. Singh, and C. Singh, "Modified $f(R, T)$ gravity theory and scalar field cosmology," Astrophysics and Space Science, **356**, 153-162 (2015). <https://doi.org/10.1007/s10509-014-2183-5>
- [37] T.B. Gonçalves, J.L. Rosa, and F.S.N. Lobo, "Cosmology in scalar-tensor $f(R, T)$ gravity," Physical Review D, **105**, 064019 (2022). <https://doi.org/10.1103/PhysRevD.105.064019>
- [38] V. Rao, and D.P. Rao, "Five dimensional anisotropic dark energy model in $f(R, T)$ gravity," Astrophysics and Space Science, **357**, 65 (2015). <https://doi.org/10.1007/s10509-015-2256-0>
- [39] M.F. Shamir, "Exact solutions of bianchi type v spacetime in $f(R, T)$ gravity," International Journal of Theoretical Physics, **54**, 1304-1315 (2015). <https://doi.org/10.1007/s10773-014-2328-x>
- [40] P. Sahoo, S. Bhattacharjee, S. Tripathy, and P. Sahoo, "Bouncing scenario in $f(R, T)$ gravity," Modern Physics Letters A, **35**, 2050095 (2020). <https://doi.org/10.1142/S0217732320500959>
- [41] S. Bhattacharjee, and P. Sahoo, "Comprehensive analysis of a non-singular bounce in $f(R, T)$ gravitation," Physics of the Dark Universe, **28**, 100537 (2020). <https://doi.org/10.1016/j.dark.2020.100537>
- [42] S. Bhattacharjee, and P. Sahoo, "Big bang nucleosynthesis and entropy evolution in $f(R, T)$ gravity," The European Physical Journal Plus, **135**, 350 (2020). <https://doi.org/10.1140/epjp/s13360-020-00361-4>
- [43] P. Sahoo, and S. Bhattacharjee, "Gravitational baryogenesis in non-minimal coupled $f(R, T)$ gravity," International Journal of Theoretical Physics, **59**, 1451-1459 (2020). <https://doi.org/10.1007/s10773-020-04414-3>
- [44] J.L. Rosa, M.A. Marques, D. Bazeia, and F.S. Lobo, "Thick branes in the scalar-tensor representation of $f(R, T)$ gravity," The European Physical Journal C, **81**, 981 (2021). <https://doi.org/10.1140/epjc/s10052-021-09783-5>
- [45] J.L. Rosa, D. Bazeia, and A. Lobao, "Effects of cuscuton dynamics on braneworld configurations in the scalar-tensor representation of $f(r, t)$ gravity," The European Physical Journal C, **82**, 250 (2022). <https://doi.org/10.1140/epjc/s10052-022-10196-1>
- [46] F.G. Alvarenga, M.J.S. Houndjo, A.V. Monwanou, and J.B.C. Orou, "Testing some $f(R, T)$ gravity models from energy conditions," Journal of Modern Physics, **4**, 130 (2013). <http://dx.doi.org/10.4236/jmp.2013.41019>

- [47] M. Sharif, S. Rani, and R. Myrzakulov, "Analysis of $f(R, T)$ gravity models through energy conditions," *The European Physical Journal Plus*, **128**, 123 (2013). <https://doi.org/10.1140/epjp/i2013-13123-0>
- [48] M. Sharif, and M. Zubair, "Energy conditions constraints and stability of power law solutions in $f(R, T)$ gravity," *Journal of the Physical Society of Japan*, **82**, 014002 (2012). <https://doi.org/10.7566/JPSJ.82.014002>
- [49] P.K. Sahoo, S. Mandal, and S. Arora, "Energy conditions in non-minimally coupled $f(R, T)$ gravity," *Astronomische Nachrichten*, **342**, 89 (2021). <https://doi.org/10.1002/asna.202113886>
- [50] E. Elizalde, N. Godani, and G.C. Samanta, "Cosmological dynamics in R^2 gravity with logarithmic trace term," *Physics of the Dark Universe*, **30**, 100618 (2020). <https://doi.org/10.1016/j.dark.2020.100618>
- [51] D.C. Maurya, and L.K. Gaur, "Dark energy nature in logarithmic $f(R, T)$ cosmology," (2022). <https://arxiv.org/abs/2212.05605>
- [52] X. Zhang, C.-Y. Chen, and Y. Reymuaji, "Modified gravity models for inflation: In conformity with observations," *Physical Review D*, **105**, 043514 (2022). <https://doi.org/10.1103/PhysRevD.105.043514>
- [53] A.P. Jeakel, J. Silva, and H. Velten, "Revisiting $f(R, T)$ cosmologies," (2023). <https://arxiv.org/abs/2303.15208>
- [54] S.K. Srivastava, *General relativity and cosmology*, (PHI Learning Pvt. Ltd., 2008).
- [55] A. Einstein, "Kosmologische betrachtungen zur allgemeinen relativit"ats-theorie," in: *Das Relativit"atsprinzip*, (Springer, 1922) pp.130–139.
- [56] A. Friedmann, "Uber die krummung des raumes," *Z. Phys.* **10**, 377-386 (1922). <https://doi.org/10.1007/BF01332580>

ОБМЕЖУВАЛЬНА ЛОГАРИФМІЧНА МОДЕЛЬ $f(R, T)$ ІЗ ВИКОРИСТАННЯМ ПАРАМЕТРА ЩІЛЬНОСТІ ТЕМНОЇ ЕНЕРГІЇ Ω_Λ І ПАРАМЕТРА ХАББЛА H_0

Бісваджит Деб, Атрі Дешамукх'я

Факультет фізики, Ассамський університет, Сілчар, Індія

З багатьох розширених теорій гравітації гравітація $f(R, T)$ останнім часом викликала розумний інтерес, оскільки вона дає цікаві результати в космології. Логарифмічні поправки в модифікованих теоріях гравітації були широко вивчені. У цій роботі ми розглянули логарифмічну поправку до члена сліду T і прийняли функціональну форму як $f(R, T) = R + 16\pi G\alpha \ln T$, де α є вільним параметром. Вільний параметр обмежується за допомогою параметра щільності темної енергії Ω_Λ і параметра Хаббла H_0 . Нижня межа становить $\alpha \geq -9,85 \times 10^{-29}$. Також вивчаються космологічні наслідки.

Ключові слова: $f(R, T)$ гравітація, темна енергія

FIVE-DIMENSIONAL STRANGE QUARK BIANCHI TYPE-I COSMOLOGICAL MODEL IN THE FRAMEWORK OF SAEZ-BALLESTER THEORY OF GRAVITY

 Mahesh Netnaskar^{a,c},  Kalpana Pawar^b,  Abhishek Dabre^{c*}

^aBapumiya Sirajoddin Patel Arts, Commerce and Science College, Pimpalgaon Kale, Dist. Buldhana (M.S.), India

^bShri Shivaji Education Society Amravati's Science College, Nagpur (M.S.), India

^cShri R. R. Lahoti Science College, Morshi, Dist. Amravati (M.S.), India

*Corresponding Author E-mail: ankitdabre@live.com

Received May 1, 2024; revised June 12, 2024; accepted June 19, 2024

In this paper, we have constructed a five-dimensional Bianchi type I cosmological model with strange quark matter in the context of Saez-Ballester theory of gravitation. We have discussed a five-dimensional cosmological model by using the special rule of variation for the Hubble's parameter in the shape of $H = Da^{-1}$ and the equation of state for strange quark matter. Two different models for $n \neq 0$ and $n = 0$ has been discussed. Furthermore, the accelerated expansion of the universe has been discussed by using different physical parameters along with their graphical representations.

Keywords: Bianchi Type-I; Strange Quark Matter; Saez and Ballester Theory

PACS: 95.30.Sf, 04.50.-h, 11.10.Kk, 04.20.Jb, 02.90.+p, 98.80.Jk

1. INTRODUCTION

In recent years, analysis of diverse observational data has revealed that the universe is experiencing a rapid expansion. This phenomenon has sparked significant interest in formulating cosmological models within different gravitational theories. The general theory of relativity (GTR) offers a mathematically precise and physically robust explanation of gravity, serving as a foundation for developing cosmological models of the universe. But, describing the present state of the universe requires more than what is GTR explained. As a result, numerous efforts have been undertaken to modify Einstein's GTR, incorporating alternative and modified theories of gravitation. Hence, recently, researchers have shown significant interest in formulating cosmological models by employing alternative theories of gravitation such as Lyra Geometry, Brans Dicke Theory, Barber's first, second self-creation theory and Saez - Ballester theory [1-4].

Saez and Ballester [4] have formulated a theory in which the metric is interconnected with a dimensionless scalar field φ , and this coupling of φ provides a satisfactory explanation for weak fields. The scalar-tensor theory contributes to resolving issues within non-flat Friedmann-Robertson-Walker (FRW) cosmologies. Bali and Chandnani [5-6], studied the cosmological model of Bianchi type-I, considering a time-varying gauge function β to accommodate a perfect fluid distribution and string dust magnetized in the context of Lyra geometry.

Many authors have explored cosmological models using Saez and Ballester's scalar-tensor theory of gravitation. The Bianchi type- I, III, V, VI₀, and Kantowski-Sachs type models were examined within a scalar tensor theory by Singh and Agrawal [7]. Ram and Singh [8-9] have investigated a metric that exhibits spatially homogeneity, local rotational symmetry (LRS), and allows for a group of motions conforming to the Bianchi-I pattern on hypersurfaces with constant time t . Also, an investigation is conducted on a Robertson-Walker model of the universe that is both spatially homogeneous and isotropic, and possesses zero-curvature in the context of the Saez-Ballester scalar-tensor theory of gravity. Reddy [10] investigated Bianchi type-I metric together with cosmic string in a scalar – tensor theory of gravity. He observed that scalar field and the density are free from initial singularity and the universe is expanding with cosmic time. Mohanty and Sahu [11-12] have studied Bianchi type-VI₀ and Bianchi type-I cosmological models in the context of scalar- tensor theory of gravitation. Reddy, Subba Rao and Koteswara Rao [13] investigated exact solutions for a spatially homogeneous and LRS Bianchi type-I space time with negative constant deceleration parameters by employing special law of variations for Hubble parameter in the Saez-Ballester scalar tensor theory. Samanta *et al.* [14] discussed LRS Bianchi type-I cosmological models with bulk viscosity in the Saez-Ballester theory of gravitation and found that cosmic strings do not sustain when $\rho + \lambda = 0$, but they do sustain for Takabayasi and Geometric strings. Pawar and Agrawal [15] examined cosmological models with five dimensions within the Kaluza-Klein space-time in the framework Saez and Ballester theory of gravity. Mahurley *et al.* [16] focused on examination of cosmological models in scalar-tensor theory of gravitation. Specifically, the study explores spatially homogeneous anisotropic five-dimensional Bianchi type-I model with a perfect fluid.

Strange quark matter (SQM) in the influence of magnetic flux with five-dimensional Bianchi type-I cosmological model in Saez-Ballester theory has been considered. The SQM has been important and interesting topic in nuclear, astrophysics and cosmology due to its far-reaching theoretical significance and determine primitive magnetic fields. The

SQM is possibly produced by energetic heavy-ion collision experiments [17], or exists in cosmic rays and in the interior of compact stars. A magnetic field has strong effects on the properties and stability of SQM [18,19]. The surface of a pulsar may exhibit a characteristic strength approaching approximately 10^{12} Gauss. In comparison, certain magnets can possess even higher magnetic fields, reaching surface values as extensive as 10^{13} – 10^{15} Gauss. At present, our understanding of the genesis of these intense magnetic fields is lacking. The magneto hydrodynamic dynamo mechanism, in which a protoneutron star's revolving plasma creates a strong magnetic field, is a widely accepted theory. Many investigations have been carried out to explain the primordial magnetic field and quark-gluon matter in the early universe. In exploring the initial phase of the cosmos, examining the quark-gluon plasma proves to be a valuable approach. Following the Big Bang, the universe experienced a transition to quark-gluon plasma at the crucial temperature $T_c \equiv 100$ – 200 MeV, leading to the expulsion of quark matter (QM). Quark-gluon plasmas have many diverse implications for cosmology and astrophysics. The challenge in isolating a quark stems from the fact that quarks are never found in isolation; rather, they always exist in groups. There are mainly six types of quarks: charm (c), top (t), bottom (b), up (u), down (d) and strange (s) [20-23]. The suggestion that a theoretical concept known as strange quark matter (SQM) could exhibit complete stability at zero temperature and in β -equilibrium has sparked significant research and exploration.

The equation of state (EoS) of SQM is given by $p = \rho - 4B_c/3$, where B_c is Bag constant and the difference between the energy density of the perturbative and non-perturbative QCD vacuum and ρ , p are the energy density and thermodynamic pressure of the QM, respectively. Fundamentally, this is the EoS of a gas of massless particles with corrections due to the QCD trace glitch and perturbative interactions. At the surface of the star as $p \rightarrow 0$, we have $\rho \rightarrow 4B_c$. The characteristic value of the bag constant is of the order $B = 57\text{MeV}/\text{fm}^3 \approx 10^{15} \text{ g/cm}^3$. Several researchers have explored SQM with General relativity (GR), scalar tensor theory and other modified theories of gravity [24-28].

Motivated by the above discussion and work done by Pawar et al. [28], here we consider five-dimensional Bianchi type-I cosmological model with strange quark matter the framework of Saez-Ballester theory of gravity. The paper organized as follows: Section 2 contains field equations of Saez and Ballesters theory. Section 3 deals with metric and field equations. In section 4 we have obtained the solutions of field equations. Section 5 deals with the model for $n \neq 0$ with some physical and kinematical parameter of the model. Again, Section 6 deals with the model for $n = 0$ with some physical and kinematical parameter of the model. In Section 7 we have kept the graphical representation of dynamical parameters of Model-I and Model-II. Lastly, in section 8 is the discussion and conclusion are provided.

2. FIELD EQUATION OF SAEZ AND BALLESTER THEORY

The field equations given by Saez and Ballester (1985) for the combined scalar and tensor fields are

$$G_i^j - \omega \varphi^n \left(\varphi_{,i} \varphi^{,j} - \frac{1}{2} \delta_i^j \varphi_{,k} \varphi^{,k} \right) = -T_i^j. \quad (1)$$

The scalar field φ satisfies the equation

$$2\varphi^n \varphi^i_{,i} + n\varphi^{n-1} \varphi_{,k} \varphi^{,k} = 0, \quad (2)$$

where, $G_i^j = R_i^j - \frac{1}{2} R \delta_i^j$ is the Einstein's tensors, ω and n are constants, T_i^j is stress energy-momentum tensor, comma and semicolon represents partial and covariant differentiation respectively.

The energy-momentum tensor for Strange Quark Matter is given by

$$T_i^j = (\rho + p + h^2) u^j u_i + \left(\frac{h^2}{2} - p \right) \delta_i^j - h_i h^j, \quad (3)$$

where, ρ is the density, p is the pressure, h^2 is the magnetic flux. The magnetic flux is considered in the x -direction with $h_i u^i = 0$. The four velocity vectors are given by $u^i = (0, 0, 0, 0, 1)$ with $u_i u^i = 1$.

3. THE METRIC AND FIELD EQUATIONS

The homogeneous five-dimensional Bianchi type-I metric is given as

$$ds^2 = -dt^2 + A^2 dx^2 + B^2 (dy^2 + dz^2) + C^2 dm^2, \quad (4)$$

where, A , B , and C are functions of cosmic time t only.

From equation (1) - (3) for the equation (4) we have obtained,

$$\frac{2\dot{A}\dot{B}}{AB} + \frac{2\dot{B}\dot{C}}{BC} + \frac{\dot{A}\dot{C}}{AC} + \frac{\dot{B}^2}{B} + \frac{\omega}{2} \varphi^n \dot{\varphi}^2 = - \left(\rho + \frac{3h^2}{2} \right), \quad (5)$$

$$\frac{2\ddot{B}}{B} + \frac{\ddot{C}}{C} + \frac{2\dot{B}\dot{C}}{BC} + \frac{B^2}{B} - \frac{\omega}{2}\dot{\varphi}^2 = \left(p - \frac{h^2}{2}\right), \quad (6)$$

$$\frac{\ddot{A}}{A} + \frac{\ddot{B}}{B} + \frac{\ddot{C}}{C} + \frac{\dot{A}\dot{B}}{AB} + \frac{\dot{B}\dot{C}}{BC} + \frac{\dot{A}\dot{C}}{AC} - \frac{\omega}{2}\dot{\varphi}^2 = \left(p - \frac{h^2}{2}\right), \quad (7)$$

$$\frac{\ddot{A}}{A} + \frac{2\ddot{B}}{B} + \frac{2\dot{A}\dot{B}}{AB} + \frac{B^2}{B} - \frac{\omega}{2}\dot{\varphi}^2 = \left(p - \frac{h^2}{2}\right), \quad (8)$$

$$\ddot{\varphi} + \dot{\varphi} \left(\frac{\dot{A}}{A} + \frac{2\dot{B}}{B} + \frac{\dot{C}}{C} \right) + \frac{n}{2} \frac{\dot{\varphi}^2}{\varphi} = 0. \quad (9)$$

The contracted covariant derivative of energy-momentum tensor vanishes. i. e. from the energy conservation equation we get

$$T_{,j}^j = 0, \quad (10)$$

which yield to

$$\dot{\rho} + (\rho + p + 2h^2) \left(\frac{\dot{A}}{A} + \frac{2\dot{B}}{B} + \frac{\dot{C}}{C} \right) = 0. \quad (11)$$

4. SOLUTIONS OF THE FIELD EQUATIONS

Einstein's field equations (5) - (9) are system of highly non-linear differential equations which contains five independent equations containing seven unknowns $A, B, C, p, \rho, \varphi$ and h^2 . To obtain the solution of system of equations we have to consider two additional conditions. Initially, we examine the variation law for the generalized Hubble's parameter in space-time (4), as provided by Berman (1983). This law yields a constant deceleration parameter. Cosmological models with a constant deceleration parameter have been examined by numerous authors. Kumar and Singh [29] have investigated Bianchi type-I models in general relativity, where a constant deceleration parameter was maintained. This was achieved by employing a specific law for the variation of Hubble's parameter, resulting in constant value of deceleration parameter.

The special law of variation for the Hubble's parameter given by Berman (1983) is expressed as

$$H = Da^{-n} = D(AB^2C)^{\frac{n}{4}}, \quad (12)$$

where, $D > 0$ and $n \geq 0$ are constants.

On solving equation (12), we get

$$a = (AB^2C)^{\frac{1}{4}}. \quad (13)$$

The dynamical parameters for metric (4) are given as follows:

The spatial volume is defined as

$$V = a^4 = (AB^2C), \quad (14)$$

The mean Hubble's parameter is given by

$$H = \frac{\dot{a}}{a} = \frac{1}{4} \left(\frac{\dot{A}}{A} + 2\frac{\dot{B}}{B} + \frac{\dot{C}}{C} \right), \quad (15)$$

The Expansion Scalar θ is obtained by

$$\theta = 4H, \quad (16)$$

The mean Anisotropy Parameter A_m is given by

$$A_m = \frac{1}{4} \sum_{i=1}^4 \left(\frac{H_i}{H} - 1 \right)^2, \quad (17)$$

The Shear Scalar is

$$\sigma^2 = \frac{3}{2} A_m H^2, \tag{18}$$

The deceleration parameter (q) is defined to be

$$q = -\frac{a\ddot{a}}{\dot{a}^2}, \tag{19}$$

Solving equation (15), we get

$$a = (nDt + c_1)^{\frac{1}{4}}, \quad n \neq 0, \tag{20}$$

$$a = c_2 e^{Dt}, \quad n = 0, \tag{21}$$

where, c_1 & c_2 are integrating constants.

From equations (5) to (8), the metric potentials are obtained as follows,

$$A = a_1 a e^{b_1 \int a^{-4} dt}, \tag{22}$$

$$B = a_2 a e^{b_2 \int a^{-4} dt}, \tag{23}$$

$$C = a_3 a e^{b_3 \int a^{-4} dt}, \tag{24}$$

where,

$$a_1 = k_1^{\frac{1}{2}} k_2^{\frac{1}{4}}, \quad a_2 = k_1^{\frac{1}{4}} k_3^{\frac{1}{4}}, \quad a_3 = k_2^{\frac{1}{4}} k_3^{\frac{1}{2}} \quad \text{and} \quad b_1 = \frac{2d_1 + d_2}{4}, \quad b_2 = \frac{d_3 + d_1}{4}, \quad b_3 = \frac{-d_2 - 2d_3}{4}$$

which satisfy the relations

$$a_1 a_2^2 a_3 = 1, \quad b_1 + 2b_2 + b_3 = 0. \tag{25}$$

Equation (9) gives

$$\varphi(t) = \left[\frac{k_4(n+2)}{2} \int a^{-4} dt \right]^{\frac{2}{n+2}}, \tag{26}$$

here, k_4 is constant of integration.

5. MODEL I: when $n \neq 0$.

Using equation (20) in (22) - (24) and (26), we get the metric potentials and scalar field as follows:

$$A = a_1 (nDt + c_1)^{\frac{1}{n}} e^{b_1 \left[\frac{(nDt+c_1)^{\frac{n-4}{n}}}{D(n-4)} \right]}, \tag{27}$$

$$B = a_2 (nDt + c_1)^{\frac{1}{n}} e^{b_2 \left[\frac{(nDt+c_1)^{\frac{n-4}{n}}}{D(n-4)} \right]}, \tag{28}$$

$$C = a_3 (nDt + c_1)^{\frac{1}{n}} e^{b_3 \left[\frac{(nDt+c_1)^{\frac{n-4}{n}}}{D(n-4)} \right]}, \tag{29}$$

$$\varphi(t) = \left[\frac{k_4(n+2)}{2} \right]^{\frac{2}{n+2}} \left[nDt + c_1 \right]^{\frac{2(n-4)}{n(n+2)}}. \tag{30}$$

Equation (27) to (30) satisfy the equation of conservation of energy (11) and hence the metric in (4) can be expressed as

$$\begin{aligned}
 ds^2 = -dt^2 + & \left(a_1(nDt + c_1)^{\frac{1}{n}} e^{b_1 \left[\frac{(nDt + c_1)^{\frac{n-4}{n}}}{D(n-4)} \right]} \right)^2 dx^2 + \left(a_2(nDt + c_1)^{\frac{1}{n}} e^{b_2 \left[\frac{(nDt + c_1)^{\frac{n-4}{n}}}{D(n-4)} \right]} \right)^2 (dy^2 + dz^2) \\
 & + \left(a_3(nDt + c_1)^{\frac{1}{n}} e^{b_3 \left[\frac{(nDt + c_1)^{\frac{n-4}{n}}}{D(n-4)} \right]} \right)^2 dm^2.
 \end{aligned} \tag{31}$$

The EoS for SQM given by Pawar et al, [28] as

$$p = \frac{\rho - 4B_c}{3}, \tag{32}$$

where, p, ρ, B_c represents pressure, energy density and Bag constant respectively.

Using equation (27) - (30) in (5) and (8) with (32) we get, p, ρ, h^2 as

$$p = 2D^2[3n - 6] - D^2[2(nDt + c_1)^{-2}] - Q_1(nDt + c_1)^{-\frac{8}{n}} - \frac{4}{3}B_c, \tag{33}$$

$$\rho = 3D^2[(n - 2) + (nDt + c_1)^{-2}] - Q_2(nDt + c_1)^{-\frac{8}{n}} - \frac{4}{3}B_c, \tag{34}$$

$$h^2 = D^2[2(nDt + c_1)^{-2} - (3n - 6)] - Q_3(nDt + c_1)^{-\frac{8}{n}} + \frac{4}{3}B_c, \tag{35}$$

where,

$$Q_1 = 2b_1^2 + \frac{19}{3}b_2^2 + \frac{13}{3}b_1b_2 + \frac{2}{3}b_2b_3 + \frac{1}{3}b_1b_3 + \frac{1}{6}\omega k_4^2.$$

$$Q_2 = \frac{3}{2}b_1^2 + 6b_2^2 + \frac{11}{2}b_1b_2 + 3b_2b_3 + \frac{3}{2}b_1b_3 + \frac{3}{2}\omega k_4^2.$$

$$Q_3 = b_1^2 + \frac{10}{3}b_2^2 + \frac{7}{3}b_1b_2 + \frac{2}{3}b_2b_3 + \frac{1}{3}b_1b_3 + \frac{2}{3}\omega k_4^2.$$

The directional Hubble's parameters $H_i(i = 1, 2, 3, 4)$ in x, y, z and m direction are obtained as

$$H_i = D(nDt + c_1)^{-1} + b_i(nDt + c_1)^{-\frac{4}{n}}. \tag{36}$$

Using (15) we get,

$$H = D(nDt + c_1)^{-1}. \tag{37}$$

The Expansion Scalar θ using (16) is obtained as

$$\theta = 4D(nDt + c_1)^{-1}. \tag{38}$$

The mean Anisotropy parameter A_m given by (17) is

$$A_m = \frac{(nDt + c_1)^{\frac{2n-8}{n}}}{4D^2}. \tag{39}$$

Using (14), the spatial volume is given by

$$V = a^4 = (nDt + c_1)^{\frac{1}{n}}. \tag{40}$$

On solving (18), the Shear scalar is given by

$$\sigma^2 = \frac{3}{2}A_m H^2 = \frac{3}{8}(nDt + c_1)^{-\frac{8}{n}}(b_1^2 + 2b_2^2 + b_3^2). \tag{41}$$

From (19) and (20) we get,

$$q = (n - 1), \tag{42}$$

From the above findings, it is observed that the volume of the universe is zero at $t = -(c_1 / nD)$ and expansion scalar tends to infinity which indicates that the universe evolved with zero volume with infinite rate of expansion. As time t increases, the scale factors and spatial volume increases but expansion scalar decreases. Thus, the rate of expansion of universe slows down with increasing time. Also, as t tends to infinity the scalar field, pressure, density, magnetic flux, mean Hubble's Parameter, Shear scalar, mean anisotropic parameter tends to 0. Hence, the model initially shows an empty universe for large time t . Thus, the from equation (42) it is observed that the model representing accelerating expansion of the universe for non-zero values of $n < 1$ and shows decelerating nature for $n > 1$.

6. Model II: when $n = 0$

Using equation (21) in (22) - (24) and (26), we get the metric potentials and scalar field as follows:

$$A = a_1 c_2 e^{\left[\frac{Dt - \frac{b_1}{4Dc_2^4} e^{-4Dt}}{4Dc_2^4} \right]}, \tag{43}$$

$$B = a_2 c_2 e^{\left[\frac{Dt - \frac{b_2}{4Dc_2^4} e^{-4Dt}}{4Dc_2^4} \right]}, \tag{44}$$

$$C = a_3 c_2 e^{\left[\frac{Dt - \frac{b_3}{4Dc_2^4} e^{-4Dt}}{4Dc_2^4} \right]}, \tag{45}$$

$$\varphi(t) = \left[\frac{k_4(n+2)}{8Dc_2^4} \right]^{\frac{2}{n+2}} e^{\frac{-8Dt}{n+2}}. \tag{46}$$

Equation (43) - (46) satisfy the equation of conservation of energy (11) and hence, the metric in (4) can be expressed as

$$ds^2 = -dt^2 + \left(a_1 c_2 e^{\left[\frac{Dt - \frac{b_1}{4Dc_2^4} e^{-4Dt}}{4Dc_2^4} \right]} \right)^2 dx^2 + \left(a_2 c_2 e^{\left[\frac{Dt - \frac{b_2}{4Dc_2^4} e^{-4Dt}}{4Dc_2^4} \right]} \right)^2 (dy^2 + dz^2) + \left(a_3 c_2 e^{\left[\frac{Dt - \frac{b_3}{4Dc_2^4} e^{-4Dt}}{4Dc_2^4} \right]} \right)^2 dm^2. \tag{47}$$

Using equation (43) - (46) in (5) and (8) with (32) we get the values of p, ρ, h^2 as

$$p = 2D^2 + Q_1 c_2^{-8} e^{-8Dt} + \frac{2}{3} B_c, \tag{48}$$

$$\rho = -\frac{2}{3} D^2 + Q_2 c_2^{-8} e^{-8Dt} - \frac{8}{9} B_c, \tag{49}$$

$$h^2 = -8D^2 - Q_3 c_2^{-8} e^{-8Dt} + \frac{4}{3} B_c, \tag{50}$$

where,

$$Q_4 = \frac{b_1^2}{2} + \frac{4}{3} b_2^2 + \frac{2}{3} b_1 b_2 - \frac{1}{3} b_2 b_3 - \frac{1}{6} b_1 b_3 - \frac{5}{6} \omega k_4^2,$$

$$Q_5 = \frac{2}{3} b_1^2 + \frac{11}{9} b_2^2 - \frac{2}{9} b_1 b_2 - \frac{14}{9} b_2 b_3 - \frac{7}{9} b_1 b_3 + \frac{1}{18} \omega k_4^2,$$

$$Q_6 = b_1^2 + \frac{10}{3} b_2^2 + \frac{8}{3} b_1 b_2 + \frac{2}{3} b_2 b_3 + \frac{1}{3} b_1 b_3 - \frac{2}{3} \omega k_4^2.$$

The directional Hubble's parameters $H_i (i = 1, 2, 3, 4)$ in x, y, z and m direction are obtained as

$$H_i = D + b_i (c_2^{-4} e^{-4Dt}). \tag{51}$$

Using (15) the mean Hubble's parameter is given by

$$H = D. \tag{52}$$

Using (16), the Expansion scalar θ is obtained as

$$\theta = 4D. \tag{53}$$

Using (17), the anisotropy parameter A_m is given by

$$A_m = \frac{1}{4D^2}(b_1^2 + 2b_2^2 + b_3^2)c_2^{-8}e^{-4Dt}. \tag{54}$$

Using (14), the spatial volume is given by

$$V = a^4 = (c_2e^{Dt})^4. \tag{55}$$

Using (18), the shear scalar is given by

$$\sigma^2 = \frac{3}{2}A_mH^2 = \frac{3}{8}c_2^{-8}e^{-8Dt}(b_1^2 + 2b_2^2 + b_3^2). \tag{56}$$

Using (19) and (21), the deceleration parameter turns out to be

$$q = -1. \tag{57}$$

The spatial volume, scale factors, scalar field, pressure, density, magnetic flux, and other kinematical parameters are all constant at $t = 0$. Hence, the universe begins with a constant volume and expands exponentially. As t increases, the scale factors and spatial volume increases and scalar field, pressure, density, magnetic flux, and other kinematical parameters decrease. The expansion scalar and deceleration parameter are constant and hence the universe is expanding and accelerating for $n = 0$.

7. GRAPHICAL REPRESENTATION OF DYNAMICAL PARAMETERS FOR THE MODEL-I AND MODEL-II

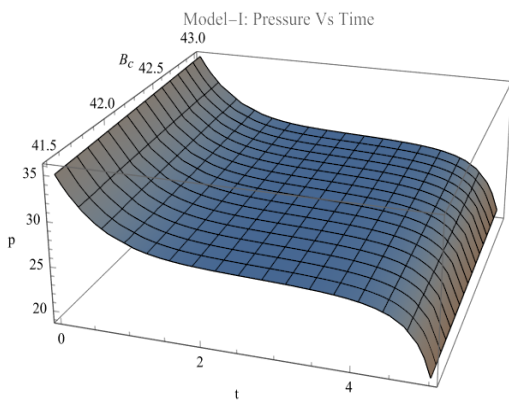


Figure 1. Pressure verses Time has been plotted by considering the values $D = 0.2, n = -0.9, c_1 = 1, Q_1 = -10$

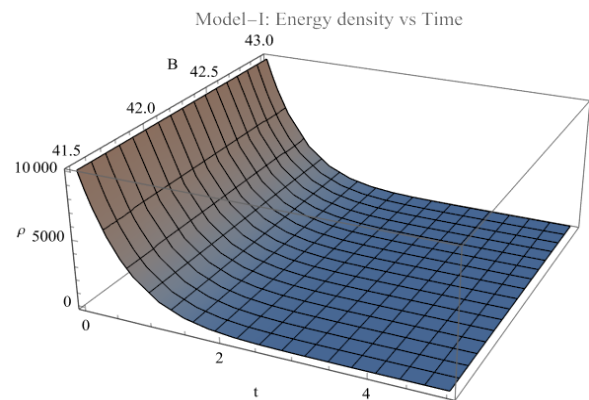


Figure 2. Energy density verses Time has been plotted by considering the values $D = 0.2, n = -0.9, c_1 = 1, Q_2 = -10 \times 10^3$

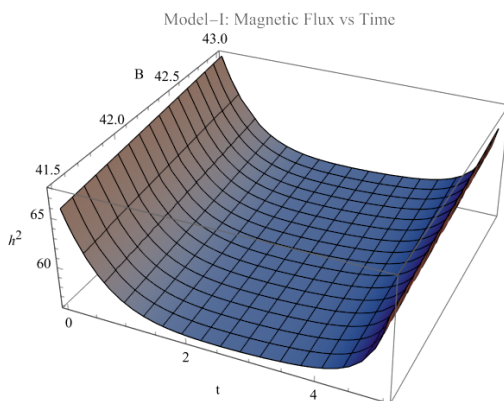


Figure 3. Magnetic flux verses Time has been plotted by considering the values $D = 0.2, n = -0.9, c_1 = 1, Q_3 = -10$

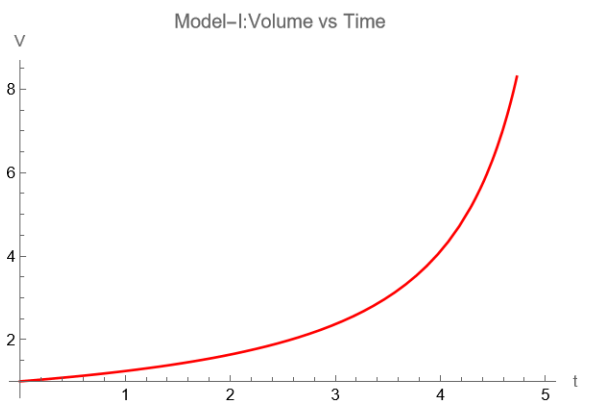


Figure 4. Volume verses time has been plotted by considering the values $D = 0.2, n = -0.9, c_1 = 1$

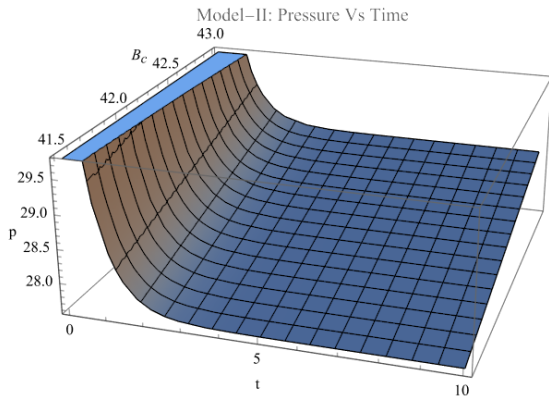


Figure 5. Pressure versus time has been plotted by considering the values $D = 0.2, n = -0.9, c_2 = -1, Q_4 = 5$

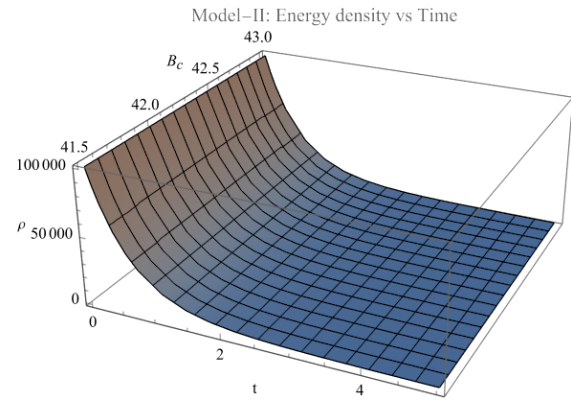


Figure 6. Energy density versus time has been plotted by considering the values $D = 0.2, n = -0.9, c_2 = -1, Q_5 = 10 \times 10^4$

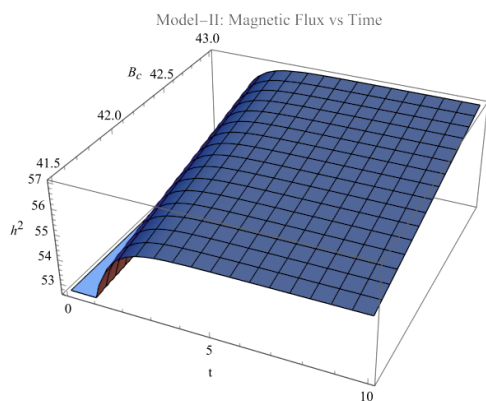


Figure 7. Magnetic flux versus time has been plotted by considering the values $D = 0.2, n = -0.9, c_2 = -1, Q_6 = -10$

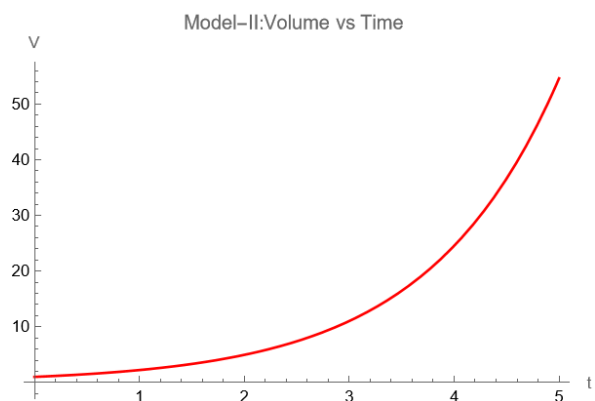


Figure 8. Volume versus time has been plotted by considering the values $D = 0.2, c_2 = -1,$

8. CONCLUSION

In this paper, we have investigated a five-dimensional model by considering five-dimensional Bianchi Type-I spacetime with strange quark matter in the framework of Saez and Ballester theory of gravity. By using special law of variation of Hubble's parameter, we have solved the field equations to obtain the values of metric potentials A, B and C . Here we have discussed two models, for $n \neq 0$ and for $n = 0$, by considering the equation of state for strange quark matter and obtained the physical parameters pressure p , density ρ , magnetic flux h^2 , mean Hubble's parameter H , expansion scalar θ , mean anisotropy parameter A_m , shear scalar σ^2 , spatial volume V and discussed their physical behavior in details. We have observed that for model-I ($n \neq 0$) as $t \rightarrow \infty$ the scale factors and volume of the universe became infinitely large, whereas the scalar field ϕ , mean anisotropy parameter, shear scalar tends to 0. For large value of time t , the model approaches to isotropy, the pressure, density, mean Hubble's parameter becomes constant. Thus, the constructed model resembles with the accelerating expansion of the universe.

In model-II ($n = 0$), we have obtained the deceleration parameter $q = -1$ which leads to $dH/dt = 0$. This gives the maximum value of the mean Hubble's parameter, which shows the fastest rate of accelerating expansion of the universe. Thus, the graphical results of the obtained models are in good agreement with the observational data.

Acknowledgement

The authors would like to convey their deepest appreciation to the Editor and anonymous Referees for their valuable comments and suggestions.

ORCID

Mahesh Netnaskar, <https://orcid.org/0000-0002-7405-9430>;
 Kalpana Pawar, <https://orcid.org/0000-0002-4388-039X>
 Abhishek Dabre, <https://orcid.org/0000-0002-6811-582X>

REFERENCES

- [1] G. Lyra, "Über eine Modifikation der Riemannschen Geometrie," *Mathematische Zeitschrift*, **54**(1), 52-64 (1951). <https://doi.org/10.1007/BF01175135>
- [2] C. Brans, and R.H. Dicke, "Mach's Principle and a Relativistic Theory of Gravitation," *Physical Review*, **124**(3), (1951). http://www.weylmann.com/brans_dicke.pdf

- [3] G.A. Barber, "On Two Self-Creation Cosmology," *General Relativity and Gravitation*, **14**, 117-136 (1982). <http://dx.doi.org/10.1007/s10509-007-9387-x>
- [4] D. Saez, and V.J. Ballester, "A simple coupling with cosmological implications," *Physics Letters A*, **113**(9), (1986). [https://doi.org/10.1016/0375-9601\(86\)90121-0](https://doi.org/10.1016/0375-9601(86)90121-0)
- [5] R. Bali, and N.K. Chandnani, "Bianchi type-I cosmological model for perfect fluid distribution in Lyra geometry," *Journal of Mathematical Physics*, **49**(3). 032502 (2008). <https://doi.org/10.1063/1.2898477>
- [6] R. Bali, N.K. Chandnani, and L.K. Gupta, "Bianchi type I string dust magnetized cosmological models in Lyra geometry," *Communications in Theoretical Physics*, **54**(1), 197 (2010). <https://doi.org/10.1088/0253-6102/54/1/36>
- [7] T. Singh, and A.K. Agrawal, "Some Bianchi-type cosmological models in a new scalar- tensor theory," *Astrophys. Space Sci.* **182**, 289–312 (1991). <https://doi.org/10.1007/BF00645008>
- [8] S. Ram, and J.K. Singh, "Cosmological models in certain scalar-tensor theories," *Astrophys. Space Sci.* **234**, 325–334 (1995). <https://doi.org/10.1007/BF00627675>
- [9] C.P. Singh, and S. Ram, "Unified Description of Early Universe in Scalar-Tensor Theory," *Astrophysics and Space Science*, **284**, 1199-1206 (2003). <https://doi.org/10.1023/A:1023637627922>
- [10] D. Reddy, "A string cosmological model in a scalar – Tensor theory of gravitation," *Astrophysics and Space Science*, **286**, 359-363 (2003). <https://doi.org/10.1023/A:1026370732619>
- [11] G. Mohanty, and S.K. Sahu, "Bianchi VI0 cosmological model in Saez and Ballester theory," *Astrophysics and Space Science*, **288**(4), 509-516 (2003). <https://doi.org/10.1023/B:ASTR.0000005124.75571.11>
- [12] G. Mohanty, and S.K. Sahu, "Bianchi type-I cosmological effective stiff fluid model in Saez and Ballester theory," *Astrophysics and Space Science*, **291**, 75–83 (2004). <https://doi.org/10.1023/B:ASTR.0000029962.07483.40>
- [13] D.R.K. Reddy, M.V. Subba Rao, and G.A. Koteswara Rao, "Cosmological Model with Negative Constant Deceleration Parameter in a Scalar-Tensor Theory," *Astrophys. Space Sci.* **306**, 171–174 (2006). <https://doi.org/10.1007/s10509-006-9210-0>
- [14] G.C. Samanta, S.K. Biswal, and P.K. Sahoo, "Five-Dimensional Bulk Viscous String Cosmological Models in Saez and Ballester Theory of Gravitation," *Int. J. Theor. Phys.* **52**, 1504–1514 (2013). <https://doi.org/10.1007/s10773-012-1470-6>
- [15] K. Pawar, and R. Agrawal, "Five-Dimensional Kaluza-Klein Space-time in the framework of Saez Ballester," *IJSR*, **3**(7), 1509-1512 (2014). <https://www.ijrsr.net/getabstract.php?paperid=20141023>
- [16] I.S. Mohurley, D.H. Gahane, R.K. Jumale, and J.K. Jumale, "Five-Dimensional Exact Bianchi Type-I Cosmological Models in a Scalar-Tensor Theory," *Prespacetime Journal*, **7**(8), 1165-1175 (2016). <https://prespacetime.com/index.php/pst/article/download/1012/999>
- [17] U. Heinz, "The Little bang: Searching for quark gluon matter in relativistic heavy ion collisions," *Nucl. Phys. A*, **685**, 414 (2001). [https://doi.org/10.1016/S0375-9474\(01\)00558-9](https://doi.org/10.1016/S0375-9474(01)00558-9)
- [18] C. Alcock, E. Farhi, and A. Olinto, "Strange Stars," *Astrophys. J.* **310**, 261 (1986). <https://doi.org/10.1086/164679>
- [19] J. Madsen, "Physics and astrophysics of strange quark matter," in: *Lecture Notes in Physics*, vol. 516, (Springer, Berlin, Heidelberg, 1999), pp. 162–203. <https://doi.org/10.1007/BFb0107314>
- [20] B. Paczynski, "GB 790305 as a Very Strongly Magnetized Neutron Star," *Acta Astronomica*, **42**, 145-153 (1992). https://acta.astrouw.edu.pl/Vol42/n3/pap_42_3_1.pdf
- [21] C. Thompson, and R.C. Duncan, "Formation of Very Strongly Magnetized Neutron Stars: Implications for Gamma-Ray Bursts," *Astrophysical Journal Letters*, **392**, L9 (1992). <https://doi.org/10.1086/186413>
- [22] C. Kouveliotou, *et al.*, "An X-ray pulsar with a superstrong magnetic field in the soft γ -ray repeater SGR1806–20," *Nature*, **393**(6682), 235-237 (1998). <https://doi.org/10.1038/30410>
- [23] R. Nagpal, J.K. Singh, and S. Aygün, "FLRW cosmological models with quark and strange quark matters in $f(R,T)$ gravity," *Astrophys. Space Sci.* **363**, 114 (2018). <https://doi.org/10.1007/s10509-018-3335-9>
- [24] C. Aktaş, and S. Aygün, "Magnetized strange quark matter solutions in $f(R, T)$ gravity with cosmological constant," *Chin. J. Phys.* **55**(1), 71–78 (2017). <https://doi.org/10.1016/j.cjph.2016.12.003>
- [25] K.L. Mahanta, A.K. Biswal, and P.K. Sahoo, "Bulk viscous string cloud with strange quark matter in Brans-Dicke theory," *Eur. Phys. J. Plus*, **129**, 141 (2014). <https://doi.org/10.1140/epjp/i2014-14141-0>
- [26] P.K. Sahoo, P. Sahoo, B.K. Bishi, and S. Aygün, "Magnetized strange quark model with Big Rip singularity in $f(R,T)$ gravity," *Mod. Phys. Lett. A*, **32**, 1750105 (2017). <https://doi.org/10.1142/S021773231750105X>
- [27] G.S. Khadekar, and R.D. Shelote, "Higher Dimensional Cosmological Model with Quark and Strange Quark Matter," *International Journal of Theoretical Physics*, **51**, 1442-1447 (2011). <https://doi.org/10.1007/s10773-011-1020-7>
- [28] D.D. Pawar, B.L. Jakore, and V.J. Dagwal, "Kaluza-Klein cosmological model with strange-quark-matter in Lyra geometry," *Int. J. Geom. Meth. Mod. Phys.* **20**(05), 2350079 (2023). <https://doi.org/10.1142/S0219887823500792>
- [29] S. Kumar, and C.P. Singh, "Exact Bianchi Type-I Cosmological Models in a Scalar-Tensor Theory," *International Journal of Theoretical Physics*, **47**, 1722-1730 (2008). <https://doi.org/10.1007/s10773-007-9614-9>

П'ЯТИВИМІРНА КОСМОЛОГІЧНА МОДЕЛЬ Б'ЯНЧІ ТИПУ І З ДИВНОЮ КВАРКОВОЮ МАТЕРІЄЮ В РАМКАХ ТЕОРІЇ ГРАВІТАЦІЇ САЕЗА-БАЛЛЕСТЕРА

Махеш Негнаскар^{a,c}, Калпана Павар^b, Абхішек Дабре^c

^aКоледж мистецтв, комерції та науки Бапумія Сіражоддін Пател, Пімпагаон Кале, округ Булдохана (М. С.), Індія

^bНауковий коледж Амраваті Освітнього товариства Шрі Шіваджі, Нагпур (Міссічі), Індія

^cШрі Р.Р. Лахоті науковий коледж, Морші, округ Амраваті (М. С.), Індія

У цій статті ми побудували п'ятивимірну космологічну модель Б'янкі типу І з дивною кварковою матерією в контексті теорії гравітації Саез-Баллестера. Ми обговорили п'ятивимірну космологічну модель за допомогою спеціального правила варіації для параметра Хаббла у формі $H = Da^{-1}$ та рівнянні стану дивної кваркової матерії. Обговорювалися дві різні моделі для $n \neq 0$ і $n = 0$. Крім того, прискорене розширення Всесвіту обговорювалося з використанням різних фізичних параметрів разом із їх графічним зображенням.

Ключові слова: *Bianchi Type-I; дивна кваркова матерія; теорія Саеза-Баллестера*

LRS BIANCHI COSMOLOGICAL MODEL IN SÁEZ-BALLESTER THEORY OF GRAVITY WITH TIME VARYING COSMOLOGICAL CONSTANT

Chandra Rekha Mahanta, Anindita Basumatary

Department of Mathematics, Gauhati University, Guwahati -781014, India

*Corresponding Author e-mail: anibasus3@gmail.com

Received June 30, 2024; revised July 26, 2024; accepted August 12, 2024

The present work deals with the study of a locally rotationally symmetric (LRS) Bianchi type-I cosmological model in the framework of a scalar-tensor theory of gravity formulated by Sáez and Ballester with time varying cosmological constant. To obtain the explicit solutions of the Sáez-Ballester field equations we assume the average scale factor to obey a power law expansion and the cosmological constant to be proportional to the energy density of the cosmic fluid. The dynamical behaviour of relevant cosmological parameters including the Hubble parameter, the deceleration parameter, the energy density, the pressure, the equation of state parameter, the cosmological constant, the shear scalar, the expansion scalar etc. are investigated graphically by examining their evolution versus the redshift parameter. The validation of the four energy conditions are also checked. We find the outcomes of the constructed model to be in good agreement with the recent observational data.

Keywords: Cosmological constant; Deceleration parameter; Hubble parameter; LRS Bianchi type-I; Sáez-Ballester theory

PACS: 04.20.Jb, 04.50.Kd, 98.80.-k, 98.80.Jk

1. INTRODUCTION

Throughout the last few decades, a number of observations in the field of cosmology and astrophysics have been indicating that our universe is currently passing through a phase of accelerated expansion. The list of the observations includes Supernova type Ia (SNIa), Large Scale Structure (LSS), Cosmic Microwave Background (CMB), Wilkinson Microwave Anisotropy Probe (WMAP) [1]- [10] etc. These observations have contradicted the earlier beliefs of the cosmologists that the expansion of the universe would be decelerating due to the gravitationally attractive nature of the matter in the universe. As a result of the contradiction in the belief, cosmologists become more inquisitive to know the root cause of the accelerated cosmic expansion. Within the framework of General Relativity, the leading cause behind the late time acceleration in the expansion of the universe is considered to be a mysterious form of energy with anti-gravity effect and tremendous negative pressure. This exotic form of energy is named dark energy which consists of nearly 68.3% of the total energy budget of the present universe. Another exotic component of the universe is the dark matter which takes approximately 26.8% of the total matter-energy content of the universe. The yet unknown nature of these two exotic components consisting of more than 95% of the universe raises some fundamental questions which can not be explained from the General Theory of Relativity although this theory is very successful in describing many gravitational phenomena up to cosmological scales. In order to ascertain the true nature of dark energy and the root cause of the observed cosmic acceleration, a variety of theoretical models are proposed in the literature which can be classified into two broad categories - the dark energy models and the modified gravity models. The dark energy models are constructed by modifying the matter part of the Einstein-Hilbert action. On the other hand, the modified gravity models are constructed by modifying the gravitational part of the Einstein-Hilbert action.

Among the several dark energy models, Λ CDM model is the simplest and the best fit model of the universe but it is plagued with some theoretical challenges such as the fine-tuning and cosmic coincidence problems. To overcome these problems, different dynamical scalar field models such as quintessence, k-essence, phantom, tachyons etc. [11], Chaplygin gas models [12], Holographic dark energy models [13]- [17] etc. are proposed in the literature. Several modified gravity models are also proposed in the literature such as the $f(R)$ gravity, $f(G)$ gravity, $f(Q)$ gravity, $f(R, T)$ gravity, $f(R, G)$ gravity, $f(Q, T)$ gravity etc., where R is the Ricci scalar curvature, G is the Gauss-Bonnet invariant, Q is the non-metricity scalar, T is the trace of the energy-momentum tensor and some scalar-tensor theories of gravity such as Brans-Dicke theory [18], Sáez-Ballester theory [19] etc. in order to unfold the mystery behind the late time acceleration in the cosmic expansion as well as to study various other aspects of the universe. The Sáez-Ballester theory of gravity was formulated by Sáez and Ballester in 1986. This theory is a scalar-tensor theory in which the metric is coupled with a dimensionless scalar field ϕ in a simple manner. The coupling satisfactorily describes the weak fields and also provides a possible way of removing the missing matter problem in non-flat Friedmann-Lemaître-Robertson-Walker cosmologies. After the discovery of the acceleration in the rate of expansion of the universe, many researchers have constructed different cosmological models in Sáez-Ballester theory and investigated various aspects of the universe as it can be shown that there exists an antigravity regime in this theory. Rao *et al.* [20] presented exact string cosmological

models for Bianchi type II, VIII and IX. Rao *et al.* [21] also discussed the exact Bianchi type II, VIII and IX perfect fluid cosmological models. Naidu *et al.* [22] investigated a Bianchi type-III universe in the presence of anisotropic dark energy. Mishra and Chand [23] studied the dynamical nature of Bianchi type-I model considering a bilinearly varying deceleration parameter. Mishra and Dua [24] investigated a Bianchi type-I model with cosmological constant, considering the deceleration parameter to be a linear function of the Hubble parameter. They have also studied the statefinder diagnostic and some cosmographic parameters graphically. Naidu *et al.* [25] investigated the dynamical behaviour of FRW type Kaluza-Klein (KK) cosmological model taking the Planck Collaboration data as a special reference and discussed three different models by using hybrid expansion law and varying deceleration parameters. Singh, *et al.* [26] examined a FRW model with bulk viscous fluid. Mishra and Dua [27] examined the behaviours of bulk viscous string cosmological models in the tilted Bianchi type-VI₀ universe. Wath and Nimkar [28] studied a Bianchi type VIII anisotropic dark matter fluid cosmological model. Dabgar and Bhabor [29] investigated a five-dimensional Bianchi type-III model with string cosmology considering both power law and exponential law models.

In the present work, we also consider the Sáez-Ballester theory of gravity and study the cosmological dynamics of a locally rotationally symmetric Bianchi type-I universe with a time varying cosmological constant Λ . The paper is organised as follows: In section 2, we derive the Sáez-Ballester field equations corresponding to a locally rotationally symmetric Bianchi type-I line-element. In section 3, we obtain cosmological solution of Sáez-Ballester field equations by considering the cosmological constant Λ to be proportional to the energy density ρ , and by using a power law expansion for the average scale factor. In section 4, we express the relevant cosmological parameters in terms of the redshift parameter and study their physical behaviour as the universe evolves. In section 5, the validity of the energy conditions are checked. The paper is concluded in section 6 with a brief summary of the main outcomes of our model.

2. BASIC EQUATIONS GOVERNING THE MODEL

The action for the Sáez-Ballester theory of gravity along with time-varying cosmological constant Λ can be expressed as

$$S = \int_{\Sigma} \left[(R - 2\Lambda) + 16\pi\mathcal{L} - W\phi^n\phi_{,i}\phi^{,i} \right] \sqrt{-g} dX^1 dX^2 dX^3 dX^4 \quad (1)$$

where, R is the Ricci scalar curvature, \mathcal{L} is the matter Lagrangian, W and n are arbitrary dimensionless constants, ϕ is a dimensionless scalar field, $\phi_{,i}$ is the partial derivative of ϕ with respect to the coordinate X^i , $\phi^{,i}$ is the contraction $\phi_{,\alpha}g^{\alpha i}$ and $g = |g_{ij}|$.

By considering the scalar field ϕ to be vanishing at the boundary of the arbitrary region Σ of integration, the variation of the action (1) with respect to the tensor g^{ij} and the scalar field ϕ leads to the field equations

$$R_{ij} - \frac{R}{2}g_{ij} + \Lambda g_{ij} - W\phi^n \left(\phi_{,i}\phi_{,j} - \frac{1}{2}g_{ij}\phi_{,k}\phi^{,k} \right) = -8\pi T_{ij} \quad (2)$$

and

$$2\phi^n\phi^{,k}{}_{;k} + n\phi^n\phi_{,k}\phi^{,k} = 0 \quad (3)$$

where R_{ij} is the Ricci tensor, T_{ij} is the energy-momentum tensor and semicolon represents the covariant derivative.

Now, in order to construct a cosmological model, we consider a locally rotationally symmetric (LRS) Bianchi type-I space-time characterised by the metric

$$ds^2 = dt^2 - A^2 dx^2 - B^2 (dy^2 + dz^2) \quad (4)$$

where A and B are the functions of the cosmic time t .

We assume the matter-energy distribution of the universe to be as isotropic perfect fluid of density ρ and pressure p so that the energy-momentum tensor T_{ij} can be taken as

$$T_{ij} = (\rho + p)u_i u_j - p g_{ij} \quad (5)$$

where u^i is the four velocity with $u_i u^i = 1$.

In a comoving coordinate system, the field equations (2) and (3) with equations (5) for the metric (4) lead to the following set of field equations:

$$2\frac{\ddot{B}}{B} + \frac{\dot{B}^2}{B^2} - \frac{W}{2}\phi^n \dot{\phi}^2 - \Lambda = -8\pi p \quad (6)$$

$$\frac{\ddot{A}}{A} + \frac{\ddot{B}}{B} + \frac{\dot{A}\dot{B}}{AB} - \frac{W}{2}\phi^n \dot{\phi}^2 - \Lambda = -8\pi p \quad (7)$$

$$2 \frac{\dot{A} \dot{B}}{A B} + \frac{\dot{B}^2}{B^2} + \frac{W}{2} \phi^n \dot{\phi}^2 - \Lambda = 8\pi\rho \tag{8}$$

$$\frac{\ddot{\phi}}{\dot{\phi}} + \frac{\dot{A}}{A} + 2 \frac{\dot{B}}{B} + \frac{n \dot{\phi}}{2 \phi} = 0 \tag{9}$$

Integration of equation (9) yields

$$\phi = \left[E \left(\frac{n}{2} + 1 \right) \right]^{\frac{2}{n+2}}, \quad n \neq -2 \tag{10}$$

where $E(t) = \int \frac{k_1}{a^3} dt$, k_1 is a constant of integration.

From the equations (6) and (7), we have

$$\frac{\ddot{B}}{B} - \frac{\ddot{A}}{A} + \frac{\dot{B}}{B} \left(\frac{\dot{B}}{B} - \frac{\dot{A}}{A} \right) = 0 \tag{11}$$

On integration, it gives

$$\frac{B}{A} = D(t) \tag{12}$$

where $D(t) = e^{\int \frac{k_2}{a^3} dt}$, k_2 is an integrating constant.

Therefore, the average scale factor, $a(t)$ can be expressed as

$$a = \left(AB^2 \right)^{\frac{1}{3}} = AD^{\frac{2}{3}} \tag{13}$$

Equations (6)-(8) can be written in terms of the average scale factor a as

$$2 \frac{\ddot{a}}{a} + \frac{\dot{a}^2}{a^2} + \frac{k_2^2}{3a^6} - \frac{W k_1^2}{2 a^6} - \Lambda = -8\pi p \tag{14}$$

$$3 \frac{\dot{a}^2}{a^2} - \frac{k_2^2}{3a^6} + \frac{W k_1^2}{2 a^6} - \Lambda = 8\pi\rho \tag{15}$$

3. ASSUMPTIONS AND SOLUTION OF THE FIELD EQUATIONS

We have three equations and five unknowns a, Λ, p, ρ and ϕ , which allows us to take two conditions in consideration in order to find the exact solutions of the field equations.

We assume the average scale factor a to obey a power law expansion as

$$a = a_0 t^\alpha \tag{16}$$

where $\alpha > 0$, a_0 is a constant and represents the present value of a .

In view of equation (15), we consider the cosmological constant $\Lambda(t)$ to be proportional to the energy density $\rho(t)$ with h as the constant of proportionality as

$$\Lambda = h\rho \tag{17}$$

Then, from the equations (10) and (14)-(17) the expressions for ϕ, Λ, p and ρ are obtained as

$$\phi(t) = \left[\frac{k_1}{a_0^3} \left(\frac{n}{2} + 1 \right) \left(\frac{t^{1-3\alpha}}{1-3\alpha} \right) \right]^{\frac{2}{n+2}}, \quad n \neq -2 \tag{18}$$

$$\Lambda(t) = \frac{h}{8\pi + h} \left[\frac{3\alpha^2}{t^2} - \frac{k_2^2}{3(a_0 t^\alpha)^6} + \frac{W k_1^2}{2(a_0 t^\alpha)^6} \right] \tag{19}$$

$$p(t) = \frac{1}{8\pi} \left[\frac{2\alpha}{t^2} - \frac{2k_2^2}{3(a_0 t^\alpha)^6} + W \frac{k_1^2}{(a_0 t^\alpha)^6} \right] - \frac{1}{8\pi + h} \left[\frac{3\alpha^2}{t^2} - \frac{k_2^2}{3(a_0 t^\alpha)^6} + \frac{W k_1^2}{2(a_0 t^\alpha)^6} \right] \tag{20}$$

$$\rho(t) = \frac{1}{8\pi + h} \left[\frac{3\alpha^2}{t^2} - \frac{k_2^2}{3(a_0 t^\alpha)^6} + \frac{W k_1^2}{2(a_0 t^\alpha)^6} \right] \tag{21}$$

4. PROPERTIES OF THE MODEL

The Hubble parameter H measures the rate of expansion of the universe. It is related to the scale factor a by the relation $H = \frac{\dot{a}}{a}$ and therefore, $H > 0$ infers the expanding universe. The deceleration parameter q reveals whether the expansion of the universe is uniform, accelerating or decelerating. It is defined by the relation $q = -\frac{a\ddot{a}}{\dot{a}^2}$ and therefore, q is

related to the Hubble parameter H through the relation $q = -1 - \frac{\dot{H}}{H^2}$.
For our model, these two parameters are obtained as

$$H(t) = \frac{\dot{a}}{a} = \frac{\alpha}{t} \quad (22)$$

$$q(t) = -1 + \frac{1}{\alpha} \quad (23)$$

The spatial volume (V), the expansion scalar (θ), the shear scalar (σ^2), the mean anisotropy parameter (A_m) and the equation of state (EoS) parameter (η) are obtained as

$$V(t) = a^3 = (a_0 t^\alpha)^3 \quad (24)$$

$$\theta(t) = 3H = 3\frac{\alpha}{t} \quad (25)$$

$$\sigma^2(t) = \frac{1}{3} \frac{k_2^2}{(a_0 t^\alpha)^6} \quad (26)$$

$$A_m(t) = \frac{2}{9} \left(\frac{t}{\alpha}\right)^2 \frac{k_2^2}{(a_0 t^\alpha)^6} \quad (27)$$

$$\eta(t) = \frac{p(t)}{\rho(t)} = \frac{(8\pi + h) \left[\frac{2\alpha}{t^2} - \frac{2k_2^2}{3(a_0 t^\alpha)^6} + W \frac{k_1^2}{(a_0 t^\alpha)^6} \right]}{8\pi \left[\frac{3\alpha^2}{t^2} - \frac{k_2^2}{3(a_0 t^\alpha)^6} + \frac{W}{2} \frac{k_1^2}{(a_0 t^\alpha)^6} \right]} - 1 \quad (28)$$

The scale factor redshift relation is given by

$$a = \frac{a_0}{1+z} \quad (29)$$

Using equation (16), we obtain

$$t = (1+z)^{-\frac{1}{\alpha}} \quad (30)$$

Therefore, the cosmic time t dependent cosmological parameters of our model can be expressed in terms of the redshift z as
Hubble parameter,

$$H(z) = \alpha (1+z)^{\frac{1}{\alpha}} \quad (31)$$

Deceleration parameter,

$$q(z) = -1 + \frac{1}{\alpha} \quad (32)$$

Spatial volume,

$$V(z) = a^3 = a_0^3 (1+z)^{-3} \quad (33)$$

Expansion scalar,

$$\theta(z) = 3H = 3\alpha (1+z)^{\frac{1}{\alpha}} \quad (34)$$

Shear scalar,

$$\sigma^2(z) = \frac{1}{3} \frac{k_2^2}{a_0^6} (1+z)^6 \quad (35)$$

Mean anisotropy parameter,

$$A_m(z) = \frac{2}{9\alpha^2} \frac{k_2^2}{a_0^6} (1+z)^{6-\frac{2}{\alpha}} \quad (36)$$

Also, scalar field,

$$\phi(z) = \left[\frac{k_1}{a_0^3} \left(\frac{n}{2} + 1 \right) \left(\frac{1}{1-3\alpha} \right) (1+z)^{\frac{3\alpha-1}{\alpha}} \right]^{\frac{2}{n+2}}, \quad n \neq -2 \quad (37)$$

Cosmological constant,

$$\Lambda(z) = \frac{h}{8\pi + h} \left[3\alpha^2 (1+z)^{\frac{2}{\alpha}} - \frac{k_2^2}{3a_0^6} (1+z)^6 + \frac{W}{2} \frac{k_1^2}{a_0^6} (1+z)^6 \right] \quad (38)$$

Pressure,

$$p(z) = \frac{1}{8\pi} \left[2\alpha (1+z)^{\frac{2}{\alpha}} - \frac{2k_2^2}{3a_0^6} (1+z)^6 + W \frac{k_1^2}{a_0^6} (1+z)^6 \right]$$

$$-\frac{1}{8\pi + h} \left[3\alpha^2 (1+z)^{\frac{2}{\alpha}} - \frac{k_2^2}{3a_0^6} (1+z)^6 + \frac{W k_1^2}{2 a_0^6} (1+z)^6 \right] \tag{39}$$

Energy density,

$$\rho(z) = \frac{1}{8\pi + h} \left[3\alpha^2 (1+z)^{\frac{2}{\alpha}} - \frac{k_2^2}{3a_0^6} (1+z)^6 + \frac{W k_1^2}{2 a_0^6} (1+z)^6 \right] \tag{40}$$

The EoS (equation of state) parameter,

$$\eta(z) = \frac{8\pi + h \left[2\alpha (1+z)^{\frac{2}{\alpha}} - \frac{2k_2^2}{3a_0^6} (1+z)^6 + W \frac{k_1^2}{a_0^6} (1+z)^6 \right]}{8\pi \left[3\alpha^2 (1+z)^{\frac{2}{\alpha}} - \frac{k_2^2}{3a_0^6} (1+z)^6 + \frac{W k_1^2}{2 a_0^6} (1+z)^6 \right]} - 1 \tag{41}$$

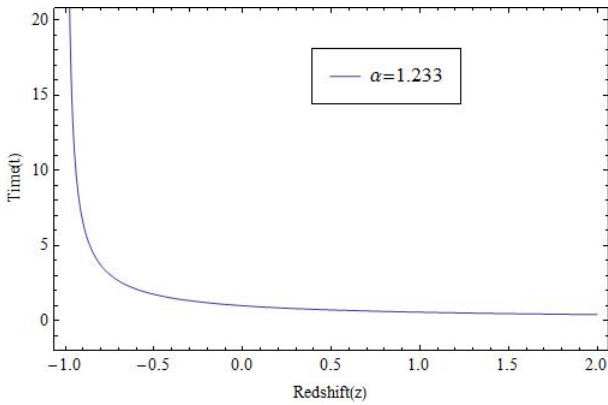


Figure 1. Plot of the cosmic time t v/s redshift z for $\alpha = 1.233$

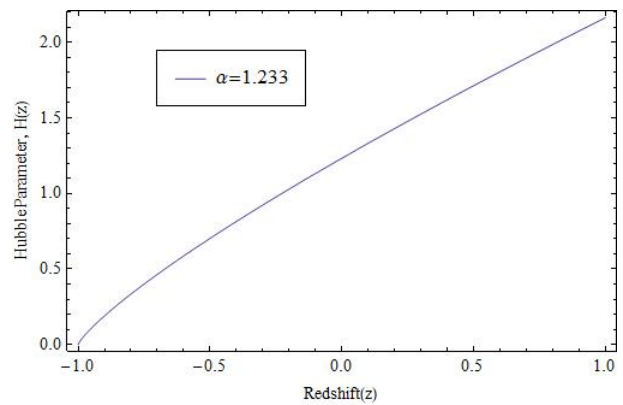


Figure 2. Evolution of the Hubble parameter H v/s redshift z for $\alpha = 1.233$

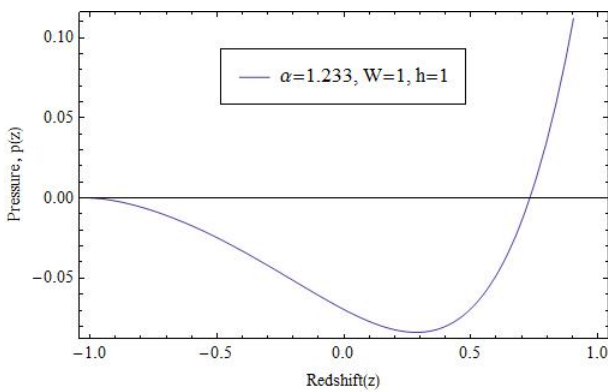


Figure 3. Evolution of the pressure p v/s redshift z for $\alpha = 1.233, h = 1, W = 1, a_0 = k_1 = k_2 = 1$

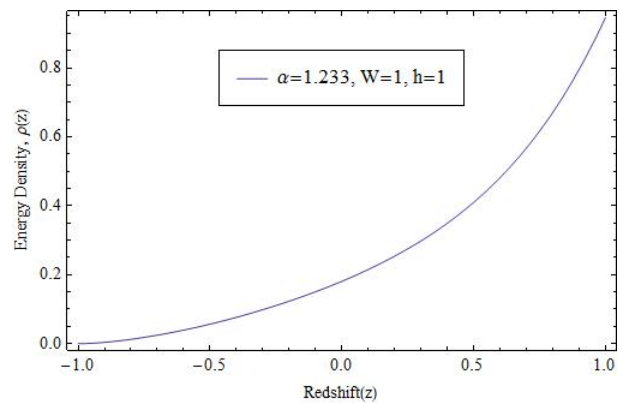


Figure 4. Evolution of the energy density ρ v/s redshift z for $\alpha = 1.233, h = 1, W = 1, a_0 = k_1 = k_2 = 1$

Figure 1 shows the graphical plot of cosmic time t v/s redshift z . From Figure 2 and Figure 8 we can see the decreasing and positive nature of the Hubble parameter H and the expansion scalar θ . In Figure 3, we observe that the pressure p of the cosmic fluid has a peculiar behaviour. It is positive in the early phases of the universe, subsequently becomes negative in the later phase and keeps increasing to attain the zero value at far future. Figure 4 depicts the behaviour of the energy density ρ . It decreases as the universe evolves, remains positive throughout the evolution of the universe and tends to zero at far future, thereby hinting about the expanding universe during the cosmic evolution. Figure 5 shows that the cosmological constant Λ is an increasing function of the redshift z , or equivalently it is a decreasing function of the cosmic time t . The Figure also depicts the positive nature of Λ in the evolving universe which fades away at far future. In Figure 6 we observe the decreasing nature of the EoS parameter η with the universe's evolution. The Figure indicates that the model starts in the radiation-dominated phase and subsequently it enters into the matter-dominated phase. At the late phase of universe's evolution, the model behaves as in the quintessence phase $(-1 < \eta < -\frac{1}{3})$. Figure 7 depicts the increasing nature of the spatial volume V , with the evolution of the universe, which gives the indication of the acceleration

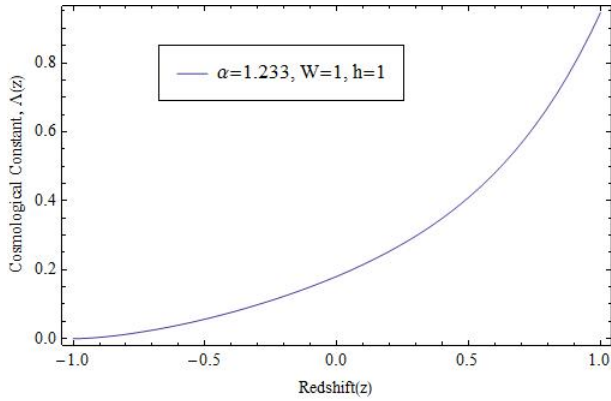


Figure 5. Evolution of the cosmological constant Λ v/s redshift z for $\alpha = 1.233, h = 1, W = 1, a_0 = k_1 = k_2 = 1$

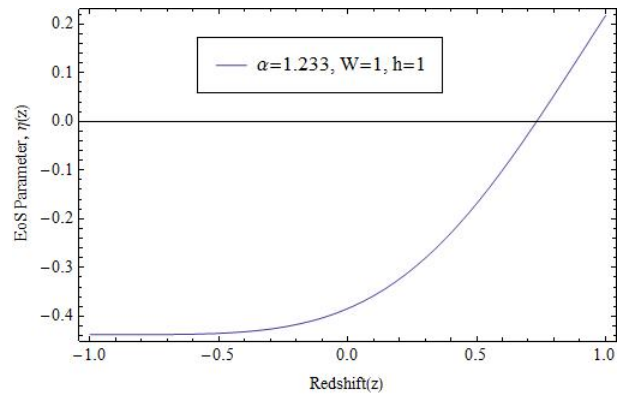


Figure 6. Evolution of the EoS parameter η v/s redshift z for $\alpha = 1.233, h = 1, W = 1, a_0 = k_1 = k_2 = 1$

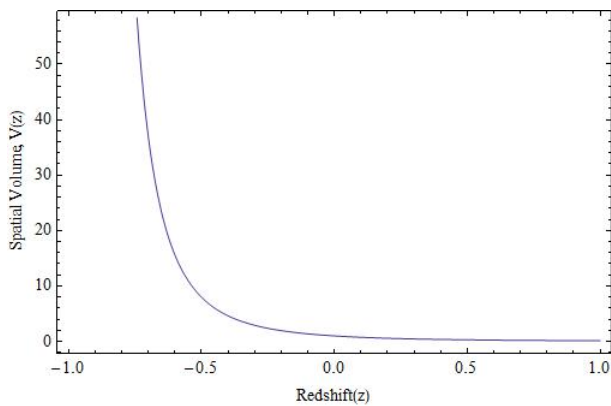


Figure 7. Evolution of the spatial volume V v/s redshift z for $a_0 = 1$

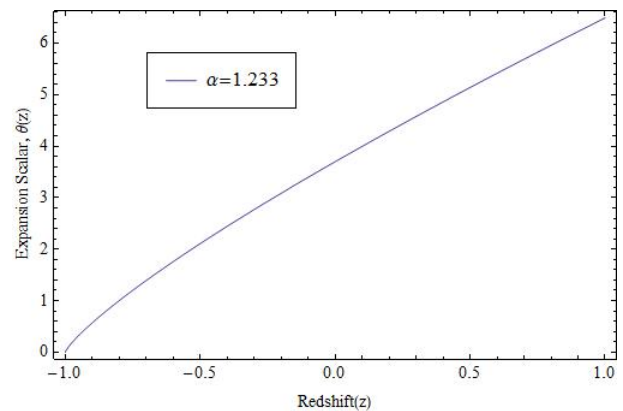


Figure 8. Evolution of the expansion scalar θ v/s redshift z for $\alpha = 1.233$

in the expansion rate of the universe at late times. Figure 9 and Figure 10 show the decreasing nature of the shear scalar σ^2 and the mean anisotropy parameter A_m which tends to zero at late times, thereby indicating the transition from early anisotropic phase to an isotropic phase at late time.

5. ENERGY CONDITIONS:

Energy conditions are simply some linear combinations of the energy density and the pressure with constraints. These conditions are helpful in studying the characteristics of the universe. A normal matter always satisfies all the energy conditions, for the reason that the energy density and the pressure of the normal matter are positive. Violation of the energy conditions hints about the presence of some unknown matter energy which is not normal in the universe. The four energy conditions are: Strong Energy Condition (SEC), Weak Energy Condition (WEC), Dominant Energy Condition (DEC) and Null Energy Condition (NEC).

The SEC suggests that the rate of expansion of the universe decelerates, independent of whether the universe is open, flat, or closed [30]. The WEC suggests that the energy density is always positive and non-increasing. The DEC provides an upper bound on the energy density and therefore an upper bound on the rate of expansion. The NEC implies a (very weak) upper bound on the Hubble parameter and indicates that the energy density of the universe goes down as its size increases.

The energy conditions are given as:

SEC: $\rho + 3p \geq 0$ and $\rho + p \geq 0$

WEC: $\rho + p \geq 0$ and $\rho \geq 0$

DEC: $\rho + p \geq 0, \rho - p \geq 0$ and $\rho \geq 0$

NEC: $\rho + p \geq 0$

For our model,

$$(\rho + 3p)(z) = \frac{3}{8\pi} \left[2\alpha(1+z)^{\frac{2}{\alpha}} - \frac{2k_2^2}{3a_0^6}(1+z)^6 + W\frac{k_1^2}{a_0^6}(1+z)^6 \right]$$

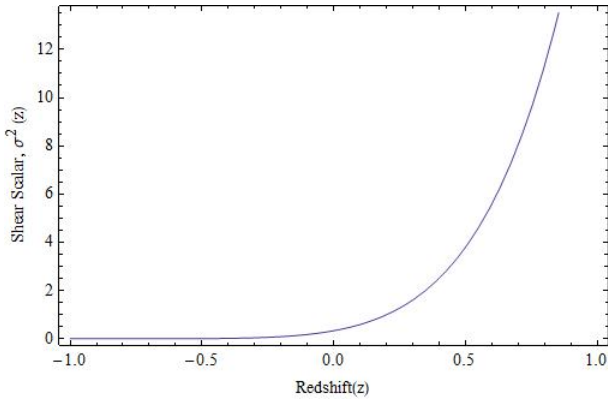


Figure 9. Evolution of the shear scalar σ^2 v/s redshift z for $a_0 = k_2 = 1$

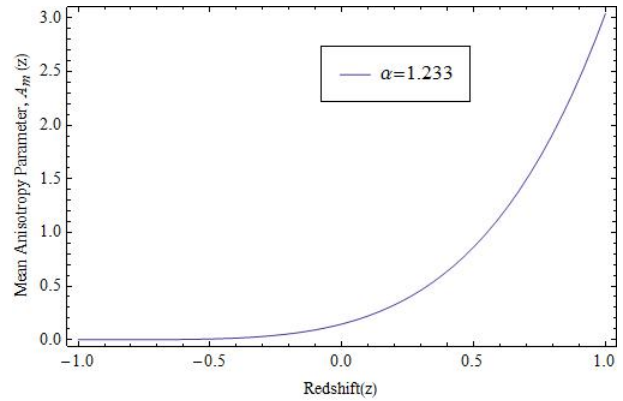


Figure 10. Evolution of the mean anisotropy parameter A_m v/s redshift z for $\alpha = 1.233, a_0 = k_2 = 1$

$$-\frac{2}{8\pi + h} \left[3\alpha^2 (1+z)^{\frac{2}{\alpha}} - \frac{k_2^2}{3a_0^6} (1+z)^6 + \frac{W k_1^2}{2 a_0^6} (1+z)^6 \right] \tag{42}$$

$$(\rho + p)(z) = \frac{1}{8\pi} \left[2\alpha (1+z)^{\frac{2}{\alpha}} - \frac{2k_2^2}{3a_0^6} (1+z)^6 + W \frac{k_1^2}{a_0^6} (1+z)^6 \right] \tag{43}$$

$$\begin{aligned} (\rho - p)(z) = & -\frac{1}{8\pi} \left[2\alpha (1+z)^{\frac{2}{\alpha}} - \frac{2k_2^2}{3a_0^6} (1+z)^6 + W \frac{k_1^2}{a_0^6} (1+z)^6 \right] \\ & + \frac{2}{8\pi + h} \left[3\alpha^2 (1+z)^{\frac{2}{\alpha}} - \frac{k_2^2}{3a_0^6} (1+z)^6 + \frac{W k_1^2}{2 a_0^6} (1+z)^6 \right] \end{aligned} \tag{44}$$

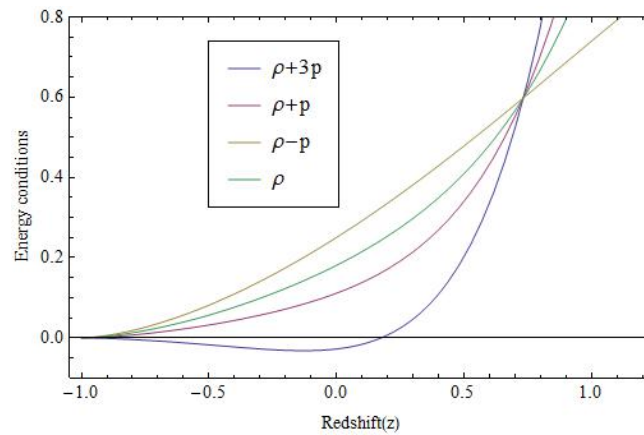


Figure 11. Plot of the energy conditions v/s redshift z for $\alpha = 1.233, h = 1, W = 1, a_0 = k_1 = k_2 = 1$

In Figure 11 we observe that at the very early stage of the universe, all the four energy conditions are satisfied and the three conditions other than the SEC are satisfied throughout the cosmic evolution. However, at a later stage the SEC is violated hinting about the accelerated rate of the universe’s expansion, which is in agreement with recent observational data.

6. CONCLUDING REMARKS

In this paper, we explore LRS Bianchi type-I universe with a power law expansion in the framework of Sáez-Ballester scalar-tensor theory with a cosmological term Λ which is assumed to be directly proportional to the matter-energy density ρ . We study the evolution of some parameters of cosmological importance such as the Hubble parameter H , the deceleration parameter q , the equation of state (EoS) parameter η , spatial volume V , the expansion scalar θ , Shear scalar σ^2 and the mean anisotropy parameter A_m graphically by choosing the values of the parameters as $\alpha = 1.233, h = 1, W = 1, a_0 = k_1 = k_2 = 1$. We observe that

- The increasing nature of the scale factor a and the Spatial volume V of the universe throughout the cosmic evolution implies the acceleration in the rate of cosmic expansion.
- The decreasing nature of the Hubble parameter H and the expansion scalar θ gives the hint of accelerated expansion of

the universe.

- The deceleration parameter q is constant in nature which may be positive, negative or zero according as $0 < \alpha < 1$, $\alpha > 1$ or $\alpha = 1$.
 - With the evolving universe, the cosmological constant Λ and the energy density ρ decrease and tend to zero at later phase of the universe's evolution.
 - The decreasing nature of the EoS parameter η with the universe's evolution is seen in Figure 6, which indicates that the model starts in the radiation-dominated phase and subsequently it enters into the matter-dominated phase. At the late phase of universe's evolution, the model behaves as in the quintessence phase $(-1 < \eta < -\frac{1}{3})$.
 - The decreasing nature of the shear scalar σ^2 and the mean anisotropy parameter A_m which gradually fades away signifies the transitioning from early anisotropic phase to a later isotropic phase.
 - Violation of the SEC is indicating the accelerated cosmic expansion agreeing with the observation.
- Thus the results of our model, are found to be satisfactory with the current observational data.

Acknowledgments

The author (Anindita Basumatary) is extremely grateful to the Ministry of Tribal Affairs (Scholarship Division), Govt. of India, for providing the financial support to carry out this research work.

ORCID

 Chandra Rekha Mahanta, <https://orcid.org/0000-0002-8019-8824>;  Anindita Basumatary, <https://orcid.org/0009-0001-8747-0456>

REFERENCES

- [1] S. Perlmutter, *et al.*, "Measurements of the cosmological parameters Ω and Λ from the first seven supernovae at $z \geq 0.35$," The Astrophysical Journal, **483**, 565-581 (1997). <https://doi.org/10.1086/304265>
- [2] S. Perlmutter, *et al.*, "Discovery of a supernova explosion at half the age of the Universe," Nature, **391**, 51-54 (1998). <https://doi.org/10.1038/34124>
- [3] A.G. Riess, *et al.*, "Observational evidence from supernovae for an accelerating universe and a cosmological constant," The Astronomical Journal, **116**, 1009-1038 (1998). <https://doi.org/10.1086/300499>
- [4] S. Perlmutter, *et al.*, "Measurements of Ω and Λ from 42 high- redshift supernovae," The Astrophysical Journal, **517**, 565-586 (1999). <https://doi.org/10.1086/307221>
- [5] A.D. Miller, *et al.*, "A Measurement of The Angular Power Spectrum of The Cosmic Microwave Background From $l = 100$ to 400," The Astrophysical Journal, **524**, L1-L4 (1999). <https://doi.org/10.1086/312293>
- [6] D.N. Spergel, *et al.*, "First- Year Wilkinson Microwave Anisotropy Probe (WMAP) Observations: Determination of Cosmological Parameters," The Astrophysical Journal Supplement Series, **148**, 175-194 (2003). <https://doi.org/10.1086/377226>
- [7] C.L. Bennett, *et al.*, "First-Year Wilkinson Microwave Anisotropy Probe (WMAP) Observations: Preliminary Maps and Basic Results," The Astrophysical Journal Supplement Series, **148**, 1-27 (2003). <https://doi.org/10.1086/377253>
- [8] K. Abazajian, *et al.*, "The Second Data Release of The Sloan Digital Sky Survey," The Astronomical Journal, **128**, 502-512 (2004). <https://doi.org/10.1086/421365>
- [9] M. Tegmark, *et al.*, "The Three-Dimensional Power Spectrum of Galaxies from The Sloan Digital Sky Survey," The Astrophysical Journal, **606**, 702-740 (2004). <https://doi.org/10.1086/382125>
- [10] D.N. Spergel, *et al.*, "Three-Year Wilkinson Microwave Anisotropy Probe (WMAP) Observations: Implications for Cosmology," The Astrophysical Journal Supplement Series, **170**, 377-408 (2007). <https://doi.org/10.1086/513700>
- [11] E.J. Copeland, M. Sami, and S. Tsujikawa, "Dynamics of Dark Energy," International Journal of Modern Physics D, **15**(11), 1753-1935 (2006). <https://doi.org/10.1142/S021827180600942X>
- [12] A. Kamenshchik, U. Moschella, and V. Pasquier, "An alternative to quintessence," Physics Letters B, **511**, 265-268 (2001). [https://doi.org/10.1016/S0370-2693\(01\)00571-8](https://doi.org/10.1016/S0370-2693(01)00571-8)
- [13] M. Li, "A model of holographic dark energy," Physics Letters B, **603**, 1-5 (2004). <https://doi.org/10.1016/j.physletb.2004.10.014>
- [14] L.N. Granda, and A. Oliveros, "Infrared cut-off proposal for the holographic density," Physics Letters B, **669**, 275-277 (2008). <https://doi.org/10.1016/j.physletb.2008.10.017>
- [15] M. Tavayef, "Tsallis holographic dark energy," Physics Letters B, **781**, 195-200 (2018). <https://doi.org/10.1016/j.physletb.2018.04.001>
- [16] H. Moradpour, *et al.*, "Thermodynamic approach to holographic dark energy and the Rényi entropy," The European Physical Journal C, **78**, 829 (2018). <https://doi.org/10.1140/epjc/s10052-018-6309-8>
- [17] E.N. Saridakis, "Barrow holographic dark energy," Physical Review D, **102**, 123525 (2020). <https://doi.org/10.1103/PhysRevD.102.123525>
- [18] C. Brans, and R. H. Dicke, "Mach's Principle and a Relativistic Theory of Gravitation," Physical Review, **124**, 925 (1961). <https://doi.org/10.1103/PhysRev.124.925>

- [19] D. Sáez, and V.J. Ballester, "A simple coupling with cosmological implications," *Physics Letters*, **113A**(9), (1986). [https://doi.org/10.1016/0375-9601\(86\)90121-0](https://doi.org/10.1016/0375-9601(86)90121-0)
- [20] V.U.M. Rao, M.V. Santhi, and T. Vinutha, "Exact Bianchi type II, VIII and IX string cosmological models in Saez-Ballester theory of gravitation," *Astrophysics and Space Science*, **314**, 73–77 (2008). <https://doi.org/10.1007/s10509-008-9739-1>
- [21] V.U.M. Rao, M.V. Santhi, and T. Vinutha, "Exact Bianchi type-II, VIII and IX perfect fluid cosmological models in Saez-Ballester theory of gravitation," *Astrophysics and Space Science*, **317**, 27–30 (2008). <https://doi.org/10.1007/s10509-008-9849-9>
- [22] R.L. Naidu, B. Satyanarayana, and D.R.K. Reddy, "Bianchi Type-III Dark Energy Model in a Saez-Ballester Scalar-Tensor Theory," *International Journal of Theoretical Physics*, **51**, 2857–2862 (2012). <https://doi.org/10.1007/s10773-012-1161-3>
- [23] R.K. Mishra, and A. Chand, "Cosmological models in Sáez-Ballester theory with bilinear varying deceleration parameter," *Astrophysics and Space Science*, **365**, 76 (2020). <https://doi.org/10.1007/s10509-020-03790-w>
- [24] R.K. Mishra, and H. Dua, "Bianchi type-I cosmological model in Sáez-Ballester theory with variable deceleration parameter," *Astrophysics and Space Science*, **366**, 47 (2021). <https://doi.org/10.1007/s10509-021-03952-4>
- [25] R.L. Naidu, *et al.*, "Kaluza-Klein FRW dark energy models in Saez-Ballester theory of gravitation," *New Astronomy*, **85**, 101564 (2021). <https://doi.org/10.1016/j.newast.2020.101564>
- [26] S.S. Singh, *et al.*, "Causal Viscous Universe in Sáez-Ballester Theory," *Canadian Journal of Physics*, **102**(1), (2023). <https://doi.org/10.1139/cjp-2022-0342>
- [27] R.K. Mishra, and H. Dua, "Certain Investigations on Bulk Viscous String Models of the Universe with BVDP," *Bulgarian Journal of Physics*, **50**, 95–114 (2023). [doi:https://doi.org/10.55318/bgjp.2023.50.2.095](https://doi.org/10.55318/bgjp.2023.50.2.095)
- [28] J.S. Wath, and A.S. Nimkar, "Cosmological Parameters and Stability of Bianchi Type-VIII in Sáez-Ballester Theory of Gravitation," *Bulgarian Journal of Physics*, **50**, 255–264 (2023). <https://doi.org/10.55318/bgjp.2023.50.3.255>
- [29] R.K. Dabgar, and A.K. Bhabor, "Higher dimensional Bianchi type-III string cosmological models with dark energy in Saez-Ballester scalar-tensor theory of gravitation," *Journal of Astrophysics and Astronomy*, **44**, 78 (2023). <https://doi.org/10.1007/s12036-023-09971-7>
- [30] M. Visser, "General Relativistic Energy Conditions: The Hubble expansion in the epoch of galaxy formation," *Physical Review D*, **56**(12), 7578 (1997). <https://doi.org/10.1103/PhysRevD.56.7578>

КОСМОЛОГІЧНА МОДЕЛЬ LRS БІАНЧІ В ТЕОРІЇ ГРАВІТАЦІЇ САЙЄЗ-БАЛЕСТЕРА ЗІ ЗМІННОЮ В ЧАСІ КОСМОЛОГІЧНОЮ КОНСТАНТОЮ

Чандра Рекха Маханга, Андіта Басуматарі

Факультет математики, Університет Гаухаті, Гувахаті - 781014, Індія

Ця робота присвячена вивченню локально-обертально-симетричної (LRS) космологічної моделі Б'янкі типу I в рамках скалярно-тензорної теорії гравітації, сформульованої Сайєзом і Балестером, зі змінною в часі космологічною сталою. Щоб отримати явні розв'язки рівнянь поля Сайєз-Балестера, ми припускаємо, що середній масштабний коефіцієнт підкоряється степеневому закону розширення, а космологічна стала пропорційна щільності енергії космічної рідини. Динамічну поведінку відповідних космологічних параметрів, включаючи параметр Хаббла, параметр уповільнення, щільність енергії, тиск, параметр рівняння стану, космологічну постійну, скаляр зсуву, скаляр розширення тощо, досліджується графічно шляхом вивчення їх еволюції проти параметр червоного зсуву. Також перевіряється перевірка чотирьох енергетичних умов. Ми вважаємо, що результати побудованої моделі добре узгоджуються з останніми даними спостережень.

Ключові слова: космологічна стала; параметр уповільнення; параметр Хаббла; LRS Б'янкі тип-I; теорія Сайєз-Балестера

ANISOTROPIC COSMOLOGICAL MODEL WITH SQM IN $f(R, L_m)$ GRAVITY

Pravin Bolke^{a*}, Vasudeo Patil^b, Sachin Waghmare^c, Neha Mahajan^b

^aDepartment of Mathematics, Prof Ram Meghe college of Engineering and Management, Badnera, Dist. Amravati (MS), India-444701

^bDepartment of Mathematics, Arts, Science and Commerce College, Chikhaldara, Dist. Amravati (MS), India-444807

^cDepartment of Mathematics, TGPCET, Nagpur (MS), India-441108

*Corresponding Author e-mail: mrpravin.bolke@gmail.com

Received June 28, 2024; revised July 27, 2024; accepted August 9, 2024

A locally rotationally symmetric Bianchi-I model filled with strange quark matter (SQM) is explored in $f(R, L_m)$ gravity as a non-linear functional of the form $f(R, L_m) = \frac{R}{2} + L_m^\alpha$, where α is the free model parameter. We considered the special law of variation of Hubble's parameter proposed by Berman (1983) and also used the power law relation between the scale factors to obtain the exact solution of the field equation, which matches the model of the universe. We also analyze the physical and geometrical aspects of the universe's kinematic and dynamic behavior. Additionally, we employ equation-of-state (EoS) parameters and statefinder parameters as analytical tools to gain insights into the evolution of the universe. We use the Λ CDM model as a benchmark to validate the results. By placing the deviations of the universe from Λ CDM model and yet making important contributions to the study of the anisotropic nature of $f(R, L_m)$ gravity within the framework of cosmological dynamics, the paper increases our comprehension of our cosmic evolution.

Keywords: LRS Bianchi type I cosmological model; $f(R, L_m)$ gravity; Strange quark matter; Cosmic time

PACS: 04.20.-q; 04.20.Jb; 04.50.Kd

1. INTRODUCTION

Over the last twenty years, plenty of cosmological investigations have come out to suggest that we are living in an accelerated growth phase of the universe. Strong evidence from Type Ia supernovae [1, 2, 3], which are crucial probes of cosmic distances and expansion rates, supports this fast expansion. Moreover, studies on Baryon Acoustic Oscillations (BAO) [4, 5], Wilkinson Microwave Anisotropy Probe [6], the large-scale structure of the universe [7, 8], assessments of galaxy redshifts [9], and examinations of the cosmic microwave background radiation (CMBR) [10, 11] all provide convincing empirical proof for this phenomenon. Collectively, these several lines of evidence indicate the impressive fact that two mysterious substances, referred to as dark matter (DM) and dark energy (DE) with negative pressure, constitute 95% of the total universe [12]. Dark energy is thought to be the driving force causing the expanding universe's noticeable accelerated expansion, while dark matter, a substance that is gravitationally effective but unable to produce light, interacts mostly through gravitational forces. The enormous significance of these mysterious components for determining the evolution and fate of our universe is brought into focus by the convergence of universe facts.

Numerous theoretical descriptions of this acceleration have been suggested in the literature. The concept of dark energy is basically associated with the rapid acceleration of the universe. It can be understood in two different ways. The first one argues that the universe is currently expanding not due to the gravitation force but because of the existence of an unknown force with a negative pressure higher than that of gravitation, and this force is called "dark energy" (DE). The literature proposes time-varying dark energy models such as quintessence [13], k-essence [14, 15], and even the perfect fluid models, especially the Chaplygin gas model [16, 17] as a solution to this problem. Interpreting spacetime's geometry is the second tactic for explaining the universe's acceleration. The left-hand side of the Einstein equation can be changed for this purpose. Modified theories of gravity are the alteration of the Einstein-Hilbert action of general relativity to reach the acceleration of the universe. These theories are geometric extensions of relativity by Einstein. Among the recent developments, cosmologists have been detecting dark energy through the modified gravity theories as an explanation. It is argued that dark energy would be the product of introducing a modification to the force of gravity. Various scientific evidence shows that modified versions of gravity theories are likely to be the reasons for the acceleration of the universe at the early and late stages, forming a consistent picture of the universe. Hence, there are many reasons to search for theories that extend beyond general relativity, and the theories of gravity need to be revised. In the literature, there are several modified theories that have been proposed. A few of the modified theories consist of $f(R)$ gravity, the modification of general relativity by introducing an arbitrary function of the Ricci scalar (R) into the gravitational action [18], the $f(R, T)$ theory, an extension of $f(R)$ gravity coupled with the trace of energy-momentum tensor T [19], $f(G)$ theory where G is the Gauss-Bonnet invariant [20, 21, 22], $f(R, G)$ theory [23, 24], $f(T)$ gravity [25, 26, 27], $f(Q, T)$ theory [28] and $f(R, L_m)$ gravity [29].

The $f(R, L_m)$ gravity [29, 30] is a theory that is based on general relativity, attaching additional terms to the action that are dependent on matter density Lagrangian (L_m) and the Ricci scalar (R), respectively. It is an attempt to overcome

the arising issues of general relativity and observation, such as the need for dark matter and dark energy to explain universe occurrences. This function $f(R, L_m)$ is likely to be required for several theoretical reasons, such as resolving the cosmological constant puzzle, broadcasting the universe’s accelerated expansion, or offering an alternative explanation for gravitational incidents observed at the universe scales. Researchers [31] derived the energy condition and Dolgov-Kawasaki (DK) instability criterion [32] in $f(R, L_m)$ gravity and provided the highly versatile energy requirements that can reduce commonly accepted energy conditions found in $f(R)$ theories of gravity and general relativity with any connection between matter and geometry, non-minimal connection, and non-coupling. Geometry-matter couplings in the presence of scalar fields were discussed in [33]. Kasner-type static, cylindrically symmetric interior string solutions in the $f(R, L_m)$ theory of modified gravity are studied [34]. Some of the researchers discussed various cosmological models [35, 36] and phenomenon of gravitational baryogenesis [37] in $f(R, L_m)$ gravity. Kavya et al. [38] have discussed the anisotropic cosmological model in $f(R, L_m)$ gravity. The universe’s accelerating scenarios [39] and warmhole solution [40] have all been investigated recently.

The LRS Bianchi-type I cosmological model is a homogeneous and anisotropic cosmological solution to Einstein’s field equations. It specifies a spatially homogeneous universe that allows anisotropic expansion since it experiences different rates of expansion along distinct spatial directions. This model has been extensively studied in the context of both general relativity (GR) and modified gravity theories to understand its implications and test the viability of such theories against observations. Yadav et al. [41] have studied the LRS Bianchi I bulk viscous cosmological model in $f(R, T)$ gravity. Interacting two fluid dark energy radiating cosmological models [42] and power-exponential law models [43] have been investigated in $f(R)$ gravity. Later on, several researchers [44, 45, 46] discussed the various cosmological aspects of the LRS Bianchi type I cosmological model in $f(R, T)$ gravity. Recently, Solanke et al.[47] investigated the LRS Bianchi type-I cosmological model in the $f(Q, T)$ theory of gravity with observational constraints.

This research paper emphasizes the exploration of an exact solution for the LRS Bianchi Type I space-time within the framework of $f(R, L_m)$ gravity, Hubble’s law, and incorporating the presence of strange quark matter (SQM). The study aims to advance understanding regarding the universe’s dynamics and properties within this gravitational framework. The article is organized as follows: The basic field equation and detailed review of $f(R, L_m)$ modified gravity, including the metric and energy momentum tensor, are given in Sections 2 and 3. Moving to Section 4, efforts are directed to find the exact solution of the $f(R, L_m)$ cosmological model. The subsequent Sections, 5 and 6, covered the details about the strange quark model and some physical parameters respectively, within the framework of the discussed modified gravity theory. The important analytical tool statefinder parameters are discussed in Section 7. The figures and conclusion are summarized in sections 8 and 9.

2. BASIC FIELD EQUATIONS IN $f(R, L_m)$ GRAVITY

The action integral for the framework of $f(R, L_m)$ interpreted with the matter Lagrangian density L_m and the Ricci scalar R is given as,

$$S = \int f(R, L_m)\sqrt{-g}dx^4, \tag{1}$$

where $f(R, L_m)$ is arbitrary function of Ricci scalar R and matter Lagrangian L_m . By contracting the Ricci tensor R_{mn} , one may get the Ricci scalar R ,

$$R = g^{ij}R_{ij} \tag{2}$$

where, the Ricci tensor is defined by,

$$R_{ij} = -\delta_\lambda^i \Gamma_{ij}^\lambda + \delta_j^i \Gamma_{i\lambda}^\lambda - \Gamma_{\lambda\sigma}^i \Gamma_{ij}^\sigma + \Gamma_{j\sigma}^\lambda \Gamma_{i\lambda}^\sigma \tag{3}$$

Here $\Gamma_{\beta\gamma}^\alpha$ represents the components of well-known Levi-Civita connection defined by

$$\Gamma_{\beta\gamma}^\alpha = \frac{1}{2}g^{\alpha\lambda} \left(\frac{\delta g_{\gamma\lambda}}{\delta x^\beta} + \frac{\delta g_{\lambda\beta}}{\delta x^\gamma} - \frac{\delta g_{\beta\gamma}}{\delta x^\lambda} \right) \tag{4}$$

The corresponding field equations of $f(R, L_m)$ gravity are obtained by varying the action (1) for metric g_{ij} is given by,

$$f_R(R, L_m)R_{ij} + (g_{ij}\nabla^i\nabla_j - \nabla_i\nabla_j)f(R, L_m) - \frac{1}{2}[f(R, L_m) - f_{L_m}(R, L_m)L_m]g_{ij} = \frac{1}{2}f_{L_m}(R, L_m)T_{ij} \tag{5}$$

Where, $f_R(R, L_m) = \frac{\delta f(R, L_m)}{\delta R}$, $f_{L_m}(R, L_m) = \frac{\delta f(R, L_m)}{\delta L_m}$ Here covariant derivative is represented by ∇_i and the energy momentum tensor T_{ij} can be expressed as,

$$T_{ij} = -\frac{2}{\sqrt{-g}} \frac{\delta(\sqrt{-g}L_m)}{\delta g^{ij}} = g_{ij}L_m - 2\frac{\delta L_m}{\delta g^{ij}} \tag{6}$$

Now, from the explicit form of the field equation (5), the covariant divergence of Energy momentum tensor T_{ij} can be obtained as,

$$\nabla^i T_{ij} = 2 \nabla^i \ln [f_{L_m}(R, L_m)] \frac{\delta L_m}{\delta g^{ij}} \tag{7}$$

The relation between the trace of energy momentum-tensor T , Ricci scalar R , and the Lagrangian density of the matter L_m obtained by contracting the field equation (5)

$$f_R(R, L_m) R + 3 \nabla_i \nabla^i f_R(R, L_m) - 2 [f(R, L_m) - f_{L_m}(R, L_m) L_m] = \frac{1}{2} f_{L_m}(R, L_m) T \tag{8}$$

The relation between the trace of the energy momentum tensor $T = T^i_i$, L_m , and R can be established by taking account of the previously mentioned equation.

3. METRIC AND FIELD EQUATION IN $f(R, L_m)$ GRAVITY

The spatially homogeneous and anisotropic LRS Bianchi type I spacetime can be written in the form of,

$$ds^2 = -dt^2 + L^2 dx^2 + M^2 (dy^2 + dz^2) \tag{9}$$

Where L and M are the metric potential that are the functions of cosmic time t only. The Ricci scalar for LRS Bianchi - I spacetime can be expressed as

$$R = -2 \left[\frac{\ddot{L}}{L} + 2 \frac{\ddot{M}}{M} + 2 \frac{\dot{L}\dot{M}}{LM} + \frac{\dot{M}^2}{M^2} \right] \tag{10}$$

The overhead dot ($\dot{}$) denotes the derivative with respect to time t . The spatial volume V of the universe is defined as

$$V = LM^2 \tag{11}$$

The generalized mean Hubble parameter (H), which describes the space-time expansion rate, can be stated as

$$H = \frac{1}{3} (H_1 + H_2 + H_3) \tag{12}$$

where H_1, H_2, H_3 are the directional Hubble's parameters in the direction of the x-, y-, and z-axes, respectively. In order to figure out whether the models approach isotropy or not, we define the expansion's anisotropy parameter as

$$A_m = \frac{1}{3} \sum_{i=1}^3 \left(\frac{H_i - H}{H} \right)^2 \tag{13}$$

The expansion scalar and shear scalar are defined as follows:

$$\theta = u^i_{;i} = \frac{\dot{L}}{L} + 2 \frac{\dot{M}}{M} \tag{14}$$

$$\sigma^2 = \frac{3}{2} H^2 A_m \tag{15}$$

Let us take the matter that contains the energy momentum tensor for quark matter, which is of the form

$$T_i^{j(\text{quark})} = (p + \rho) u^j u_i + p g_i^j = \text{diag}(-\rho, p, p, p) \tag{16}$$

where $\rho = \rho_q + B_c$ is a quark matter total energy density, $p = p_q - B_c$ is the quark matter total pressure, and u_i is the four-velocity vector such that $u_i u^i = -1$.

The EoS parameter for quark matter is defined as,

$$p_q = \omega \rho_q, \quad 0 \leq \omega \leq 1 \tag{17}$$

The linear equation of state for strange quark matter is provided by

$$p = \omega (\rho - \rho_0) \tag{18}$$

where ω is constant and ρ_0 is the energy density at zero pressure. When $\omega = \frac{1}{3}$ and $\rho_0 = 4B_c$, in the bag model, strange quark matter changes the above linear equation of state to the one that follows EoS.

$$p = \frac{(\rho - 4B_c)}{3} \tag{19}$$

where B_c is the bag constant.

By using the help of equation (16), the field equation (5) can be translated into the action of metric (10) in the co-moving coordinate system as,

$$-\left(\frac{\ddot{L}}{L} + 2\frac{\dot{L}\dot{M}}{LM}\right) f_R - \frac{1}{2} (f - f_{L_m} L_m) - 2\frac{\dot{M}}{M} \dot{f}_R - \ddot{f}_R = \frac{1}{2} f_{L_m} (p_q - B_c) \tag{20}$$

$$-\left(\frac{\ddot{M}}{M} + \frac{\dot{M}^2}{M^2} + \frac{\dot{L}\dot{M}}{LM}\right) f_R - \frac{1}{2} (f - f_{L_m} L_m) - \left(\frac{\dot{L}}{L} + \frac{\dot{M}}{M}\right) \dot{f}_R - \ddot{f}_R = \frac{1}{2} f_{L_m} (p_q - B_c) \tag{21}$$

$$-\left(\frac{\ddot{L}}{L} + 2\frac{\dot{M}}{M}\right) f_R - \frac{1}{2} (f - f_{L_m} L_m) - \left(\frac{\dot{L}}{L} + 2\frac{\dot{M}}{M}\right) \dot{f}_R - \ddot{f}_R = -\frac{1}{2} f_{L_m} (\rho_q + B_c) \tag{22}$$

4. COSMOLOGICAL $f(R, L_m)$ MODEL

In the present study, to examine the dynamics of the cosmological model in $f(R, L_m)$ gravity, we use the relation between R and L_m [38]

$$f(R, L_m) = \frac{R}{2} + L_m^\alpha \tag{23}$$

where $\alpha \neq 0$ is a parameter and one can retain GR for $\alpha = 1$.

For this particular $f(R, L_m)$ model, we have to consider $L_m = \rho$ [48]

Using the above particular choice of L_m , the field equations (20),(21) and (22) becomes,

$$2\frac{\ddot{M}}{M} + \frac{\dot{M}^2}{M^2} - (1 - \alpha) (\rho_q + B_c)^\alpha = \alpha (\rho_q + B_c)^{\alpha-1} (p_q - B_c) \tag{24}$$

$$\frac{\ddot{L}}{L} + \frac{\dot{M}}{M} + \frac{\dot{L}\dot{M}}{LM} - (1 - \alpha) (\rho_q + B_c)^\alpha = \alpha \alpha (\rho_q + B_c)^{\alpha-1} (p_q - B_c) \tag{25}$$

$$\frac{\dot{M}^2}{M^2} + 2\frac{\dot{L}\dot{M}}{LM} = (1 - 2\alpha) (\rho_q + B_c)^\alpha \tag{26}$$

The field equations (24), (25) and (26) are three independent differential equations with four unknowns: L , M , ρ_q , and p_q . Hence, to determine solutions, we have to use physically plausible conditions.

Berman [49] indicate that there exists a connection between the deceleration parameter as well as the average scale factor given as,

$$q = -\frac{a\ddot{a}}{\dot{a}^2} \tag{27}$$

Here, a is the average scale factor with $a = (LM^2)^{\frac{1}{3}}$ and q is the deceleration parameter. If we use Hubble's law and relate Hubble's parameter H to the average scale factor a then we get a constant value of the deceleration parameter q .

Hence the Hubble's law gives,

$$H = ba^{-m} \tag{28}$$

where b and m are constants. Also, Hubble's parameter (12) can be written as

$$H = \frac{1}{3} \left(\frac{\dot{L}}{L} + 2\frac{\dot{M}}{M}\right) = \frac{\dot{a}}{a} \tag{29}$$

Using equation (29), we can re-write equation (28) as

$$\dot{a} = ba^{-m+1} \tag{30}$$

Using the equations (28), (29), and (30) in (27), we get

$$q = -m + 1 \quad (31)$$

This equation demonstrates that the deceleration parameter is going to stay constant, whatever its significance, and regardless of whether the value is positive or negative. The standard deceleration model is indicated by positive values of the deceleration parameters. Negative numbers, on the other hand, lead the model to accelerate or lead to inflation. on solving the equation (28) with the help of equation (29), we get

$$a = (ct + d)^{\frac{1}{q+1}}, q \neq -1 \quad (32)$$

considering that d is the integration constant and $c \neq 0$. Using equation (??) and $LM^2 = a^3$, we can obtain,

$$LM^2 = (ct + d)^{\frac{3}{q+1}}, q \neq -1 \quad (33)$$

In order to obtain a favorable solution to the field equations, we have to consider the constraining equation. Here we presume the anisotropic relation can be written in terms of expansion scalar (θ) and shear scalar (σ) as,

$$\sigma \propto \theta$$

With reference to the scale factors L and M , the above assumption leads to the following anisotropic relation:

$$L = M^k \quad (34)$$

where $k \neq 1$ is an arbitrary constant. The model becomes isotropic if $k = 1$, indicating that the distribution of matter in the universe is homogeneous; otherwise, it turns out to be anisotropic.

Using the equation (34), equation (33) implies that

$$L = (ct + d)^{\frac{3k}{(q+1)(k+2)}} \quad (35)$$

$$M = (ct + d)^{\frac{3}{(q+1)(k+2)}} \quad (36)$$

Equations (35) and (36) indicate that the model's metric potentials L and M are time-dependent functions that rise with time at $q > -1$, $k \neq -2$ and fall with time at $q < -1$, $k \neq -2$; they also do not exist at $q = -1$ or $k = -2$. Moreover, it is important to note that for $q > -1$, $k \neq -2$, these parameters begin at a constant value, but at the point $t = -\frac{d}{c}$, they start at zero, indicating that the model exhibits point-type singularity at that point.

Thus, the metric (9) with the help of equations (35) and (36) can be written as,

$$ds^2 = -dt^2 + (ct + d)^{\frac{6k}{(q+1)(k+2)}} dx^2 + (ct + d)^{\frac{6}{(q+1)(k+2)}} (dy^2 + dz^2) \quad (37)$$

Equation (37) represents the homogeneous anisotropic plane symmetric cosmological model with quark and strange quark matter in the framework of $f(R, L_m)$ gravity. The model increases with time for the constants $q < -1$, $k \neq -2$ and has a singularity at the point $t = -\frac{d}{c}$.

5. STRANGE QUARK MATTER FOR COSMOLOGICAL MODEL

From the equations (25) and (26), with the help of metric potential, the energy density and pressure of strange quark matter are given as,

$$\rho = \left[\frac{9(1+2k)c^2}{(1-2\alpha)(q+1)^2(k+2)^2(ct+d)^2} \right]^{\frac{1}{\alpha}} \quad (38)$$

$$p = D \left[\frac{9c^2(1+2k)^{1-\alpha}}{(1-2\alpha)(q+1)^2(k+2)^2(ct+d)^2} \right]^{\frac{1}{\alpha}} \quad (39)$$

where, $D = \frac{[(2\alpha-1)q+(2-4\alpha)]k^2+[3q(2\alpha-1)+6(\alpha-1)]k+[2(2\alpha-1)q+(\alpha-2)]}{3\alpha}$

Using the above equations, the pressure and energy density of the quark matter as follows:

$$\rho_q = \left[\frac{9(1+2k)c^2}{(1-2\alpha)(q+1)^2(k+2)^2(ct+d)^2} \right]^{\frac{1}{\alpha}} - B_c \quad (40)$$

$$p_q = D \left[\frac{9c^2(1+2k)^{1-\alpha}}{(1-2\alpha)(q+1)^2(k+2)^2(ct+d)^2} \right]^{\frac{1}{\alpha}} + B_c \tag{41}$$

Using the equations (38) and (39), the equation of state (EoS) for strange quark matter and quark matter are given as

$$\omega = \frac{D}{(1+2k)} \tag{42}$$

$$\omega_q = \frac{D \left[\frac{9c^2(1+2k)^{1-\alpha}}{(1-2\alpha)(q+1)^2(k+2)^2(ct+d)^2} \right]^{\frac{1}{\alpha}} + B_c}{\left[\frac{9(1+2k)c^2}{(1-2\alpha)(q+1)^2(k+2)^2(ct+d)^2} \right]^{\frac{1}{\alpha}} - B_c} \tag{43}$$

6. SOME PHYSICAL PARAMETERS

The spatial volume V of the universe is given as

$$V = (ct+d)^{\frac{3}{q+1}} \tag{44}$$

The spatial volume of the universe increases with increasing cosmic time, starting with a constant value at $t = 0$ and with a big bang at $t = -\frac{d}{c}$. As a result of this approach, inflation. This illustrates that the universe begins to evolve at zero volume and grows over cosmic time. The mean generalized Hubble's parameter (29) of the model is given by

$$H = \frac{c}{(q+1)(ct+d)} \tag{45}$$

The expansion scalar of the model turns out to be

$$\theta = \frac{3c}{(q+1)(ct+d)} \tag{46}$$

At the initial stage, both the Hubble's parameter and the expansion scalar are constant and approach zero steadily at $t \rightarrow \infty$, but at $t = -\frac{d}{c}$ both are infinitely large. The mean anisotropic parameter of the model is given as

$$A_m = \frac{2k^2 - 4k + 2}{k^2 + 4k + 4} \tag{47}$$

The shear scalar of the model is represented as

$$\sigma^2 = \frac{3c^2}{(q+1)^2} \frac{k^2 - 2k + 1}{k^2 + 4k + 4} \frac{1}{(ct+d)^2} \tag{48}$$

The shear scalar, the scalar expansion, and the Hubble parameter are all the functions of time that are rapidly decreasing with the increase of cosmic time and getting closer to zero in the later stages. This fact reveals that in the earliest stages of the universe, the rate of expansion was very high for a while, but gradually it became slower. This shows that the evolution of the universe starts at an infinite rate, but with expansion, it declines.

7. STATEFINDER PARAMETERS

The so-called cosmic acceleration may arise from a quite wide range of dark energy models, many of which are distinguishable by the utilization of the statefinder diagnostic tool. It is a model-free way of quantifying the dark energy intrinsic properties of higher derivatives to the scale factor. Through employing the cosmic statefinder diagnostic fiction pair $\{r, s\}$, the technique permits research to investigate dark energy properties, free of any particular models. The statefinder parameters are defined as [50, 51].

$$r = \frac{1}{aH^3} \frac{d^3}{dt^3} (a), \quad s = \frac{r-1}{3(q-\frac{1}{2})} \tag{49}$$

Identifying between different cosmological domains is mostly dependent on the paths in the $\{r, s\}$ plane. For example, in the $\{r, s\}$ plane, the λ CDM model is characterized by the point $(r = 1, s = 0)$, Standard Cold Dark Matter is for $(r = 1, s = 1)$, and the holographic DE model is represented by $(r = 1, s = \frac{2}{3})$. The phantom region is associated with $(r > 1, s < 0)$, and the quintessence region is identified by $(r < 1, s > 0)$. with the help of equations (32), (44) and (45), the equation (49) becomes

$$\{r, s\} = \left\{ 2q^2 + q, \frac{2}{3}(q+1) \right\} \tag{50}$$

We can see that for a given model, q, r, s are constant. For different values of q , we have different expansion factors, which can be analyzed in the following Table 1.

Table 1. Description of Models

q	r	s	Type of Model
0.5	1	1	SCDM
-0.5	0	$\frac{1}{3}$	quintessence
-1	1	0	λ CDM
-2	6	$-\frac{2}{3}$	Phantom

8. FIGURES

In this section, in order to gain a deeper insight into our cosmological model, let us plot different physical and dynamic parameters against cosmic time.

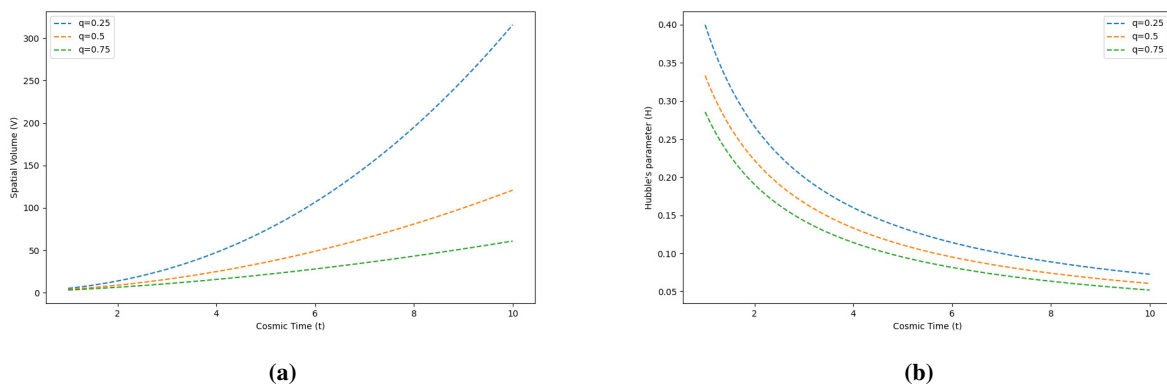


Figure 1. The Variation of Spatial volume (V) (left) and Hubble’s parameter (H) (right) as a function of cosmic time (t) are shown. V, H and t are in arbitrary units. To derive above plot we have used $c = d = 1$.

- The graph of volume against cosmic time is increasing in nature (Fig. 1(a)), and that of the Hubble parameter H is a decreasing function of cosmic time (t) in the positive region (Fig. 1(b)). From it, we collect important insights about the expansion of the universe. This observation serves as a necessary foundation for our understanding of the universe’s dynamics.

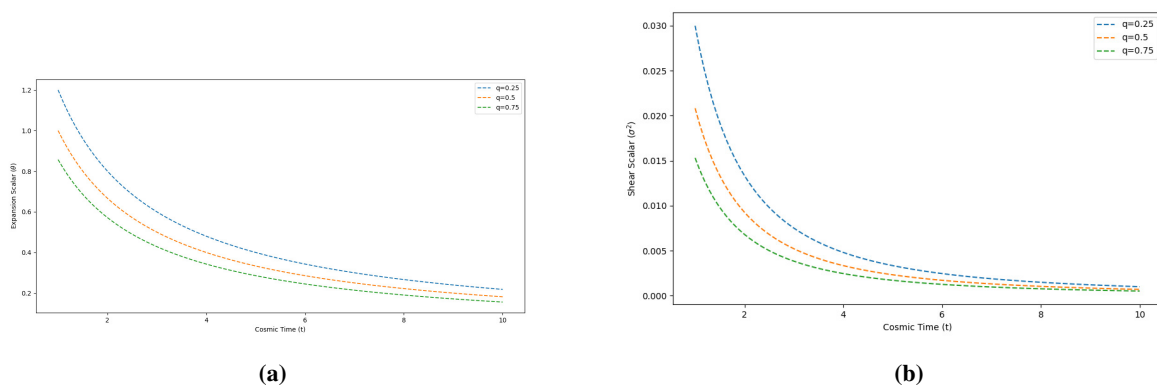


Figure 2. Variation of Expansion scalar (θ) (left) and Shear scalar (σ^2) (right) as a function of cosmic time (t) are shown. θ, σ^2 and t are in arbitrary units. To derive above plot we have used $c = d = 1$.

- We found that the expansion scalar (Fig. 2(a)) and shear scalar (Fig. 2(b)) are the diminishing functions of cosmic time (t).

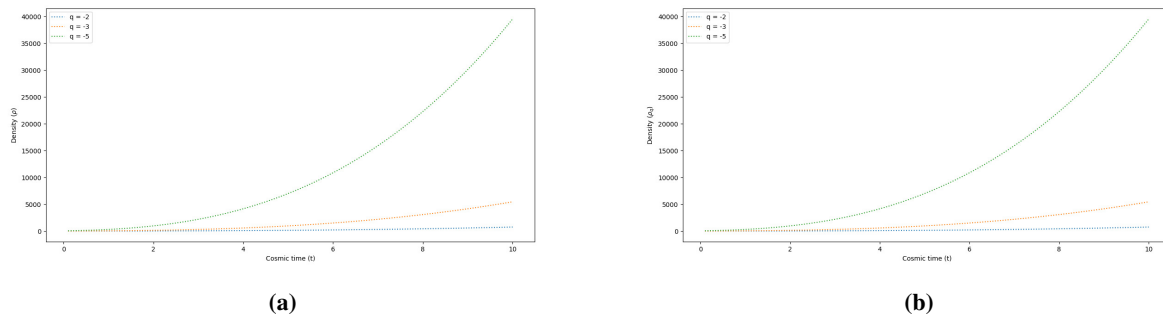


Figure 3. Variations of energy density of strange quark matter(ρ) (left) and quark matter(ρ_q) (right) as a function of cosmic time (t) for $q < -1$. All quantities are in arbitrary units. These plots are derived using $c = d = B_c = 1, k = 2$.

- The energy density of strange quark matter (ρ) and quark matter (ρ_q) both appear constant at the initial stage and becomes infinite as t tends to infinity, as shown in Fig. 3.

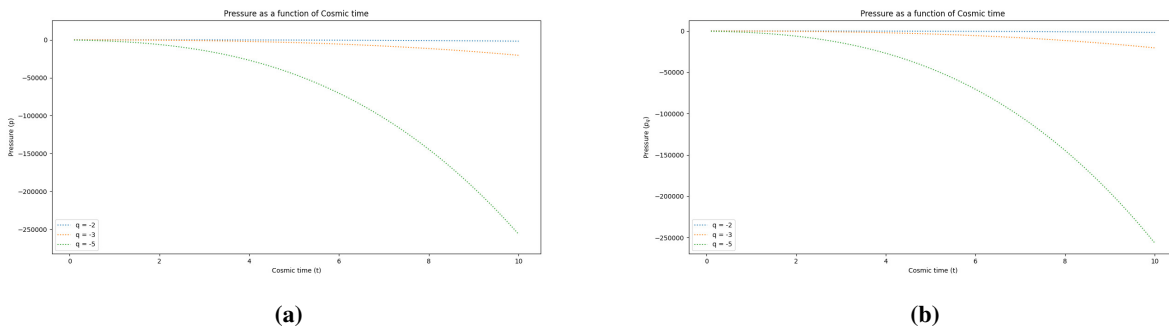


Figure 4. Variations of pressure of strange quark matter(p) and quark matter(p_q) as a function of cosmic time (t) for $q < -1$. All quantities are in arbitrary units. These plots are derived using $c = d = B_c = 1, k = 2$.

- The pressure of strange quark matter (p) and quark matter (p_q), both decreasing functions of time, remains negative throughout the evolution, as shown in Fig. 4.

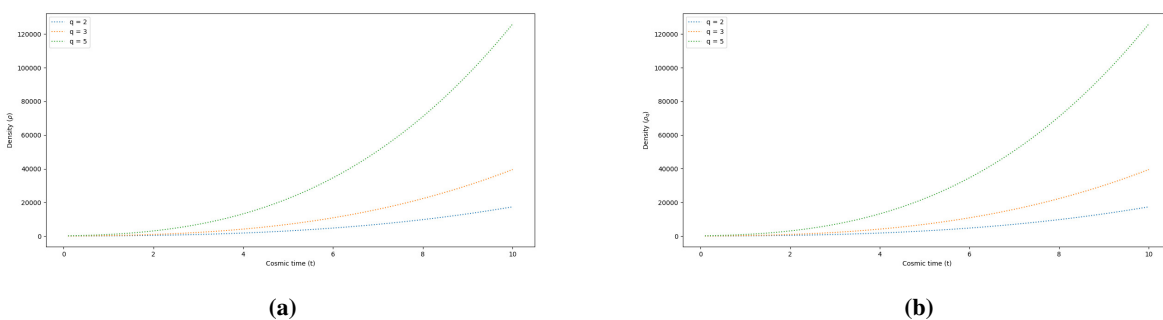


Figure 5. Variations of energy density of strange quark matter (ρ) and quark matter (ρ_q) as a function of cosmic time (t) for $q > -1$. All quantities are in arbitrary units. These plots are derived using $c = d = B_c = 1, k = 2$.

9. CONCLUSIONS

In this article, we explore an accelerating model of the universe in the context of the $f(R, L_m)$ theory of gravity as a non-linear functional of the form $f(R, L_m) = \frac{R}{2} + L_m^\alpha$, where α is the free model parameter. Utilizing a unique formulation of the deceleration parameter, we derive cosmological solutions that closely resemble the characteristics of the dark energy-driven λ CDM model. We assumed a power law relation between the scale factors. We also considered the special

law of variation of Hubble's parameter proposed by Berman (1983), which yields the constant deceleration parameter. The findings of the research are very interesting and ultimately result in the following conclusions:

Around $t = 0$, the metric potentials L and M are constant, and then both vanish. This brings one to the conclusion that the model exhibits an initial singularity at $t = -\frac{d}{c}$. As a result, similar to the standard Big Bang theory, the values of L and M increase steadily over time. At a singular point, the model is similar to the work of [52]. We discovered that the spatial volume (V), expansion scalar (θ), shear scalar (σ^2), and mean Hubble's parameter (H) are all functions of cosmic time (t). These parameters tend to zero as t tends to infinity ($t \rightarrow \infty$), but they diverge with the exception of spatial volume when cosmic time approaches $t = -\frac{c}{d}$, as shown in Fig.(1) and Fig.(2) The spatial volume (V) of the model is zero when cosmic time is $t = -\frac{d}{c}$. Depending on the value of q we have the following two cases:

case(i) when $q < -1$: The proposed model starts expanding with the Big Bang singularity at $t = -\frac{d}{c}$. At $t = 0$, both the pressure p and energy density ρ of strange quark matter are constant, and at $t \rightarrow \infty$, both p and ρ become infinite, as shown in Fig. 3(a) and Fig. 4(a). The pressure of strange quark matter (p) and quark matter (p_q), both decreasing functions of time, remains negative throughout the evolution. Negative pressure (p) and (p_q) corresponds to the accelerating expansion of the universe. Also, the pressure p_q and energy density ρ_q for quark matter behave the same as for strange quark matter. The shift in the ρ values than that of p_q is due to the additional term of bag constant in equation (40). In this study, we chose the bag constant as unity, as shown in Fig. 3(b) and Fig. 4(b).

case (ii) when $q > -1$: At cosmic time $t = 0$, the proposed model has constant volume, which increases with an increase in time and becomes infinite at $t \rightarrow \infty$. At $t = 0$, energy density ρ of strange quark matter are constant, and at $t \rightarrow \infty$, it become infinite, as shown in Fig. 5(a) and Fig. 5(b). The energy and pressure profiles for quark and strange quark matter are the same except from the extra bag constant. The bag constant is subtracted for energy density and added for the pressure of quarks.

For $\alpha < 0$, equations (38) to (41) give the real value of pressure and energy density for quark matter and strange quark matter (SQM), and values turn out to be complex for $\alpha > 0$. The anisotropic parameter A_m is nonzero for $k \neq 1$ provided $k \neq -2$, and in such a case, the model does not approach isotropy, but for $k = 1$ provided $k \neq -2$, the mean anisotropic parameter is zero, and the model becomes isotropic. Moreover, the mean anisotropic parameter (A_m) remains constant throughout the evolution of the universe as it is independent of the cosmic time (t). Regarding the current statefinder parameters, the value $\{r, s\} = \{1, 0\}$ generated by our investigation is in the same line with the λ CDM model, which is very close to the recent data [53, 54]

ORCID

 Pravin Bolke, <https://orcid.org/0000-0002-1212-5260>;  Vasudeo Patil, <https://orcid.org/0000-0002-0442-3962>;  Sachin Waghmare, <https://orcid.org/0000-0001-5316-0540>;  Neha Mahajan, <https://orcid.org/0009-0008-3929-5869>

REFERENCES

- [1] A.G. Riess, A.V. Filippenko, P. Challis, A. Clocchiatti, A. Diercks, P.M. Garnavich, R.L. Gilliland, *et al.*, "Observational evidence from supernovae for an accelerating universe and a cosmological constant," *The astronomical journal*, **116**(3), 1009 (1998). <https://doi.org/10.1086/300499>
- [2] S. Perlmutter, G. Aldering, G. Goldhaber, R.A. Knop, P. Nugent, P.G. Castro, S. Deustua, *et al.*, "Measurements of ω and λ from 42 high-redshift supernovae," *The Astrophysical Journal*, **517**(2), 565 (1999). <https://doi.org/10.1086/307221>
- [3] A.G. Riess, L.-G. Strolger, J. Tonry, S. Casertano, H.C. Ferguson, B. Mobasher, P. Challis, *et al.*, "Type Ia supernova discoveries at $z < 1$ from the Hubble Space Telescope: Evidence for past deceleration and constraints on dark energy evolution," *The Astrophysical Journal*, **607**(2), 665 (2004). <https://doi.org/10.1086/383612>
- [4] D.J. Eisenstein, I. Zehavi, D.W. Hogg, R. Scoccimarro, M.R. Blanton, R.C. Nichol, R. Scranton, *et al.*, "Detection of the baryon acoustic peak in the large-scale correlation function of SDSS luminous red galaxies," *The Astrophysical Journal*, **633**(2), 560 (2005). <https://doi.org/10.1086/466512>
- [5] W.J. Percival, B.A. Reid, D.J. Eisenstein, N.A. Bahcall, T. Budavari, J.A. Frieman, M. Fukugita, *et al.*, "Baryon acoustic oscillations in the Sloan Digital Sky Survey data release 7 galaxy sample," *Monthly Notices of the Royal Astronomical Society*, **401**(4), 2148–2168 (2010). <https://doi.org/10.1111/j.1365-2966.2009.15812.x>
- [6] D.N. Spergel, L. Verde, H.V. Peiris, E. Komatsu, M.R.olta, C.L. Bennett, M. Halpern, *et al.*, "First-year Wilkinson Microwave Anisotropy Probe (WMAP) observations: determination of cosmological parameters," *The Astrophysical Journal Supplement Series*, **148**(1), 175 (2003). <https://doi.org/10.1086/377226>
- [7] T. Koivisto, and D. F. Mota, "Dark energy anisotropic stress and large scale structure formation," *Physical Review D*, **73**(8), 083502 (2006). <https://doi.org/10.1103/PhysRevD.73.083502>
- [8] S.F. Daniel, R.R. Caldwell, A. Cooray, and A. Melchiorri, "Large scale structure as a probe of gravitational slip," *Physical Review D*, **77**(10), 103513 (2008). <https://doi.org/10.1103/PhysRevD.77.103513>

- [9] M. Colless, G. Dalton, S. Maddox, W. Sutherland, P. Norberg, S. Cole, J. Bland-Hawthorn, *et al.*, "The 2df galaxy redshift survey: spectra and redshifts," *Monthly Notices of the Royal Astronomical Society*, **328**(4), 1039–1063 (2001). <https://doi.org/10.1046/j.1365-8711.2001.04902.x>
- [10] C.L. Bennett, M. Bay, M. Halpern, G. Hinshaw, C. Jackson, N. Jarosik, A. Kogut, *et al.*, "The microwave anisotropy probe* mission," *The Astrophysical Journal*, **583**(1), 1 (2003). <https://doi.org/10.1086/345346>
- [11] R.R. Caldwell, and M. Doran, "Cosmic microwave background and supernova constraints on quintessence: concordance regions and target models," *Physical Review D*, **69**(10), 103517 (2004). <https://doi.org/10.1103/PhysRevD.69.103517>
- [12] B. Clegg, *Dark matter and dark energy: the hidden 95 of the universe*. (Icon Books, 2019).
- [13] T. Chiba, T. Okabe, and M. Yamaguchi, "Kinetically driven quintessence," *Physical Review D*, **62**(2), 023511 (2000). <https://doi.org/10.1103/PhysRevD.62.023511>
- [14] C. Armendariz-Picon, V. Mukhanov, and P.J. Steinhardt, "Dynamical solution to the problem of a small cosmological constant and late-time cosmic acceleration," *Physical Review Letters*, **85**(21), 4438 (2000). <https://doi.org/10.1103/PhysRevLett.85.4438>
- [15] C. Armendariz-Picon, V. Mukhanov, and P.J. Steinhardt, "Essentials of k-essence," *Physical Review D*, **63**(10), 103510 (2001). <https://doi.org/10.1103/PhysRevD.63.103510>
- [16] M.C. Bento, O. Bertolami, and A.A. Sen, "Generalized chaplygin gas, accelerated expansion, and dark-energy-matter unification," *Physical Review D*, **66**(4), 043507 (2002). <https://doi.org/10.1103/PhysRevD.66.043507>
- [17] A. Kamenshchik, U. Moschella, and V. Pasquier, "An alternative to quintessence," *Physics Letters B*, **511**(2-4), 265–268 (2001). [https://doi.org/10.1016/S0370-2693\(01\)00571-8](https://doi.org/10.1016/S0370-2693(01)00571-8)
- [18] H.A. Buchdahl, "Non-linear lagrangians and cosmological theory," *Monthly Notices of the Royal Astronomical Society*, **150**(1), 1–8 (1970). <https://doi.org/10.1093/mnras/150.1.1>
- [19] T. Harko, F.S.N. Lobo, S. Nojiri, and S.D. Odintsov, " $f(R,T)$ gravity," *Physical Review D*, **84**(2), 024020 (2011). <https://doi.org/10.1103/PhysRevD.84.024020>
- [20] B. Li, J. D Barrow, and D.F. Mota, "Cosmology of modified gauss-bonnet gravity," *Physical Review D*, **76**(4), 044027 (2007). <https://doi.org/10.1103/PhysRevD.76.044027>
- [21] A. De Felice, and S. Tsujikawa, "Construction of cosmologically viable $f(G)$ gravity models," *Physics Letters B*, **675**(1), 1–8 (2009). <https://doi.org/10.1016/j.physletb.2009.03.060>
- [22] K. Bamba, M. Ilyas, M.Z. Bhatti, and Z. Yousaf, "Energy conditions in modified $f(G)$ gravity," *General Relativity and Gravitation*, **49**, 112 (2017). <https://doi.org/10.1007/s10714-017-2276-x>
- [23] Á. De la Cruz-Dombriz, and D. Sáez-Gómez, "On the stability of the cosmological solutions in $f(R,G)$ gravity," *Classical and Quantum Gravity*, **29**(24), 245014 (2012). <https://doi.org/10.1088/0264-9381/29/24/245014>
- [24] M. De Laurentis, M. Paoella, and S. Capozziello, "Cosmological inflation in $f(R,G)$ gravity," *Physical Review D*, **91**(8), 083531 (2015). <https://doi.org/10.1103/PhysRevD.91.083531>
- [25] E.V. Linder, "Einstein's other gravity and the acceleration of the universe," *Physical Review D*, **81**(12), 127301 (2010). <https://doi.org/10.1103/PhysRevD.81.127301>
- [26] K. Bamba, C.-Q. Geng, C.-C. Lee, and L.-W. Luo, "Equation of state for dark energy in $f(T)$ gravity," *Journal of Cosmology and Astroparticle Physics*, **2011**(01), 021 (2011). <https://doi.org/10.1088/1475-7516/2011/01/021>
- [27] B. Li, T.P. Sotiriou, and J.D. Barrow, "Large-scale structure in $f(T)$ gravity," *Physical Review D*, **83**(10), 104017 (2011). <https://doi.org/10.1103/PhysRevD.83.104017>
- [28] Y. Xu, G. Li, T. Harko, and S.-D. Liang, " $f(Q,T)$ gravity," *The European Physical Journal C*, **79**, 708 (2019). <https://doi.org/10.1140/epjc/s10052-019-7207-4>
- [29] T. Harko, and F.S.N. Lobo, " $f(R,L_m)$ gravity," *The European Physical Journal C*, **70**, 373–379 (2010). <https://doi.org/10.1140/epjc/s10052-010-1467-3>
- [30] O. Bertolami, C.G. Boehmer, T. Harko, and F.S.N. Lobo, "Extra force in $f(R)$ modified theories of gravity," *Physical Review D*, **75**(10), 104016 (2007). <https://doi.org/10.1103/PhysRevD.75.104016>
- [31] J. Wang and K. Liao, "Energy conditions in $f(R,L_m)$ gravity," *Classical and Quantum Gravity*, **29**(21), 215016 (2012). [10.1088/0264-9381/29/21/215016](https://doi.org/10.1088/0264-9381/29/21/215016)
- [32] Y.-B. Wu, Y.-Y. Zhao, Y.-Y. Jin, L.-L. Lin, J.-B. Lu, and X. Zhang, "Constraints of energy conditions and dk instability criterion on $f(R,L_m)$ gravity models," *Modern Physics Letters A*, **29**(22), 1450089 (2014). <https://doi.org/10.1142/S0217732314500898>
- [33] T. Harko, F.S.N. Lobo, and O. Minazzoli, "Extended $f(R,L_m)$ gravity with generalized scalar field and kinetic term dependences," *Physical Review D*, **87**(4), 047501 (2013). <https://doi.org/10.1103/PhysRevD.87.047501>
- [34] T. Harko, and M.J. Lake, "Cosmic strings in $f(R,L_m)$ gravity," *The European Physical Journal C-Particles and Fields*, **75**(2), 60 (2015). <https://doi.org/10.1140/epjc/s10052-015-3287-y>
- [35] L.V. Jaybhaye, R. Solanki, S. Mandal, and P.K. Sahoo, "Cosmology in $f(R,L_m)$ gravity," *Physics Letters B*, **831**, 137148 (2022). <https://doi.org/10.1016/j.physletb.2022.137148>
- [36] L.V. Jaybhaye, S. Mandal, and P.K. Sahoo, "Constraints on energy conditions in $f(R,L_m)$ gravity," *International Journal of Geometric Methods in Modern Physics*, **19**(04), 2250050 (2022). <https://doi.org/10.1142/S0219887822500505>

- [37] L.V. Jaybhaye, S. Bhattacharjee, and P.K. Sahoo, "Baryogenesis in $f(R, L_m)$ gravity," *Physics of the Dark Universe*, **40**, 101223 (2023). <https://doi.org/10.1016/j.dark.2023.101223>
- [38] N.S. Kavya, V. Venkatesha, S. Mandal, and P.K. Sahoo, "Constraining anisotropic cosmological model in $f(R, L_m)$ gravity," *Physics of the Dark Universe*, **38**, 101126 (2022). <https://doi.org/10.1016/j.dark.2022.101126>
- [39] D.C. Maurya, "Accelerating scenarios of massive universe in $f(R, L_m)$ -gravity," *New Astronomy*, **100**, 101974 (2023). <https://doi.org/10.1016/j.newast.2022.101974>
- [40] R. Solanki, Z. Hassan, and P.K. Sahoo, "Wormhole solutions in $f(R, L_m)$ gravity," *Chinese Journal of Physics*, **85**, 74–88 (2023). <https://doi.org/10.1016/j.cjph.2023.06.005>
- [41] A.K. Yadav, L.K. Sharma, B.K. Singh, and P.K. Sahoo, "Existence of bulk viscous universe in $f(R, T)$ gravity and confrontation with observational data," *New Astronomy*, **78**, 101382 (2020). <https://doi.org/10.1016/j.newast.2020.101382>
- [42] K.S. Wankhade, A.Y. Shaikh, and S.N. Khan, "Interacting two fluid dark energy bianchi type-i radiating cosmological model in $f(R)$ gravity," *Prespacetime Journal*, **13**(3), (2022).
- [43] V.R. Patil, P.A. Bolke, S.K. Waghmare, and J.L. Pawade. Cosmological power law model and exponential model in $f(R)$ gravity. *Prespacetime Journal*, **14**(6), 2023. <https://prespacetime.com/index.php/pst/article/view/1852/1734>
- [44] V. Singh, and A. Beesham, "LRS Bianchi I model with strange quark matter and $\Lambda(t)$ in $f(R, T)$ gravity," *New Astronomy*, **89**, 101634 (2021). <https://doi.org/10.1016/j.newast.2021.101634>
- [45] A. Pradhan, A. Dixit, and G. Varshney, "LRS bianchi type-i cosmological models with periodic time varying deceleration parameter in $f(R, T)$ gravity," *International Journal of Modern Physics A*, **37**(18), 2250121 (2022). <https://doi.org/10.1142/S0217751X22501214>
- [46] V.R. Patil, P.A. Bolke, S.K. Waghmare, and J.L. Pawde, "Energy conditions and statefinder diagnostic of cosmological model with special law of hubble parameter in $f(R, T)$ gravity," *East European Journal of Physics*, (3), 53–61 (2023). <https://doi.org/10.26565/2312-4334-2023-3-03>
- [47] Y.S. Solanke, A.P. Kale, D.D. Pawar, and V.J. Dagwal, "LRS bianchi type-i cosmological model in $f(Q, T)$ theory of gravity with observational constraints," *International Journal of Geometric Methods in Modern Physics*, **20**(12), 2350212 (2023). <https://doi.org/10.1142/S0219887823502122>
- [48] T. Harko, F.S.N. Lobo, J.P. Mimoso, and D. Pavón, "Gravitational induced particle production through a nonminimal curvature–matter coupling," *The European Physical Journal C*, **75**, 386 (2015). <https://doi.org/10.1140/epjc/s10052-015-3620-5>
- [49] M.S. Berman, "A special law of variation for hubble's parameter," *Nuovo Cimento B Serie*, **74**, 182–186 (1983). <https://doi.org/10.1007/BF02721676>
- [50] V. Sahni, T.D. Saini, A.A. Starobinsky, and U. Alam, "Statefinder—a new geometrical diagnostic of dark energy," *Journal of Experimental and Theoretical Physics Letters*, **77**, 201–206 (2003). <https://doi.org/10.1134/1.1574831>
- [51] U. Alam, V. Sahni, T.D. Saini, and A.A. Starobinsky, "Exploring the expanding universe and dark energy using the statefinder diagnostic," *Monthly Notices of the Royal Astronomical Society*, **344**(4), 1057–1074 (2003). <https://doi.org/10.1046/j.1365-8711.2003.06871.x>
- [52] P.K. Agrawal, and D.D. Pawar, "Plane symmetric cosmological model with quark and strange quark matter in $f(R, T)$ theory of gravity," *Journal of Astrophysics and Astronomy B*, **38**, 2 (2017). <https://doi.org/10.1007/s12036-016-9420-y>
- [53] S.-L. Cao, S. Li, H.-R. Yu, and T.-J. Zhang, "Statefinder diagnostic and constraints on the palatini $f(R)$ gravity theories," *Research in Astronomy and Astrophysics*, **18**(3), 026 (2018). <https://doi.org/10.1088/1674-4527/18/3/26>
- [54] G. Gadbaill, S. Arora, and P.K. Sahoo, "Power-law cosmology in Weyl-type $f(Q, T)$ gravity," *The European Physical Journal Plus*, **136**(10), 1040 (2021). <https://doi.org/10.1140/epjp/s13360-021-02048-w>

Анізотропна космологічна модель із SQM у $f(R, L_m)$ гравітації

Правін Болке^a, Васудео Патіл^b, Сачин Вагмаре^c, Неха Махаджан^b

^a Факультет математики, коледж інженерії та менеджменту імені проф. Рама Меге, Баднера, Дист. Амраваті (MS), Індія

^b Коледж факультету математики, мистецтв, науки та торгівлі, Чикхалдара, округ Амраваті (MS), Індія

^c Департамент математики, TGPSET, Назпур (MS), Індія

Локально обертально-симетрична модель Біанчі-I, заповнена дивною кварковою матерією (SQM), досліджується в $f(R, L_m)$ гравітації як нелінійний функціонал у формі $f(R, L_m) = \frac{R}{2} + L_m^\alpha$, де α — вільний параметр моделі. Ми розглянули спеціальний закон зміни параметра Хаббла, запропонований Берманом (1983), а також використали степеневий зв'язок між масштабними факторами, щоб отримати точний розв'язок рівняння поля, який відповідає моделі Всесвіту. Ми також аналізуємо фізичні та геометричні аспекти кінематичної та динамічної поведінки Всесвіту. Крім того, ми використовуємо параметри рівняння стану (ЕoS) і параметри визначення стану як аналітичні інструменти, щоб отримати уявлення про еволюцію Всесвіту. Ми використовуємо модель Λ CDM як еталон для перевірки результатів. Розмішуючи відхилення Всесвіту від моделі Λ CDM і водночас роблячи важливий внесок у дослідження анізотропної природи $f(R, L_m)$ гравітації в рамках космологічної динаміки, стаття покращує наше розуміння нашої космічної еволюції.

Ключові слова: космологічна модель LRS типу Біанчі-I; $f(R, L_m)$ гравітація; дивна кваркова матерія; космічний час

COSMIC EVOLUTION IN A BIANCHI TYPE-V UNIVERSE WITH BARROW HOLOGRAPHIC DARK ENERGY WITH GRANDA-OLIVEROS LENGTH SCALE AS IR CUTOFF

 Chandra Rekha Mahanta,  Rajashree Mahanta*,  Joy Prakash Medhi

Department of Mathematics, Gauhati University, Guwahati - 781014 (INDIA)

*Corresponding Author e-mail: rajashree.mahanta@gauhati.ac.in

Received June 30, 2024; revised July 26, 2024; accepted August 5, 2024

In this work, we construct a spatially homogeneous and anisotropic Bianchi type-V cosmological model with a hybrid expansion law by considering the universe to be filled with cold dark matter and non-interacting Barrow holographic dark energy with Granda-Oliveros length scale as IR cutoff. The physical and kinematical characteristics of the resulting model are discussed by studying the evolution of various parameters of cosmological importance such as the Hubble parameter, the deceleration parameter, the anisotropic parameter, the equation of state parameter, jerk parameter etc. We also examine whether the energy conditions are satisfied or violated. Our analysis reveals that the Null, Weak, and Dominant energy conditions are fulfilled, while the Strong Energy Condition is violated, which supports the accelerated expansion of the universe. Statefinder diagnostics have also been performed based on recent cosmological observations in order to compare our model with different dark energy cosmological scenario. Additionally, we establish the correspondence between the quintessence scalar field and the Barrow holographic dark energy model, supporting our description of the universe's accelerated expansion.

Keywords: *Cosmic acceleration; Barrow holographic dark energy; Bianchi type-V; Cold dark matter; Deceleration parameter; Equation of state parameter*

PACS: 95.35.+d, 95.36.+x, 98.80.-k, 98.80.Jk, 98.80.Es, 04.20.Jb

1. INTRODUCTION

In the late twentieth century, the observational data from two independent projects, the High-redshift Supernova Search Team led by A. G. Riess [1] and the Supernova Cosmology Project led by S. Perlmutter [2], revealed that the universe is currently in a phase of accelerated expansion. Since then, various astrophysical and cosmological observations such as the temperature anisotropies in the Cosmic Microwave Background (CMB) [3, 4, 5], Large Scale Structure (LSS) such as the galaxy clustering [6, 7, 8], Baryon Acoustic Oscillations (BAO) [9] etc. have been supporting the observed acceleration. The root cause or the source for this bizarre late-time cosmic acceleration has not been identified yet and it remains as a great challenge in modern cosmology even after more than two decades of its discovery. Most of the cosmological models presented in the literature attribute the cosmic acceleration to a component with negative pressure, commonly referred to as dark energy, an enigmatic form of physical entity that dominates the universe and is causing the current universe to enter into an accelerated phase of expansion. The observational data also show that the combined dark components accounts for around 95% of the universe's total energy density, with dark matter (DM), a non-relativistic matter that interacts very weakly with baryonic *i.e.* standard matter particles, contributing about 27% and dark energy (DE) contributing approximately 68% of the entire matter-energy allocation, and only about 5% is ordinary baryonic matter, the most basic model being the concordance model, popularly known as the Λ CDM model, in which dark energy is represented by the cosmological constant Λ , introduced by Einstein in his field equations, although it needs to be fine-tuned to fit the available observational data [10, 11]. As a result, a variety of dynamically evolving scalar field models such as quintessence, k-essence, tachyon, quintom, dilatonic ghost condensate, phantom etc. and exotic fluid models like Chaplygin gas models [12] are proposed in the literature.

Recently, attention has been drawn to a number of holographic dark energy models initially originating from the Holographic Principle proposed by G't Hooft [13] in the context of black hole physics, and on the hypothesis [14] on the mutual relationship between the short distance UV cutoff and IR cutoff. However, the original holographic dark energy models [15, 16, 17] constructed by attributing Bekenstein-Hawking entropy and Hubble horizon could not provide satisfactory explanation for the current accelerated expansion. The density of holographic dark energy, as determined by Li's work [17], is $\rho_D = 3c^2 M_P^2 L^{-2}$, where L is the infrared (IR) cutoff, M_P is the Planck mass and $3c^2$ is a numerical constant. Various appropriate choice of this IR cutoff result in new cosmological problems. The Granda and Oliveros cutoff [18] is utilized in proposing a new holographic dark energy (NHDE) model, where the energy density is expressed as the square of the Hubble parameter and its time derivative. The Tsallis holographic dark energy (THDE) model was developed in 2018 [19] using the Tsallis generalized entropy $S_\delta = \gamma A^\delta$, where δ is a non-additive parameter, A is the event horizon's surface area and γ is a constant [20]. Another holographic dark energy model, known as the Rényi holographic

dark energy (RHDE), was formulated utilizing the Rényi entropy [21]. Barrow [22] has suggested a new approach to black hole entropy, incorporating quantum gravitational effects. This could potentially introduce intricate and fractal properties to the black hole's area, represented by $S_B = \left(\frac{A}{A_0}\right)^{1+\frac{\Delta}{2}}$, where A is the standard horizon area, A_0 is the Planck area, and the exponent Δ , ranging from 0 to 1, quantifies the quantum gravitational deformation. When Δ equals 1, the structure exhibits maximal complexity and fractal characteristics, whereas when Δ equals 0, it corresponds to the standard Bekenstein-Hawking entropy or the standard smooth structure. The standard holographic dark energy density is defined by the inequality $\rho_{HDE} L^4 \leq S$, where ' L ' represents the horizon length. When subjected to the condition $S \propto A \propto L^2$ [23], the Barrow entropy provides the energy density for Barrow holographic dark energy (BHDE) as $\rho_{BHDE} = 3c^2 M_p^2 L^{\Delta-2}$, where ' c^2 ' is the model parameter and ' M_p ' is the Planck mass. Saridakis [24] innovated the BHDE by utilizing the Barrow entropy rather than the standard Bekenstein-Hawking entropy. Furthermore, Srivastava and Sharma [25] explore the flat Friedmann-Lemaître-Robertson-Walker (FLRW) universe by employing the BHDE with the Hubble horizon as the infrared cutoff. The authors in [26], recently investigated the Barrow holographic dark energy with the Granda-Oliveros length serving as the infrared cutoff. The authors in [27] investigated Barrow holographic dark energy within a flat Friedmann-Lemaître-Robertson-Walker (FLRW) universe, employing the Granda-Oliveros length as the infrared cutoff and determined the impact of the deformation parameter Δ on the evolution of $H(z)$. When Paul *et al.* [28] examined the Bianchi type-I universe in the presence of BHDE, they found that the new exponent is crucial in determining the nature of the universe.

The Friedmann-Lemaître-Robertson-Walker model characterizes the universe as homogeneous and isotropic on a large scale. But it is essential to note that there is no observable evidence definitively excluding the existence of an anisotropic universe. Anisotropic cosmological models [29, 30, 31] have gained prominence due to observations of the Cosmic Microwave Background Radiation (CMBR) and the formation of Helium in the early stages of the universe's evolution. The presence of anisotropy in cosmic expansion is a significant factor, supported by critical arguments and experimental data suggesting the existence of an anisotropic phase transitioning towards isotropy over time. Hence, it is crucial to consider models incorporating an anisotropic background. Spatially homogeneous and anisotropic Bianchi models are commonly taken into consideration to gain a better understanding of the dynamics of the expanding universe. This is because they are the most basic models with an anisotropic background and are important in explaining the large-scale behavior of the universe. In order to properly connect the homogeneous and isotropic FLRW models with the inhomogeneous and anisotropic models, Bianchi type models provide means of incorporating the influence of anisotropy. As a result, a large number of scholars have investigated anisotropic and spatially homogeneous Bianchi cosmological models in many contexts.

In this study, we develop a cosmological model of Bianchi type-V, which is both spatially homogeneous and anisotropic. This model incorporates a hybrid expansion law, assuming the universe to be filled with cold dark matter and non-interacting Barrow holographic dark energy with the Granda-Oliveros length scale serving as the IR cutoff. The paper is structured in the following manner: In section 2, we derive the Einstein field equations for the Bianchi type-V metric. In Section 3, exact solutions to the field equations are obtained by employing a hybrid expansion law. Furthermore, we consider several cosmologically relevant parameters. In section 4, we examine the model's kinematical and physical characteristics as well as its energy conditions. In Section 5, we explore the Statefinder diagnostics and examine its consequences. In Section 6, we explore the correlation between BHDE and a quintessence scalar field. In Section 7, we provide concluding remarks on our findings.

2. THE METRIC AND BASIC FIELD EQUATIONS

We consider the spatially homogeneous and anisotropic Bianchi type-V universe characterised by the metric:

$$ds^2 = -dt^2 + A^2 dx^2 + e^{2\eta x} \{B^2 dy^2 + C^2 dz^2\} \quad (1)$$

where η is a positive constant and $A(t)$, $B(t)$ and $C(t)$ are the directional scale factors with t being the cosmic time.

With natural units of ($8\pi G = 1, c = 1$), the Einstein field equations are given by

$$R_{ij} - \frac{1}{2} g_{ij} R = T_{ij} \quad (2)$$

where R_{ij} is the Ricci tensor, g_{ij} is the metric tensor, $R = g^{ij} R_{ij}$ is the Ricci scalar curvature and T_{ij} is the energy momentum tensor of the cosmic fluid.

We consider the universe to be filled with a mixture of pressureless cold dark matter and non-interacting Barrow holographic dark energy with Granda Oliveros (GO) length scale as IR cutoff given by

$$\rho_{BHDE} = 3 \left(\alpha H^2 + \beta \dot{H} \right)^{\frac{2-\Delta}{2}} \quad (3)$$

where ρ_{BHDE} is the energy density of Barrow holographic dark energy (BHDE) and $[L]^{\frac{-2\Delta}{2-\Delta}}$ is the dimension of the

constant parameters α and β . H represents the Hubble parameter.

The energy-momentum tensor T_{ij} can be written as

$$T_{ij} = \rho_m u_i u_j + (\rho_{BHDE} + p_{BHDE}) u_i u_j + g_{ij} p_{BHDE} \tag{4}$$

where ρ_m represents the energy density of cold dark matter, ρ_{BHDE} and p_{BHDE} are the energy density and pressure of Barrow holographic dark energy, respectively and u_i is the four velocity satisfying $u^i u_i = -1$.

In a comoving coordinate system, the Einstein field equations (2), along with equation (4) for the metric (1), result in the following system of field equations:

$$\frac{\ddot{B}}{B} + \frac{\ddot{C}}{C} + \frac{\dot{B}\dot{C}}{BC} - \frac{\eta^2}{A^2} = -p_{BHDE} \tag{5}$$

$$\frac{\ddot{A}}{A} + \frac{\ddot{C}}{C} + \frac{\dot{A}\dot{C}}{AC} - \frac{\eta^2}{A^2} = -p_{BHDE} \tag{6}$$

$$\frac{\ddot{A}}{A} + \frac{\ddot{B}}{B} + \frac{\dot{A}\dot{B}}{AB} - \frac{\eta^2}{A^2} = -p_{BHDE} \tag{7}$$

$$\frac{\dot{A}\dot{B}}{AB} + \frac{\dot{A}\dot{C}}{AC} + \frac{\dot{B}\dot{C}}{BC} - \frac{3\eta^2}{A^2} = \rho_m + \rho_{BHDE} \tag{8}$$

$$\frac{2\dot{A}}{A} - \frac{\dot{B}}{B} - \frac{\dot{C}}{C} = 0 \tag{9}$$

where a dot above indicates a differentiation with respect to t .

From equation (9), we obtain:

$$A^2 = BC \tag{10}$$

The conservation of energy-momentum yields

$$\dot{\rho}_m + \dot{\rho}_{BHDE} + 3H(\rho_m + \rho_{BHDE} + p_{BHDE}) = 0 \tag{11}$$

We can divide equation (11) into the following two continuity equations as the BHDE and cold dark matter are non-interacting:

$$\dot{\rho}_m + 3H\rho_m = 0 \tag{12}$$

$$\dot{\rho}_{BHDE} + 3H(\rho_{BHDE} + p_{BHDE}) = 0 \tag{13}$$

3. COSMOLOGICAL SOLUTIONS OF THE FIELD EQUATIONS

From Einstein's field equations (5) – (8), we obtain:

$$\frac{A}{B} = d_1 e^{k_1 \int a^{-3} dt} \tag{14}$$

$$\frac{A}{C} = d_2 e^{k_2 \int a^{-3} dt} \tag{15}$$

$$\frac{B}{C} = d_3 e^{k_3 \int a^{-3} dt} \tag{16}$$

where $d_1, d_2, d_3, k_1, k_2, k_3$ are the constants of integration and a is the average scale defined by.

$$a = (ABC)^{\frac{1}{3}} \tag{17}$$

which parameterizes the universe's relative expansion.

The metric functions from equations (14) – (16) and (10) can be directly obtained as

$$A = a \quad (18)$$

$$B = ma e^{l \int a^{-3} dt} \quad (19)$$

$$C = \frac{a}{m} e^{-l \int a^{-3} dt} \quad (20)$$

$$\text{where } m = (d_2 d_3)^{\frac{1}{3}}, \quad l = \frac{k_2 + k_3}{3}, \quad d_2 = d_1^{-1}, \quad k_2 = -k_1 \quad (21)$$

To derive a complete solution for the field equations, we take into account a hybrid expansion law in the form:

$$a = a_0 \left(t^k e^t \right)^{\frac{1}{n}} \quad (22)$$

where a_0 , k and n are positive constants.

Using (22) in (18), (19), (20), we then obtain

$$A = a_0 \left(t^k e^t \right)^{\frac{1}{n}} \quad (23)$$

$$B = ma_0 \left(t^k e^t \right)^{\frac{1}{n}} e^{lF(t)} \quad (24)$$

$$C = \frac{a_0}{m} \left(t^k e^t \right)^{\frac{1}{n}} e^{-lF(t)} \quad (25)$$

where $F(t) = \int a_0 \left(t^k e^t \right)^{\frac{-3}{n}} dt$.

4. PHYSICAL AND KINEMATICAL PROPERTIES OF THE MODEL

In order to comprehend the universe's evolution, we now introduce a few cosmic parameters: the mean Hubble parameter H , which determines the universe's rate of expansion, the spatial volume V , the scalar expansion (θ), shear scalar (σ), average anisotropic parameter (A_m) defined for the metric(1) by

$$V = a^3 = ABC \quad (26)$$

$$H = \frac{1}{3} (H_1 + H_2 + H_3) \quad (27)$$

$$\theta = 3H \quad (28)$$

$$\sigma^2 = \frac{1}{3} \left[\left(\frac{\dot{A}}{A} \right)^2 + \left(\frac{\dot{B}}{B} \right)^2 + \left(\frac{\dot{C}}{C} \right)^2 - \frac{\dot{A}\dot{B}}{AB} - \frac{\dot{B}\dot{C}}{BC} - \frac{\dot{C}\dot{A}}{CA} \right] \quad (29)$$

$$A_m = \frac{1}{3} \sum_{i=1}^3 \left(\frac{H_i - H}{H} \right)^2 \quad (30)$$

where the directional Hubble parameters along the three spatial directions x , y , and z , are respectively, $H_1 = \frac{\dot{A}}{A}$, $H_2 = \frac{\dot{B}}{B}$, $H_3 = \frac{\dot{C}}{C}$.

The universe's relative rate of expansion (or contraction) is measured by the expansion scalar θ , its deformation due to density fluctuations is measured by the shear scalar σ , and its divergence from isotropy is measured by the anisotropy parameter A_m .

The directional Hubble parameters and the mean Hubble parameter (H) are obtained for the metric in (1) as :

$$H_1 = \frac{\dot{A}}{A} = \frac{k+t}{nt} \tag{31}$$

$$H_2 = \frac{\dot{B}}{B} = \frac{k+t}{nt} + lF'(t) \tag{32}$$

$$H_3 = \frac{\dot{C}}{C} = \frac{k+t}{nt} - lF'(t) \tag{33}$$

$$H = \frac{1}{3} \left(\frac{\dot{A}}{A} + \frac{\dot{B}}{B} + \frac{\dot{C}}{C} \right) = \frac{k+t}{nt} \tag{34}$$

The evolution of the Hubble parameter (H) with respect to cosmic time t are shown in figure 1. We can see from the figure that, for all values of n and k , H diverges at $t = 0$ and then decreases with cosmic time t .

The deceleration parameter can be found as follows using the relation $q = \frac{-a\ddot{a}}{\dot{a}^2}$:

$$q = \frac{kn}{(k+t)^2} - 1 \tag{35}$$

The dynamics of deceleration parameter (q) is determined by the two free parameters, n and k , as shown in Figure 2. The universe is accelerating from the beginning for $n = 1, k = 1.5$ (Red solid line) and $n = 0.5, k = 1$ (Green solid line); but, for $n = 1.1, k = 1$ (Blue solid line) and $n = 1.05, k = 1$ (Black solid line), it is transitioning from an early decelerating phase to the current accelerating phase. It is noted that our model is transitioning from the deceleration phase to the acceleration phase for $0 < \frac{k}{n} < 1$. Furthermore, current SNIa data reveal that the universe is expanding and that the deceleration parameter's value falls somewhere between the interval $-1 < q < 0$.

We select $n = 1.1$ and $k = 1$ for plotting the graphs of the cosmological parameters to study their behaviour as the universe evolves. This is the most appropriate choice as we are looking for a model that describes the universe from early decelerating phase to current accelerating phase.

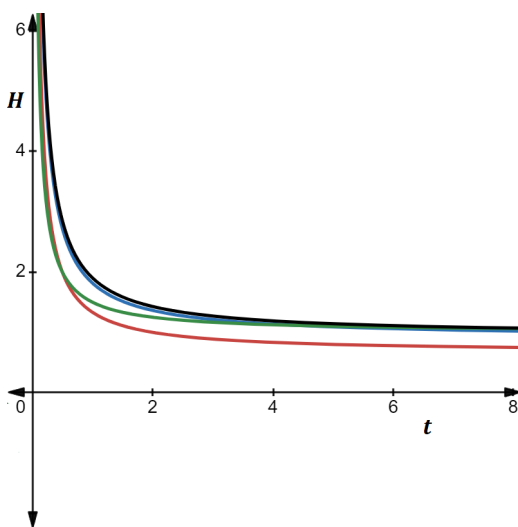


Figure 1. Plotting the Hubble parameter (H) vs cosmic time (t) for $n = 1, k = 1.5$ (Red solid line) , $n = 0.5, k = 1$ (Green solid line), $n = 1.1, k = 1$ (Blue solid line) and $n = 1.05, k = 1$ (Black solid line)

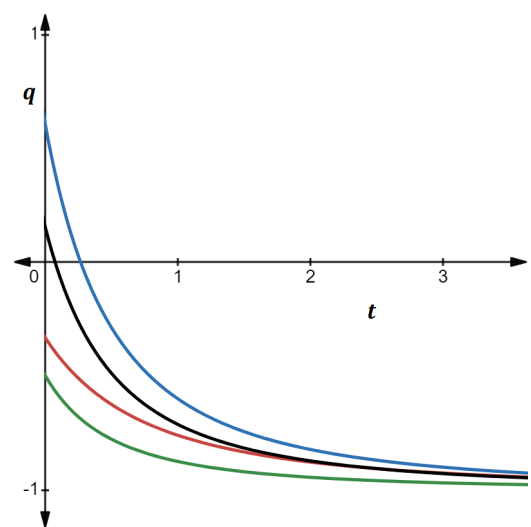


Figure 2. Plotting the deceleration parameter (DP) vs cosmic time (t) for $n = 1, k = 1.5$ (Red solid line) , $n = 0.5, k = 1$ (Green solid line), $n = 1.1, k = 1$ (Blue solid line) and $n = 1.05, k = 1$ (Black solid line)

For our model, the spatial volume V , shear scalar σ , expansion scalar θ , and average anisotropy parameter A_m are determined as follows:

$$V = a_0^3 \left(t^k e^t \right)^{\frac{3}{n}} \quad (36)$$

$$\sigma^2 = \frac{l^2}{\left(t^k e^t \right)^{\frac{6}{n}}} \quad (37)$$

$$\theta = 3 \left(\frac{k+t}{nt} \right) \quad (38)$$

$$A_m = \frac{2}{3} \frac{l^2 \left(t^k e^t \right)^{\frac{-6}{n}}}{\left(\frac{k+t}{nt} \right)^2} \quad (39)$$

From equations (36)–(39), we may infer that at the beginning of the universe, the spatial volume V is zero. Therefore, the Big Bang singularity is where our model begins. Both the shear scalar σ and the expansion scalar θ diverge at $t = 0$ and decrease as cosmic time t increases up to a fixed limit. The anisotropic parameter (A_m) varies with cosmic time, as seen in figure 3. It is demonstrated that for sufficiently long times, A_m diminishes with time and tends to zero for large t . As a result, the universe's anisotropic behavior eventually ends, and the derived model can produce the universe's observed isotropy.

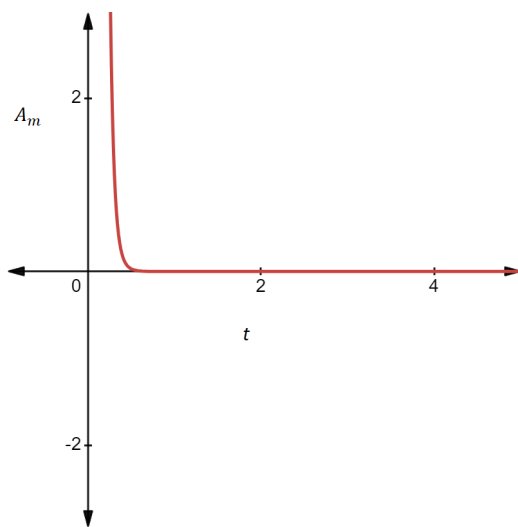


Figure 3. Plotting the anisotropic parameter vs cosmic time (t) for $n = 1.1$ and $k = 1$

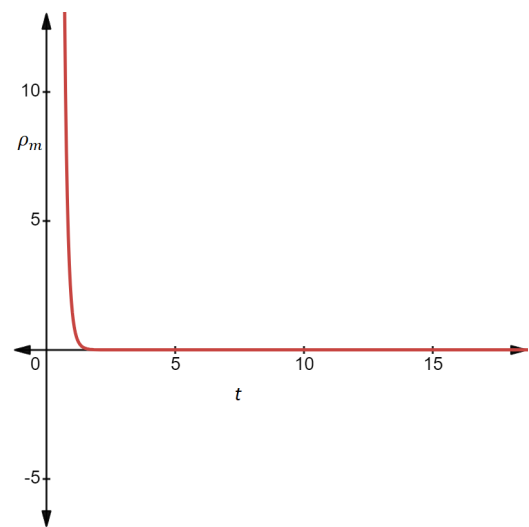


Figure 4. Plotting the matter energy density vs cosmic time (t) for $c_1 = 100$, $n = 1.1$ and $k = 1$

Using equation (34), from equations (12) and (3), we obtain

$$\rho_m = c_1 t^{-\frac{3k}{n}} e^{-\frac{3t}{n}} \quad (40)$$

where c_1 is the integration constant.
And

$$\rho_{BHDE} = 3 \left(\alpha \left(\frac{k+t}{nt} \right)^2 + \beta \left(\frac{-k}{nt^2} \right)^{\frac{2-\Delta}{2}} \right) \quad (41)$$

We can see that both the energy densities are decreasing functions of cosmic time t . The evolution of the matter energy density (ρ_m) is shown in Figure 4, showing that it is large in the early stages of the universe and tends to zero in the later stages. For $\Delta = 0$, the BHDE density provided by equation (41) behaves like the standard HDE. A different cosmic scenario will arise from the deviation of BHDE's behavior from the standard one, contingent on the Δ parameter. Plotting

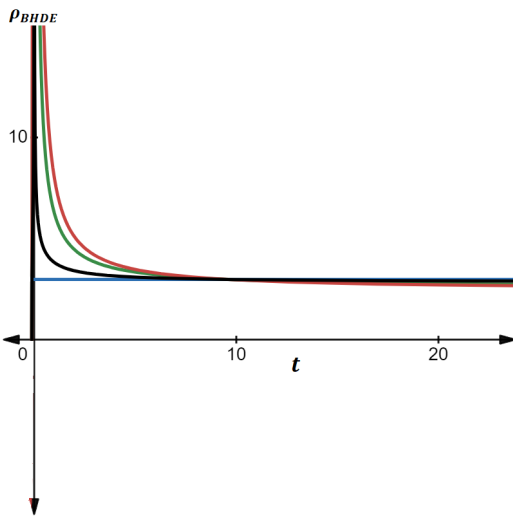


Figure 5. Plotting the Barrow HDE density vs cosmic time (t) for $\alpha = 1, \beta = 0.7$ with $\Delta = 0$ (Red solid line), $\Delta = 0.5$ (Green solid line), $\Delta = 1.5$ (Black solid line) and $\Delta = 2$ (Blue solid line)

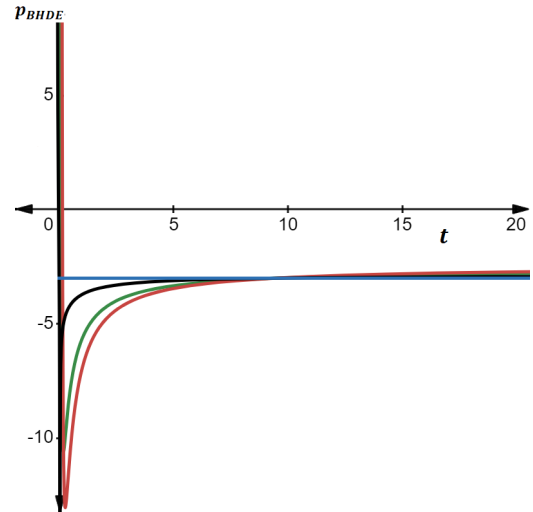


Figure 6. Plotting the Barrow HDE pressure p_{BHDE} vs cosmic time (t) for $\alpha = 1, \beta = 0.7$ with $\Delta = 0$ (Red solid line), $\Delta = 0.5$ (Green solid line), $\Delta = 1.5$ (Black solid line) and $\Delta = 2$ (Blue solid line)

BHDE against cosmic time t for various values of Δ allows us to comprehend its evolution. Figure 5 illustrates that the BHDE density decreases as cosmic time t increases for values of $\Delta = 0, 0.5$ and 1.5 , and eventually tends to a constant value. The BHDE density, on the other hand, remains constant throughout the evolution of the universe for $\Delta = 2$. In this case, the model is referred to as the Λ CDM model, and the BHDE acts like a cosmological constant. Volume of the universe is increasing, according to the physical consequences of the decline in energy densities.

We obtain pressure p_{BHDE} of the Barrow HDE as follows by using equations (34) and (41) in equation (13) as

$$p_{BHDE} = - \left[\alpha \left(\frac{k+t}{nt} \right)^2 + \beta \left(\frac{-k}{nt^2} \right) \right]^{\frac{-\Delta}{2}} \left[\frac{(2-\Delta)nt}{k+n} \left(-\alpha k \left(\frac{n+k}{n^2 t^3} \right) + \frac{\beta k}{nt^3} \right) + 3 \left(\alpha \left(\frac{k+t}{nt} \right)^2 + \beta \left(\frac{-k}{nt^2} \right) \right) \right] \quad (42)$$

Equation (42) gives the Barrow holographic dark energy pressure (p_{BHDE}) with respect to cosmic time t , which is shown in Figure 6. For $\Delta = 0, 0.5$ and 1.5 , the pressure p_{BHDE} is extremely negative at the beginning and rises gradually as cosmic time t increases until it reaches a certain constant value. However for $\Delta = 2$, the pressure is constantly negative in the entire evolution of the universe. This indicates that the universe is undergoing accelerated expansion for all the values of Δ , as the pressure remains negative throughout the evolution.

Equation of state parameter (EoS parameter) ω_{BHDE} of Barrow HDE is determined as follows by using equations (41) and (42).

$$\omega_{BHDE} = \frac{p_{BHDE}}{\rho_{BHDE}} = -1 + \frac{(\Delta - 2) \frac{k}{nt^2} \left(\frac{\beta}{t} - \alpha \left(\frac{k+t}{nt} \right) \right)}{\left(\frac{k+t}{nt} \right) \left[\alpha \left(\frac{k+t}{nt} \right)^2 - \frac{\beta k}{nt^2} \right]} \quad (43)$$

According to equation (43), when $\Delta < 2$, the EoS parameter ω_{BHDE} in our model is a strictly decreasing function of cosmic time t . For various values of Δ , Figure 7 shows how the EoS parameter ω_{BHDE} varies with cosmic time t . The graph shows that, after a specific point in time throughout its evolution, initially the EoS parameter ω_{BHDE} in our model varies in the quintessence region $\left(-1 < \omega_{BHDE} < -\frac{1}{3} \right)$ for $\Delta = 0, 0.5$, and 1.5 and after 5 billion years (approx), the EoS parameter ω_{BHDE} eventually approaches the Λ CDM ($\omega_{BHDE} = -1$) model as it converges to -1 at late times. With $\Delta = 2$, the evolution of the EoS parameter ω_{BHDE} never changes and always has a value of -1 . The Barrow holographic dark energy behaves like the cosmological constant Λ , as was previously mentioned. After taking into account every scenario in our model, we can say that the expansion rate will accelerate more with large values of cosmic time t .

The total energy density is obtained from equations (34), (40) and (41) as

$$\Omega = \frac{\rho_m}{3H^2} + \frac{\rho_{BHDE}}{3H^2} = \Omega_m + \Omega_{BHDE}$$

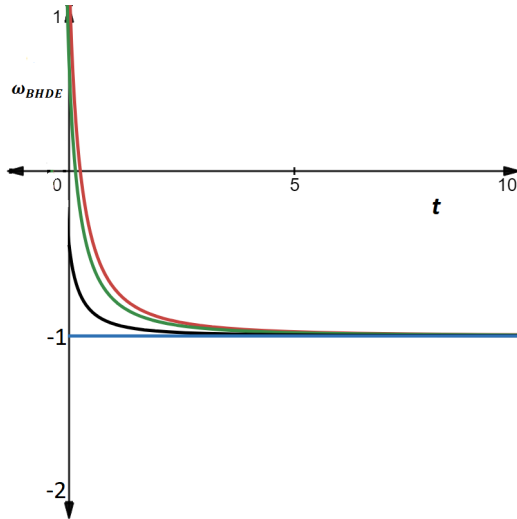


Figure 7. Plotting the equation of state parameter (EoS parameter) ω_{BHDE} vs cosmic time (t) for $\alpha = 1, \beta = 0.7$ with $\Delta = 0$ (Red solid line), $\Delta = 0.5$ (Green solid line), $\Delta = 1.5$ (Black solid line) and $\Delta = 2$ (Blue solid line)

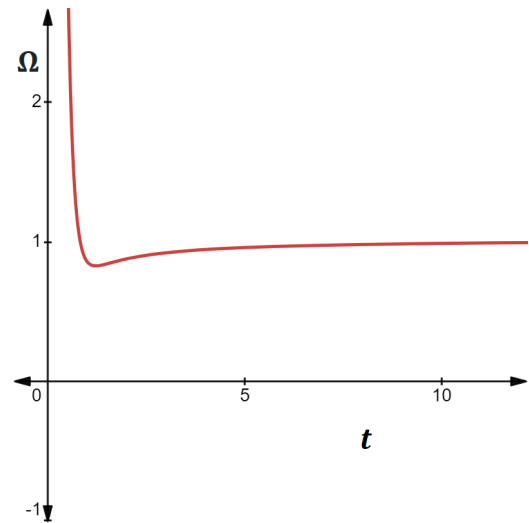


Figure 8. Plotting the total energy density parameter (Ω) vs cosmic time (t) for $\alpha = 1, \beta = 0.7, c_1 = 100$ with $\Delta = 0.5$

$$= \frac{c_1 t^{-\frac{3k}{n}} e^{-\frac{3t}{n}}}{3 \left(\frac{k+t}{nt}\right)^2} + \frac{\left(\alpha \left(\frac{k+t}{nt}\right)^2 + \beta \left(\frac{-k}{nt^2}\right)\right)^{\frac{2-\Delta}{2}}}{\left(\frac{k+t}{nt}\right)^2} \quad (44)$$

The total energy density Ω varies throughout cosmic time t as seen in the graph shown in Figure 8. The parameters denoting the total energy density, $\Omega > 1$, $\Omega = 1$, and $\Omega < 1$, respectively, correspond to the open, flat, and closed universe. The overall density parameter Ω decreases with time, as the figure shows. The universe eventually becomes flat at later times, as indicated by the total density parameter Ω eventually approaching 1.

4.1. Jerk parameter (j)

The universe's acceleration, or how quickly the rate of expansion is changing throughout cosmic time t , is measured by the cosmic jerk parameter, j . It is a dimensionless quantity that gives crucial information on the universe's expansion and is defined as the third derivative of the scale factor a with respect to cosmic time t . The universe transitions from an era of decelerated expansion to one of accelerated expansion, when the jerk parameter, j , is positive. The jerk parameter j for the widely used Λ CDM model has a value of one.

The jerk parameter j is defined mathematically as

$$j = \frac{1}{aH^3} \frac{d^3 a}{dt^3} \quad (45)$$

We derive the jerk parameter j for our model as

$$j = \frac{\left(\frac{1}{n}\right)^3 + \frac{3k}{n^3} + \frac{3k}{n^2} \left(\frac{k}{n} - 1\right) + \frac{k}{n} \left\{ \left(\frac{k}{n}\right)^2 - 3\left(\frac{k}{n}\right) + 2 \right\}}{\left(\frac{t+k}{nt}\right)^3} \quad (46)$$

Figure 9 displays the graph of the jerk parameter j . It is clear from the figure that the jerk parameter j stays positive during the universe's evolution, indicating a growing rate of expansion. Furthermore, figure 9 shows that the jerk parameter j converges to 1 at late times, suggesting that the model mimics the behavior of the Λ CDM model.

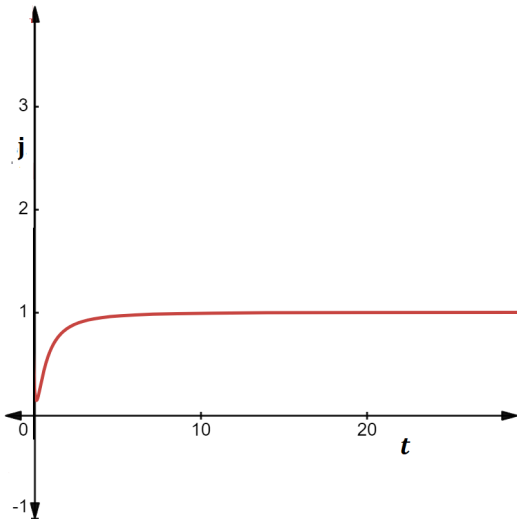


Figure 9. Plotting the jerk parameter vs cosmic time (t) for $n = 1.1$ and $k = 1$

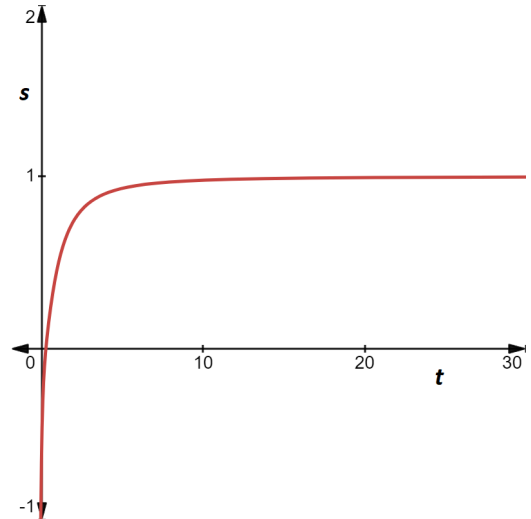


Figure 10. Plotting the snap parameter vs cosmic time (t) for $n = 1.1$ and $k = 1$

4.2. Snap parameter(s):

The fourth order derivative of the scale factor a with respect to cosmic time t is known as the snap parameter (s), a dimensionless quantity. It aids in understanding the dynamics of the universe by describing the pace at which the acceleration of the universe’s expansion is changing. Mathematically, the snap parameter (s) is defined as

$$s = \frac{1}{aH^4} \frac{d^4 a}{dt^4} \tag{47}$$

The snap parameter (s) for our model is found as

$$s = \frac{\left(\frac{1}{n}\right)^4 + \frac{4k}{n^4} + \frac{6k}{n^3} \left(\frac{k}{n} - 1\right) + \frac{4k}{n^2} \left(\left(\frac{k}{n}\right)^2 - 3\left(\frac{k}{n}\right) + 2\right) + \frac{\left(\frac{k}{n}\right)^4 - 6\left(\frac{k}{n}\right)^3 + 11\left(\frac{k}{n}\right)^2 - 6\left(\frac{k}{n}\right)}{t^4}}{\left(\frac{k+t}{nt}\right)^4} \tag{48}$$

The variation of the snap parameter s with respect to cosmic time t is shown in Figure 10. The increasing behavior is displayed by the snap parameter (s). It is negative when $t \rightarrow 0$ and increases with cosmic time t . Eventually, the snap parameter s converges to 1 at late times. This indicates an accelerated expansion phase of the universe.

4.3. Lerk parameter(l):

Another dimensionless quantity is the lerk parameter l , which is the fifth order derivative of the scale factor a with respect to cosmic time t .

The lerk parameter l is described mathematically as

$$l = \frac{1}{aH^5} \frac{d^5 a}{dt^5} \tag{49}$$

We derive the lerk parameter l for our model as

$$l = \frac{\left(\frac{1}{n}\right)^5 + \frac{5k}{n^5} + \frac{10k}{n^4} \left(\frac{k}{n} - 1\right) + \frac{10\left(\frac{k}{n^3}\right) \left(\left(\frac{k}{n}\right)^2 - 3\left(\frac{k}{n}\right) + 2\right) + 5\left(\frac{k}{n^2}\right) \left(\left(\frac{k}{n}\right)^3 - 6\left(\frac{k}{n}\right)^2 + 11\left(\frac{k}{n}\right) - 6\right) + \frac{\left(\frac{k}{n}\right)^5 - 10\left(\frac{k}{n}\right)^4 + 35\left(\frac{k}{n}\right)^3 - 50\left(\frac{k}{n}\right)^2 + 24\left(\frac{k}{n}\right)}{t^5}}{\left(\frac{t+k}{nt}\right)^5} \tag{50}$$

The variation of the lerk parameter l with respect to cosmic time t is shown in Figure 11. The figure illustrates that the lerk parameter, l , is high at $t \rightarrow 0$ and decreases progressively as cosmic time t , increases. At late times, it converges to 1.

4.4. Energy conditions:

In the context of general relativity, energy conditions are a collection of theoretical inequalities which operate as linear combinations of energy density and pressure that describe the behavior of energy and matter in a given spacetime. These conditions are derived from the Einstein field equations of general relativity and play a crucial role in understanding the properties and evolution of the universe. They often place constraints on the possible forms of energy and matter that can exist in the universe. There are several types of energy conditions, each with its own implications for the nature of matter and energy in the universe. The null energy condition (NEC), the weak energy condition (WEC), the strong energy condition (SEC), and the dominant energy condition (DEC) are the linear energy conditions among them.

The four energy conditions are as follows:

$$\text{Null energy condition(NEC)} \Leftrightarrow (\rho + p) \geq 0 \quad (51)$$

$$\text{Weak energy condition(WEC)} \Leftrightarrow (\rho \geq 0) \text{ and } (\rho + p \geq 0) \quad (52)$$

$$\text{Strong energy condition(SEC)} \Leftrightarrow (\rho + 3p \geq 0) \text{ and } (\rho + p \geq 0) \quad (53)$$

$$\text{Dominant energy condition(DEC)} \Leftrightarrow (\rho \geq 0) \text{ and } (\rho \pm p \geq 0) \quad (54)$$

For our model,

$$\rho = \rho_m + \rho_{BHDE} \quad \text{and} \quad p = p_{BHDE}$$

consequently,

$$\rho + p = c_1 t^{\frac{-3k}{n}} e^{\frac{-3t}{n}} - \left(\alpha \left(\frac{k+t}{nt} \right)^2 + \beta \left(\frac{-k}{nt^2} \right) \right)^{-\frac{\Delta}{2}} \cdot \left[\frac{(2-\Delta)nt}{k+n} \left\{ -\alpha k \left(\frac{n+k}{n^2 t^3} \right) + \frac{\beta k}{nt^3} \right\} \right] \quad (55)$$

$$\rho - p = c_1 t^{\frac{-3k}{n}} e^{\frac{-3t}{n}} + \left(\alpha \left(\frac{k+t}{nt} \right)^2 + \beta \left(\frac{-k}{nt^2} \right) \right)^{-\frac{\Delta}{2}} \cdot \left[\frac{(2-\Delta)nt}{k+n} \left\{ -\alpha k \left(\frac{n+k}{n^2 t^3} \right) + \frac{\beta k}{nt^3} \right\} + 6 \left\{ \alpha \left(\frac{k+t}{nt} \right)^2 - \frac{\beta k}{nt^2} \right\} \right] \quad (56)$$

$$\rho + 3p = c_1 t^{\frac{-3k}{n}} e^{\frac{-3t}{n}} - 3 \left(\alpha \left(\frac{k+t}{nt} \right)^2 + \beta \left(\frac{-k}{nt^2} \right) \right)^{-\frac{\Delta}{2}} \cdot \left[\frac{(2-\Delta)nt}{k+n} \left\{ -\alpha k \left(\frac{n+k}{n^2 t^3} \right) + \frac{\beta k}{nt^3} \right\} + 2 \left\{ \alpha \left(\frac{k+t}{nt} \right)^2 - \frac{\beta k}{nt^2} \right\} \right] \quad (57)$$

However, the SEC is known to be violated in an accelerated expansion phase of the universe. Figure 12 shows a plot of the energy conditions, which indicates that in our model, initially, the NEC, WEC, SEC and DEC are all satisfied, but at late times, the SEC gets violated. The violation of the SEC results in the acceleration of the universe.

4.5. Coincidence parameter (\bar{r}):

The coincidence parameter, symbolized by \bar{r} , is a measure representing the ratio between two energy densities within the universe, namely $\bar{r} = \frac{\rho_{BHDE}}{\rho_m}$. According to current data, the coincidence parameter's value must either stay constant or vary very slowly as the universe expands. However, the simplest and most widely acknowledged dark energy model, the Λ CDM model, doesn't align with these observations. Numerous different models are therefore taken into consideration to get over this problem of coincidence.

The coincidence parameter (\bar{r}) for our model can be found as

$$\bar{r} = \frac{3 \left(\alpha \left(\frac{k+t}{nt} \right)^2 + \beta \left(\frac{-k}{nt^2} \right) \right)^{\frac{2-\Delta}{2}}}{c_1 t^{\frac{-3k}{n}} e^{\frac{-3t}{n}}} \quad (58)$$

The graph in Figure 13 illustrates the change in the coincidence parameter \bar{r} over cosmic time t . It's evident that \bar{r} increases rapidly in later stages, indicating that our model doesn't resolve the coincidence problem. As we've assumed no interaction between BHDE and dark matter, exploring an interacting model could be insightful. Therefore, a specific form

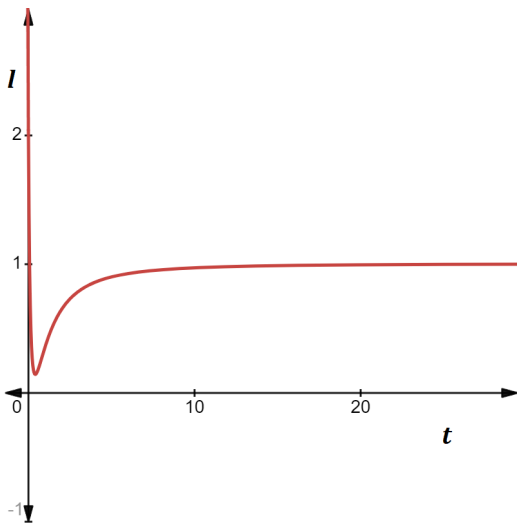


Figure 11. Plotting the lerk parameter vs cosmic time (t) for $n = 1.1$ and $k = 1$

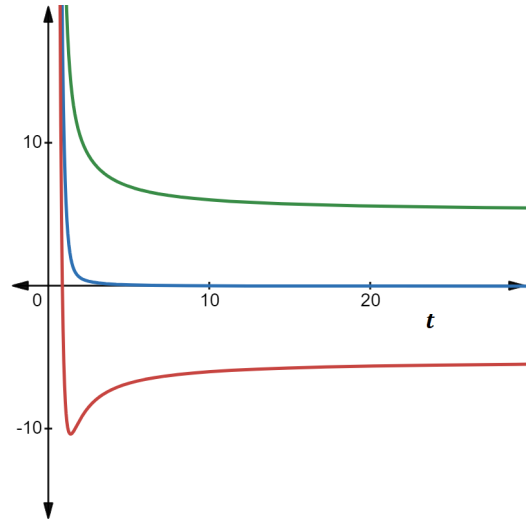


Figure 12. Plotting the energy conditions vs cosmic time (t) for $n = 1.1, k = 1, c_1 = 100, \Delta = 0.5, \alpha = 1, \beta = 0.7, \rho + p$ (blue line), $\rho - p$ (green line), $\rho + 3p$ (red line)

of interaction between Barrow holographic dark energy and dark matter might keep their density ratios relatively constant over the course of the universe’s evolution.

5. STATEFINDER DIAGNOSTIC

In order to differentiate between different dark energy-related cosmological scenarios, a precise and robust method for evaluating DE models is important. In order to do this, Sahni *et al.* [32] proposed the Statefinder diagnostic, that uses the parameter pair $\{r, s\}$. Different dark energy models, including the cosmological constant, quintessence, Chaplygin gas, braneworld models, and models with interacting dark energy, can be effectively distinguished by the pair. The construction of the dimensionless Statefinder diagnostic involves taking into account the universe’s scale factor a and its higher order derivative just with regard to cosmic time t . The parameter r represents the hierarchy of geometrical cosmological parameters, succeeding the Hubble parameter H and the deceleration parameter q . The parameter s , on the other hand, is independent of the density associated to dark energy as it is obtained as a linear combination of q and r . The definition of the Statefinder diagnostic pair $\{r, s\}$ is

$$r = \frac{1}{aH^3} \frac{d^3 a}{dt^3} \quad \text{and} \quad s = \frac{r - 1}{3(q - \frac{1}{2})}, \quad \text{where} \quad q \neq \frac{1}{2} \tag{59}$$

In case of our model, r and s are found to be as

$$r = \frac{\left(\frac{1}{n}\right)^3 + \frac{3k}{n^3} + \frac{3k}{n^2} \frac{(k-1)}{t^2} + \frac{k}{n} \left\{ \left(\frac{k}{n}\right)^2 - 3\left(\frac{k}{n}\right) + 2 \right\}}{\left(\frac{t+k}{nt}\right)^3} \tag{60}$$

$$s = \frac{-6\left(\frac{k}{n^2}\right)t - 6\left(\frac{k}{n}\right)^2 + 4\left(\frac{k}{n}\right)}{3\left(\frac{1}{n}\right)(t+k) \left\{ 2\left(\frac{k}{n}\right) - 3\left(\frac{1}{n}t + \frac{k}{n}\right)^2 \right\}} \tag{61}$$

For these cosmological parameters, the $r - s$ plane is $(1, 0)$ for Λ CDM and $(1, 1)$ for standard CDM(SCDM). While the trajectories for Chaplygin gas are located in the range $(r > 1, s < 0)$, the quintessential dark energy epochs are represented by the region $(r < 1, s > 0)$. The Statefinder diagnostic pair in our model is dependent on the cosmic time t , as shown by equations (60) and (61). The diagnostic pair results in $r = 1$ and $s = 0$ as t approaches infinity. Additionally, figure 14 verifies that later stages of our model coincide with the Λ CDM model.

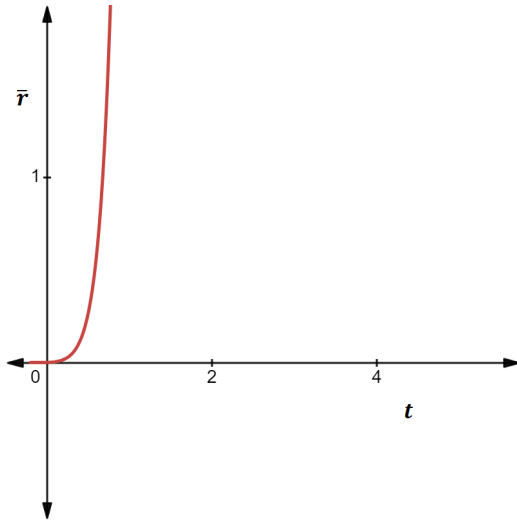


Figure 13. Plotting the coincidence parameter vs cosmic time (t) for $n = 1.1, k = 1, c_1 = 100, \Delta = 0.5, \alpha = 1, \beta = 0.7$

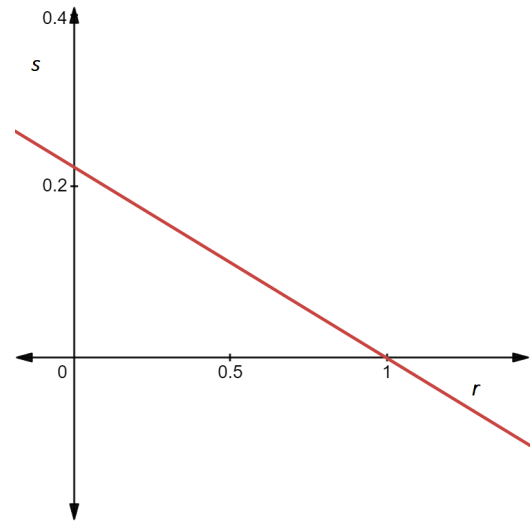


Figure 14. Plotting the statefinder parameters s vs r (t) for $n = 1.1$ and $k = 1$

6. CORRESPONDENCE BETWEEN THE BARROW HOLOGRAPHIC DARK ENERGY MODEL AND QUINTESSENCE SCALAR FIELD MODEL

To establish correspondence between holographic dark energy with quintessence dark energy models, we compare their equations of state and dark energy densities. For the universe to undergo accelerated expansion, the equation of state parameter for quintessence must be less than $-\frac{1}{3}$.

The energy density and pressure for the quintessence scalar field model are defined by:

$$\rho_\phi = \frac{\dot{\phi}^2}{2} + V(\phi) \quad (62)$$

$$p_\phi = \frac{\dot{\phi}^2}{2} - V(\phi) \quad (63)$$

where ϕ represents the quintessence scalar field and $V(\phi)$ denotes the potential of the scalar field ϕ . The equation of state parameter for the scalar field is expressed as

$$\omega_\phi = \frac{p_\phi}{\rho_\phi} = \frac{\dot{\phi}^2 - 2V(\phi)}{\dot{\phi}^2 + 2V(\phi)} \quad (64)$$

Equations (62) and (63) provide

$$\dot{\phi}^2 = \rho_\phi + p_\phi \quad (65)$$

$$V(\phi) = \frac{\rho_\phi - p_\phi}{2} \quad (66)$$

By using equations (43) and (64), we obtain

$$-1 + \frac{(\Delta - 2) \frac{k}{nt^2} \left(\frac{\beta}{t} - \alpha \left(\frac{k+t}{nt} \right) \right)}{\left(\frac{k+t}{nt} \right) \left[\alpha \left(\frac{k+t}{nt} \right)^2 - \frac{\beta k}{nt^2} \right]} = \frac{\dot{\phi}^2 - 2V(\phi)}{\dot{\phi}^2 + 2V(\phi)} \quad (67)$$

By equating ρ_ϕ with ρ_{BHDE} and p_ϕ with p_{BHDE} , we can compute the kinetic energy $\dot{\phi}^2$ and the scalar potential $V(\phi)$ as

$$\dot{\phi}^2 = - \left[\alpha \left(\frac{k+t}{nt} \right)^2 + \beta \left(\frac{-k}{nt^2} \right) \right]^{\frac{-\Delta}{2}} \left[\frac{(2-\Delta)}{k+n} \left(-\alpha k \left(\frac{n+k}{nt^2} \right) + \frac{\beta k}{t^2} \right) \right] \quad (68)$$

$$V(\phi) = 3 \left[\alpha \left(\frac{k+t}{nt} \right)^2 + \beta \left(\frac{-k}{nt^2} \right) \right]^{\frac{2-\Delta}{2}} + \frac{1}{2} \left[\alpha \left(\frac{k+t}{nt} \right)^2 + \beta \left(\frac{-k}{nt^2} \right) \right]^{\frac{-\Delta}{2}} \left[\frac{(2-\Delta)}{k+n} \left(-\alpha k \left(\frac{n+k}{nt^2} \right) + \frac{\beta k}{t^2} \right) \right] \quad (69)$$

Thus, we have determined the potential $V(\phi)$ and the scalar field ϕ for the quintessence scalar field model corresponding to the BHDE model. The kinetic energy $\dot{\phi}^2$ is shown in Figure 15, illustrating that it decreases over cosmic time t and eventually diminishes at late times. Figure 16 depicts the scalar field potential $V(\phi)$ for the quintessence model, indicating that $V(\phi)$ also decreases over cosmic time t and tends to a constant value at late times. This type of potential and kinetic energy can lead to the accelerated expansion of the universe.

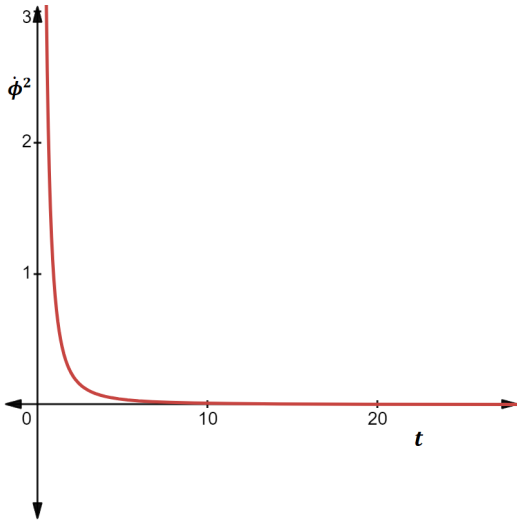


Figure 15. Plotting the kinetic energy $\dot{\phi}^2$ vs (t) for $n = 1.1, k = 1, \Delta = 0.5, \alpha = 1$ and $\beta = 0.7$

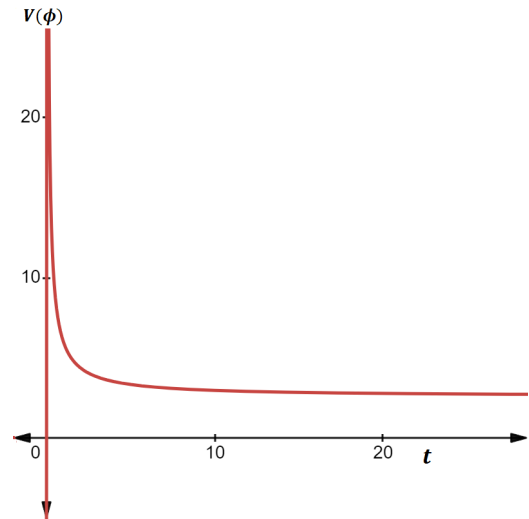


Figure 16. Plotting the potential energy $V(\phi)$ vs (t) for $n = 1.1, k = 1, \Delta = 0.5, \alpha = 1$ and $\beta = 0.7$

7. CONCLUSION

In this study, we consider Barrow holographic dark energy with Granda - Oliverso length scale as the infrared cutoff to construct a spatially homogeneous and anisotropic Bianchi type-V universe within the framework of General Relativity. The universe is assumed to be filled with a mixture of cold dark matter and the Barrow holographic dark energy which does not interact with the cold dark matter. Exact solution of the Einstein field equations are obtained by imposing the condition that the average scale factor a obeys a hybrid expansion law. We then investigate the physical and kinematic characteristics of the model by analyzing its parameters of cosmological importance and find that:

- At time $t \rightarrow 0$, the volume V of the universe is zero, indicating that the universe starts from a point of zero volume and expands throughout its evolution. This suggests that the universe began with a Big Bang singularity.
- The universe transitions from an early deceleration phase to a recent acceleration phase, as illustrated in Figure 2, and this aligns well with recent observations.
- The Hubble parameter H , the expansion scalar θ , and the shear scalar σ each diverges at $t \rightarrow 0$, and then all decrease with increasing cosmic time t but remains positive.
- The anisotropic parameter A_m approaches zero for sufficiently large time. Thus, the present model becomes isotropic at late times.
- The matter energy density ρ_m and the Barrow holographic dark energy density ρ_{BHDE} both decrease as cosmic time t increases. This decrease in energy densities over time results in the expansion of the universe.
- In later epochs, the pressure of Barrow holographic dark energy p_{BHDE} becomes negative, indicating the universe's accelerated expansion.
- In the beginning, the equation of state parameter ω_{BHDE} for Barrow holographic dark energy experiences variation within the quintessence region, gradually approaching the Λ CDM model as time progresses.

- The total energy density parameter Ω tends to 1 as $t \rightarrow \infty$. This implies that the universe is approaching towards a flat universe in its later stage.
- The Null energy condition, Weak energy condition, and Dominant energy condition are all satisfied, but in the later stages, the Strong energy condition is violated, indicating the universe's accelerated expansion.
- The cosmic jerk parameter (j), snap parameter (s), and lerk parameter (l) all approach the value 1 as time progresses. This convergence, particularly of j , indicates that our model aligns with the Λ CDM model at late time.
- Throughout the evolution of the universe, the coincidence parameter, \bar{r} varies. In our model, the coincidence problem remains unresolved.
- The Statefinder parameters intersect at the point (1, 0), signifying alignment with the Λ CDM model.
- The correlation between the Barrow holographic dark energy model and the quintessence scalar field model explains the accelerated expansion phase of the universe.

ORCID

 **Chandra Rekha Mahanta**, <https://orcid.org/0000-0002-8019-8824>;  **Rajashree Mahanta**, <https://orcid.org/0009-0009-2656-115X>;  **Joy Prakash Medhi**, <https://orcid.org/0009-0004-5275-5330>

REFERENCES

- [1] A.G. Riess, *et al.*, "Observational evidence from supernovae for an accelerating universe and a cosmological constant," *The Astronomical Journal*, **116**, 1009-1038 (1998). <https://doi.org/10.1086/300499>
- [2] S. Perlmutter, *et al.*, "Measurements of Ω and Λ from 42 high-redshift supernovae," *The Astrophysical Journal*, **517**, 565-586 (1999). <https://doi.org/10.1086/307221>
- [3] D.N. Spergel, *et al.*, "First-year Wilkinson Microwave Anisotropy Probe (WMAP) observations: Determination of cosmological parameters," *Astrophys. J. Suppl. Ser.* **148**, 175-194 (2003). <https://doi.org/10.1086/377226>
- [4] D.N. Spergel, *et al.*, "Three-Year Wilkinson Microwave Anisotropy Probe (WMAP) Observations: Implications for Cosmology," *Astrophys. J. Suppl. Ser.* **170**, 377 (2007). <https://doi.org/10.1086/513700>
- [5] E. Komatsu, *et al.*, "Five-Year Wilkinson Microwave Anisotropy Probe observation: cosmological interpretation," *Astrophys. J. Suppl. Ser.* **180**, 330 (2009). <https://doi.org/10.1088/0067-0049/180/2/330>
- [6] M. Tegmark, *et al.*, "Cosmological parameters from SDSS and WMAP," *Phys. Rev. D*, **69**, 103501 (2004). <https://doi.org/10.1103/PhysRevD.69.103501>
- [7] U. Seljak, *et al.*, "Cosmological parameter analysis including SDSS Ly α forest and galaxy bias: constraints on the primordial spectrum of fluctuations, neutrino mass, and dark energy," *Phys. Rev. D*, **71**, 103515 (2005). <https://doi.org/10.1103/PhysRevD.71.103515>
- [8] M. Tegmark, *et al.*, "Cosmological constraints from the SDSS luminous red galaxies," *Phys. Rev. D*, **74**, 123507 (2006). <https://doi.org/10.1103/PhysRevD.74.123507>
- [9] D.J. Eisenstein, *et al.*, "Detection of the Baryon Acoustic Peak in the Large-Scale correlation function of SDSS luminous red galaxies," *The Astronomical Journal*, **633**, 560-574 (2005). <https://doi.org/10.1086/466512>
- [10] P.J.E Peebles and Bharat Ratra, "The cosmological constant and dark energy," *Rev. Mod. Phys.* **75**, 559 (2003). <https://doi.org/10.1103/RevModPhys.75.559>
- [11] Planck Collaboration, "Planck 2018 results VI. Cosmological parameters," *A&A*, **641**, A6 (2020). <https://doi.org/10.1051/0004-6361/201833910>
- [12] Edmund J. Copeland, "Dynamics of Dark Energy," *AIP Conf. Proc.* **957**, 21-29 (2007). <https://doi.org/10.1063/1.2823765>
- [13] G.'t Hooft, "Dimensional reduction in quantum gravity," *arXiv.gr-qc/9310026* (2009). <https://doi.org/10.48550/arXiv.gr-qc/9310026>
- [14] A.G. Cohen, D.B. Kaplan, and A.E. Nelson, "Effective Field Theory, Black Holes, and the Cosmological Constant," *Phys. Rev. Lett.* **82**, 4971-4974 (1999). <https://doi.org/10.1103/PhysRevLett.82.4971>
- [15] P. Hořava, and D. Minic, "Probable Values of the Cosmological Constant in a Holographic Theory," *Phys. Rev. Lett.* **85**, 1610-1613 (2000). <https://doi.org/10.1103/PhysRevLett.85.1610>
- [16] S.D.H. Hsu, "Entropy bounds and dark energy," *Phys. Lett. B*, **594**, 13 (2004). <https://doi.org/10.1016/j.physletb.2004.05.020>
- [17] M. Li, "A model of holographic dark energy," *Phys. Lett. B*, **603**, 1-5 (2004). <https://doi.org/10.1016/j.physletb.2004.10.014>
- [18] L.N. Granda, and A. Oliveros, "Infrared cut-off proposal for the holographic density," *Phys. Lett. B*, **669**(5), 275-277 (2008). <https://doi.org/10.1016/j.physletb.2008.10.017>
- [19] M. Tavayef, A. Sheykhi, K. Bamba, and H. Moradpour, "Tsallis holographic dark energy," *Phys. Lett. B*, **781**, 195-200 (2018). <https://doi.org/10.1016/j.physletb.2018.04.001>

- [20] C. Tsallis, and L.J.L. Cirto, "Black hole thermodynamical entropy," Eur. Phys. J. C, **73**, 2487 (2013). <https://doi.org/10.1140/epjcs/10052-013-2487-6>
- [21] H. Moradpour, et al.: "Thermodynamic approach to holographic dark energy and the Rényi entropy," Eur. Phys. J. C, **78**, 829 (2018). <https://doi.org/10.1140/epjcs/10052-018-6309-8>
- [22] J.D. Barrow, "The area of a rough black hole," Phys. Lett. B, **808**, 135643 (2020). <https://doi.org/10.1016/j.physletb.2020.135643>
- [23] S. Wang, Y. Wang, and M. Li, "Holographic dark energy," Phys. Rep. **696**, 1–57 (2017). <https://doi.org/10.1016/j.physrep.2017.06.003>
- [24] E.N. Saridakis, "Barrow holographic dark energy," Phys. Rev. D, **102**, 123525 (2020). <https://doi.org/10.1103/PhysRevD.102.123525>
- [25] S. Srivastava, and U.K. Sharma, "Barrow holographic dark energy with Hubble horizon as IR cutoff," Int. J. Geo. Methods in Mod. Phys. **18**, 2150014 (2021). <https://doi.org/10.1142/S0219887821500146>
- [26] N. K. P and T. K. Mathew, "Barrow Holographic Dark Energy Model with GO Cut-off – An Alternative Perspective," <https://doi.org/10.48550/arXiv.2112.07310>
- [27] A. Oliverosa, M.A. Sabogal, M.A. Acero, "Barrow holographic dark energy with Granda–Oliveros cutoff," Eur. Phys. J. Plus, **137**, 783 (2022). <https://doi.org/10.1140/epjp/s13360-022-02994-z>
- [28] B.C. Paul, et al., "Bianchi-I anisotropic universe with Barrow holographic dark energy," Eur. Phys. J. C, **82**, 76 (2022). <https://doi.org/10.1140/epjcs/10052-022-10041-5>
- [29] C.L. Bennett et al., "The Microwave Anisotropy Probe* Mission," The Astrophysical Journal, **583**, 1-23 (2003). <https://doi.org/10.1086/345346>
- [30] Bernardis, et al., "MAXIMA-1: A Measurement of the Cosmic Microwave Background Anisotropy on Angular Scales of 10'–5°," The Astrophysical Journal, **545**, (2000). <https://doi.org/10.1086/317322>
- [31] G. Hinshaw et al., "Five-Year Wilkinson Microwave Anisotropy Probe* Observations: Data Processing, Sky Maps, and Basic Results," The Astrophysical Journal Supplement Series, **180**, 225–245 (2009). <https://doi.org/10.1088/0067-0049/180/2/225>
- [32] V. Sahni, T.D. Saini, A.A. Starobinsky, and U. Alam, "Statefinder—a new geometrical diagnostic of dark energy," JETP Lett. **77**, 201-206 (2003). <https://doi.org/10.1134/1.1574831>

КОСМІЧНА ЕВОЛЮЦІЯ У ВСЕСВІТІ БІАНКІ ТИПУ V З ГОЛОГРАФІЧНОЮ ТЕМНОЮ ЕНЕРГІЄЮ БАРРОУ ЗІ ШКАЛОЮ ДОВЖИНИ ГРАНДА-ОЛІВЕРОСА ЯК ІЧ ВІДСІЧЕННЯ

Чандра Рекха Маханга, Раджашрі Маханга, Джой Пракаш Медхі

Факультет математики, Університет Гаухаті, Гувахаті - 781014, Індія

У цій роботі ми будемо просторово однорідну та анізотропну космологічну модель типу Б'янки V із гібридним законом розширення, розглядаючи Всесвіт як заповнений холодною темною матерією та незв'язаною голографічною темною енергією Барроу зі шкалою довжини Гранда-Олівероса як ІЧ-відсічення. Фізичні та кінематичні характеристики отриманої моделі обговорюються шляхом вивчення еволюції різних параметрів космологічного значення, таких як параметр Хаббла, параметр уповільнення, анізотропний параметр, параметр рівняння стану, параметр ривка тощо. Ми також досліджуємо, чи енергетичні умови виконуються або порушуються. Наш аналіз показує, що умови нульової, слабкої та домінуючої енергії виконуються, тоді як умова сильної енергії порушена, що підтримує прискорене розширення Всесвіту. Діагностика вимірювача стану також була виконана на основі останніх космологічних спостережень, щоб порівняти нашу модель з різними космологічними сценаріями темної енергії. Крім того, ми встановлюємо відповідність між квінтесенційним скалярним полем і голографічною моделлю темної енергії Барроу, що підтверджує наш опис прискореного розширення Всесвіту.

Ключові слова: космічне прискорення; голографічна темна енергія Барроу; Біанкі тип-V; холодна темна матерія; параметр уповільнення; рівняння параметра стану

EXAMINING THE VISCOUS RICCI DARK ENERGY COSMOLOGICAL MODEL IN GENERAL THEORY OF GRAVITATION

 T. Chinnappalanaidu^a,  M. Vijaya Santhi^b,  N. Sri Lakshmi Sudha Rani^b

^aDepartment of Mathematics, Vignan's Institute of Information Technology(Autonomous), Visakhapatnam 530049, India

^bDepartment of Applied Mathematics, College of Science and Technology, Andhra University, Visakhapatnam 530003, India

*Corresponding Author e-mail: chinnappalanaidu.tadi@gmail.com

Received June 30, 2024; revised July 24, 2024; accepted August 15, 2024

This study focuses on dynamically exploring Marder-type spacetime containing viscous Ricci dark energy within the framework of general relativity theory. To find a solution of the field equations, we use the relation between metric potentials and the average scale factor $a(t) = (\sinh \beta_1 t)^{\frac{1}{\beta_2}}$, this leads to a seamless transition of the Universe from its initial decelerating phase to the current accelerating phase. Here, we have obtained the cosmological parameters and $\omega_{de} - \omega'_{de}$ plane for the derived model. Also, dynamical features of the derived cosmological model are analyzed through diagrams.

Keywords: Dark energy; Viscous Ricci dark energy; Marder type metric; General relativity

PACS: 04.20. - q; 98.80. - k; 95.36. + x

1. INTRODUCTION

Dark Energy(DE), which has yet to be identified, is thought to be the cause of the Universe's recent aggressive expansion. One of the pillars of contemporary cosmology is DE. Many measurements, like the cosmic microwave background radiation(CMB) [1], the distant modulus of the type Ia supernova (SnIa) [2–4] and more recently by large-scale structure studies [5], show that DE is a peculiar phenomena that is developing into an Einstein-de Sitter structure. Just $\sim 4\%$ of the entire Universe's energy density is represented by baryonic matter, $\sim 24\%$ by non-baryonic matter, and almost $\sim 72\%$ by an unidentified component that has negative pressure, which is the most unexpected and counter intuitive outcome of these studies. A cosmic acceleration could be produced by the cosmological constant, which represents quantum vacuum energy density. In general relativity (GR), this simple DE model is plagued by coincidence. The accelerating universe is explained by different dynamical DE models. There are several notable models in this group, including K -essence and Quintessence [6, 7]. You might want to also note that there are other modified matter models based on perfect fluids, such as pilgrim DE models [8–10], generalized Chaplygin gas models [11], and holographic DE models [12, 13]. GR is modified by another class of DE models. Models of DE correspond to modified theories of gravity [14, 15] and scalar-tensor theories of gravity [16, 17].

In 1916, Einstein [18] presented his GR, which gives a geometrical account of gravity. Even today, GR is an elegant scientific as well as geometrical framework used to accurately characterizes gravity fields. As well as being useful for discussing cosmological models of the Universe. Even so, Einstein admitted that some desirable characteristics were not accounted for in his theory. By way of instance, such an approach fails to take into account Mach's principle. In the simplest instance, gravity is maintained by Einstein's equations of GR. The Einstein-Maxwell equations are a set of differential second order equations with partial derivatives that are extremely nonlinear. On the one hand, these equations provide formulas for the elements of energy-momentum tensor. Because metric potentials are formed from Ricci tensors, they enter in a more complicated manner.

Holographic dark energy (HDE) has recently received significant attention as a possible candidate for DE. The holographic principle inspired this type of model [19, 20], a model that was further developed into string theory [20]. Using this principle for cosmology, Li [21] suggested that HDE energy density can be calculated as $\rho_d = 3b^2 M_p^2 L^{-2}$, where L denotes the infrared (IR) cut-off, $b^2 = \text{constant}$ and $M_p^{-2} = 8\pi G$. Using Hubble's horizon as a cutoff for the IR distance from HDE, it was found that there is no evidence that the Universe accelerates. The infrared cut-off of the Universe was later considered by him to be a prospective event horizon for the Universe that will emerge in the future. The HDE model can give insight into our current observations indicating an accelerated Universe expansion. Meanwhile, many works have been published [22–27] on HDE models to illustrate the rapid behavior of the cosmos. Based on the Ricci dark energy (RDE) model proposed by Gao et al. [28], DE density appears to be oppositely related to Ricci scalar curvature. In RDE, the future event horizon is replaced by the inverse of the Ricci scalar curvature. In the case of RDE, the energy density can be expressed as follows:

$$\rho_d = 3\alpha \left(\dot{H} + 2H^2 \right), \quad (1)$$

where H is the Hubble parameter, a is the scale factor and there is no dimension to α , but it describes how the energy density runs. Over dot refers to a derivative of cosmic time t .

Generally, it is recognized as a fact the Cosmos' content in the form of a perfect fluid is aggressive because dissipation is not involved, dissipation being something that exists extensively and supposedly plays a vital role in the cosmos's development. Most practically, the cosmos is thought to consist of a series of mediums which are made up of scattering media. The development of the Universe is characterized by a series of scattering operations. These mechanisms include shear viscosity, heat transmission and bulk viscosity. Numerous writers [29–32] have examined their involvement with the explanation of the Universe's initial inflation as well as its subsequent cosmic development. Over the past few decades, the concept of viscous DE models is being developed to better comprehend the development of the Universe. Based on the writings [33–44], many studies have been conducted to investigate viscosity of the bulk fluid in light of possibility of DE, without the cosmological constant, cosmological expansion may be explained by even the correct form of viscosity of the bulk fluid [45]. The main concept of viscous cosmology for the ancient and modern Universes was given by Brevik et al. [46]. Norman and Brevik [47, 48] have investigated the characteristics of two different viscous cosmology models and established general mathematics formulations for bulk viscous fluids. Several recent literature [49, 50] have examined the HDE model under the impact of bulk viscosity on the model. By assuming a linear barotropic fluid and an RDE with bulk viscosity, researchers Feng and Li [51] have developed a viscous RDE model. In their paper [52], Singh and Kumar propose a diagnostic method for viscous HDE cosmology using a statefinder.

Furthermore, the Universe's homogeneity and isotropic characteristics have been ascertained from various investigations. Inflationary Universes were homogeneous and isotropic at the end of the inflationary period [53], and FLRW models were essential in depicting cosmos that were both spatially homogeneous and isotropic. Yet the theoretical justification and anomalies found in the CMB facilitate the identification of a phase of anisotropy that is later referred to as an isotropic phase. Immediately following the Planck probe data was released [54], it was discovered that the early cosmos was not entirely uniform. As a result, cosmological models constructed with anisotropic backgrounds have gained popularity due to the inhomogeneous and anisotropic nature of the Universe. Accordingly, the attributes of the Universe change based on the direction in which they're observed, which indicates that we live in an anisotropic Universe. Based on the data provided by WMAP, the current Universe can be described as anisotropic [55]. Marder space time possesses certain traits that help elucidate the genesis of galaxies in the early phases of universal evolution [56, 57]. Given that the Marder line element represents an anisotropic and homogeneous space time, it aids in comprehending the Universe's inception and its shift from anisotropy to isotropy. This encourages us to contemplate such space time configurations. Moreover, employing the transformation $t \rightarrow \int A(t)dt$, allows for the simplification of Marder spacetime to the Bianchi type-I model, subsequently converging to the FRW Universe. Thus, we categorize the line element accordingly based on whether anisotropy is prevalent in later times or during the early stages of the Universe [58]. Therefore, Marder spacetime not only enables us to study an anisotropic universe but also an isotropic one. We opted Marder's space-time in Einstein's GR and scalar-tensor theories, which is an anisotropic and homogeneous space-time that facilitates an anisotropic to isotropic transition. Many authors have discussed Marder space-time for different matter content. Aygün et al., [59], Aygün [60, 61], Kömürcü and Aktas [62] analyzed the Marder's type Universe in the $f(R, T)$ theory of gravity in different contexts. Aygün et al., [56, 63], Kabak and Aygun [64], Ali et al. [65] provide a couple of references to some authors who have examined Marder's space-time in various theories with a variety of tensors of energy and momentum. Singh et al., [66], Prakash [67] have used Marder's metric in the development of plane-symmetric models of the universe. Roy and Chatterjee [68], Mukherjee [69] study the Sen-Dunn theory of gravitation and obtain exact solutions to Marder's metric. Pawar and Solanke [70], Pawar and Panpatte [71] studied Marder's space-time in the Saez–Ballester framework. Pawar et al., [72] developed an anisotropic homogeneous Marder's space-time model of wet dark fluids. Santhi et al., [73, 74] have examined a cosmological model based on a bulk viscous string in a modified theory of gravity, as well as a viscous HDE cosmological model with Marder space-time in GR respectively. It was just studied by Santhi and Naidu [75] that Marder space-time with Tsallis HDE in GR.

With the help of the GR, we look at Marder-type metric with a viscous RDE (VRDE). The paper looks like this: Section 2 contains the metric and field equations. We derive solutions for Marder-type cosmological models in section 3. Our physical discussion of the cosmological parameters is in section 4. The last section summarizes the results.

2. METRIC AND FIELD EQUATIONS

A space time of Marder type that is anisotropic and spatially homogeneous looks like this:

$$-b_1^2(t)dt^2 + b_1^2(t)dx^2 + b_2^2(t)dy^2 + b_3^2(t)dz^2 = ds^2. \tag{2}$$

- The average scale factor ($a(t)$) and volume (V) of the Marder type metric as follows:

$$V = [a(t)]^3 = b_1^2 b_2 b_3. \tag{3}$$

- The anisotropic parameter \mathcal{A}_h is given by

$$\mathcal{A}_h = \frac{1}{3} \sum_{i=1}^3 \left(\frac{H_i - H}{H} \right)^2, \tag{4}$$

where $H_1 = \frac{\dot{b}_1}{b_1}$, $H_2 = \frac{\dot{b}_2}{b_2}$, $H_3 = \frac{\dot{b}_3}{b_3}$ are directional Hubble's parameters and $H = \frac{1}{3} \left(2\frac{\dot{b}_1}{b_1} + \frac{\dot{b}_2}{b_2} + \frac{\dot{b}_3}{b_3} \right)$ is mean Hubble's parameter. Cosmological time t differentiation is indicated by an overhead dot.

- The expansion scalar (θ) is given by

$$\theta = \frac{1}{b_1} \left(\frac{\dot{b}_2}{b_2} + 2\frac{\dot{b}_1}{b_1} + \frac{\dot{b}_3}{b_3} \right). \quad (5)$$

- The shear scalar (σ^2) is given by

$$\sigma^2 = \frac{1}{2} \left(\sum_{i=1}^3 H_i^2 - \frac{\theta^2}{3} \right). \quad (6)$$

In Einstein's theory of GR, the equations of fields are defined as follows:

$$G_{ij} = -T_{ij}, \quad (7)$$

where T_{ij} is the energy momentum tensor and $G_{ij} = R_{ij} - \frac{1}{2}Rg_{ij}$ is an Einstein tensor. As well as that, the equation for conservation is as follows:

$$T^{ij}{}_{;j} = 0. \quad (8)$$

With viscosity of the bulk fluid and a deviation from thermodynamic equilibrium of the first order, the stress-energy-momentum tensor takes the form (Wilson et al. [76]).

$$T_{ij} = (\rho_m + \rho_d)u_i u_j + \bar{p}_d (g_{ij} + u_i u_j), \quad (9)$$

where ρ_d and ρ_m are the energy densities of RDE and DM, respectively and $\bar{p}_d = p_d - 3\zeta H$, where \bar{p}_d is the effective pressure of RDE, H is Hubble parameter and ζ is the bulk viscous coefficient which is given as $\zeta = \zeta_0 + \zeta_1 h + \zeta_2 h'$, where $h = \frac{H}{H_0}$ and ζ_0, ζ_1 are positive constants and $u_i u^i = -1$.

By using Eq. (9), the field equations (7) can be written as follows:

$$\frac{1}{b_1^2} \left(\frac{\ddot{b}_2}{b_2} + \frac{\ddot{b}_3}{b_3} + \frac{\dot{b}_2 \dot{b}_3}{b_2 b_3} - \frac{\dot{b}_1 \dot{b}_2}{b_1 b_2} - \frac{\dot{b}_1 \dot{b}_3}{b_1 b_3} \right) = -\bar{p}_d, \quad (10)$$

$$\frac{1}{b_1^2} \left(\frac{\ddot{b}_1}{b_1} + \frac{\ddot{b}_3}{b_3} - \frac{\dot{b}_1^2}{b_1^2} \right) = -\bar{p}_d, \quad (11)$$

$$\frac{1}{b_1^2} \left(\frac{\ddot{b}_1}{b_1} + \frac{\ddot{b}_2}{b_2} - \frac{\dot{b}_1^2}{b_1^2} \right) = -\bar{p}_d, \quad (12)$$

$$\& \frac{1}{b_1^2} \left(\frac{\dot{b}_1 \dot{b}_2}{b_1 b_2} + \frac{\dot{b}_2 \dot{b}_3}{b_2 b_3} + \frac{\dot{b}_3 \dot{b}_1}{b_3 b_1} \right) = \rho_m + \rho_d. \quad (13)$$

Furthermore, the energy conservation equation leads to

$$(\dot{\rho}_m + \dot{\rho}_d) + \left(2\frac{\dot{b}_1}{b_1} + \frac{\dot{b}_2}{b_2} + \frac{\dot{b}_3}{b_3} \right) (\rho_m + \rho_d + \bar{p}_d) = 0. \quad (14)$$

3. SOLUTION OF THE FIELD EQUATIONS

There are four independent equations in (10)-(13) which have six independent components : $\bar{p}_d, \rho_m, \rho_d, b_1, b_2,$ and b_3 . In order to resolve the equations mentioned above, the following conditions are required:

- There is a relationship between the metric potentials when the shear scalar (σ) is proportional to the expansion scalar (θ) (Collins et al. [77]). That is

$$b_1 = (b_2 b_3)^n, \quad (15)$$

as long as $n \neq 1$ is constant, space-time's anisotropy is preserved.

- Mishra et al. [78] proposed a varying deceleration parameter as

$$q(t) = -\frac{a\ddot{a}}{\dot{a}^2} = b(t), \quad (16)$$

where $b(t)$ is an arbitrary function of time, where $a(t)$ is the average scale factor of the Universe. We can get the average scale factor by solving the above Eq. (16) using some suitable assumptions (Mishra et al. [78]).

$$a(t) = (\sinh \beta_1 t)^{\frac{1}{\beta_2}}, \tag{17}$$

where β_1 and β_2 represent arbitrary positive constants. Using such an average scale factor, we obtain a deceleration parameter(DP) (q) that changes from an early deceleration phase to a current acceleration phase. Santhi et al. [79] and Rao and Prasanthi [80], Reddy et al. [81] used this average scale factor to evaluate various cosmological models.

From Eqs.(11) and (12), we have

$$b_2 = \gamma_2^2 b_3, \tag{18}$$

here, $\gamma_2^2 \neq 1$ & $\gamma_2^2 > 0$.

The metric potentials are derived from equations (3), (15), (17), and (18) as depicted below:

$$b_1 = (\sinh(\beta_1 t))^{\frac{3n}{\beta_2(n+1)}}, \tag{19}$$

$$b_2 = \gamma_2 (\sinh(\beta_1 t))^{\frac{3}{\beta_2(2n+2)}}, \tag{20}$$

$$b_3 = \frac{(\sinh(\beta_1 t))^{\frac{3}{\beta_2(2n+2)}}}{\gamma_2}. \tag{21}$$

The energy density of VRDE is expressed as follows:

$$\rho_d = \frac{6\alpha (\beta_2 - 2) \beta_1^3 \cosh(\beta_1 t)}{\beta_2^2 \sinh(\beta_1 t)^3}. \tag{22}$$

Matter's energy density is given by

$$\rho_m = \frac{3\beta_1^2 \left(3 (\cosh(\beta_1 t)^2 - 1) \cosh(\beta_1 t)^2 \left(n + \frac{1}{4} \right) \sinh(\beta_1 t)^{\frac{2\beta_2(n+1)+(-4n-4)\beta_2-6n}{\beta_2(n+1)}} + \alpha(n+1)^2 (\beta_2 - 2 \cosh(\beta_1 t)^2) \right)}{\beta_2^2(n+1)^2 \sinh(\beta_1 t)^2}. \tag{23}$$

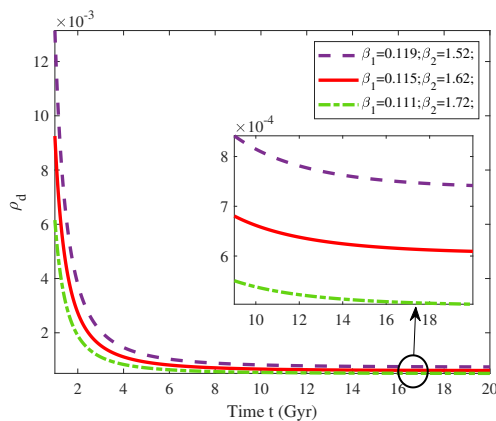


Figure 1. VRDE energy density (ρ_d) v/s time (t) (Gyr)

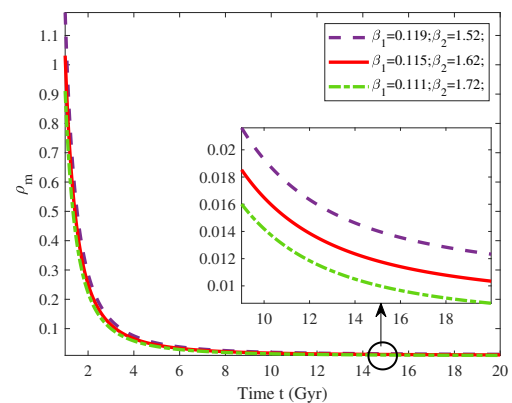


Figure 2. Matter energy density(ρ_m) v/s time (t) (Gyr)

The pressure of VRDE is given by

$$\bar{p}_d = - \frac{2\beta_1^2 (\sinh(\beta_1 t))^{\frac{(-2n-2)\beta_2-6n}{\beta_2(n+1)}} \left(\left(\frac{3n}{2} - \frac{15}{8} \right) \cosh(\beta_1 t)^2 + \beta_2(n+1)^2 \right)}{\beta_2^2(n+1)^2}. \tag{24}$$

The bulk viscosity is given by

$$\zeta = \frac{\zeta_1 \beta_1 \cosh(\beta_1 t) \sinh(\beta_1 t) H_0 + H_0 \beta_2 \cosh(\beta_1 t)^2 \zeta_0 - \zeta_0 \beta_2 H_0 - \zeta_2 \beta_1^2}{\beta_2 H_0 \sinh(\beta_1 t)^2}. \tag{25}$$

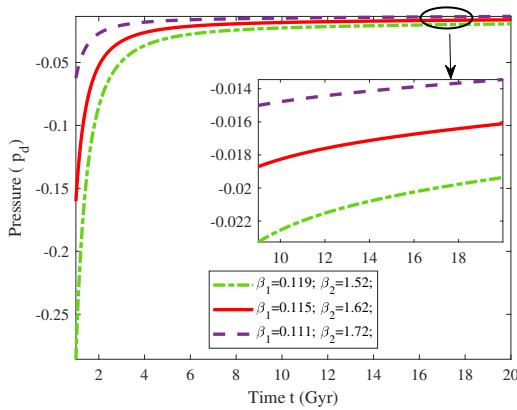


Figure 3. VRDE pressure (\bar{p}_d) v/s time t (Gyr)

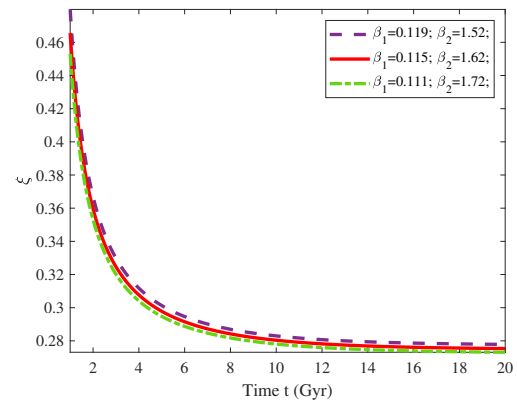


Figure 4. Bulk viscosity (ξ) v/s time t (Gyr)

We used the following constants as a constraint in our analysis as well as diagrammatic illustrations of the Marder VRDE model of the universe in which our analysis discussed the corresponding parameters: $\beta_1 = 0.199, 0.115, 0.111; \beta_2 = 1.52, 1.62, 1.72; n = 0.019; \alpha = 0.02; \zeta_0 = 0.25; \zeta_1 = 0.35; \zeta_2 = 0.15; H_0 = 65$. It is shown in Fig.(1) and (2) that the characteristics of VRDE energy density (ρ_d) and matter energy density (ρ_m) is plotted against cosmic time t . Observing the trajectories of VRDE energy density (ρ_d) and matter energy density (ρ_m) for various values of β_1 and β_2 , as we can see a variation towards the positive region, through time, which indicates that the Universe is expanding. The total pressure (p) for different values of β_1 and β_2 can also be observed by examining Fig. (3). With the passing of time (t), the total pressure (p) becomes negative. According to Fig. (4), the trajectory of bulk viscosity decreases with time t , while it varies in the positive region.

It is now possible to write the metric (2) as

$$ds^2 = (\sinh(\beta_1 t))^{\frac{6n}{\beta_2(n+1)}} dx^2 + \left(\gamma_2^2 (\sinh(\beta_1 t))^{\frac{6}{\beta_2(2n+2)}} \right) dy^2 + \left(\frac{(\sinh(\beta_1 t))^{\frac{6}{\beta_2(2n+2)}}}{\gamma_2^2} \right) dz^2 - (\sinh(\beta_1 t))^{\frac{6n}{\beta_2(n+1)}} dt^2. \quad (26)$$

Thereby, in the general theory of gravitation, Eq. (26) corresponds to a Marder-type space time that is spatially homogeneous and anisotropic with VRDE.

- The average scale factor ($a(t)$) and volume (V) of the Marder type space time are given by

$$V = (\sinh(\beta_1 t))^{\frac{3}{\beta_2}} \quad \text{and} \quad a(t) = [V]^{\frac{1}{3}} = (\sinh(\beta_1 t))^{\frac{1}{\beta_2}}. \quad (27)$$

- The Hubble parameter (H) is given by the following equation:

$$H = \frac{\beta_1 \coth(\beta_1 t)}{\beta_2}. \quad (28)$$

- The expansion scalar (θ) is given by

$$\theta = 3 \left(\frac{\beta_1 \coth(\beta_1 t)}{\beta_2} \right) \left(\sinh(\beta_1 t)^{\frac{(-n-1)\beta_2-3n}{\beta_2(n+1)}} \right). \quad (29)$$

- The shear scalar (σ^2) is given by

$$\sigma^2 = \left(\frac{-3}{2} \right) \frac{\beta_1^2 \cosh(\beta_1 t)^2 \left((n+1)^2 \sinh(\beta_1 t)^{\frac{2\beta_2(n+1)+(-2n-2)\beta_2-6n}{\beta_2(n+1)}} - 3n^2 - \frac{3}{2} \right)}{\beta_2^2 (n+1)^2 \sinh(\beta_1 t)^2}. \quad (30)$$

- You can find the anisotropic parameter by

$$\mathcal{A}_h = \frac{(2n-1)^2}{2(n+1)^2}. \quad (31)$$

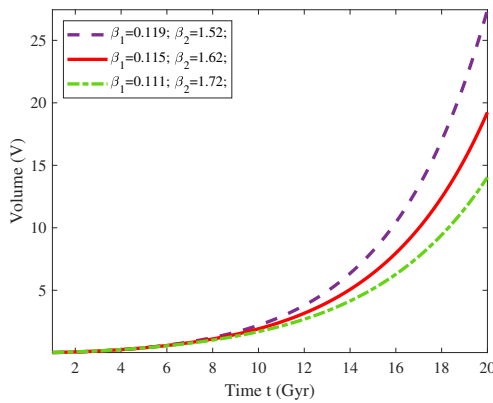


Figure 5. V v/s time t (Gyr)

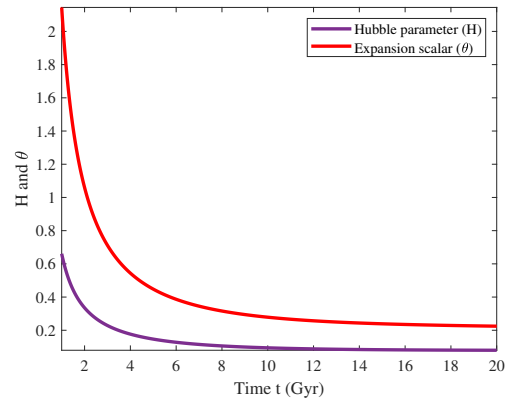


Figure 6. Hubble parameter (H), expansion scalar (θ) v/s time t (Gyr)

We observe from Eq.(31) that $\mathcal{A}_h \neq 0$ represents the likelihood that the Marder type cosmic model will always be anisotropic(except $n = \frac{1}{2}$). For different values of β_1 and β_2 , the volume has monotonously increased against time (t) in Fig. (5). This describes the spatial volume (V) is growing a significant increase and presents the Universe’s growth in an exponential manner. As can also be observed from the equations (27)-(30) within the scope of the earliest phase *i.e.*, at $t = 0$, the average scale factor $a(t)$ and the volume (V) decrease as time passes, indicating an expanding Universe. Hubble parameter H , expansion scalar θ , and shear scalar σ diverge at the initial epoch but attain constant values later. The graphical representation of the θ & H can be found in figure (6). As time progresses, both functions decrease and become constant. Based upon these observations, it can be seen that with respect to time, the model begins its intensification as a volume-zero model, and as it expands further, it reaches an infinite-volume model.

4. COSMIC PARAMETERS

We will investigate the Universe expands in terms of well recognized parameters relevant to the study of the cosmos, namely the EoS parameter (ω_{de}), squared sound speed (v_s^2), jerk parameter (j), DP (q), density parameters *i.e.*, Ω_m , Ω_d & Ω , energy conditions and $\omega_{de} - \omega'_{de}$ plane, statefinder ($r - s$) for constructing an anisotropic VRDE model.

- **Deceleration Parameter:** A further parameter that we have to consider as a result of to examine the transition phase of the Universe is referred to as the DP. This measure quantifies the Universe’s expansion rate in a dimensionless form. q represents this value and it can be described in the following manner:

$$q = \frac{d}{dt} \left(\frac{1}{H} \right) - 1 = \beta_2 \operatorname{sech}(\beta_1 t)^2 - 1. \tag{32}$$

Depending on its sign, it signifies either deceleration (if positive) or acceleration (if negative), whereas de-Sitter expansion is observed at $q = -1$ and marginal inflation happens when $q = 0$. The model indicates a super exponential expansion for $q < -1$ and an accelerated expansion for $-1 \leq q < 0$. According to Fig. (7), we can see that the DP q is plotted against time t , and by looking at the trajectory of the DP we observe that it shows a nice line with three different values of β_1 and β_2 corresponding to the shift from the initial slowing down to the current speeding up.

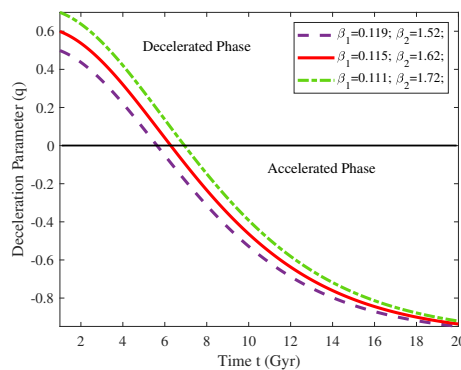


Figure 7. VRDE deceleration parameter(q) v/s time t (Gyr)

- **Jerk Parameter:** It is widely accepted that the jerk parameter(JP) in cosmology is the third derivative of the scale factor with respect to time, expressed without dimensions, and it is defined as follows:

$$j = \frac{\ddot{a}}{aH^3} = \frac{2\beta_2^2 + \cosh(\beta_1 t)^2 - 3\beta_2}{\cosh(\beta_1 t)^2}. \tag{33}$$

Nowadays it is generally accepted that in modern cosmology, the JP can be used to describe how the Universe transitions from a decelerating phase into an accelerating phase as a result of its jerk. It seems that this transition of the Universe occurs in various models if the JP is set to a positive value and the DP is set to a negative value (Chiba and Nakamura [82]; Visser [83]). Based on three different values of β_1 and β_2 , we have plotted a graphical representation of the JP against time (t) in Fig. (8). Throughout the evolution, the JP varies in positive regions and achieves a value of one at the end of the process. Thus, we can conclude from our model that recent observations are consistent with it. Additionally, we observe that β_1 and β_2 completely affect the JP.

- **Statefinder diagnostics:** For the purpose of distinguishing between multiple candidates for dark energy, Sahni et al. [84] has developed an analytical tool that can be used to identify and quantify the statefinder pair of terms $\{r, s\}$, for which the term r able to derived as a result of $a(t)$ and in terms of cosmic time (t), it is a third-order derivative and s can be derived as a function of r and the DP q . The parameters for Statefinder are as follows:

$$r = \frac{\ddot{a}}{aH^3} = \frac{2\beta_2^2 + \cosh(\beta_1 t)^2 - 3\beta_2}{\cosh(\beta_1 t)^2}, \quad s = \frac{r - 1}{3(q - \frac{1}{2})} = \frac{4\beta_2^2 - 6\beta_2}{6\beta_2 - 9\cosh(\beta_1 t)^2}. \tag{34}$$

“A few useful regions can be described by these parameters: $(r, s) = (1, 0)$ indicates Λ CDM, $(r, s) = (1, 1)$ shows CDM limit, Chaplygin gas region $(r > 1, s < 0)$, quintessence and phantom regions $(r < 1, s > 0)$. Fig. (9) shows the behavior of $r - s$ plane of our model. A Λ CDM model is observed within our model of the Universe.”

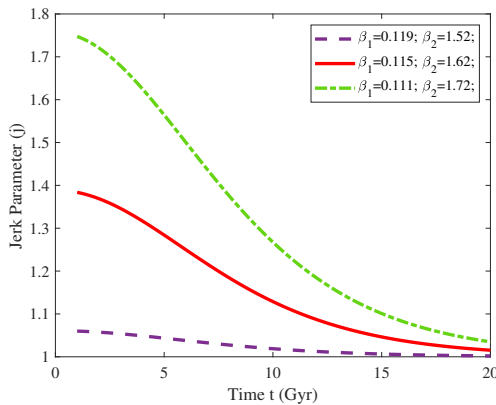


Figure 8. VRDE JP (j) v/s time t (Gyr)

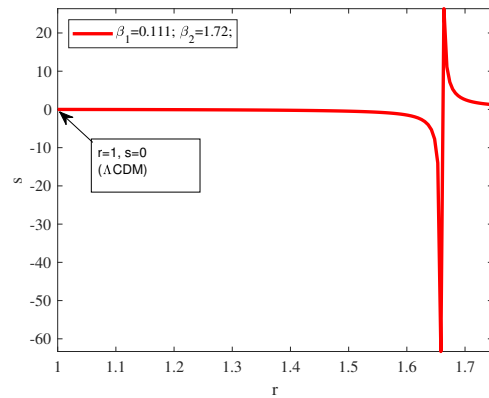


Figure 9. $r - s$ plane

- **EoS Parameter:** The following equation will be used to obtain EoS parameter

$$\omega_{de} = \frac{\bar{p}_d}{\rho_d}. \tag{35}$$

Here, ρ_d and \bar{p}_d are used to represent the DE density and the pressure of the VRDE, respectively. It is estimated that the EoS parameter can be used to define the Universe’s progression into stages of deceleration and acceleration. It is possible to divide the DE dominated phase into the following eras:

- (i) $\omega_{de} = 0$ corresponds to non-relativistic matter.
- (ii) $-1 < \omega_{de} < -\frac{1}{3}$ quintessence.
- (iii) $\omega_{de} = -1$ cosmological constant.
- (iv) $\omega_{de} < -1$ phantom.

In the model, the EoS parameter is represented as the following:

$$\omega_{de} = \frac{2\beta_1^2 \sinh(\beta_1 t) \frac{\beta_2(-2n-2)-6n}{\beta_2(n+1)} \left(\left(\frac{3n}{2} - \frac{15}{8} \right) \cosh(\beta_1 t)^2 + \beta_2(n+1)^2 \right)}{(n+1)^2 6\alpha (\beta_2 - 2) \beta_1^3 \coth(\beta_1 t) \operatorname{cosech}(\beta_1 t)^2}. \tag{36}$$

VRDE's EoS parameter is given in Eq. (26). For the model (26), we present in figure (10) the development of the EoS parameter ω_{de} in terms of time (t), which has various numbers for β_1 and β_2 . It is clear from the figures that the EoS parameter for model (26) starts from phantom region and vary in high phantom region.

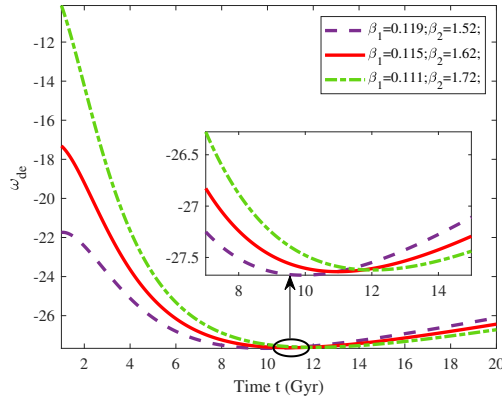


Figure 10. VRDE EoS parameter(ω_{de}) v/s time t (Gyr)

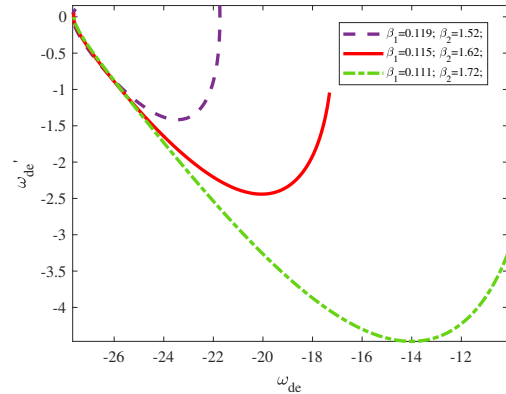


Figure 11. $\omega_{de} - \omega'_{de}$ plane

- **$\omega_{de} - \omega'_{de}$ plane:** Caldwell and Linder [85] propose the $\omega_{de} - \omega'_{de}$ plane analysis, which is a useful tool for distinguishing DE models based on the trajectory of their planes. Using this approach, we can create two types of planes in the essence model, *i.e.*, the region $\omega_{de} < 0, \omega'_{de} < 0$ implies the freezing region and the region $\omega_{de} < 0, \omega'_{de} > 0$ a region of thawing. The expression for ω'_{de} can be obtained by taking the derivative of Eq. (36) with respect to $\ln a$

$$\omega'_{de} = \left. \begin{aligned} & \frac{(-1) \left(4 \left(\frac{9n^2}{2} - \frac{45n}{8} \right) \cosh(\beta_1 t)^2 \sinh(\beta_1 t) \frac{3\beta_2(n+1)+\beta_2(-3n-3)-6n}{\beta_2(n+1)} \right)}{\beta_2(n+1)^3 6\alpha (\beta_2 - 2)} \\ & + \frac{(-4) \left(\beta_2(n+1)^2 + 3n^2 + \frac{9n}{2} - \frac{15}{8} \right) \sinh(\beta_1 t) \frac{3\beta_2(n+1)+\beta_2(-3n-3)-6n}{\beta_2(n+1)}}{(n+1)^2 6\alpha (\beta_2 - 2)} \\ & + \frac{(-1) \sinh(\beta_1 t) \frac{3\beta_2(n+1)+\beta_2(-2n-2)-6n}{\beta_2(n+1)} \left(\left(\frac{3n}{2} - \frac{15}{8} \right) \cosh(\beta_1 t)^2 + \beta_2(n+1)^2 \right)}{(n+1)^2 6\alpha (\beta_2 - 2) \beta_1^3 \cosh(\beta_1 t)} \end{aligned} \right\} \quad (37)$$

As shown in Fig. (11), all values of β_1 and β_2 place the model in the freezing region. According to observations, the Universe is expanding relatively fast in the freezing region. For the obtained model (26), $\omega_{de} - \omega'_{de}$ plane analysis gives the Universe is expanding faster than ever.

- **Energy conditions:** Astrophysical and cosmological energy conditions (ECs) are derived from Raychaudhuri equations [86]. In general, the energy momentum tensor (EMT) is an important factor to consider when studying energy conditions, so, for this discussion, we are going to use the term EMT in relation to pressure \bar{p}_d and energy density ρ_d , therefore, all four of the energy conditions can be written in the following ways: null energy condition (NEC), dominant energy condition (DEC), strong energy condition (SEC), and weak energy condition (WEC). As part of this paper, we have examined how energy conditions have evolved over time. In general, these energy conditions serve as a measure of the expansion of the Universe. It is imperative to recognize that these conditions impose additional limitations on the cosmological model's viability. These conditions include the following:

- WEC: $\rho_d \geq 0$
- NEC: $\rho_d + \bar{p}_d \geq 0$
- DEC: $\rho_d - \bar{p}_d \geq 0$
- SEC: $\rho_d + 3\bar{p}_d \geq 0$

It's important to mention that SEC represents a strong energy condition, DEC represents a dominant energy condition, and NEC represents a null energy condition, and WEC represents a weak energy condition.

Fig. (12) shows the behavior of these energy conditions in the constructed model. In cosmic evolution, WEC and DEC are well satisfied while NEC and SEC are violated at late times, which corresponds to accelerated expansion.

Our model also clearly shows that DEC dominates NEC and SEC in accordance with our observation. I think this is an interesting observation that should be taken into account.

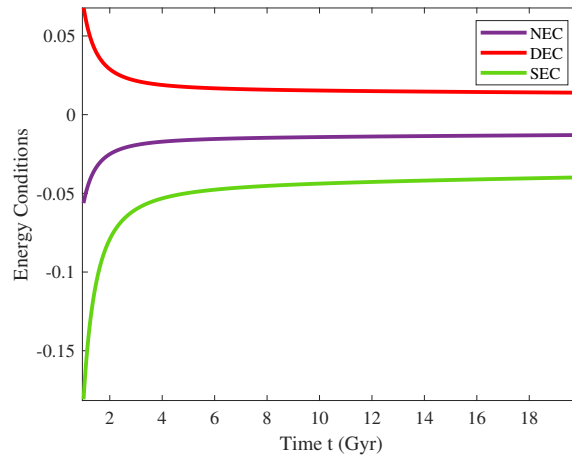


Figure 12. VRDE ECs v/s time t (Gyr)

- Squared speed of sound (v_s^2):** Our next step will be to consider and study one of the most important quantities in cosmology, that is the squared speed of sound(v_s^2), which is an important quantity to take into account when checking every DE model’s stability. Depending on the sign of this parameter, we can examine stability of DE models. Models with $v_s^2 < 0$ are unstable whereas models with $v_s^2 > 0$ are stable. Here is a definition of the squared speed of sound:

$$v_s^2 = \frac{\dot{p}_d}{\dot{\rho}_d} = \frac{-2 \left(\left(\frac{9n^2}{2} - \frac{45n}{8} \right) \cosh(\beta_1 t)^2 + (n+1) \left(\beta_2(n+1)^2 + 3n^2 + \frac{92}{2} - \frac{15}{8} \right) \beta_2 \right) \sinh(\beta_1 t) \beta_2^{-\frac{6n}{n+1}}}{3\alpha(\beta_2 - 2)\beta_2(n+1)^3} \quad (38)$$

Fig. (13) illustrates v_s^2 versus time t for various values of β_1 and β_2 . All values of β_1 and β_2 show trajectories in the negative region, which indicates unstable cosmos behavior.

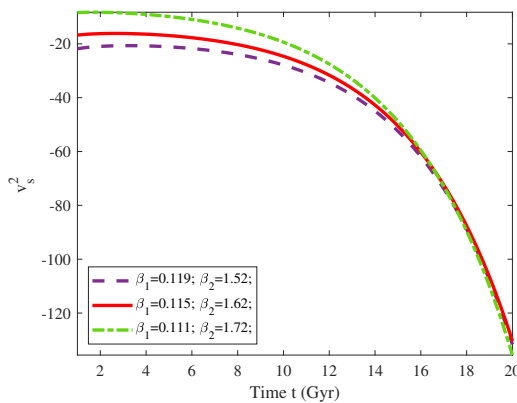


Figure 13. VRDE squared speed of sound(v_s^2) v/s time t (Gyr)

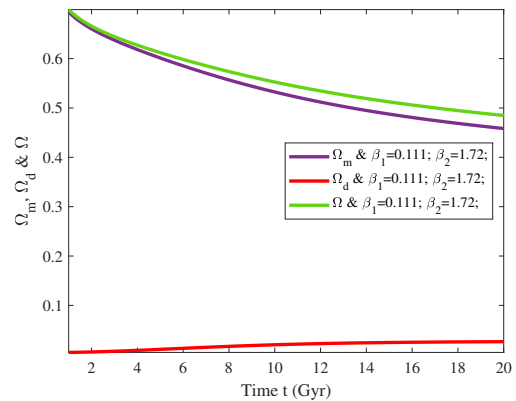


Figure 14. VRDE density parameters ($\Omega, \Omega_d, \Omega_m$) v/s time t (Gyr)

- Density parameters:** “It has been suggested by most authors that the $\Omega \approx 1$. The ultimate destiny of the Universe can be revealed by knowing whether Ω is greater than 1, less than 1, or exactly equal to 1. Eventually, the Universe will stop expanding and collapse if $\Omega > 1$. In the case where $\Omega < 1$, then the Universe is open and will continue to expand forever, whereas if $\Omega = 1$, then the Universe is flat and has enough material to stop expansion, but not enough to collapse. As a result of this definition, a dimensionless density parameter expression can be found as follows:”

$$\Omega_d = \frac{\rho_d}{3H^2}, \quad (39)$$

$$\Omega_m = \frac{\rho_m}{3H^2}, \tag{40}$$

$$\Omega = \Omega_d + \Omega_m. \tag{41}$$

For model (26), the density parameters of VRDE, matter, and total density are given by

$$\Omega_d = \frac{-\alpha (\beta_2 - 2 \cosh(\beta_1 t)^2)}{\cosh(\beta_1 t)^2}, \tag{42}$$

$$\Omega_m = \frac{12 (\cosh(\beta_1 t)^2 - 1) \cosh(\beta_1 t)^2 \left(n + \frac{1}{4}\right) \sinh(\beta_1 t)^{\frac{\beta_2(-2n-2)-6n}{\beta_2(n+1)}}}{4 \cosh(\beta_1 t)^2 (n+1)^2} + \frac{4\alpha(n+1)^2 (\beta_2 - 2 \cosh(\beta_1 t)^2)}{4 \cosh(\beta_1 t)^2 (n+1)^2}, \tag{43}$$

$$\& \quad \Omega = \frac{3(4n+1) \sinh(\beta_1 t)^{\frac{-6n}{\beta_2(n+1)}}}{4(n+1)^2}. \tag{44}$$

According to Fig. (14), we analyze the behavior of the density parameters of VRDE (Ω_d), matter (Ω_m) as well as the total density (Ω) as a function of cosmic time t for model (26) with β_1 and β_2 . Based on the trajectory of density parameters, we observe that Ω_d , Ω_m & Ω decrease with cosmic time and approach a number less than one at later times, subsequently the total density (Ω) dominates the VRDE and matter parameters.

5. CONCLUSION

Using Einstein GR, we have constructed a Marder type cosmological model with viscous Ricci dark energy. A variable declaration parameter has been applied to study the dynamics of the Universe and to determine solutions to the field equations. A transition from a decelerating to accelerating phase was observed in DP. This model has the following main outcomes:

Our obtained model at present accelerated and deceleration at past, based on the assumed form of DP. Observations agree well with these aspects of the model. At first V , a are dies whereas H , θ , & σ tends to ∞ but as time passes V , a are tends to ∞ and H , θ , & σ are become constant. It can be seen that our constructed model is anisotropic throughout the evolution of the Universe since (A_h) is constant and does not vanish ($A_h \neq 0$). Throughout cosmic expansion, VRDE has a positive energy density. Furthermore, cosmic pressure increases over time and is negative. Also, the changes of EoS parameter $\omega_{de} = \frac{p_d}{\rho_d}$ has been graphically observed. According to this analysis, ω_{de} evolves from the phantom region and varies in the high phantom region. Our constructed model's evolution of $\omega_{de} - \omega'_{de}$ varies in the freezing phase. In the freezing region of the Universe, according to the observations, the growth of the Universe is relatively accelerating at the present time and also we examine that ECs for obtained model and hence notice that SEC, NEC are breach whereas DEC is fulfilled. We observe that Ω_d , Ω_m & Ω decrease with cosmic time and approach a number less than one at later times Throughout the evolution, the JP is positive and reaches one. In general, (r, s) trajectories start from the chaplygin gas region and finally reach SCDM, where $s = 0$, $r = 1$. Consequently, in the future, the constructed model of the Universe will behave in a manner similar to the Λ CDM model.

Compliance with Ethical Standards

Funding: not applicable.

Conflict of interest: The Authors declare that they have no conflicts of interest.

Author contribution: The study was carried out in collaboration of all authors. All authors read and approved the final manuscript.

Ethical Conduct.

Data Availability: The data used to support the findings of this study are included within the article and are cited at relevant places within the text as references.

Acknowledgments MVS acknowledges Department of Science and Technology (DST), Govt of India, New Delhi for financial support to carry out the Research Project [No. EEQ/2021/000737, Dt. 07/03/2022].

ORCID

 T. Chinnappalanaidu, <https://orcid.org/0000-0001-6902-2820>;  M. Vijaya Santhi, <https://orcid.org/0000-0002-0050-3033>;  N. Sri Lakshmi Sudha Rani, <https://orcid.org/0009-0009-9593-954X>

REFERENCES

- [1] N. Aghanim, et al., (Planck Collaboration), (2018). <https://doi.org/10.48550/arXiv.1807.06209>
- [2] A.G. Riess, et al., Astron. J. **116**, 1009 (1998). <https://doi.org/10.1086/300499>

- [3] S.Perlmutter, *et al.*, *Astrophys. J.* **517**, 565 (1999). <https://doi.org/10.1086/307221>
- [4] D.M. Scolnic, *et al.*, *Astrophys. J.* **859**, 101 (2018). arXiv:1710.00845 [astro-ph.CO] <https://doi.org/10.3847/1538-4357/aab9bb>
- [5] S.Nadathur, *et al.*, *Phys.Rev.Lett.* **124**, 221301 (2020). <https://doi.org/10.1103/PhysRevLett.124.221301>
- [6] B. Ratra, and P. Peebles, *Am. Phys. Soc.* **37**(12), 3406 (1988). <https://doi.org/10.1103/PhysRevD.37.3406>
- [7] T. Chiba, *et al.*, *Phys. Rev. D*, **62**, 023511 (2000). <https://doi.org/10.1103/PhysRevD.62.023511>
- [8] H. Wei, and R.G. Cai, *Phys. Lett. B*, **660**(3), 113 (2008). <https://doi.org/10.1016/j.physletb.2007.12.030>
- [9] M.V. Santhi, *et al.*, *Int. J. Theor. Phys.* **56**, 362 (2017). <https://doi.org/10.1007/s10773-016-3175-8>
- [10] H. Wei, and R.G. Cai, *Phys. Lett. B*, **663**, 1 (2008). <https://doi.org/10.1016/j.physletb.2008.03.048>
- [11] A. Kamenshchik, *et al.*, *Phys. Lett. B*, **511**, 265 (2001). [https://doi.org/10.1016/S0370-2693\(01\)00571-8](https://doi.org/10.1016/S0370-2693(01)00571-8)
- [12] A. Cohen, *et al.*, *Phys. Rev. Lett.* **82**, 4971 (1999). <https://doi.org/10.1103/PhysRevLett.82.4971>
- [13] P. Horava, and D. Minic, *Phys. Rev. Lett.* **85**, 1610 (2000). <https://doi.org/10.1103/PhysRevLett.85.1610>
- [14] V. Husain, and O. Winkler, *Phys. Rev. D*, **75**, 024014 (2007). <https://doi.org/10.1103/PhysRevD.75.024014>
- [15] T. Harko, *et al.*, *Phys. Rev. D*, **84**, 024020 (2011). <https://doi.org/10.1103/PhysRevD.84.024020>
- [16] C.H. Brans, and R.H. Dicke, *Phys. Rev.* **124**, 925 (1961). <https://doi.org/10.1103/PhysRev.124.925>
- [17] D. Saez, and V.J. Ballester, *Phys. Lett.* **113**, 467 (1986). [https://doi.org/10.1016/0375-9601\(86\)90121-0](https://doi.org/10.1016/0375-9601(86)90121-0)
- [18] A. Einstein, *Ann. Phys.* **354**, 769 (1916). <https://doi.org/10.1002/andp.19163540702>
- [19] G t'Hooft, arXiv:gr-qc/9310026 (1993). <https://arxiv.org/abs/gr-qc/9310026>
- [20] L. Susskind, *J. Math. Phys.* **36**, 6377 (1995). <https://doi.org/10.1063/1.531249>
- [21] M. Li, *Phys. Lett. B*, **603**, 1 (2004). <https://doi.org/10.1016/j.physletb.2004.10.014>
- [22] W. Fischler, and L. Susskind, arXiv:hep-th/9806039 (1998). <https://arxiv.org/abs/hep-th/9806039>
- [23] Y. Gong, *Phys. Rev. D*, **70**, 064029 (2004). <https://doi.org/10.1103/PhysRevD.70.064029>
- [24] B.Wang, *et al.*, *Phys. Lett. B*, **624**, 141 (2005). <https://doi.org/10.1016/j.physletb.2005.08.008>
- [25] X. Zhang, *Int. J. Mod. Phys. D*, **14**, 1597 (2005). <https://doi.org/10.1142/S0218271805007243>
- [26] D. Pavon, and W. Zimdahl, arXiv:hep-th/0511053 (2005). <https://arxiv.org/abs/hep-th/0511053>
- [27] A.G. Cohen, *et al.*, *Phys. Rev. Lett.* **82**, 4971 (1999). <https://doi.org/10.1103/PhysRevLett.82.4971>
- [28] C. Gao, *et al.*, *Phys. Rev. D*, **79**, 043511 (2009). <https://doi.org/10.1103/PhysRevD.79.043511>
- [29] J.D. Barrow, *Phys. Lett. B*, **180**, 335 (1986). [https://doi.org/10.1016/0370-2693\(86\)91198-6](https://doi.org/10.1016/0370-2693(86)91198-6)
- [30] I. Brevik, and S.D. Odintsov, *Phys. Rev. D*, **65**, 067302 (2002). <https://doi.org/10.1103/PhysRevD.65.067302>
- [31] I. Brevik, and O. Gorbunova, *Gen. Relativ. Gravit.* **37**, 2039 (2005). <https://doi.org/10.1007/s10714-005-0178-9>
- [32] D.J. Liu, and X.Z. Li, *Phys. Lett. B*, **611**, 8 (2005). <https://doi.org/10.1016/j.physletb.2005.02.048>
- [33] S. Nojiri, and S.D. Odintsov, *Phys. Rev. D*, **72**, 023003 (2005). <https://doi.org/10.1103/PhysRevD.72.023003>
- [34] S. Capozziello, *et al.*, *Phys. Rev. D*, **73**, 043512 (2006). <https://doi.org/10.1103/PhysRevD.73.043512>
- [35] J. Ren, and X.H. Meng, *Phys. Lett. B*, **633**, 1 (2006). <https://doi.org/10.1016/j.physletb.2005.11.055>
- [36] Hu M.G., Meng X.H., *Phys. Lett. B*, **635**, 186 (2006). <https://doi.org/10.1016/j.physletb.2006.02.059>
- [37] N. Cruz, S. Lepe, and F. Pena, *Phys. Lett. B*, **646**, 177 (2007). <http://dx.doi.org/10.1016/j.physletb.2017.01.035>
- [38] X.H. Meng, J. Ren, and M.G. Hu, *Commun. Theor. Phys.* **47**, 379 (2007). <https://doi.org/10.1088/0253-6102/47/2/036>
- [39] C.P. Singh, S. Kumar, and A. Pradhan, *Class. Quantum Gravit.* **24**, 455 (2007). <https://doi.org/10.1088/0264-9381/24/2/011>
- [40] C.P. Singh, *Pramana J. Phys.* **71**, 33 (2008). <https://doi.org/10.1007/s12043-008-0139-4>
- [41] C.J. Feng, and X.Z. Li, *Phys. Lett. B*, **680**, 355 (2009). <https://doi.org/10.1016/j.physletb.2009.09.013>
- [42] Y.D.Xu, Z.G. Huang, and X.H. Zhai, *Astrophys. Space Sci.* **337**, 493 (2012). <https://doi.org/10.1007/s10509-011-0850-3>
- [43] C.P. Singh, P. Kumar, *Eur. Phys. J. C*, **74**, 3070 (2014). <https://doi.org/10.1140/epjc/s10052-014-3070-5>
- [44] P. Kumar, and C.P. Singh, *Astrophys. Space Sci.* **357**, 120 (2015). <https://doi.org/10.1007/s10509-015-2348-x>
- [45] J.S. Gagnon, and J. Lesgourgues, *J Cosmol. Astropart. Phys.* **09**, 026 (2011). <https://doi.org/10.1088/1475-7516/2011/09/026>
- [46] I. Brevik, *et al.*, *Int. J. Mod. Phys. D*, **26**, 1730024 (2017). <https://doi.org/10.1142/S0218271817300245>
- [47] B.D. Normann, and I. Brevik, *Mod. Phys. Lett. A*, **32**, 1750026 (2017). <https://doi.org/10.1142/S0217732317500262>
- [48] B.D. Normann, and I. Brevik, *Entropy*, **18**, 215 (2016). <https://doi.org/10.3390/e18060215>
- [49] M. Jamil, and M.U. Farooq, *Int. J. Theor. Phys.* **49**, 42 (2010). <https://doi.org/10.1007/s10773-009-0176-x>
- [50] S. Chattopadhyay, *Int. J. Mod. Phys. D*, **26**, 1750042 (2017) <https://doi.org/10.1142/S0218271817500420>
- [51] C.J. and Feng, X.Z. Li, *Phys. Lett. B*, **680**, 355 (2009). <https://doi.org/10.1016/j.physletb.2009.09.013>

- [52] C.P. Singh, and P. Kumar, *Astrophys. Space Sci.* **361**, 157 (2016). <https://doi.org/10.1007/s10509-016-2740-1>
- [53] A.D. Linde, *Inflationary cosmology*, *Lect. Notes Phys.* **738**, 1 (2008). https://doi.org/10.1007/978-3-540-74353-8_1
- [54] P.A.R. Ade, *et al.*, *Planck Collab.*, *Planck 2013 results. XVI. Cosmological parameters*, *Astron. Astrophys.* **571**, A16 (2014). <https://doi.org/10.1051/0004-6361/201321591>
- [55] E. Komatsu, *et al.*, *Astrophys. J. Suppl.* **180**, 330 (2008). <https://doi.org/10.1088/0067-0049/180/2/330>
- [56] S. Aygün, *et al.*, *Journal of Geometry and Physics*, **62**, 100 (2012). <https://doi.org/10.1016/j.geomphys.2011.09.011>
- [57] C.B. Kilinc, *Astrophys. Space Sci.* **222**, 171 (1994). <https://doi.org/10.1007/BF00627091>
- [58] M. Sharif, and H.R. Kausar, *Phys. Lett. B*, **697**, 1 (2011). <https://doi.org/10.1016/j.physletb.2011.01.027>
- [59] S. Aygün, *et al.*, *Astrophys. Space Sci.* **361**, 380 (2016). <https://doi.org/10.1007/s10509-016-2956-0>
- [60] S. Aygün, *Turk. J.Phys.* **41**, 436 (2017). <https://doi.org/10.3906/fiz-1704-14>
- [61] S. Aygün, *et al.*, *Indian J.Phys.* **93**, 407 (2019). <https://doi.org/10.1007/s12648-018-1309-y>
- [62] C. Kömürçü, and C. Aktas, *Mod. Phys. Lett. A*, **2050263**, 1 (2020). <https://doi.org/10.1142/S0217732320502636>
- [63] Aygün, S., *et al.*, *Pramana J. Phys.* **68**, 21 (2007). <https://doi.org/10.1007/s12043-007-0002-z>
- [64] A. Kabak, and S. Aygün, *Int. J. Mod. Phys.* **9**, 50 (2019).
- [65] A. Ali, *et al.*, *Int. J. innov. sci. math.* **7**, 2347 (2019). https://www.ijism.org/administrator/components/com_jresearch/files/publications/IJISM_798_FINAL.pdf
- [66] K.P. Singh, *et al.*, *Journal of Physics A: Mathematical, Nuclear and General*, **6** 1090, (1973). <https://doi.org/10.1088/0305-4470/6/7/029>
- [67] S. Prakash, *Astrophys. space sci.* **111**, 383, (1985). <https://doi.org/10.1007/BF00649977>
- [68] A.R. Roy, and B. Chatterjee, *Acta Phys. Acad. Sci. Hung.* **48**, 383, (1980). <https://doi.org/10.1007/BF03155547>
- [69] B. Mukherjee, *Heavy Ion Phys.* **18**, 115 (2003).
- [70] D.D. Pawar, and Y.S. Solanke, *arXiv:1602.05222*, (2016). <https://arxiv.org/abs/1602.05222>
- [71] D.D. Pawar, and M.K. Panpatte, *Prespacetime Journal*, **7**, 1187 (2016). <https://prespacetime.com/index.php/pst/issue/view/83>
- [72] D.D. Pawar, *et al.*, *New Astronomy*, **87**, 101599 (2021). <https://doi.org/10.1016/j.newast.2021.101599>
- [73] M.V. Santhi, *et al.*, *MSEA*, **71** 1056 (2022).
- [74] M.V. Santhi, *et al.*, *Indian J. Phys.* **97**, 1641 (2022). <https://doi.org/10.1007/s12648-022-02515-9>
- [75] M.V. Santhi, and T. Chinnappalanaidu, *Int. J. Geom. Methods Mod.* **19** 2250211 (2022). <https://doi.org/10.1142/S0219887822502115>
- [76] J.R. Wilson, G.J. Mathews, and G.M. Fuller, *Phys. Rev. D*, **75** 043521 (2007). <https://doi.org/10.1103/PhysRevD.75.043521>
- [77] C.B. Collins, *et al.*, *Gen. Relativ. Gravit.* **12**, 805 (1980). <https://doi.org/10.1007/BF00763057>
- [78] R.K. Mishra, *et al.*, *Int. J. Theor. Phys.* **55**, 1241 (2016). <https://doi.org/10.1007/s10773-015-2766-0>
- [79] M.V. Santhi, *et al.* *Can. J. Phys.* **95**, 381 (2017). <https://doi.org/10.1139/cjp-2016-0781>
- [80] V.U.M. Rao, and U.Y. Divya Prasanthi, *Eur. Phys. J. Plus*, **132**, 64 (2017). <https://doi.org/10.1140/epjp/i2017-11328-9>
- [81] D.R.K. Reddy, *et al.*, *arXiv:1601.02648* (2016). <https://arxiv.org/abs/1601.02648>
- [82] T. Chiba, and T. Nakamura, *Prog. Theor. Phys.* **100**, 1077 (1998). <https://doi.org/10.1143/PTP.100.1077>
- [83] M. Visser, *Class. Quantum Gravity*, **21**, 2603 (2004). [10.1088/0264-9381/21/11/006](https://doi.org/10.1088/0264-9381/21/11/006)
- [84] V. Sahni, *et al.*, *J. Exp. and Theor. Phys. Lett.* **77**, 201 (2003). <https://doi.org/10.1134/1.1574831>
- [85] R. Caldwell, and E.V. Linder, *Phys. Rev. Lett.* **95**, 141301 (2005). <https://doi.org/10.1103/PhysRevLett.95.141301>
- [86] A. Raychaudhuri, *Phys. Rev.* **98**, 1123 (1955). <https://doi.org/10.1103/PhysRev.98.1123>

АНАЛІЗ КОСМОЛОГІЧНОЇ МОДЕЛІ В'ЯЗКОЇ ТЕМНОЇ ЕНЕРГІЇ РІЧЧІ В ЗАГАЛЬНІЙ ТЕОРІЇ ГРАВІТАЦІЇ

Т. Чіннаппаланаїду^a, М. Віджая Санті^b, Н. Шрі Лакшмі Судха Рані^b

^a Департамент математики, Інститут інформаційних технологій Віньяна (автономний), Вісакхапатнам 530049, Індія

^b Департамент прикладної математики, Коледж науки і технологій, Університет Андхра, Вісакхапатнам 530003, Індія
Це дослідження зосереджено на динамічному дослідженні простору-часу типу Мардера, що містить в'язку темну енергію Річчі, в рамках загальної теорії відносності. Щоб знайти розв'язок рівнянь поля, ми використовуємо співвідношення між метричними

потенціалами та середнім масштабним коефіцієнтом $a(t) = (\sinh \beta_1 t)^{\frac{1}{2}}$, це призводить до плавного переходу Всесвіту від початкової фази уповільнення до поточної фази прискорення. Тут ми отримали космологічні параметри та площину $\omega_{de} - \omega'_{de}$ для похідної моделі. Також за допомогою діаграм аналізуються динамічні особливості отриманої космологічної моделі.

Ключові слова: темна енергія; в'язка темна енергія Річчі; метрика типу Мардера; загальна теорія відносності

A STUDY OF TIME EVOLUTION OF SOME COSMOLOGICAL PARAMETERS IN THE FRAMEWORK OF AN ANISOTROPIC KALUZA-KLEIN METRIC USING AN EMPIRICAL EXPONENTIAL SCALE FACTOR

Sudipto Roy

Department of Physics, St. Xavier's College, Kolkata, West Bengal, India

Corresponding Author e-mail: roy.sudipto@sxccal.edu

Received June 8, 2024; revised July 7, 2024; accepted July 15, 2024

The present study attempts to determine the time dependence of some cosmological parameters in flat space (i.e., a space of zero spatial curvature), in the framework of an anisotropic Kaluza-Klein metric. The field equations for this work have been derived from the metric by assuming a power-law relation between the normal scale factor and the scale factor corresponding to the extra (i.e., the fifth) dimension. An empirical scale factor, having the expression of $a = B \exp(at^\beta)$, has been used here in order to derive the expressions for some cosmological parameters as functions of time. The reason for choosing this scale factor is that it generates an expression for the deceleration parameter which undergoes a change of sign, as time goes on, from positive to negative, indicating a transition of the universe from an initial state of decelerated expansion to that of an accelerated expansion (which is its present state), as has been inferred from astrophysical observations. We have graphically depicted the evolution of some cosmological parameters with respect to what one may call the *relative time*, expressed as t/t_0 , where t_0 is the present age of the universe. The present study finds the dynamical cosmological constant (Λ) to be negative, and it becomes less negative with time, changing at a gradually decreasing rate. The dependence of pressure of the all-pervading cosmic fluid upon density, corresponding to the fifth dimension, has been described in terms of a skewness parameter (δ) which comes out to be decreasing with time. The anisotropy factor has been calculated in this study, whose numerical value has been found to be decreasing with time, indicating a journey of the universe towards phases of gradually smaller anisotropy.

Keywords: *Dark energy; Kaluza-Klein theory; Cosmological parameter (Λ); Anisotropy; Exponential scale factor*

PACS: 04.20.-q; 04.50.+h; 04.50.-h; 98.80.Es; 98.80.-k

1. INTRODUCTION

Based on cosmological observations throughout the world, it has been convincingly established that the universe undergoes a process of expansion with acceleration. Research is going on extensively to understand the nature of the agent causing an accelerated expansion. If gravitation had been the only interaction governing the motions of celestial bodies, the expansion of the universe would have continued with deceleration. On the basis of the observational findings from supernova 1a, it was concluded that there is a negative pressure generated by an exotic form of energy, referred to as dark energy (DE), which is considered to be responsible for the present phase of accelerated expansion of the universe [1, 2]. The functioning of this mysterious DE can only be determined by extensive investigations. A thorough analysis of supernova data has led to an inference that the universe has changed its phase from decelerated expansion to accelerated expansion, resulting in the change of sign of the deceleration parameter from positive to negative [3-5]. In the vast scientific literature regarding investigations to find the nature of cosmic acceleration, one generally finds approaches through mainly two ways. One of these ways is to construct mathematical models using modified theories of gravity (which are based on modifications of Einstein's theory of general relativity) and explore their characteristics. The other way is to investigate the cosmological observations by formulating dark energy models. A parameter, named cosmological constant (denoted by Λ), has been said to be representing DE in lots of models on cosmology. There are various dark energy models in scientific literature, namely quintessence, phantom, k-essence and quintom [6-9]. Although Λ was introduced in Einstein's theory as a constant parameter [10], but, due to some limitations connected with the coincidence problem and the cosmological constant problem, it is presently regarded as a time-dependent quantity [11]. By modifying Einstein's theory of gravity in various ways, researchers have formulated theories such as $f(R)$ and $f(R, T)$ [12-14] and scalar tensor models like Saez-Ballester (SB) and Brans-Dicke (BD) theories of gravity [15, 16]. Wide range of investigations have been carried out by constructing models on cosmological phenomena involving DE [17-20].

In order to unify electromagnetic force with gravitational force, two scientists, Kaluza and Klein, proposed a new theory in last century's first half, and it has always been referred to Kaluza-Klein (KK) theory since then [21, 22]. This theory talked about a new dimension (or the *fifth* dimension) which acted as a link between the two forces. A contraction of this new dimension with time was proved by Chodos and Detweiler through a five-dimensional model based on KK theory [23]. The current four-dimensional representation of the universe is theoretically demonstrated to be preceded by an era of a multidimensional state. The extra dimension shrinks along with the evolution of the universe and it cannot be detected now by the experimental techniques at our disposal. These phenomena have inspired many

researchers to carry out studies by formulating models involving higher dimensions. The KK theory can be looked upon as a five-dimensional generalization of the general theory of relativity. Theoretical investigations, which are considered to be of great importance in this field, are those carried out by Chodos & Detweller [23], Witten [24], Appelquist et al. [25], Appelquist & Chodos [26] and Marchiano [27]. The motivation for the present work was obtained from a formulation of an anisotropic dark energy model based on KK theory by N. I. Jain [28].

An approximate solution to Kaluza-Klein's equations was shown in a study undertaken by J.A. Ferrari for a spherically symmetric charged system [29]. This study was carried out to find how a test particle behaves in a field of force produced by a charged particle. According to this study, Kaluza-Klein's theory allows us to determine the corrections to the Lorentz force. The five-dimensional relativity in KK framework is validated by these experimental observations. It is possible to verify experimentally the existence of an extra spacetime dimension, as obtained from a study by Kalligas et al. [30]. A set of equations was derived in this study which contains terms connected with the existence of an extra dimension. Using the data obtained from observations of the solar system it has been established that the terms representing the fifth dimension is extremely small in comparison to the usual dimensions of spacetime, in our region of space. It has been found that the parameters corresponding to the KK theory cannot be treated as universal constants, and, there can be place to place variation of these parameters depending upon the local characteristic of matter. Several non-asymptotically flat solutions of Kaluza-Klein space-time were found by Dzhunushaliev et al., which had both electric and magnetic charges [31]. It was proved that these solutions could be regarded to be acting as virtual quantum handles (wormholes) in the models on space-time foam. It was shown that, within an external magnetic and/or electric field, which is sufficiently large, these solutions might be *inflated* from a quantum state to a classical state. This finding leads to the expectation, in a multidimensional gravity, for a possible experimental signal for higher dimensions. An improvement of the theory based five-dimensional Kaluza-Klein metric is possible, according to a recent study by Jean Paul Mbelek [32], by incorporating an external scalar field (ψ). It came out of that formulation that the observational data (for the experiments in the laboratory and also in the context of astrophysics and cosmology) are consistent with the theoretical findings. It has been found in the study that, in consistency with predictions based on the theory, one measured a torque acting upon a torsion pendulum. Based on a novel experimental investigation, by Tajmar and Williams [33], a macroscopic interpretation of the fifth dimension of the Kaluza-Klein theory has been obtained. This experiment was carried out to verify an important aspect of theoretical findings which shows the fifth dimension to somehow correspond to the electric charge. Based on Kaluza-Klein theory, they arrived at an interpretation of the observations regarding the time dilation effect in an electrically charged clock. They explained it by saying that the five-dimensional metric should have a timelike signature for a classical explanation of the extra dimension.

The objective of the present study is to investigate the nature of time dependence of some cosmological parameters, based on an anisotropic Kaluza-Klein spacetime. This study involves a time-dependent cosmological term (Λ). A power-law type relation (*i. e.*, $A = a^n$) has been assumed between the normal scale factor (a) and the scale factor representing the extra dimension (A), both of which belong to the Kaluza-Klein metric used here.

To obtain the solution of field equations, we have used an *ansatz* for the scale factor (*i.e.*, $a = B \exp[at^\beta]$). The reason for choosing this function is that, the deceleration parameter ($q = -\ddot{a}a/\dot{a}^2$), obtained from this scale factor, undergoes a signature flip with time from positive to negative, which is consistent with the fact that the present phase of accelerated expansion of the universe was preceded by a phase of decelerated expansion [3-5]. Using this exponential scale factor, we have derived expressions for some cosmological quantities such as, Hubble parameter (H), deceleration parameter (q), energy density (ρ), cosmological constant (Λ), equation of state (EoS) parameter (ω), skewness parameter (δ) and the anisotropy factor (σ^2/θ). We have depicted their time variation by plotting them graphically as functions of the relative cosmic time (*i.e.*, t/t_0) where t_0 denotes the age of the universe at the present time, which is nearly 13.7×10^9 years.

Based on our findings regarding both skewness parameter (δ) and the anisotropy factor (σ^2/θ) it can be said that we are heading towards phases of smaller anisotropy. The dynamical cosmological term (Λ), in our study, comes out to be negative (becoming less negative with time) and it changes very slowly in the present universe, indicating probably a slow rise in the dark energy content, which is considered to be causing the cosmic acceleration.

This article has six sections including the one for *introduction*. Sections 2 and 3 are respectively about the field equations and their solutions. Determination of cosmological quantities has been dealt with in the 4th section. Sections 5 and 6 are respectively about the findings of this theoretical investigation and its conclusions.

2. THE METRIC AND THE FIELD EQUATIONS

In order to obtain the cosmological field equations, we have used the Kaluza-Klein space-time of the following type [34].

$$ds^2 = -dt^2 + a^2(t) \left[\frac{dr^2}{1-kr^2} + r^2 d\theta^2 + r^2 \sin^2\theta d\phi^2 \right] + A^2(t) d\psi^2. \quad (1)$$

In equation (1), $a(t)$ and $A(t)$ are the fourth and fifth-dimension scale factors respectively. The symbol k is a measure of the spatial curvature, having the values -1 , 0 and $+1$ respectively for the *open*, *flat* and *closed* universes. The energy-momentum tensor (T^i_j), for the anisotropic space-time metric represented by equation (1), is given below [35].

$$T_j^i = \text{diag}(T_0^0, T_1^1, T_2^2, T_3^3, T_4^4) = \text{diag}(-\rho, p, p, p, p_\psi). \quad (2)$$

In equation (2), the symbols ρ and p denote respectively the energy density and pressure of the cosmic fluid (dark energy) pervading the universe. The symbol p_ψ denotes the pressure corresponding to the extra dimension. The barotropic equation of state (EoS) parameter for the normal dimensions is $\omega = p/\rho$. Based on some studies on anisotropy, in the framework of Kaluza-Klein theory, we have used the equation, $p_\psi = (\delta + \omega)\rho$, as the directional equation of state for the fifth dimension, where δ is the skewness parameter which represents the deviation from the normal equation-of-state parameter ω [28, 36-41]. The parameter δ serves as a measure of deviation from isotropy. Thus, the energy-momentum tensor of equation (2) can be rewritten as,

$$T_j^i = \text{diag}(-\rho, \omega\rho, \omega\rho, \omega\rho, (\omega + \delta)\rho) \quad (3)$$

The time dependence of ω and δ has been investigated in the present study. Gravitational field equations are obtained from the following equation.

$$G_j^i = R_j^i - \frac{1}{2}R\delta_j^i = -8\pi GT_j^i + \Lambda\delta_j^i \quad (4)$$

To formulate the field equations, we have used an *ansatz* for the fifth-dimension scale factor (A), which is $A = a^n$ [42]. We have also used $8\pi G = c = 1$ and $k = 0$ (i.e., flat space). Combining equations (1), (3) and (4), one gets the following field equations.

$$(n + 2)\dot{H} + (n^2 + 2n + 3)H^2 = -\omega\rho + \Lambda \quad (5)$$

$$3\dot{H} + 6H^2 = -(\omega + \delta)\rho + \Lambda \quad (6)$$

$$3(n + 1)H^2 = \rho + \Lambda \quad (7)$$

Divergence of Einstein's tensor can be expressed as,

$$\left(R_j^i - \frac{1}{2}R\delta_j^i\right)_{;j} = (-T_j^i + \Lambda\delta_j^i)_{;j} = 0 \quad (8)$$

Based on equation (8), the equation representing energy conservation [35] is given by,

$$\dot{\rho} + 3(\rho + p)H + n(\rho + p_\psi)H + \dot{\Lambda} = 0 \quad (9)$$

Substituting the equations of state for the normal dimension and the extra dimension [i.e., $p = \omega\rho$ and $p_\psi = (\omega + \delta)\rho$ respectively] in equation (9), we get,

$$\dot{\rho} + (3 + n)(1 + \omega)\rho H + n\rho\delta H + \dot{\Lambda} = 0 \quad (10)$$

Equation (10) can be written as a sum of two equations which are equations (11) and (12), as given below.

$$\dot{\rho} + (3 + n)(1 + \omega)\rho H = Q \quad (11)$$

$$n\rho\delta H + \dot{\Lambda} = -Q \quad (12)$$

In equations (11) and (12), Q is an arbitrary parameter.

Subtracting equation (6) from equation (5), we get,

$$(n - 1)\dot{H} + (n^2 + 2n - 3)H^2 = \rho\delta \quad (13)$$

Substitution for $\rho\delta$ in equation (12), based on equation (13), leads to the following differential equation.

$$\dot{\Lambda} = -Q - nH(n - 1)[\dot{H} + (n + 3)H^2] \quad (14)$$

3. SOLUTION OF THE FIELD EQUATIONS USING AN EMPIRICAL SCALE FACTOR

To solve the field equations, we have used the following *ansatz* for the scale factor.

$$a = B \exp(\alpha t^\beta) \quad (15)$$

where the constant parameters $B, \alpha, \beta > 0$.

The reason for using this scale factor (expressed by eqn. 15) is that it leads to a deceleration parameter (given by equation no. 17) which (with suitable parameter values) undergoes a change of sign (as a function of time) from positive to negative, which is in agreement with the inferences drawn from recent astrophysical observations [ref. nos. 3-5] demonstrating a transition from decelerated expansion to accelerated expansion of the expanding universe. For the same purpose, one often uses a hybrid scale factor which is a combination of an *exponential* and a *power-law* function of time. It has been used in several recent cosmological studies [43-49]. There are some studies where hyperbolic functions of time have been used as empirical scale factors [50-55], having the same property (i.e., deceleration-to-

acceleration transition) of cosmic expansion. The parameter B in the expression for the scale factor (eqn. 15) does not appear in the equations representing the Hubble parameter and the deceleration parameter (eqns. 16 & 17 respectively), because of their expressions, which are, $H = \frac{\dot{a}}{a}$ and $q = -\frac{\ddot{a}a}{\dot{a}^2}$ respectively. All functions of H and q are therefore independent of B . The left-hand sides of equations (5), (6) and (7) are functions of the Hubble parameter (H) and its time derivative and they are thus independent of the parameter B . This is the reason why the parameter B is not found in any expression of the present article except that of the scale factor (eqn. 15).

Based on our empirical scale factor (eqn. 15), the Hubble parameter (H) is given by,

$$H = \frac{\dot{a}}{a} = \alpha\beta t^{\beta-1} \tag{16}$$

Based on our empirical scale factor (eqn. 15), the deceleration parameter (q) is given by,

$$q = -\frac{\ddot{a}a}{\dot{a}^2} = \frac{1-\beta}{\alpha\beta t^\beta} - 1 \tag{17}$$

In the present article, we have used the symbols, H_0 and q_0 , which stand for the values of H and q respectively at the present time (i.e., $t = t_0$) where t_0 denotes the age of the universe ($t_0 = 13.7 \times 10^9$ years).

Putting $H = H_0$, $q = q_0$ and $t = t_0$ in equations (16) and (17), we get,

$$H_0 = \alpha\beta t_0^{\beta-1} \tag{18}$$

$$q_0 = \frac{1-\beta}{\alpha\beta t_0^\beta} - 1 \tag{19}$$

Combining equations (18) and (19) we get the following expressions for the constants α and β .

$$\alpha = \frac{H_0 t_0^{(q_0+1)H_0 t_0}}{1-(q_0+1)H_0 t_0} \tag{20}$$

$$\beta = 1 - (q_0 + 1)H_0 t_0 \tag{21}$$

4. DETERMINATION OF COSMOLOGICAL PARAMETERS

Using equation (16) in equation (14) and solving the differential equation for Λ , we get,

$$\Lambda = C - Qt + \frac{n(1-n)\alpha^2\beta^2}{2}t^{2\beta-2} + \frac{n(1-n)(3+n)\alpha^3\beta^3}{3\beta-2}t^{3\beta-2} \tag{22}$$

where C is the integration constant. Using equations (16) and (22) in equation (7), the energy density (ρ) is obtained as,

$$\rho = -C + Qt + \frac{(n^2+5n+6)\alpha^2\beta^2}{2}t^{2\beta-2} - \frac{n(1-n)(3+n)\alpha^3\beta^3}{3\beta-2}t^{3\beta-2} \tag{23}$$

Using equation (5), we get equation (24) which represents the EoS parameter (ω).

$$\omega = \frac{\Lambda - (n+2)\dot{H} - (n^2+2n+3)H^2}{\rho} \tag{24}$$

Using equations (16), (22) and (23) in equation (24), we get,

$$\omega = \frac{C - Qt + \frac{n(1-n)(3+n)\alpha^3\beta^3}{3\beta-2}t^{3\beta-2} - (n+2)\alpha\beta(\beta-1)t^{\beta-2} - \frac{3\alpha^2\beta^2}{2}(n^2+n+2)t^{2\beta-2}}{-C + Qt + \frac{(n^2+5n+6)\alpha^2\beta^2}{2}t^{2\beta-2} - \frac{n(1-n)(3+n)\alpha^3\beta^3}{3\beta-2}t^{3\beta-2}} \tag{25}$$

Using equation (13) we get,

$$\delta = \frac{(n-1)\dot{H} + (n^2+2n-3)H^2}{\rho} \tag{26}$$

Using equations (16) and (23) in equation (26), we get,

$$\delta = \frac{(n-1)\alpha\beta(\beta-1)t^{\beta-2} + (n^2+2n-3)\alpha^2\beta^2t^{2\beta-2}}{-C + Qt + \frac{(n^2+5n+6)\alpha^2\beta^2}{2}t^{2\beta-2} - \frac{n(1-n)(3+n)\alpha^3\beta^3}{3\beta-2}t^{3\beta-2}} \tag{27}$$

Combining equation (16) with equation (22), Λ can be expressed as,

$$\Lambda = C - Qt + \frac{n(1-n)}{2}H^2 + \frac{n(1-n)(3+n)\alpha\beta}{3\beta-2}t^\beta H^2 \tag{28}$$

Using equation (28) in equation (7) we get,

$$\rho = -C + Qt + H^2 \left[3(n+1) - \frac{n(1-n)}{2} - \frac{n(1-n)(3+n)\alpha\beta}{3\beta-2}t^\beta \right] \tag{29}$$

Putting $\rho = \rho_0$, $H = H_0$ and $t = t_0$ in equation (29), we get the following equation from which one can determine the value of C .

$$C = -\rho_0 + Qt_0 + H_0^2 \left[3(n+1) - \frac{n(1-n)}{2} - \frac{n(1-n)(3+n)\alpha\beta}{3\beta-2} t_0^\beta \right] \quad (30)$$

Thus, among the three parameters n , Q and C (which are present in the expressions for Λ , ρ , ω , δ), it is evident from equation (30) that the parameter C can be calculated using the values of the parameters n and Q . One may also express Q as a function of n and C in the following way.

$$Q = \frac{\rho_0 + C - H_0^2 \left[3(n+1) - \frac{n(1-n)}{2} - \frac{n(1-n)(3+n)\alpha\beta}{3\beta-2} t_0^\beta \right]}{t_0} \quad (31)$$

In the present formulation, we have used n and Q as independent parameters, which determine the value of C , in accordance with equation (30).

The expansion scalar (θ) and the shear scalar (σ^2) are given by the following equations.

$$\theta = 3\frac{\dot{a}}{a} + \frac{\dot{A}}{A} = (n+3)H \quad (32)$$

$$\sigma^2 = \frac{3}{8} \left(\frac{\dot{a}}{a} - \frac{\dot{A}}{A} \right)^2 = \frac{3}{8} (1-n)^2 H^2 \quad (33)$$

Using equations (32) and (33), the anisotropy factor (σ^2/θ) can be expressed as,

$$\frac{\sigma^2}{\theta} = \frac{3(1-n)^2}{8(n+3)} H = \frac{3(1-n)^2}{8(n+3)} \alpha\beta t^{\beta-1} \quad (34)$$

5. RESULTS AND DISCUSSION

In the present article, we have discussed the results of a theoretical investigation carried out to determine the time evolution of an anisotropic universe in terms of the time-variations of the directional equation-of-state (EoS) parameters for the normal and extra dimensions (ω & δ), defined respectively by the relations $p = \omega\rho$ and $p_\psi = (\omega + \delta)\rho$. Time-variations of different cosmological parameters, such as scale factor, Hubble parameter, deceleration parameter, energy density, cosmological constant, etc. have been shown graphically.

Using equations (20) and (21), respectively, we have obtained $\alpha = 4.925 \times 10^{-10}$ and $\beta = 0.543$. The time variations of Hubble parameter and deceleration parameter depend upon these parameters, according to equations (16) and (17) respectively. Apart from α and β , the scale factor (a) depends upon the parameter B , according to equation (15). Any change in B causes a proportionate change in the scale factor (a) and its time derivative (da/dt) without affecting the values of the Hubble parameter ($H = \frac{\dot{a}}{a}$) and deceleration parameter ($q = -\frac{\ddot{a}a}{\dot{a}^2}$) because they are independent of B . As per equation (29), the energy density (ρ) depends upon the parameters n , C and Q , where C itself depends upon Q & n according to equation (30). Based on equation (7) we have, $\Lambda = 3(n+1)H^2 - \rho$. Thus, Λ has a similar dependence upon Q , which is evident from equation (28). The larger the value of Q , the faster would be the change in Qt with time, which is present in both Λ and ρ . The parameter C was introduced in the expression for Λ (eqn. 22) as a constant of integration. Based on equation (30), we have $C = -8.043 \times 10^{-27}$ for $Q = 0$ and $n = -500$. For this study, we have used $Q = 0$, otherwise the energy density (ρ) comes out to be negative for a certain range of values of t . For $n > 0$, we have found the energy density (ρ) to be increasing with time which is not possible for an universe which is expanding with time. For $n = 0$, there is almost no change of ρ with time. For these reasons, we have depicted our findings graphically for $n < 0$ in this article.

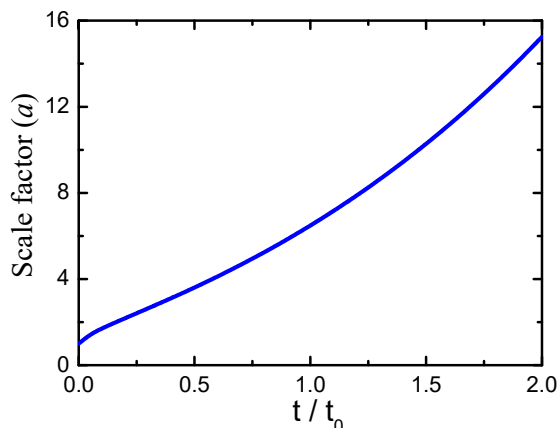


Figure 1. The scale factor versus time

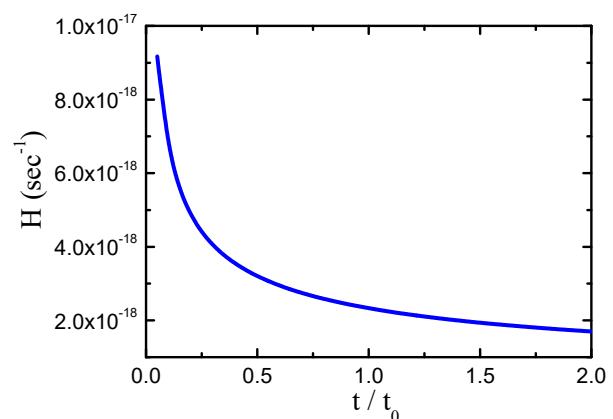


Figure 2. The Hubble parameter versus time

Figure 1 shows the time-variation of the scale factor (a). This cosmological quantity increases with time, which is in accordance with the property of an expanding universe. This figure shows that the rate of change of scale factor increases with time.

Figure 2 depicts the Hubble parameter (H) as a function of time. This plot shows this parameter to be decreasing with time. Its positive value is in accordance with the property of an expanding universe. Its decrease with time indicates that the scale factor (a) increases faster with time in comparison to the increase in its rate of change (\dot{a}). One can also say that, the time-rate of fractional change of the scale factor (a) decreases with time.

Figure 3 shows the time variation of the deceleration parameter (q). It shows a signature flip, from positive to negative, indicating clearly a transition of the universe from a phase of decelerated expansion to a phase of accelerated expansion, which is in agreement with the inferences drawn from astrophysical observations [3-5].

Figure 4 depicts the time dependence of the energy density (ρ) for three values of the parameter n , where we have $Q = 0$. The energy density decreases with time which is expected for a universe which is expanding with time. This figure shows that, more negative values of n cause a faster fall in ρ . We have found that, for $Q \neq 0$ and $n \geq 0$, ρ is often found to negative (which is not allowed by its definition) and increasing with time (which is not admissible for an expanding universe). For this reason, we have used same values, i.e., $Q = 0$ and $n < 0$ to depict the time dependence of other parameters (Λ , ω and δ).

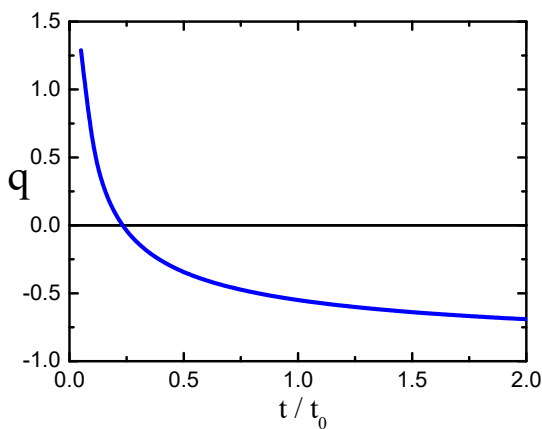


Figure 3. The deceleration parameter versus time

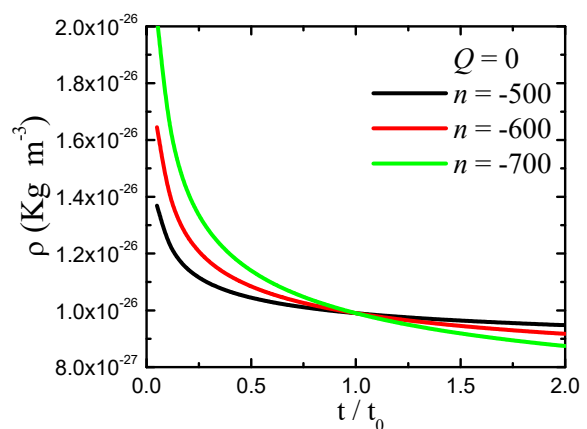


Figure 4. The energy density versus time for three values of the parameter n

Figure 5 shows the nature of dependence of the cosmological constant (Λ) upon time for three values of the parameter n , with $Q = 0$. The cosmological constant (Λ) is often used to represent the dark energy which is generally held responsible for the accelerated expansion of the universe. It is found to be negative in our study, becoming less negative with time at a gradually decreasing rate. This behaviour is found to be consistent with the observations of some recent studies [48, 56-58]. This figure shows the cosmological constant (Λ) to have a faster rise with time for more negative values of n .

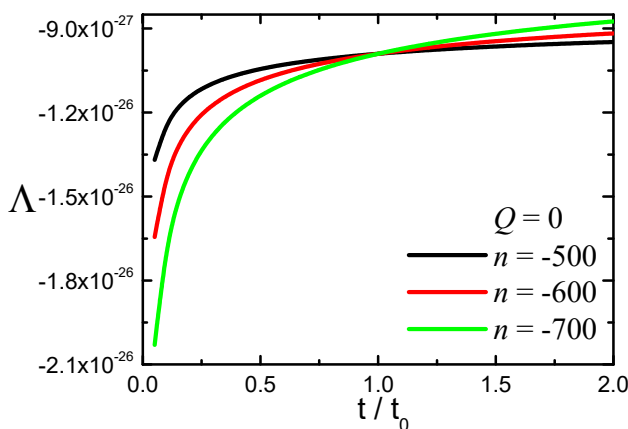


Figure 5. The dynamical cosmological parameter versus time for three values of the parameter n

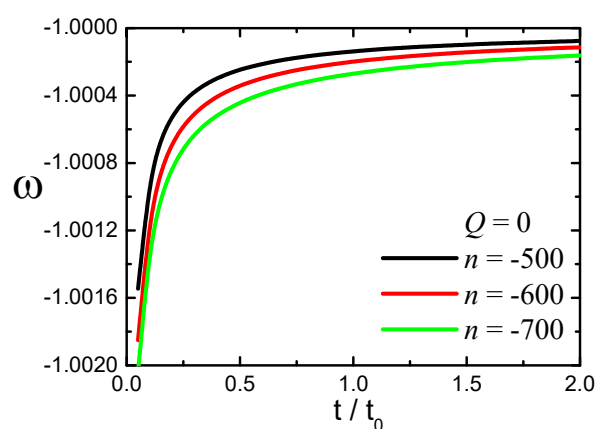


Figure 6. The EoS parameter versus time for three values of the parameter n

Figure 6 shows the nature of dependence of the EoS parameter (ω) upon time for three values of the parameter n , with $Q = 0$. It is negative and it becomes closer to -1 (minus one) with time at a rate which decreases gradually with time. Its values show that the universe is dominated by *phantom* dark energy (i.e., $\omega < -1$) at the early stage and also

at the present time (i.e., $t = t_0$), but it is gradually making a transition to a state where it will be dominated by vacuum fluid (i.e., $\omega = -1$) in future, and thereafter to a state of *quintessence* dark energy (i.e., $\omega > -1$) later. These findings are in agreement with the results of some studies carried out in theoretical frameworks which are totally different from the Kaluza-Klein framework that we have used here [59-61]. As per SN Ia data we have $-1.67 < \omega < -0.6237$ while the range obtained by a combination of galaxy clustering statistics and SN Ia data (with CMB anisotropy) and is $-1.33 < \omega < -0.79$ [62, 63]. The values of ω at $t = t_0$, as obtained from equation (24), are consistent with these ranges obtained experimentally. It is found in this figure that less negative values of n makes ω closer to -1 , causing a faster approach towards a vacuum fluid dominated universe.

Figure 7 shows the time dependence of the skewness parameter delta (δ) for three different values of the parameter n , with $Q = 0$. Its value is positive and it decreases with time at a gradually smaller rate. Its value is smaller for less negative values of n . Its present value is of the order of 10^{-4} , implying a very small anisotropy in the present universe, and this anisotropy is shown by this graph to become smaller with time. This finding is in sufficient agreement with some recent studies based on Kaluza-Klein anisotropic metric [28].

Figure 8 depicts the time-variation of the ratio σ^2/θ (anisotropy factor) for three different values of the parameter n , with $Q = 0$. Its values are negative and approaches smaller negative values with time at a gradually smaller rate. Its present value is nearly of the order of 10^{-16} , indicating a small anisotropy of the universe at the present time, and this anisotropy becomes smaller with time. It is observed that, the condition for isotropy, i.e., $\sigma^2/\theta \rightarrow 0$ as $t \rightarrow \infty$, is satisfied. This observation is consistent with the findings by Shamir *et al*, based on Bianchi type III space-time [64, 65]. Its absolute value, (i.e., $|\sigma^2/\theta|$), is closer to zero for less negative values of the parameter n .

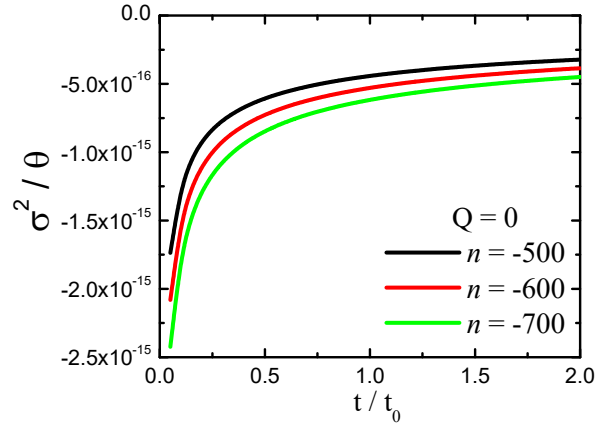
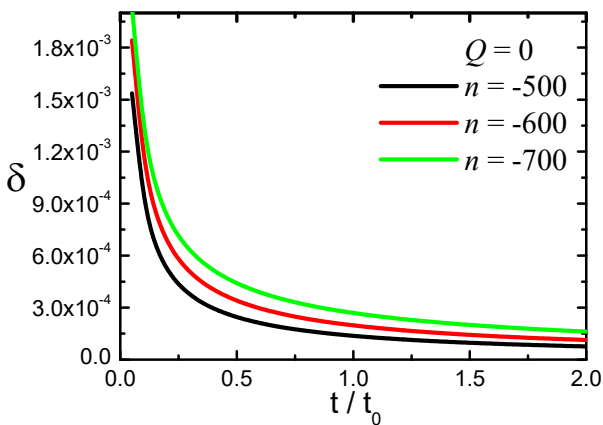


Figure 7. The skewness parameter (δ) versus time for three values of the parameter n

Figure 8. The anisotropy factor (σ^2/θ) versus time for three values of the parameter n

In the present article, we have used the following values of the measurable cosmological parameters, obtained from recent scientific literature [66-72]: $H_0 = 72.20 \text{ km s}^{-1} \text{ Mpc}^{-1} = 2.34 \times 10^{-18} \text{ s}^{-1}$, $q_0 = -0.55$, $\rho_0 = 9.83 \times 10^{-27} \text{ Kg m}^{-3}$. The graph of cosmological parameter Λ versus time, in Fig. 5, is based on equations (28), where the value of C has been obtained from equation (30). The value of Λ at the present time (i.e., at $t = t_0$), obtained from these equations, is -9.9×10^{-27} . One of the values of the cosmological parameter (Λ), as determined from observational data, is $1.25 \times 10^{-52} \text{ m}^{-2}$, according to recent scientific literature [73-76]. But, one finds a very long range of values, which is spread over several orders of magnitude, as its estimates from theoretical and observational investigations [76-78]. The objective of determining the cosmological constant (Λ) in the present study is to find the nature of its evolution with time in an anisotropic Kaluza-Klein space-time where an exponential function of time (Eqn. 15) has been used as an ansatz for the scale factor. Our findings regarding the time-variation of Λ are in qualitative agreement with some recent studies based on models quite different from ours [48, 56-58].

6. CONCLUDING REMARKS

The present study has been carried out in the framework of an anisotropic Kaluza-Klein space-time, having a time-dependent cosmological constant (Λ), to determine the time variation of various cosmological parameters. For this purpose, we have used an empirical scale factor of such a form that it leads to a deceleration parameter which changes sign with time from positive to negative, indicating clearly a transition from decelerated expansion to accelerated expansion, remaining consistent with inferences drawn from observations [3-5]. To enhance the theoretical validity and the ability of prediction of the model constructed here, we have determined the values of three constants (α, β, C) associated with this model by using the presently accepted values of H_0, q_0 and ρ_0 . Due to lack of experimental evidence, we have not been able to fix the value of the parameter n , although it has been shown here that we must have $n < 0$ to get physically acceptable results. It is evident from Figure-4 that the slopes of the curves for ρ are different for different values of n at all values of t/t_0 . The value of n could probably have been determined if we had any

experimentally obtained estimate of the rate of change of energy density (i.e., $d\rho/dt$) at the present time (i.e., $t = t_0$). An important finding of this study is that the dynamical cosmological parameter (Λ) comes out to be negative and it becomes less negative with time, changing at a gradually decreasing rate. At the present time ($t = t_0$), its value is found to be -9.9×10^{-27} , irrespective of the value of n . This value is numerically equal to the value of ρ_0 (expressed in $Kg m^{-3}$). The time evolution of the EoS parameter (ω) shows that the universe has been in the *phantom* regime (i.e., $\omega < -1$) of dark energy since the earliest phase and we are gradually moving towards a vacuum fluid dominated stage (i.e., $\omega = -1$). This model shows that, as $t \rightarrow \infty$, $\sigma^2/\theta \rightarrow 0$, indicating a journey of the universe towards phases of gradually smaller anisotropy. In the present formulation, we have not been able to use equation (11), though it was obtained from equation (10) which is one of the field equations used here. Using $\omega = -1$ in equation (11), one can obtain an expression for ρ where the integration constant can be determined by using the fact that $\rho = \rho_0$ at $t = t_0$. Proceeding in this manner, the time dependence of other cosmological quantities can be determined. We have plans to use this method in a future project.

ORCID

✉ Sudipto Roy, <https://orcid.org/0000-0002-8811-2511>

REFERENCES

- [1] A.G. Riess, et al., "Observational Evidence from Supernovae for an Accelerating Universe and a Cosmological Constant," *Astron. J.* **116**(3), 1009–1038 (1998). <https://doi.org/10.1086/300499>
- [2] S. Perlmutter, et al., "Measurements of Ω and Λ from 42 High-Redshift Supernovae," *Astrophys. J.* **517**(2), 565–586 (1999). <https://doi.org/10.1086/307221>
- [3] A.G. Riess, et al., "The Farthest Known Supernova: Support for an Accelerating Universe and a Glimpse of the Epoch of Deceleration," *Astrophys. J.* **560**(1), 49–71 (2001). <https://doi.org/10.1086/322348>
- [4] T. Padmanabhan and T. R. Choudhury, "A theoretician's analysis of the supernova data and the limitations in determining the nature of dark energy," *Mon. Not. R. Astron. Soc.* **344**(3), 823–834 (2003). <https://doi.org/10.1046/j.1365-8711.2003.06873.x>
- [5] L. Amendola, "Acceleration at $z > 1$," *Mon. Not. R. Astron. Soc.* **342**(1), 221–226 (2003). <https://doi.org/10.1046/j.1365-8711.2003.06540.x>
- [6] B. Ratra and P. J. E. Peebles, "Cosmological consequences of a rolling homogeneous scalar field," *Phys. Rev. D* **37**(12), 3406–3427 (1988). <https://doi.org/10.1103/physrevd.37.3406>
- [7] T. Chiba, T. Okabe, and M. Yamaguchi, "Kinetically driven quintessence," *Phys. Rev. D*, **62**(2), (2000). <https://doi.org/10.1103/physrevd.62.023511>
- [8] E. Elizalde, S. Nojiri, and S. D. Odintsov, "Late-time cosmology in a (phantom) scalar-tensor theory: Dark energy and the cosmic speed-up," *Phys. Rev. D*, **70**(4), (2004). <https://doi.org/10.1103/physrevd.70.043539>
- [9] R.R. Caldwell, "A phantom menace? Cosmological consequences of a dark energy component with super-negative equation of state," *Phys. Lett. B*, **545**(1-2), 23–29 (2002). [https://doi.org/10.1016/s0370-2693\(02\)02589-3](https://doi.org/10.1016/s0370-2693(02)02589-3)
- [10] D. Janzen, "Einstein's cosmological considerations," arXiv:1402.3212 (2014). <https://doi.org/10.48550/arXiv.1402.3212>
- [11] J.M. Overduin and F. I. Cooperstock, "Evolution of the scale factor with a variable cosmological term," *Phys. Rev. D*, **58**(4), (1998). <https://doi.org/10.1103/physrevd.58.043506>
- [12] S. Nojiri, S. D. Odintsov, and S. Tsujikawa, "Properties of singularities in the (phantom) dark energy universe," *Phys. Rev. D*, **71**(6), (2005). <https://doi.org/10.1103/physrevd.71.063004>
- [13] S. Nojiri, S. D. Odintsov, and M. Sasaki, "Gauss-Bonnet dark energy," *Phys. Rev. D*, **71**(12), (2005). <https://doi.org/10.1103/physrevd.71.123509>
- [14] T. Harko, F. S. N. Lobo, S. Nojiri, and S. D. Odintsov, "f(R,T)gravity," *Phys. Rev. D*, **84**(2), (2011). <https://doi.org/10.1103/physrevd.84.024020>
- [15] D. Sáez and V. J. Ballester, "A simple coupling with cosmological implications," *Phys. Lett. A*, **113**(9), 467–470 (1986). [https://doi.org/10.1016/0375-9601\(86\)90121-0](https://doi.org/10.1016/0375-9601(86)90121-0)
- [16] C. Brans and R. H. Dicke, "Mach's Principle and a Relativistic Theory of Gravitation," *Phys. Rev.* **124**(3), 925–935 (1961). <https://doi.org/10.1103/physrev.124.925>
- [17] M. Kiran, D. R. K. Reddy, and V. U. M. Rao, "Minimally interacting holographic dark energy model in a scalar-tensor theory of gravitation," *Astrophys. Space Sci.* **354**(2), 577–581 (2014). <https://doi.org/10.1007/s10509-014-2099-0>
- [18] Y. Aditya, V. U. M. Rao, and M. Vijaya Santhi, "Bianchi type-II, VIII and IX cosmological models in a modified theory of gravity with variable Λ ," *Astrophys. Space Sci.* **361**(2) (2016). <https://doi.org/10.1007/s10509-015-2617-8>
- [19] V.U.M. Rao, U. Y. D. Prasanthi, and Y. Aditya, "Plane symmetric modified holographic Ricci dark energy model in Saez-Ballester theory of gravitation," *Results Phys.* **10**, 469–475 (2018). <https://doi.org/10.1016/j.rinp.2018.06.027>
- [20] Y. Aditya and D. R. K. Reddy, "FRW type Kaluza–Klein modified holographic Ricci dark energy models in Brans–Dicke theory of gravitation," *Eur. Phys. J. C*, **78**(8), (2018). <https://doi.org/10.1140/epjc/s10052-018-6074-8>
- [21] T. KALUZA, "On the Unification Problem in Physics," *Int. J. Mod. Phys. D* **27**(14), 1870001 (2018). <https://doi.org/10.1142/s0218271818700017>
- [22] O. Klein, "Quantentheorie und fünfdimensionale Relativitätstheorie," *Zeitschrift für Physik*, **37**(12), 895–906 (1926). <https://doi.org/10.34663/9783945561317-10>
- [23] A. Chodos, and S. Detweiler, "Where has the fifth dimension gone?," *Phys. Rev. D*, **21**(8), 2167–2170 (1980). <https://doi.org/10.1103/physrevd.21.2167>
- [24] E. Witten, "Some properties of O(32) superstrings," *Phys. Lett. B*, **149**(4-5), 351–356 (1984). [https://doi.org/10.1016/0370-2693\(84\)90422-2](https://doi.org/10.1016/0370-2693(84)90422-2)
- [25] T. Appelquist, A. Chodos, and G.O.P. Freund, *Modern Kaluza-Klein theories*, (Addison-Wesley Pub. Co., Menlo Park, Calif, 1987). <http://pi.lib.uchicago.edu/1001/cat/bib/719574>

- [26] T. Appelquist, and A. Chodos, "Quantum Effects in Kaluza-Klein Theories," *Phys. Rev. Lett.* **50**(3), 141–145 (1983). <https://doi.org/10.1103/physrevlett.50.141>
- [27] W.J. Marciano, "Time Variation of the Fundamental "Constants" and Kaluza-Klein Theories," *Phys. Rev. Lett.* **52**(7), 489–491 (1984). <https://doi.org/10.1103/physrevlett.52.489>
- [28] N. Indrakumar Jain, "Dark energy cosmological model with anisotropic fluid and time varying lambda in Kaluza-Klein metric," *Int. J. Math. Phys.* **14**(1), (2023). <https://doi.org/10.26577/ijmph.2023.v14.i1.011>
- [29] J.A. Ferrari, "On an approximate solution for a charged object and the experimental evidence for the Kaluza-Klein theory," *Gen. Relativ. Gravit.* **21**(7), 683–695 (1989). <https://doi.org/10.1007/bf00759078>
- [30] D. Kalligas, P.S. Wesson, and C.W.F. Everitt, "The classical tests in Kaluza-Klein gravity," *Astrophys. J.* **439**, 548 (1995). <https://doi.org/10.1086/175195>
- [31] V. Dzhunushaliev, and D. Singleton, "Experimental Test for Extra Dimensions in Kaluza–Klein Gravity," *Gen. Relativ. Gravit.* **32**(2), 271–280 (2000). <https://doi.org/10.1023/a:1001943725858>
- [32] J.P. Mbelek, "Experimental tests of an improved 5D Kaluza-Klein theory," *Int. J. Mod. Phys. A*, **35**(02n03), 2040027 (2020). <https://doi.org/10.1142/s0217751x20400278>
- [33] M. Tajmar, and L.L. Williams, "An Experimental Test of the Classical Interpretation of the Kaluza Fifth Dimension," *Physics*, **2**(4), 587–595 (2020). <https://doi.org/10.3390/physics2040033>
- [34] N.I. Jain, and S. S. Bhoga, "Kaluza-Klein Bulk Viscous Cosmological Model with Time Dependent Gravitational Constant and Cosmological Constant," *Int. J. Theor. Phys.* **54**(8), 2991–3003 (2015). <https://doi.org/10.1007/s10773-015-2538-x>
- [35] S.D. Katore, M. M. Sancheti, and N. K. Sarkate, "Kaluza-Klein Anisotropic Magnetized Dark Energy Cosmological Model in Brans-Dicke Theory of Gravitation," *Astrophysics*, **57**(3), 384–400 (2014). <https://doi.org/10.1007/s10511-014-9344-7>
- [36] K.S. Adhav, A.S. Bansod, R.P. Wankhade, and H.G. Ajmire, "Kaluza-Klein Cosmological Models with Anisotropic Dark Energy," *Mod. Phys. Lett. A*, **26**(10), 739–750 (2011). <https://doi.org/10.1142/s0217732311035080>
- [37] D.R.K. Reddy, and R. Santhi Kumar, "Kaluza-Klein dark energy cosmological model in scale Co-variant Theory of Gravitation," *Astrophys. Space Sci.* **349**(1), 485–489 (2013). <https://doi.org/10.1007/s10509-013-1656-2>
- [38] R.L. Naidu, Y. Aditya, and D. R. K. Reddy, "Bianchi type-V dark energy cosmological model in general relativity in the presence of massive scalar field," *Heliyon*, **5**(5), e01645 (2019). <https://doi.org/10.1016/j.heliyon.2019.e01645>
- [39] S.D. Katore, and S.P. Hatkar, "Kaluza Klein universe with magnetized anisotropic dark energy in general relativity and Lyra manifold," *New Astron.* **34**, 172–177 (2015). <https://doi.org/10.1016/j.newast.2014.07.002>
- [40] Y. Aditya, K.D. Raju, V.U.M. Rao, and D.R.K. Reddy, "Kaluza-Klein dark energy model in Lyra manifold in the presence of massive scalar field," *Astrophys. Space Sci.* **364**(11) (2019). <https://doi.org/10.1007/s10509-019-3681-2>
- [41] A.K. Mishra, U.K. Sharma, and A. Pradhan, "A comparative study of Kaluza–Klein model with magnetic field in Lyra manifold and general relativity," *New Astron.* **70**, 27–35 (2019). <https://doi.org/10.1016/j.newast.2019.02.003>
- [42] N.I. Jain, S.S. Bhoga, and G.S. Khadekar, "Implications of Time Varying Cosmological Constant on Kaluza-Klein Cosmological Model," *Int. J. Theor. Phys.* **52**(12), 4416–4426 (2013). <https://doi.org/10.1007/s10773-013-1760-7>
- [43] B. Mishra, S. K. Tripathy, and S. Tarai, "Accelerating models with a hybrid scale factor in extended gravity," *J. Astrophys. Astron.* **42**(1), (2021). <https://doi.org/10.1007/s12036-020-09655-6>
- [44] B. Mishra, S.K. Tripathy, and P.P. Ray, "Bianchi-V string cosmological model with dark energy anisotropy," *Astrophysics and Space Science*, **363**, 1-7 (2018). <https://doi.org/10.1007/s10509-018-3313-2>
- [45] B. Mishra, S.K. Tripathy, and S. Tarai, "Cosmological models with a hybrid scale factor in an extended gravity theory," *Mod. Phys. Lett. A*, **33**(09), 1850052 (2018). <https://doi.org/10.1142/s0217732318500529>
- [46] S.K. Tripathy, B. Mishra, M. Khlopov, and S. Ray, "Cosmological models with a hybrid scale factor," *Int. J. Mod. Phys. D*, **30**(16), 2140005 (2021). <https://doi.org/10.1142/s0218271821400058>
- [47] A. Pradhan, B. Saha, and V. Rikhvitsky, "Bianchi type-I transit cosmological models with time dependent gravitational and cosmological constants: reexamined," *Indian J. Phys.* **89**(5), 503–513 (2014). <https://doi.org/10.1007/s12648-014-0612-5>
- [48] M.A. Hossain, M.M. Alam, and A.H.M.M. Rahman, "Kaluza-Klein Cosmological Models with Barotropic Fluid Distribution," *Phys. & Astron. Int. J.* **1**(3), 98–103 (2017). <https://doi.org/10.15406/paij.2017.01.00018>
- [49] N. Ahmed, and S.Z. Alamri, "Cosmological determination to the values of the pre-factors in the logarithmic corrected entropy-area relation," *Astrophys. Space Sci.* **364**(6) (2019). <https://doi.org/10.1007/s10509-019-3590-4>
- [50] B. Mishra, S. K. Tripathy, and S. Ray, "Cosmological models with squared trace in modified gravity," *Int. J. Mod. Phys. D*, **29**(15), 2050100 (2020). <https://doi.org/10.1142/s021827182050100x>
- [51] F.M. Esmacili, "Anisotropic Behavior of Cosmological Models with Exponential and Hyperbolic Scale Factors," *J. High Energy Phys. Gravit. Cosmol.* **04**(02), 223–235 (2018). <https://doi.org/10.4236/jhepgc.2018.42017>
- [52] A. Chand, R. K. Mishra, and A. Pradhan, "FRW cosmological models in Brans-Dicke theory of gravity with variable q and dynamical Λ -term," *Astrophys. Space Sci.* **361**(2) (2016). <https://doi.org/10.1007/s10509-015-2579-x>
- [53] A. Pradhan, "Two-fluid atmosphere from decelerating to accelerating Friedmann–Robertson–Walker dark energy models," *Indian J. Phys.* **88**(2), 215–223 (2013). <https://doi.org/10.1007/s12648-013-0399-9>
- [54] C. Chawla, R.K. Mishra, and A. Pradhan, "String cosmological models from early deceleration to current acceleration phase with varying G and Λ Eur. Phys. J. Plus, **127**(11), (2012). <https://doi.org/10.1140/epjp/i2012-12137-4>
- [55] N. Ahmed, and T.M. Kamel, "Note on dark energy and cosmic transit in a scale-invariance cosmology," *Int. J. Geom. Methods Mod. Phys.* **18**(05), 2150070 (2021). <https://doi.org/10.1142/s0219887821500705>
- [56] R.K. Tiwari, F. Rahaman, and S. Ray, "Five Dimensional Cosmological Models in General Relativity," *Int. J. Theor. Phys.* **49**(10), 2348–2357 (2010). <https://doi.org/10.1007/s10773-010-0421-3>
- [57] A. Pradhan, "Anisotropic Bianchi Type-I Magnetized String Cosmological Models with Decaying Vacuum Energy Density $\Lambda(t)$," *Commun. Theor. Phys.* **55**(5), 931–941 (2011). <https://doi.org/10.1088/0253-6102/55/5/36>
- [58] A.K. Yadav, "Bianchi type V matter filled universe with varying Lambda term in general relativity," arXiv:0911.0177, (2009). <https://doi.org/10.48550/arXiv.0911.0177>
- [59] A.V. Prasanthi, G. Suryanarayana, Y. Aditya, and U.Y.D. Prasanthi, "Cosmological Dynamics of Anisotropic Kaniadakis Holographic Dark Energy Model in Brans-Dicke Gravity," *East Eur. J. Phys.* (2), 10-20 (2024). <https://doi.org/10.26565/2312-4334-2024-2-01>

- [60] A. Pradhan, “Accelerating dark energy models with anisotropic fluid in Bianchi type VI₀ space-time,” *Res. Astron. Astrophys.* **13**(2), 139–158 (2013). <https://doi.org/10.1088/1674-4527/13/2/002>
- [61] A. K. Yadav, F. Rahaman, and S. Ray, “Dark Energy Models with Variable Equation of State Parameter,” *Int. J. Theor. Phys.* **50**(3), 871–881 (2010). <https://doi.org/10.1007/s10773-010-0628-3>
- [62] R.A. Knop, et al., “New Constraints on Ω_M , Ω_Λ , and from an Independent Set of 11 High-Redshift Supernovae Observed with the Hubble Space Telescope,” *Astrophys. J.* **598**(1), 102–137 (2003). <https://doi.org/10.1086/378560>
- [63] M. Tegmark, et al., “The Three-Dimensional Power Spectrum of Galaxies from the Sloan Digital Sky Survey,” *Astrophys. J.* **606**(2), 702–740 (2004). <https://doi.org/10.1086/382125>
- [64] M.F. Shamir, “Plane Symmetric Vacuum Bianchi Type III Cosmology in $f(R)$ Gravity,” *Int. J. Theor. Phys.* **50**(3), 637–643 (2010). <https://doi.org/10.1007/s10773-010-0587-8>
- [65] M.F. Shamir, and A.A. Bhatti, “Anisotropic dark energy Bianchi type III cosmological models in the Brans–Dicke theory of gravity,” *Can. J. Phys.* **90**(2), 193–198 (2012). <https://doi.org/10.1139/p2012-007>
- [66] A. Pradhan, P. Garg, and A. Dixit, “FRW cosmological models with cosmological constant in $f(R, T)$ theory of gravity,” *Can. J. Phys.* **99**(9), 741–753 (2021). <https://doi.org/10.1139/cjp-2020-0282>
- [67] G.K. Goswami, “Cosmological parameters for spatially flat dust filled Universe in Brans–Dicke theory,” *Res. Astron. Astrophys.* **17**(3), 27 (2017). <https://doi.org/10.1088/1674-4527/17/3/27>
- [68] R.K. Thakur, S. Gupta, R. Nigam, and P.K. Thiruvikraman, “Investigating the Hubble tension through Hubble parameter data,” *Research in Astronomy and Astrophysics*, **23**(6), 065017 (2023). <https://doi.org/10.1088/1674-4527/acd0e8>
- [69] V.K. Bhardwaj, A. Dixit, R. Rani, G.K. Goswami, and A. Pradhan, “An axially symmetric transitioning models with observational constraints,” *Chinese Journal of Physics*, **80**, 261–274 (2022). <https://doi.org/10.1016/j.cjph.2022.09.007>
- [70] N. Myrzakulov, M. Koussour, H.A.A. Alnadhief, and El. Hassan, “Impact of dark energy on the equation of state in light of the latest cosmological data,” *Progress of Theoretical and Experimental Physics*, **9**, 093E02 (2023). <https://doi.org/10.1093/ptep/ptad110>
- [71] A.G. Riess, et al., “A Comprehensive Measurement of the Local Value of the Hubble Constant with 1 km s⁻¹ Mpc⁻¹ Uncertainty from the Hubble Space Telescope and the SH0ES Team,” *The Astrophysical Journal Letters*, **934**(1), L7 (2022). <https://doi.org/10.3847/2041-8213/ac5c5b>
- [72] Q. Wu, H. Yu, and F.Y. Wang, “A New Method to Measure Hubble Parameter $H(z)$ Using Fast Radio Bursts,” *Astrophys. J.* **895**(1), 33 (2020). <https://doi.org/10.3847/1538-4357/ab88d2>
- [73] K.K. Singh, “An interpretation of the Cosmological Constant from the Physical Constants,” *BARC Newsletter*, 22–25 (2021). https://barc.gov.in/barc_nl/2021/2021070804.pdf
- [74] U. Leonhardt, “Lifshitz theory of the cosmological constant,” *Ann. Phys.* **411**, 167973 (2019). <https://doi.org/10.1016/j.aop.2019.167973>
- [75] V. Gueorguiev, and A. Maeder, “Revisiting the Cosmological Constant Problem within Quantum Cosmology,” *Universe*, **6**(8), 108 (2020). <https://doi.org/10.3390/universe6080108>
- [76] C. Köhn, “A Solution to the Cosmological Constant Problem in Two Time Dimensions,” *J. High Energy Phys. Gravit. Cosmol.* **06**(04), 640–655 (2020). <https://doi.org/10.4236/jhepgc.2020.64043>
- [77] L. Abbott, “The Mystery of the Cosmological Constant,” *Sci. Am.* **258**(5), 106–113 (1988). <https://doi.org/10.1038/scientificamerican0588-106>
- [78] S. Weinberg, “The cosmological constant problem,” *Rev. Mod. Phys.* **61**(1), 1–23 (1989). <https://doi.org/10.1103/revmodphys.61.1>

ДОСЛІДЖЕННЯ ЧАСОВОЇ ЕВОЛЮЦІЇ ДЕЯКИХ КОСМОЛОГІЧНИХ ПАРАМЕТРІВ В РАМКАХ АНІЗОТРОПНОЇ МЕТРИКИ КАЛУЦИ-КЛЕЙНА З ВИКОРИСТАННЯМ ЕМПІРИЧНОГО ЕКСПОНЕНЦІАЛЬНОГО МАСШТАБНОГО ФАКТОРА

Судіпто Рой

Факультет фізики, Коледж Св. Ксав'єра, Колката, Західна Бенгалія, Індія

У цьому дослідженні зроблено спробу визначити залежність від часу деяких космологічних параметрів у плоскому просторі (тобто просторі нульової просторової кривизни) в рамках анізотропної метрики Калуци-Клейна. Рівняння поля для цієї роботи були отримані з метрики шляхом припущення степеневого співвідношення між нормальним масштабним фактором і масштабним фактором, що відповідає додатковому (тобто п'ятому) виміру. Емпіричний масштабний коефіцієнт, що має вираз $a = B \exp(at^b)$, був використаний тут для отримання виразів для деяких космологічних параметрів як функцій часу. Причина вибору цього масштабного коефіцієнта полягає в тому, що він створює вираз для параметра уповільнення, який зазнає зміни знака з плином часу від позитивного до негативного, що вказує на перехід Всесвіту від початкового стану уповільненого розширення до стану прискорене розширення (що є його поточним станом), як було зроблено з астрофізичних спостережень. Ми графічно зобразили еволюцію деяких космологічних параметрів відносно того, що можна назвати *відносним часом*, вираженим як t/t_0 , де t_0 — поточний вік Всесвіту. У цьому дослідженні встановлено, що динамічна космологічна константа (Λ) є від'ємною, і з часом вона стає менш від'ємною, змінюючись зі швидкістю поступового зменшення. Залежність тиску всепроникної космічної рідини від щільності, що відповідає п'ятому виміру, була описана в термінах параметра асиметрії (δ), який, як виявилось, зменшується з часом. У цьому дослідженні було розраховано коефіцієнт анізотропії, чисельне значення якого, як виявилось, зменшується з часом, що вказує на рух Всесвіту до фаз поступово меншої анізотропії.

Ключові слова: темна енергія; теорія Калуци-Клейна; космологічний параметр (Λ); анізотропія; експоненціальний масштабний коефіцієнт

PILGRIM DARK ENERGY BIANCHI TYPE-I $f(T)$ GRAVITY MODEL

 Siraj N. Khan^a,  Kishor S. Wankhade^{b*},  Alfred Y. Shaikh^c

^aProf. Ram Meghe College of Engineering & Management, Badnera - Amravati - 444701, (M.S.) India

^bP.G. Department of Mathematics, Yashwantrao Chavan Arts and Science Mahavidyalaya, Mangrulpir, Dist. Washim - 444403, (M.S.) India

^cDepartment of Mathematics, Indira Gandhi Mahavidyalaya, Ralegaon - 445402, (M.S.) India

*Corresponding Author e-mail: wankhade.kishor@rediffmail.com

Received July 1, 2024; revised August 2, 2024; accepted August 10, 2024

In this work, we have analyzed Bianchi type-I space-time (spatially homogeneous and anisotropic), using an interacting two fluid – dark matter (DM) and Pilgrim dark energy (PDE) in the framework of $f(T)$ gravity by taking into consideration the infrared (IR) cut-off as a candidate of Hubble's horizon ($L = 1/H$). We have also performed the state-finder diagnostics and in addition, energy conditions are discussed to verify accelerating expansion of the universe.

Keywords: Pilgrim dark energy; Dark matter; $f(T)$ Gravity; Bianchi type-I space-time; Cosmology

PACS: 04.50.Kd; 95.36.+x; 98.80.-k; 95.35.+d

INTRODUCTION

It is assumed that dark energy (DE) is responsible for accelerated expansion of the universe and also there is increasing evidence of DE over the last few years. Same has been confirmed by various observational experiments [1-3]. Despite the remarkable success of the standard cosmology, there are some issues which remain unresolved including the search for best DE candidate. Various approaches have been adopted for the same such as dynamical DE models and modified gravities.

Several modified theories of gravitation have been proposed to investigate accelerated expansion of the Universe, such as $f(R)$ gravity theory, $f(T)$ gravity theory, $f(R,T)$ gravity theory, $f(G)$ gravity theory, etc. As far as modified $f(R)$ gravity is concerned, Ricci scalar R is replaced by an arbitrary function of R in the Einstein-Hilbert action. Recently, Wankhade et al. [4] have investigated Renyi holographic dark energy (RHDE) with Hubble's IR cut-off in the framework of $f(R)$ gravity. Some other authors [5-8] have also recently worked on the same theory. In modified $f(R,T)$ gravity theory, the gravitational action takes in an arbitrary function of the Ricci scalar R along with trace of the stress energy momentum tensor T . Pradhan et al. [9], Singh and Kumar [10], Shaikh and Wankhade [11], Dagwal et al. [12] have investigated different aspects of $f(R,T)$ gravity.

The $f(T)$ theory of gravity [13] is the generalized teleparallel gravity, where T is the torsion scalar. This theory has attracted many people to explore it in different scenarios. Cai et al. have investigated various torsional constructions in the paradigm of $f(T)$ gravity [14]. Zubair and Waheed have studied different energy conditions in $f(T)$ gravity theory, with non-minimal torsion-matter [15]. Karami and Abdolmaleki have investigated the validity of the generalized second law of gravitational thermodynamics in the framework of $f(T)$ gravity [16]. Jamil et al. have attempted to resolve the dark matter (DM) problem in $f(T)$ gravity [17]. Bhatti et al. have investigated role of $f(T)$ gravity on the evolution of collapsing stellar model [18]. Dagwal and Pawar have worked on two fluid sources namely matter field and radiation field in the framework of $f(T)$ theory of gravity [19]. Karimzadeh and Shojaee have investigated phantom-like behavior in modified teleparallel gravity [20]. Chirde and Shekh have investigated holographic dark energy (HDE) cosmological model in modified $f(T)$ theory of gravity [21]. Bhojar et al. have used hybrid expansion law to investigate the stability of accelerating universe in $f(T)$ gravity theory with linear equation of state [22]. Shekh and Chirde have examined certain aspects of the anisotropic accelerating Bianchi type-I model where two non-interacting fluids—one regular string and one DE—are present, in $f(T)$ gravity [23]. Shaikh et al. have studied LRS Bianchi type-I domain walls cosmological models in $f(T)$ gravity using volumetric expansions laws for the depiction model [24]. Mandal and Sahoo have investigated evolution of particle production in $f(T)$ gravity [25].

The search for viable DE model is the basic key leading to reconstruction phenomenon in modified theories of gravity. Holographic dark energy (HDE) models are having significant place in discussing the accelerated expansion of universe. In PDE model [26] it is considered that a repulsive force that is accelerating the Universe is phantom type with ($\omega_{DE} < -1$) and it is so strong that it prevents formation of the black hole. The energy density of PDE has the form [27]

$$\rho_\Lambda = 3\xi^2 m_p^{4-u} L^{-u}, \tag{1}$$

where ξ and u are dimensionless constants. By taking $m_p = 1$, here we consider Hubble horizon $L = 1/H$ as the IR cutoff to find $f(T)$ model using equation (1).

Sharif and Rani have discussed pilgrim dark energy (PDE) model by taking the Hubble horizon as the IR cutoff in the framework of $f(T)$ gravity [27]. Also, cosmological evolution of PDE has been studied by Sharif and Zubair [28]. Jawad et al. have used Hubble’s cut-off, Granda–Oliveros cut-off and generalized ghost cut-off to discuss the cosmological implications of interacting PDE models with cold dark matter (CDM) in fractal cosmology by taking the flat universe [29]. Sharif and Nazir [30] have discussed evolution (cosmological) of generalized ghost PDE in modified $f(T)$ theory of gravity. Jawad and Rani [31] have worked on cosmological evolution of PDE in $f(G)$ gravity. Myrzakulov et al. [32] have recreated two instances of interacting fluid scenario – ghost and PDE with pressure less DM in the framework of $f(Q)$ gravity.

$f(T)$ GRAVITY FORMALISM AND PILGRIM DARK ENERGY

Here, we provide an overview of the $f(T)$ gravity with thorough derivation of its field equations. From here onwards, let us define the notations of the Latin subscripts or superscripts as related to the tetrad field, whereas Greek notations are allied to the space-time coordinates. The line element for a general space-time metric can be described as

$$ds^2 = g_{\mu\nu} dx^\mu dx^\nu \tag{2}$$

It can be transformed into the tetrad, Minkowski's description of the transformation, in the following way:

$$ds^2 = g_{\mu\nu} dx^\mu dx^\nu = \eta_{ij} \theta^i \theta^j \tag{3}$$

$$dx^\mu = e_i^\mu \theta^i, \theta^i = e_\mu^i dx^\mu \tag{4}$$

where η_{ij} , a metric on Minkowski space-time is given by $\eta_{ij} = \text{diag}[1, -1, -1, -1]$ and $e_i^\mu e_\nu^i = \delta_\nu^\mu$ or $e_i^\mu e_\mu^j = \delta_i^j$.

Also, $\sqrt{-g} = \det[e_\mu^i] = e$ is the root of determinant of metric. The components of the Weitzenbocks connection for a manifold – where, as per the contribution of the Levi-Civita connection, the Riemann tensor part with no torsion terms is null and the only non-zero torsion terms exist – are defined as

$$\Gamma_{\mu\nu}^\alpha = e_i^\alpha \partial_\nu e_\mu^i = -e_\mu^j \partial_\nu e_i^j \tag{5}$$

This has a zero curvature; however, the torsion is nonzero. Through this connection, various components of the torsion tensors can be defined as

$$T_{\mu\nu}^\alpha = \Gamma_{\mu\nu}^\alpha - \Gamma_{\nu\mu}^\alpha = e_i^\alpha (\partial_\mu e_\nu^i - \partial_\nu e_\mu^i) \tag{6}$$

The con-torsion tensor is a space-time tensor from the difference between Weitzenbock and the Levi-Civita connections:

$$K_\alpha^{\mu\nu} = \left(-\frac{1}{2}\right) (T^{\mu\nu}_\alpha + T^{\nu\mu}_\alpha - T_\alpha^{\mu\nu}) \tag{7}$$

Another tensor $S_\alpha^{\mu\nu}$ can be defined from the constituents of the torsion and con-torsion tensors as follows to make the description of the Lagrangian and the equation of motion easier:

$$S_\alpha^{\mu\nu} = \left(\frac{1}{2}\right) (K^{\mu\nu}_\alpha + \delta_\alpha^\mu T^{\beta\nu}_\beta - \delta_\alpha^\nu T^{\beta\mu}_\beta) \tag{8}$$

The torsion scalar T is

$$T = T_{\mu\nu}^\alpha S_\alpha^{\mu\nu} \tag{9}$$

Now we define action by generalizing the Tele-parallel Theory i.e. $f(T)$ theory as

$$S = \int [T + f(T) + L_{matter}] e d^4x \tag{10}$$

Here $f(T)$ indicates an algebraic function of the torsion scalar T . We obtain the following equation of motion by functionally varying the action in equation (9) with regard to the tetrads:

$$S_{\mu}^{\nu\rho} \partial_{\rho} T(f_{TT}) + \left[e^{-1} e_{\mu}^j \partial_{\rho} (e e_i^{\alpha} S_{\alpha}^{\nu\rho}) + T^{\alpha}{}_{\lambda\mu} S_{\alpha}^{\nu\lambda} \right] (1 + f_T) + \frac{1}{4} \delta_{\mu}^{\nu} (T + f) = T_{\mu}^{\nu} \quad (11)$$

where T_{μ}^{ν} is the energy momentum tensor and $f_T = df(T)/dT$. The field equation (11) is written in terms of tetrads and their partial derivatives; and appears very different from Einstein's equation. But by setting $f(T) = a_0 = \text{constant}$, this is dynamically equivalent to the GR.

We consider the energy momentum tensor for interacting two fluids - dark matter (DM) and pilgrim dark energy (PDE), as

$$T_{\mu\nu} = \hat{T}_{\mu\nu} + \bar{T}_{\mu\nu} \quad (12)$$

where $\hat{T}_{\mu\nu} = \rho_m u_{\mu} u_{\nu}$ and $\bar{T}_{\mu\nu} = (\rho_{\Lambda} + p_{\Lambda}) u_{\mu} u_{\nu} - p_{\Lambda} g_{\mu\nu}$, with comoving coordinates $u^{\mu} = (0, 0, 0, 1)$ and $u^{\mu} u_{\nu} = -1$, where u^{μ} is four velocity vector of fluid, p_{Λ} is pressure of PDE, ρ_m and ρ_{Λ} are energy densities of DM and PDE respectively.

For interacting DM and PDE, the continuity equation is satisfied by the total energy density as

$$(\dot{\rho}_m) + (\dot{\rho}_{\Lambda}) + 3H(\rho_m + \rho_{\Lambda} + p_{\Lambda}) = 0 \quad (13)$$

When the energy densities of DM and PDE do not conserve independently, the continuity equation of matter becomes

$$(\dot{\rho}_m) + 3H(\rho_m) = Q \quad (14)$$

$$(\dot{\rho}_{\Lambda}) + 3H(\rho_{\Lambda} + p_{\Lambda}) = -Q \quad (15)$$

where dot ($\dot{\cdot}$) denotes derivative with respect to time t , Q implies the collaboration between DM and PDE. For suitability, consider the interacting term as $Q = 3\sigma H \rho_m$ [33], where σ is coupling constant.

METRIC AND COMPONENTS OF FIELD EQUATIONS

In our work, we consider the spatially homogeneous and anisotropic Bianchi type-I space-time as

$$ds^2 = dt^2 - A^2(t) dx^2 - B^2(t) [dy^2 + dz^2], \quad (16)$$

where metric potentials A and B are the functions of cosmic time t only.

Now, the corresponding Torsion scalar T is given by

$$T = -2 \left(2 \frac{\dot{A} \dot{B}}{A B} + \frac{\dot{B}^2}{B^2} \right) \quad (17)$$

Using the equation of motion in (10), Bianchi type-I space-time in (16), for the stress energy tensors (12), can be written as

$$(T + f) + 4(1 + f_T) \left\{ \frac{\ddot{B}}{B} + \frac{\dot{B}^2}{B^2} + \frac{\dot{A} \dot{B}}{A B} \right\} + 4 \frac{\dot{B}}{B} \dot{f}_{TT} = -p_{\Lambda} \quad (18)$$

$$(T + f) + 2(1 + f_T) \left\{ \frac{\ddot{A}}{A} + \frac{\ddot{B}}{B} + \frac{\dot{B}^2}{B^2} + 3 \frac{\dot{A} \dot{B}}{A B} \right\} + 2 \left\{ \frac{\dot{A}}{A} + \frac{\dot{B}}{B} \right\} \dot{f}_{TT} = -p_{\Lambda} \quad (19)$$

$$(T + f) + 4(1 + f_T) \left\{ \frac{\dot{B}^2}{B^2} + 2 \frac{\dot{A} \dot{B}}{A B} \right\} = \rho_m + \rho_{\Lambda} \quad (20)$$

So here we got three differential equations containing five unknowns — namely A, B, f, p and ρ .

We now define few kinematical quantities of space-time such as mean scale factor and volume respectively as

$$a^3 = V = AB^2 \quad (21)$$

To express volumetric expansion rate of Universe, the mean Hubble parameter is defined as

$$H = \frac{1}{3}(H_1 + H_2 + H_3) \tag{22}$$

where H_1, H_2 and H_3 are the directional Hubble parameters in the directions of x, y and z axes respectively. Anisotropy parameter, for discussing whether Universe approach isotropy or not, is defined as

$$A_m = \frac{1}{3} \sum_{i=1}^3 \left(\frac{H_i - H}{H} \right)^2 \tag{23}$$

The expansion scalar and shear scalar are respectively defined as

$$\theta = \frac{\dot{A}}{A} + 2 \frac{\dot{B}}{B} \tag{24}$$

$$\sigma^2 = \frac{3}{2} H^2 A_m \tag{25}$$

EXACT MATTER DOMINATED SOLUTION

In order to solve the system of non-linear differential equations, we use the following physically plausible conditions. The latest findings of high red-shift type-Ia supernovae disclose that the universe is accelerating, contrary to the prediction of standard cosmology with standard matter and no cosmological constant that it is currently decelerating. Hence, the model with constant decelerating parameter have received considerable attention [34]. We extend the same results of [34] to solve the field equations by taking into consideration the variation of Hubble parameter as

$$a = (\epsilon t + \epsilon_1)^{\frac{k}{\epsilon}}, \text{ for } \epsilon \neq 0 \tag{26}$$

Now subtracting equation (18) from (19), we get,

$$\frac{d}{dt} \left(\frac{\dot{A}}{A} - \frac{\dot{B}}{B} \right) + \left(\frac{\dot{A}}{A} - \frac{\dot{B}}{B} \right) \frac{\dot{V}}{V} = 0 \tag{27}$$

Integrating above equation, it gives,

$$\frac{A}{B} = c_2 \exp \left[c_1 \int \frac{1}{V} dt \right] \tag{28}$$

where c_1 and c_2 are constants of integration.

By using equation (21), we get the metric potentials A and B in the form

$$A = M_1 V^{\frac{1}{3}} \exp \left[N_1 \int \frac{1}{V} dt \right], \tag{29}$$

$$B = M_2 V^{\frac{1}{3}} \exp \left[N_2 \int \frac{1}{V} dt \right], \tag{30}$$

where $M_1 = c_2 M_2$, $M_2 = (c_2)^{-\frac{1}{3}}$ and $N_1 = c_1 + N_2$, $N_2 = -\frac{c_1}{3}$. Also $M_i (i=1,2)$ and $N_i (i=1,2)$ satisfy the relations

$$M_1 (M_2)^2 = 1 \text{ and } N_1 + 2N_2 = 0.$$

Now we consider average scale factor of the form.

Using equation (26) in equations (29) and (30), we get,

$$A = M_1 (\epsilon t + \epsilon_1)^{\frac{k}{\epsilon}} \exp \left[\frac{\epsilon N_1}{(\epsilon - 3k)} (\epsilon t + \epsilon_1)^{1 - \frac{3k}{\epsilon}} \right], \tag{31}$$

$$B = M_2 (\epsilon t + \epsilon_1)^{\frac{k}{\epsilon}} \exp \left[\frac{\epsilon N_2}{(\epsilon - 3k)} (\epsilon t + \epsilon_1)^{1 - \frac{3k}{\epsilon}} \right], \tag{32}$$

Therefore, using equations (31) and (32), space-time (16) filled with the fluid (12) in the framework of $f(T)$ gravity becomes

$$ds^2 = dt^2 - M_1^2 \tau^{\left(\frac{2k}{\varepsilon-3k}\right)} \exp\left[\frac{2\tau\varepsilon N_1}{(\varepsilon-3k)}\right] dx^2 - M_2^2 \tau^{\left(\frac{2k}{\varepsilon-3k}\right)} \exp\left[\frac{2\tau\varepsilon N_2}{(\varepsilon-3k)}\right] [dy^2 + dz^2] \tag{33}$$

where, $\tau = (\varepsilon t + \varepsilon_1)^{\frac{3k}{\varepsilon}}$.

DYNAMICAL PARAMETERS WITH PHYSICAL ACCEPTABILITY

Deceleration parameter is

$$q = -1 + \frac{\varepsilon}{k} \tag{34}$$

From equation (34), it is found that the deceleration parameter is constant throughout the expansion of the Universe.

Anisotropy parameter is

$$A_m = \frac{\varepsilon^2 \tau^2 (N_1^2 + 2N_2^2)}{3k^2} \tag{35}$$

From above equation (35), it is observed that the nature of the anisotropic parameter is varying with the evolution of the universe.

Expansion scalar is found to be

$$\theta = \frac{3k}{(\varepsilon t + \varepsilon_1)}, \tag{36}$$

From equation (36), it is observed that the expansion scalar is a decreasing function of time. At $t \rightarrow 0$, the expansion scalar is constant and as cosmic time increases, it decreases, which shows that as time increases, the universe is expanding but its rate of expansion is decreasing.

Shear scalar is

$$\sigma^2 = \frac{1}{2} \varepsilon^2 (N_1^2 + 2N_2^2) \tau^{\left(\frac{-6k}{\varepsilon-3k}\right)}, \tag{37}$$

It is found that the shear scalar is the inverse function of time. Initially it is constant and the model is shear free at an infinite expansion.

For PDE, using equation (1), the energy density is obtained as

$$\rho_\Lambda = 3\xi^2 k^u \tau^{\left(\frac{\varepsilon u}{3k-\varepsilon}\right)}, \tag{38}$$

From Figure 1, it is observed that energy density of PDE is always positive and as time increases, energy density decreases. i.e. as $t \rightarrow \infty$, $\rho_\Lambda \rightarrow 0$, this means that at infinite time, the Universe is empty.

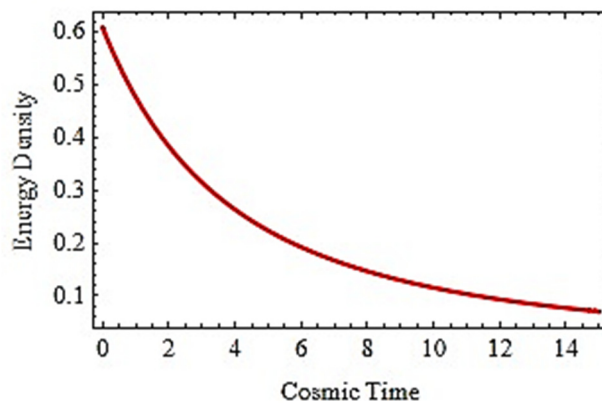


Figure 1. Graphical representation of energy density (ρ_Λ) of PDE versus cosmic time (t) by taking $\xi = 1.5$, $k = 0.3$, $u = 2$, $\varepsilon = 0.13$, $\varepsilon_1 = 1$.

Now we find exact solution of field equations using some physical quantities for depiction $f(T)$ model [35] which is,

$$f(T) = T^n \tag{39}$$

Isotropic pressure,

$$p_\Lambda = (-2)(\tau)^{\frac{-2\varepsilon}{\varepsilon-3k}} \left\{ \tau_1 \tau_2 \tau_6 + 2\tau_4 \left[1 + \eta(-2)^{\eta-1} \tau_5 \right] \right\}, \quad (40)$$

where, $\tau_1 = N_2 \varepsilon \tau + k$, $N_3 = 2N_1 + N_2$, $\tau_2 = N_3 \varepsilon \tau + 3k$, $\tau_3 = \tau_1 \tau_2^2 - 2\varepsilon k \eta (\eta - 1) [3\tau_1 (1 + N_3 \tau) + \tau_2 (1 + 3N_2 \tau)]$, $\tau_4 = 3k\tau_1 - \varepsilon k (1 + 3N_2 \tau)$, $\tau_5 = (\tau)^{\frac{2\varepsilon(1-\eta)}{\varepsilon-3k}} \tau_1^{\eta-1} \tau_2^{\eta-1}$ and $\tau_6 = -1 - (-2)^{\eta-1} \tau_1^{\eta-2} \tau_2^{\eta-3} \tau_3$.

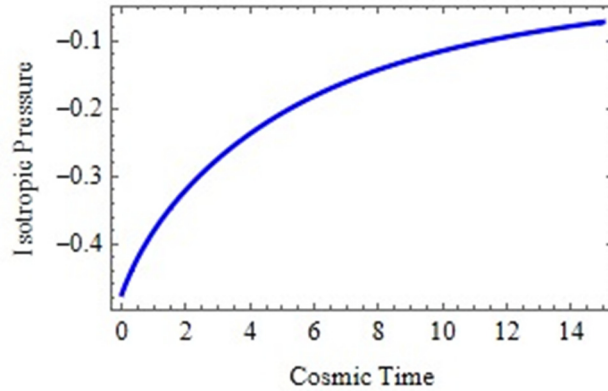


Figure 2. Graphical representation of isotropic pressure (p_Λ) of PDE versus cosmic time (t) by taking $c_1 = 0.5$, $k = 0.3$, $\varepsilon = 0.13$, $\varepsilon_1 = 1$, $\eta = 2$.

From Figure 2, one can observe that isotropic pressure of PDE model is always negative. Hence the Universe is filled with dark energy without baryonic matter.

Equation of state parameter,

$$\omega_\Lambda = \frac{-2}{3\xi^2 k^u} (\tau)^{\frac{\varepsilon(u-2)}{\varepsilon-3k}} \left\{ \tau_1 \tau_2 \tau_6 + 2\tau_4 \left[1 + \eta(-2)^{\eta-1} \tau_5 \right] \right\}, \quad (41)$$

Latterly, a considerable class of scalar field DE models has been given which includes Quintessence (if $\omega_\Lambda > -1$), Phantom (if $\omega_\Lambda < -1$) and Quinton — which can travel across Phantom to quintessence region. Also, the Quinton scenario of DE is designed to comprehend the nature of DE with ω_Λ across -1 . Setare and Saridakis [36] have examined DE models where equation of state parameter (ω_Λ) is across -1 , providing a tangible assertion to the Quinton paradigm.

Some other limits of ω_Λ — derived from observational findings obtained from SNe-Ia data and, SNe-Ia data combined with Cosmic Microwave Background (CMB) anisotropy and Galaxy clustering statistics; are respectively $-1.66 < \omega_\Lambda < -0.62$ and $-1.33 < \omega_\Lambda < -0.79$.

In the derived model, the equation of state parameter represents Quintessence region then it goes through a Λ CDM model and as time increases, it converts to a Phantom model. Same behavior can be observed from Figure 3.

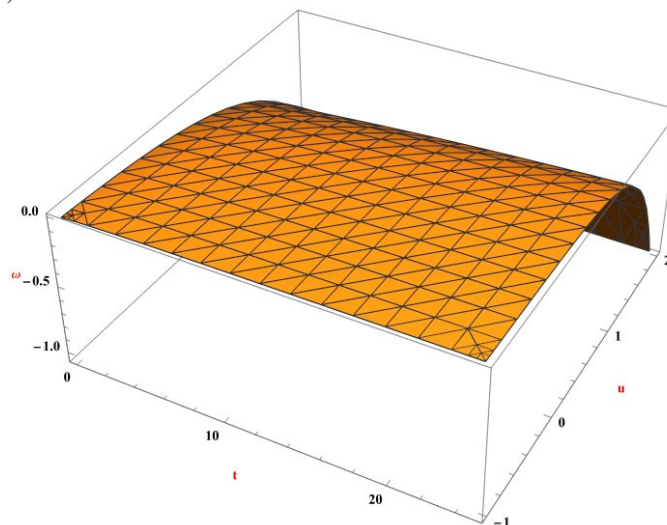


Figure 3. Graphical representation of Equation of State parameter (ω) of PDE versus cosmic time (t) by taking $\xi = 1.5$, $u = -1$ to $u = 2$, $c_1 = 0.5$, $k = 0.3$, $\varepsilon = 0.13$, $\eta = 2$, $\varepsilon_1 = 1$.

Stability factor,

$$g_s^2 = \frac{2(\varepsilon - 3k)}{3\xi^2 u k^u} (\tau)^{\frac{\varepsilon(u-1)-3k}{\varepsilon-3k}} \left\{ \begin{aligned} & \left(N_3 \tau_1 + N_2 \tau_2 \right) \tau_6 + 2\eta(\eta-1)(-2)^{(\eta-1)} \tau_4 \tau_5 \left[\frac{N_3}{\tau_2} + \frac{N_2}{\tau_1} - \frac{2}{(\varepsilon-3k)\tau} \right] \\ & - \frac{2}{(\varepsilon-3k)\tau} \left\{ \tau_1 \tau_2 \tau_6 + 2\tau_4 \left[1 + \eta(-2)^{\eta-1} \tau_5 \right] \right\} \\ & - (-2)^{\eta-1} \tau_1^{\eta-1} \tau_2^{\eta-2} \left\{ \begin{aligned} & 2N_3 \tau_1 \tau_2 + N_2 \tau_2^2 + \tau_3 \left[\frac{N_3(\eta-3)}{\tau_2} + \frac{(\eta-2)}{\tau_1} \right] \\ & - 2k\eta(\eta-1) \left\{ N_3 [3\tau_1 + \varepsilon(3N_2\tau + 1)] + 3N_2 [\tau_2 + \varepsilon(N_3\tau + 1)] \right\} \end{aligned} \right\} \end{aligned} \right\} \quad (42)$$

We should examine the physical acceptance to ensure that the appropriate solution in the current model is stable. First, the velocity of sound needs to be less than that of light in order for this to happen, i.e. within the range $0 < g_s^2$. From Figure 4, it is observed that the stability factor for the present model is negative throughout the expansion of the Universe i.e. $g_s^2 < 0$ and hence the model is unstable throughout the expansion.

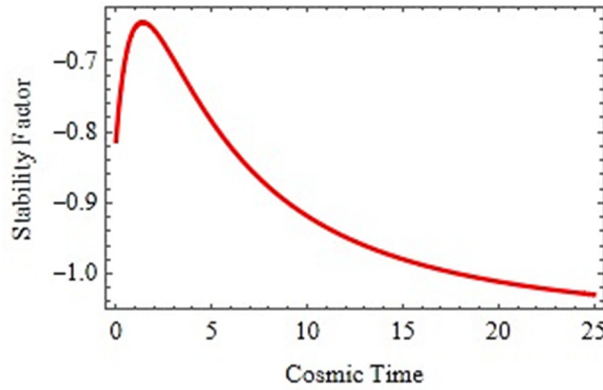


Figure 4. Graphical representation of stability factor of PDE versus cosmic time (t) by taking $\xi = 1.5$, $u = 2$, $c_1 = 0.5$, $k = 0.3$, $\varepsilon = 0.13$, $\varepsilon_1 = 1$, $\eta = 2$.

STATEFINDER PARAMETERS

Many models of DE have been developed in an attempt to comprehend its nature and provide an explanation for the Universe's accelerated expansion. Sahni et al. [37] have developed the crucial parameters known as Statefinder parameters to help differentiate between these models. The Statefinder parameters are associated to the third order derivatives of average scale factor. Different values of the pair of Statefinder parameters $\{r, s\}$ exhibit different DE models. In particular

- For Λ CDM, $(r = 1, s = 0)$,
- For SCDM, $(r = 1, s = 1)$,
- For HDE, $\left(r = 1, s = \frac{2}{3} \right)$,
- For CG, $(r > 1, s < 0)$,
- For Quintessence, $(r < 1, s > 0)$.

The Statefinder parameters for our model are

$$r = \frac{(k - \varepsilon)(k - 2\varepsilon)}{k^2} \quad (43)$$

and

$$s = \frac{2[(k - \varepsilon)(k - 2\varepsilon) - k]}{3k(2\varepsilon - 3k)} \quad (44)$$

With appropriate choice of constants $k = 0.3$ and $\varepsilon = 0.13$, it is clear that $r < 1$ and $s > 0$ which means that the model evolves around Quintessence region.

ENERGY CONDITIONS

Energy conditions are nothing but a set of certain conditions which characterize matter in the universe and are used in a variety of ways to comprehend how the universe has evolved. The objective of energy conditions in this work is to substantiate the accelerated expansion of Universe. These conditions can be obtained by the widely recognized Raychaudhuri equations [38], [39], [40], whose forms are:

$$\frac{d\theta}{dT} = -\frac{1}{3}\theta^2 - \sigma_{\mu\nu}\sigma^{\mu\nu} + \omega_{\mu\nu}\omega^{\mu\nu} - R_{\mu\nu}u^\mu u^\nu \quad \text{and} \quad \frac{d\theta}{dT} = -\frac{1}{2}\theta^2 - \sigma_{\mu\nu}\sigma^{\mu\nu} + \omega_{\mu\nu}\omega^{\mu\nu} - R_{\mu\nu}n^\mu n^\nu, \quad (45)$$

where θ is the expansion factor, n^μ is null vector and, $\sigma^{\mu\nu}$ and $\omega_{\mu\nu}$ are shear and the rotation associated with the vector field u^μ , respectively. The following energy conditions are satisfied by the attractive gravity:

- Weak energy conditions (WEC) if $\rho \geq 0, \rho + p \geq 0$,
- Null energy condition (NEC) if $p + \rho \geq 0$,
- Dominant energy conditions (DEC) if $\rho \geq 0, \rho - |p| \geq 0$,
- Strong energy condition (SEC) if $\rho + 3p \geq 0$.

WEC (Energy density together with NEC):

$$\rho \geq 0, \rho + p \geq 0 \Leftrightarrow \begin{cases} 3\xi^2 k^u (\tau)^{\frac{-\varepsilon u}{\varepsilon - 3k}} \geq 0, \\ 3\xi^2 k^u (\tau)^{\frac{-\varepsilon u}{\varepsilon - 3k}} + (-2)(\tau)^{\frac{-2\varepsilon}{\varepsilon - 3k}} \left\{ \tau_1 \tau_2 \tau_6 + 2\tau_4 \left[1 + \eta(-2)^{\eta-1} \tau_5 \right] \right\} \geq 0 \end{cases} \quad (46)$$

DEC:

$$\rho - |p| \geq 0 \Leftrightarrow 3\xi^2 k^u (\tau)^{\frac{-\varepsilon u}{\varepsilon - 3k}} - \left| (-2)(\tau)^{\frac{-2\varepsilon}{\varepsilon - 3k}} \left\{ \tau_1 \tau_2 \tau_6 + 2\tau_4 \left[1 + \eta(-2)^{\eta-1} \tau_5 \right] \right\} \right| \geq 0 \quad (47)$$

SEC:

$$\rho + 3p \geq 0 \Leftrightarrow 3\xi^2 k^u (\tau)^{\frac{-\varepsilon u}{\varepsilon - 3k}} + 3(-2)(\tau)^{\frac{-2\varepsilon}{\varepsilon - 3k}} \left\{ \tau_1 \tau_2 \tau_6 + 2\tau_4 \left[1 + \eta(-2)^{\eta-1} \tau_5 \right] \right\} \geq 0 \quad (48)$$

In the analysis of energy conditions, a violation of NEC gives rise to a violation of remaining other energy conditions, which depicts the reduction in energy density with expansion of Universe; furthermore, the violation of SEC depicts the accelerated expansion of the Universe.

Evolution of the energy conditions in the obtained Universe versus cosmic time (t), by proper choice of constants, is prescribed in Figure 5, Figure 6 and Figure 7. From these figures, along with Figure 1, we can observe that WEC ($\rho \geq 0$) together with NEC ($p + \rho \geq 0$) and DEC ($\rho - |p| \geq 0$) are verified whereas SEC ($\rho + 3p \geq 0$) violates. Hence, the violation of SEC gives rise to the accelerating expansion of the Universe.

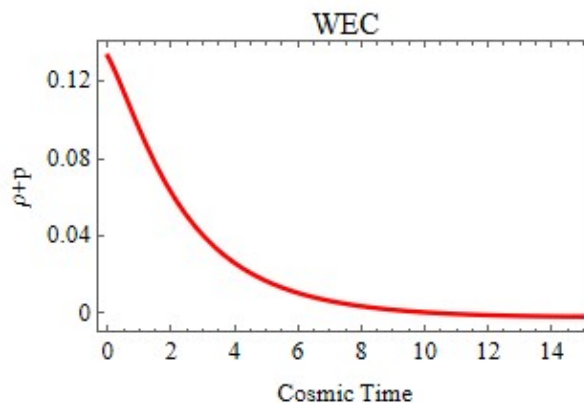


Figure 5. Graphical representation of evolution of WEC of the Universe versus cosmic time (t) by taking $\xi = 1.5, u = 2, c_1 = 0.5, k = 0.3, \varepsilon = 0.13, \varepsilon_1 = 1, \eta = 2$.

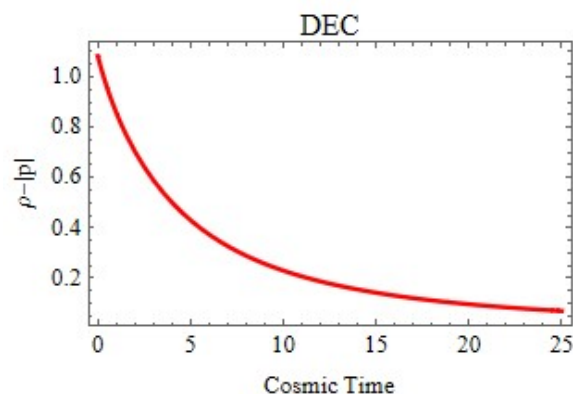


Figure 6. Graphical representation of evolution of DEC of the Universe versus cosmic time (t) by taking $\xi = 1.5$, $u = 2$, $c_1 = 0.5$, $k = 0.3$, $\varepsilon = 0.13$, $\varepsilon_1 = 1$, $\eta = 2$.

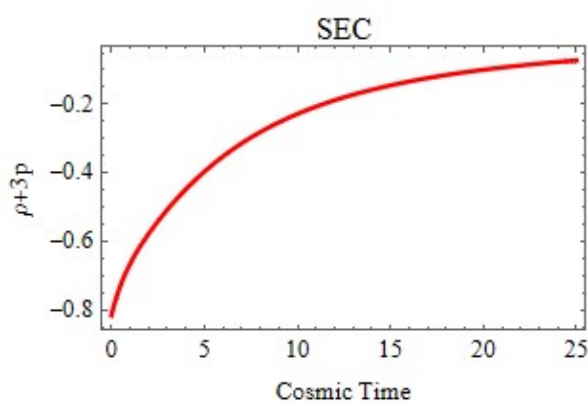


Figure 7. Graphical representation of evolution of SEC of the Universe versus cosmic time (t) by taking $\xi = 1.5$, $u = 2$, $c_1 = 0.5$, $k = 0.3$, $\varepsilon = 0.13$, $\varepsilon_1 = 1$, $\eta = 2$.

CONCLUSIONS

In present study, we considered a homogeneous and anisotropic Bianchi type-I universe with interacting DM and PDE in $f(T)$ gravity.

- It is observed that energy density of PDE is always positive and as time increases, energy density decreases [41-42].
- The equation of state parameter represents Quintessence region then it goes through a Λ CDM model and as time increases, it converts to Phantom model.
- The deceleration parameter is found to be constant throughout the expansion of the Universe.
- The stability factor for the present model is negative throughout the expansion of the Universe and hence the model is unstable [4].

ORCID

• Siraj N. Khan, <https://orcid.org/0000-0003-2246-7050>; • Kishor S. Wankhade, <https://orcid.org/0009-0004-8740-0169>;
• Alfred Y. Shaikh, <https://orcid.org/0000-0001-5315-559X>

REFERENCES

- [1] S. Perlmutter, *et al.*, *Astrophys J.* **517**(2), 565–586 (1999). <https://doi.org/10.1086/307221>
- [2] R.A. Knop, *et al.*, *Astrophys J.* **598**(1), 102–137 (2003). <https://doi.org/10.1086/378560>
- [3] G. Hinshaw, *et al.*, *Astrophys. J. Suppl. Ser.* **208**(2), 19 (2013). <https://doi.org/10.1088/0067-0049/208/2/19>
- [4] K.S. Wankhade, A.Y. Shaikh, and S. N. Khan, *East European J. of Phys.* **2023**(3), 87–95 (2023). <https://doi.org/10.26565/2312-4334-2023-3-06>
- [5] A.S. Agrawal, S.K. Tripathy, and B. Mishra, *Chin. J. of Phys.* **71**, 333–340 (2021). <https://doi.org/10.1016/J.CJPH.2021.03.004>
- [6] P. K. Sahoo, and S. Bhattacharjee, *New Astronomy*, **77**, 101351 (2020). <https://doi.org/10.1016/j.newast.2019.101351>
- [7] S. D. Katore, and R. J. Baxi, *Ind. J. of Phys.* **93**(11), 1501–1514 (2019). <https://doi.org/10.1007/s12648-019-01411-z>
- [8] S. Nojiri, S.D. Odintsov, and V.K. Oikonomou, *Ann. Phys.* **418**, (2020). <https://doi.org/10.1016/j.aop.2020.168186>
- [9] A. Pradhan, G. Goswami, and A. Beesham, *Int. J. of Geom. Meth. in Mod. Phys.* **20**(10), (2023). <https://doi.org/10.1142/S0219887823501694>
- [10] C.P. Singh, and A. Kumar, *Grav. and Cosm.* **25**(1), 58–68 (2019). <https://doi.org/10.1134/S0202289319010109>
- [11] A.Y. Shaikh, and K S. Wankhade, *Theor. Phys.* **2**(1), (2017). <https://doi.org/10.22606/tp.2017.21006>

- [12] V.J. Dagwal, D.D. Pawar, and Y.S. Solanke, Mod. Phys. Lett. A, **35**(38), 2050316 (2020). <https://doi.org/10.1142/S0217732320503162>
- [13] R. Ferraro, and F. Fiorini, Phys. Rev. D, **75**(8), 084031 (2007). <https://doi.org/10.1103/PhysRevD.75.084031>
- [14] Y.-F. Cai, S. Capozziello, M. de Laurentis, and E.N. Saridakis, Rep. Prog. Phys. **79**(10), 106901 (2016). <https://doi.org/10.1088/0034-4885/79/10/106901>
- [15] M. Zubair, and S. Waheed, Astrophys. Space Sci. **355**(2), 361 (2015). <https://doi.org/10.1007/s10509-014-2181-7>
- [16] K. Karami, and A. Abdolmaleki, J. of Cosm. and Astropart. Phys. **4**, 007 (2012). <https://doi.org/10.1088/1475-7516/2012/04/007>
- [17] M. Jamil, D. Momeni, and R. Myrzakulov, Eur. Phys. J. C, **72**(8), 1 (2012) <https://doi.org/10.1140/epjc/s10052-012-2122-y>
- [18] M.Z. ul H. Bhatti, Z. Yousaf, and S. Hanif, Physics of the Dark Universe, **16**, 34 (2017). <https://doi.org/10.1016/j.dark.2017.04.003>
- [19] V.J. Dagwal, and D.D. Pawar, Mod. Phys. Lett. A, **35** (4), (2020). <https://doi.org/10.1142/S0217732319503577>
- [20] S. Karimzadeh, and R. Shojaei, Adv. High Energy Phys. **2019**, 4026856 (2019). <https://doi.org/10.1155/2019/4026856>
- [21] V.R. Chirde, and S.H. Shekh, Ind. J. of Phys. **92**(11), 1485 (2018). <https://doi.org/10.1007/s12648-018-1236-y>
- [22] S.R. Bhoyar, V.R. Chirde, and S.H. Shekh, Astrophys. **60**(2), 259 (2017). <https://doi.org/10.1007/s10511-017-9480-y>
- [23] S.H. Shekh, and V.R. Chirde, Astrophys. Space Sci. **365**(3), 1 (2020). <https://doi.org/10.1007/s10509-020-03772-y>
- [24] A.Y. Shaikh, A.S. Shaikh, and K.S. Wankhade, arXiv:2006.12300 [gr-qc], (2020). <http://arxiv.org/abs/2006.12300>
- [25] S. Mandal, and P.K. Sahoo, Mod. Phys. Lett. A, **35**(40), 2050328 (2020). <https://doi.org/10.1142/S0217732320503289>
- [26] H. Wei, Class. Quantum Grav. **29**(17), 175008 (2012). <https://doi.org/10.1088/0264-9381/29/17/175008>
- [27] M. Sharif, and S. Rani, J. Exp. Theor. Phys. **119**(1), 75 (2014). <https://doi.org/10.1134/S1063776114070152>
- [28] M. Sharif, and M. Zubair, Astrophys. Space Sci. **352**(1), 263 (2014). <https://doi.org/10.1007/s10509-014-1889-8>
- [29] A. Jawad, S. Rani, I.G. Salako, and F. Gulshan, Int. J. Mod. Phys. D, **26**(06), 1750049 (2017). <https://doi.org/10.1142/S0218271817500493>
- [30] M. Sharif, and K. Nazir, Astrophys. Space Sci. **360**(57), 1 (2015). <https://doi.org/10.1007/S10509-015-2572-4>
- [31] A. Jawad, and S. Rani, Adv. High Energy Phys. **2015**, 952156 (2015). <https://doi.org/10.1155/2015/952156>
- [32] N. Myrzakulov, S.H. Shekh, A. Mussatayeva, and M. Koussour, Front. in Astr. Space Sci. **9**, 105 (2022). <https://doi.org/10.3389/fspas.2022.902552>
- [33] H. Wei, and R.G. Cai, Eur. Phys. J. C, **59**(1), 99 (2009). <https://doi.org/10.1140/epjc/s10052-008-0799-8>
- [34] M.S. Berman, Il Nuovo Cimento B, **74**(2), 182 (2007). <https://doi.org/10.1007/BF02721676>
- [35] A.Y. Shaikh, Bulg. J. Phys. **49**(2), 190 (2022). <https://doi.org/10.55318/bgjp.2022.49.2.190>
- [36] M.R. Setare, and E.N. Saridakis, Phys. Rev. D, **79**(4), 043005 (2009). <https://doi.org/10.1103/PhysRevD.79.043005>
- [37] V. Sahni, T.D. Saini, A.A. Starobinsky, and U. Alam, J. of Exp. Theor. Phys. Lett. **77**(5), 201 (2003). <https://doi.org/10.1134/1.1574831>
- [38] A. Raychaudhuri, Phys. Rev. **98**(4), 1123 (1955). <https://doi.org/10.1103/PhysRev.98.1123>
- [39] J. Ehlers, Int. J. Mod. Phys. D, **15**(10), 1573 (2006). <https://doi.org/10.1142/S0218271806008966>
- [40] S. Nojiri, and S.D. Odintsov, Int. J. Geom. Meth. Mod. Phys. **4**(1), 115 (2007). <https://doi.org/10.1142/S0219887807001928>
- [41] V.R. Patil, P.A. Bolke, S.K. Waghmare, and J.L. Pawde, East European J. of Phys. (3), 53 (2023). <https://doi.org/10.26565/2312-4334-2023-3-03>
- [42] K.S. Wankhade, A.Y. Shaikh, and S.N. Khan, Prespacetime J. **13**(3), 365–379 (2022). <https://www.prespacetime.com/index.php/pst/article/view/1852>

МОДЕЛЬ ГРАВИТАЦІЇ БІАНЧІ ТИПУ-I $f(T)$ З ТЕМНОЮ ЕНЕРГІЄЮ PILGRIM

Сірадж Н. Хан^a, Кішор С. Ванкхадє^b, Альфред Ю. Шейх^c

^aКоледж інженерії та менеджменту імені професора Рама Меге, Баднера - Амраваті - 444701, (M.S.) Індія

^bП.Г. Департамент математики, Коледж мистецтв і науки Яшвантрао Чаван,



Мангрултір, округ Вашім - 444403, (MS) Індія

^cДепартамент математики, Коледж Індіри Ганді, Ралегаон - 445402, (M.S.) Індія

У цій роботі ми проаналізували простір-час Б'янкі типу I (просторово однорідний та анізотропний), використовуючи дві взаємодіючі рідини – темну матерію (DM) і темну енергію Pilgrim (PDE) в рамках $f(T)$ гравітації, враховуючи інфрачервоне (ІЧ) відсікання як кандидата на горизонт Хаббла ($L = 1/H$). Ми також провели діагностику за допомогою шукача стану, а також обговорили енергетичні умови для перевірки прискореного розширення Всесвіту.

Ключові слова: темна енергія Pilgrim; темна матерія; гравітація $f(T)$; простір-час Біанчі типу I; космологія

STUDY ON ANISOTROPIC DARK ENERGY COSMOLOGICAL MODELS IN GENERALIZED BRANS-DICKE THEORY

 M. Vijaya Santhi* ,  K. SantoshRupa

Department of Applied Mathematics, Andhra University, Visakhapatnam 530003, India

*Corresponding Author e-mail: gv.santhi@live.com

Received April 22, 2024; revised June 15, 2024; accepted August 19, 2024

In this present paper, we have investigated the dark energy cosmological model in Bianchi- VI_0 spacetime by considering generalised Brans-Dicke theory, self-interacting potential, and a dynamical coupling parameter. For this purpose, we have utilised a hybrid scale factor to approximate the dynamical behaviour of the deceleration parameter. The deceleration parameter should display distinctive flipping behaviour at the transition redshift since the universe is thought to have changed from an early deceleration to a late temporal acceleration. We have studied six alternative transitioning dark energy models on the basis of observational restrictions on the transition redshift. For each model, the behaviour of the dynamical scalar field, the Brans-Dicke parameter, and the self-interacting potential are examined. On top of that, we used the generalised Brans-Dicke theory to estimate how the Newtonian gravitational constant changes over time.

Keywords: *Bianchi type- VI_0 metric; Generalized Brans-Dicke theory; Hybrid scale factor; Skewness parameter; Unified dark fluid*

PACS: 95.36+X, 98.80-k, 95.30-sf

1. INTRODUCTION

The recent observations of the universe's accelerated expansion were supported by Riess et al. [1] and Perlmutter et al. [2] through various observational facts. The universe appears to be spatially flat and dominated by dark energy, an exotic substance with high negative pressure, according to cosmological measurements and data from the cosmic microwave background [3, 4]. Additionally, it is hypothesised that dark energy makes up 68.3% of the energy in our universe, dark matter 26.8%, and baryonic matter 4.9% [5, 6]. Two methods have been put forth to explain this late-time acceleration: one is to develop different dark energy candidates, and the other is to alter Einstein's gravitational theory. Developed in 1916, Einstein's general theory of relativity offered a sophisticated description of gravitation. It has done a fantastic job of characterising gravitational phenomena. Models of the cosmos have also been built on top of it. The homogeneous isotropic expanding model based on general relativity seems to give a decent approximation to the observed large-scale features of the cosmos. In recent years, there have been some intriguing attempts to generalise general relativity by including Mach's principle and other desirable aspects that the original theory lacks, for example, general relativity does not fully account for the inertial properties of matter. Modified gravity theories of general relativity (GR) have long been a hot area for research. The Brans-Dicke (BD) theory [7] is a simple scalar tensor extension of general relativity (GR) in which a dynamical scalar field is non-minimally connected to curvature. As a result, the Newtonian constant G becomes inversely proportional to the scalar field ϕ and hence a function of coordinates. The departure of the results obtained in this theory under weak field approximation from those found in general relativity under similar approximation is determined by a dimensionless parameter \mathcal{W} , dubbed the Brans-Dicke coupling parameter. The lower the value of \mathcal{W} , the more disparate the related outcomes. General relativity is well recognized for explaining local astronomical tests very effectively, and the value of \mathcal{W} needed for BD theory to be consistent with such observations is too high ($\mathcal{W} > 500$), making BD theory nearly identical to GR in the weak field limit [8]. For numerous reasons, BD theory has a periodic renaissance, particularly in cosmology. For instance, the extended inflation suggested by BD theory [9, 10] helped remove the graceful exit issue associated with traditional inflationary models. In more recent years, the BD hypothesis has been employed to perfect the environment for the universe's late temporal acceleration [?, 11, 12, 14, 15]. The amazing aspect is that, on its own, BD theory can produce an accelerated expansion without the aid of any exotic fields by simply selecting an appropriate value for the parameter \mathcal{W} [16].

The current study examines a generalized BD(GBD) theory where the parameter is a function of the scalar field inside the framework established by Nordtvedt [17]. The presence of a potential $\mathcal{V} = \mathcal{V}(\phi)$ is also included in our study as a generalization. The stability criteria were discovered to differ as expected. Mimoso and Nunes [18] worked on a BD theory generalization with either radiation or a cosmological constant as the matter content. They worked in a conformally altered version of the theory where the action resembled that of a minimally coupled theory and discovered that GR is an attractor of the BD theory. The conformally converted version has the disadvantage that the concept of equivalence is no longer applicable because the rest mass of the test particles becomes a function of the BD scalar field. The study of the

potential impacts of anisotropy in the early universe is greatly aided by spatially homogenous and anisotropic Bianchi–type cosmological models in the presence of scalar forces.

In order to paint a realistic image of the cosmos in its infancy, a wide range of spatially homogeneous and anisotropic cosmological models have been extensively researched within the framework of general relativity. Numerous writers have examined GR-based cosmological models, scalar tensor models, and modified theories. Bianchi type– VI_0 space time in BD theory has been examined by Santhi et al [19]. Hegazy and Rahaman [20] talked about the general theory of relativity’s Bianchi type– VI_0 cosmological model, which has a variable deceleration parameter and an electromagnetic field. The anisotropic Bianchi type– VI_0 cosmological model with massive scalar field and dark energy fluid was investigated dynamically by Aditya et al [21]. The magnetized Bianchi Type– VI_0 string cosmological model for anti-stiff fluids in general relativity was studied by Chhajed et al [22]. Tripathy et al [23]. examined unified dark fluid and cosmic transit models in Brans-Dicke theory.

Inspired by all the above researchers, we take into account Bianchi type– VI_0 space time filled with anisotropic dark energy in the GBD theory with a self-interacting potential. Here we created various dark energy models with a hallmark flipping behaviour of the cosmos from early slowdown to late time acceleration in the framework of generalized BD theory. The organisation of this article is as follows. In section 2, we derived all the mathematical formations of the metric that is considered. Section 3 discussed the dark fluid model and section 4 is devoted to the study of the certain properties. In the subsequent sections, various discussions will be made regarding flipping nature, the Brans-Dicke parameter, the self-interacting potential, and the gravitational constant. In the final section, we have mentioned conclusions on the current study.

2. STRUCTURE OF THE METRIC AND THE MODEL

We consider the homogeneous and anisotropic space-time represented by the Bianchi type– VI_0 metric as

$$ds^2 = -dt^2 + \mathcal{A}^2(t)dx^2 + e^{2a_1x}\mathcal{B}^2(t)dy^2 + e^{-2a_1x}\mathcal{C}^2(t)dz^2, \tag{1}$$

where a_1 is a constant that is not zero and the scale factors \mathcal{A} , \mathcal{B} , and \mathcal{C} are purely functions of cosmic time t .

Here, we take into account the self-interacting potential of the GBD hypothesis. The BD parameter is regarded as a function of the scalar field ϕ , which mediates gravity through a dynamical scalar field. In a Jordan frame, the GBD theory’s action is provided by

$$S = \int d^4x \sqrt{-g} \left[\phi R - \frac{\mathcal{W}(\phi)}{\phi} \phi^i \phi_{,i} - \mathcal{V}(\phi) + \mathcal{L}_m \right], \tag{2}$$

where R is the scalar curvature, $\mathcal{W}(\phi)$ is the modified BD parameter, $\mathcal{V}(\phi)$ is the self-interacting potential, and \mathcal{L}_m is the matter Lagrangian.

The GBD theory’s field equations are derived as ,

$$R_{ij} - \frac{1}{2}g_{ij}R = \frac{8\pi}{\phi} T_{ij} - \frac{\mathcal{W}(\phi)}{\phi^2} \left[\phi_i \phi_j - \frac{1}{2}g_{ij} \phi_{,\alpha} \phi^{,\alpha} \right] - \frac{1}{\phi} [\phi_{,i;j} - g_{ij} \square \phi], \tag{3}$$

where

$$\square \phi = \frac{T}{2\mathcal{W}(\phi) + 3} - \frac{2\mathcal{V}(\phi) - \phi \frac{\partial \mathcal{V}(\phi)}{\partial \phi}}{2\mathcal{W}(\phi) + 3} - \frac{\frac{\partial \mathcal{W}(\phi)}{\partial \phi} \phi_{,i} \phi^{,i}}{2\mathcal{W}(\phi) + 3}. \tag{4}$$

The energy momentum tensor’s trace is represented by $T = g^{ij}T_{ij}$ in the equations above, where \square is the D’Alembert operator.

The definition of the anisotropic fluid’s energy-momentum tensor is

$$T^i_j = \text{diag}(-\rho, P_x, P_y, P_z), \tag{5}$$

where p_x, p_y and p_z are the pressures; ρ is the energy density;

Additionally, the energy conservation equation serves as

$$(T^{ij})_{;j} = 0.$$

With the aid of the energy momentum tensor, the GBD theory field equations for the metric (1) are

$$\frac{\ddot{\mathcal{B}}}{\mathcal{B}} + \frac{\ddot{\mathcal{C}}}{\mathcal{C}} + \frac{\dot{\mathcal{B}}\dot{\mathcal{C}}}{\mathcal{B}\mathcal{C}} + \frac{a_1^2}{\mathcal{A}^2} + \frac{\mathcal{W}}{2} \frac{\phi^2}{\phi^2} + \left(\frac{\dot{\mathcal{B}}}{\mathcal{B}} + \frac{\dot{\mathcal{C}}}{\mathcal{C}} \right) \frac{\dot{\phi}}{\phi} + \frac{\ddot{\phi}}{\phi} = \frac{8\pi p}{\phi} + \frac{\mathcal{V}(\phi)}{2\phi}, \tag{6}$$

$$\frac{\ddot{\mathcal{A}}}{\mathcal{A}} + \frac{\ddot{\mathcal{C}}}{\mathcal{C}} + \frac{\dot{\mathcal{A}}\dot{\mathcal{C}}}{\mathcal{A}\mathcal{C}} - \frac{a_1^2}{\mathcal{A}^2} + \frac{\mathcal{W}}{2} \frac{\phi^2}{\phi^2} + \left(\frac{\dot{\mathcal{A}}}{\mathcal{A}} + \frac{\dot{\mathcal{C}}}{\mathcal{C}} \right) \frac{\dot{\phi}}{\phi} + \frac{\ddot{\phi}}{\phi} = \frac{8\pi p}{\phi} + \frac{\mathcal{V}(\phi)}{2\phi}, \tag{7}$$

$$\frac{\ddot{\mathcal{A}}}{\mathcal{A}} + \frac{\ddot{\mathcal{B}}}{\mathcal{B}} + \frac{\dot{\mathcal{A}}\dot{\mathcal{B}}}{\mathcal{A}\mathcal{B}} - \frac{a_1^2}{\mathcal{A}^2} + \frac{\mathcal{W}\dot{\phi}^2}{2\phi^2} + \left(\frac{\dot{\mathcal{A}}}{\mathcal{A}} + \frac{\dot{\mathcal{B}}}{\mathcal{B}}\right)\frac{\dot{\phi}}{\phi} + \frac{\ddot{\phi}}{\phi} = \frac{8\pi p}{\phi} + \frac{\mathcal{V}(\phi)}{2\phi}, \tag{8}$$

$$\frac{\dot{\mathcal{A}}\dot{\mathcal{B}}}{\mathcal{A}\mathcal{B}} + \frac{\dot{\mathcal{B}}\dot{\mathcal{C}}}{\mathcal{B}\mathcal{C}} + \frac{\dot{\mathcal{A}}\dot{\mathcal{C}}}{\mathcal{A}\mathcal{C}} - \frac{a_1^2}{\mathcal{A}^2} - \frac{\mathcal{W}\dot{\phi}^2}{2\phi^2} + \left(\frac{\dot{\mathcal{A}}}{\mathcal{A}} + \frac{\dot{\mathcal{B}}}{\mathcal{B}} + \frac{\dot{\mathcal{C}}}{\mathcal{C}}\right)\frac{\dot{\phi}}{\phi} = -\frac{8\pi\rho}{\phi} + \frac{\mathcal{V}(\phi)}{2\phi}, \tag{9}$$

$$\frac{\dot{\mathcal{B}}}{\mathcal{B}} - \frac{\dot{\mathcal{C}}}{\mathcal{C}} = 0, \tag{10}$$

and

$$\ddot{\phi} + \dot{\phi} \left(\frac{\dot{\mathcal{A}}}{\mathcal{A}} + \frac{\dot{\mathcal{B}}}{\mathcal{B}} + \frac{\dot{\mathcal{C}}}{\mathcal{C}}\right) = \frac{\rho - 3p}{2\mathcal{W}(\phi) + 3} + \frac{2\mathcal{V}(\phi) - \phi \frac{\partial \mathcal{V}(\phi)}{\partial \phi}}{2\mathcal{W}(\phi) + 3} - \frac{\frac{\partial \mathcal{W}(\phi)}{\partial \phi} \dot{\phi}^2}{2\mathcal{W}(\phi) + 3}. \tag{11}$$

From the above set of equations , we obtain

$$\frac{2\ddot{\mathcal{B}}}{\mathcal{B}} + \frac{\dot{\mathcal{B}}^2}{\mathcal{B}^2} + \frac{a_1^2}{\mathcal{A}^2} + \frac{\mathcal{W}\dot{\phi}^2}{2\phi^2} + \left(\frac{2\dot{\mathcal{B}}}{\mathcal{B}}\right)\frac{\dot{\phi}}{\phi} + \frac{\ddot{\phi}}{\phi} = \frac{8\pi p}{\phi} + \frac{\mathcal{V}(\phi)}{2\phi}, \tag{12}$$

$$\frac{\ddot{\mathcal{A}}}{\mathcal{A}} + \frac{\ddot{\mathcal{B}}}{\mathcal{B}} + \frac{\dot{\mathcal{A}}\dot{\mathcal{B}}}{\mathcal{A}\mathcal{B}} - \frac{a_1^2}{\mathcal{A}^2} + \frac{\mathcal{W}\dot{\phi}^2}{2\phi^2} + \left(\frac{\dot{\mathcal{A}}}{\mathcal{A}} + \frac{\dot{\mathcal{B}}}{\mathcal{B}}\right)\frac{\dot{\phi}}{\phi} + \frac{\ddot{\phi}}{\phi} = \frac{8\pi p}{\phi} + \frac{\mathcal{V}(\phi)}{2\phi}, \tag{13}$$

$$\frac{2\dot{\mathcal{A}}\dot{\mathcal{B}}}{\mathcal{A}\mathcal{B}} + \frac{\dot{\mathcal{B}}^2}{\mathcal{B}^2} + \frac{\dot{\mathcal{A}}\dot{\mathcal{B}}}{\mathcal{A}\mathcal{B}} - \frac{a_1^2}{\mathcal{A}^2} - \frac{\mathcal{W}\dot{\phi}^2}{2\phi^2} + \left(\frac{\dot{\mathcal{A}}}{\mathcal{A}} + \frac{2\dot{\mathcal{B}}}{\mathcal{B}}\right)\frac{\dot{\phi}}{\phi} = -\frac{8\pi\rho}{\phi} + \frac{\mathcal{V}(\phi)}{2\phi}, \tag{14}$$

and

$$\ddot{\phi} + \dot{\phi} \left(\frac{\dot{\mathcal{A}}}{\mathcal{A}} + \frac{2\dot{\mathcal{B}}}{\mathcal{B}}\right) = \frac{\rho - 3p}{2\mathcal{W}(\phi) + 3} + \frac{2\mathcal{V}(\phi) - \phi \frac{\partial \mathcal{V}(\phi)}{\partial \phi}}{2\mathcal{W}(\phi) + 3} - \frac{\frac{\partial \mathcal{W}(\phi)}{\partial \phi} \dot{\phi}^2}{2\mathcal{W}(\phi) + 3}. \tag{15}$$

Where the overhead dot stands for ordinary differentiation with respect to t.

Solving equation(10), we obtain

$$C = m\mathcal{B} \tag{16}$$

The field equations (12) – (15) are now a system of four independent equations with eight unknown parameters (\mathcal{A} , \mathcal{B} , p , ρ , ϕ , δ_y , $\mathcal{V}(\phi)$ and $\mathcal{W}(\phi)$). To obtain a determinate solution to the field equations, we consider the following suitable conditions, which are physically viable.

i) We assume that the expansion scalar (θ) is proportional to the shear scalar (σ) from [25]. This condition leads to ,

$$\mathcal{A} = \mathcal{B}^n, \tag{17}$$

where $n \neq 1$ is a constant.

ii) By the motivation of Tripathy et. al. [23], we take a look at a hybrid scale factor(HSF),

$$a(t) = a_0 \left(\frac{t}{t_0}\right)^{\mathcal{H}^1} e^{\mathcal{H}^0(t-t_0)}, \tag{18}$$

where a_0 is the scale factor at the current epoch t_0 and \mathcal{H}^0 and \mathcal{H}^1 are HSF parameters whose values are positive constants, and in this work, we have assumed $a_0 = t_0 = 1$.

Spatial volume of the model and average scale factor are given by

$$V = \sqrt{-g} \quad \text{and} \quad a(t) = V^{1/3}.$$

Then we obtain,

$$\mathcal{A} = \frac{1}{m^{\frac{n}{(n+2)}}} t^{\frac{3\mathcal{H}^1 n}{(n+2)}} e^{\frac{3\mathcal{H}^0 n(t-1)}{n+2}}, \tag{19}$$

$$\mathcal{B} = \frac{1}{m^{\frac{1}{(n+2)}}} t^{\frac{3\mathcal{H}^1}{(n+2)}} e^{\frac{3\mathcal{H}^0(t-1)}{n+2}}, \tag{20}$$

and

$$C = \frac{1}{m^{\frac{1}{(n+2)}-1}} t^{\frac{3\mathcal{H}^1}{(n+2)}} e^{\frac{3\mathcal{H}^0(t-1)}{n+2}}. \tag{21}$$

From equations (12) and (13), we get

$$\frac{\dot{\mathcal{A}}}{\mathcal{A}} - \frac{\dot{\mathcal{B}}}{\mathcal{B}} = \frac{c_1}{\mathcal{A}\mathcal{B}^2\phi} e^{\int \left(\frac{2a_1^2}{\frac{\mathcal{A}^2}{\mathcal{A}-\frac{\mathcal{B}}{\mathcal{B}}}} \right) dt}, \tag{22}$$

where c_1 is an integral constant.

Assume

$$\delta_0 = e^{\int \left(\frac{2a_1^2}{\frac{\mathcal{A}^2}{\mathcal{A}-\frac{\mathcal{B}}{\mathcal{B}}}} \right) dt}. \tag{23}$$

From equations (19)– (23) , we get,

$$\frac{\phi}{\phi_0} = t^{-3\mathcal{H}^1} e^{-3\mathcal{H}^0(t-1)} \left(\frac{\mathcal{H}^1}{t} + \mathcal{H}^0 \right)^{-1}, \tag{24}$$

where $\phi_0 = \frac{m c_1 \delta_0 (n+2)}{3(n-1)}$.

The field equations (12) through (15) are used to get the Brans-Dicke parameter and the self-interacting potential, as

$$\mathcal{W}(\phi) = \left[-3 \frac{(\mathcal{H}^1 + \mathcal{H}^0 t)}{t} + \frac{\mathcal{H}^1}{t(\mathcal{H}^1 + \mathcal{H}^0 t)} \right]^{-2} \left\{ \begin{aligned} & \frac{8\pi(\rho + p)}{\phi_0 t^{-3\mathcal{H}^1} e^{-3\mathcal{H}^0(t-1)} \left(\frac{\mathcal{H}^1}{t} + \mathcal{H}^0 \right)^{-1}} - \frac{9(2n^2 + 3n + 5)(\mathcal{H}^1 + \mathcal{H}^0 t)^2}{(n + 2)^2 t^2} \\ & - 2 \left(\frac{\mathcal{H}^1}{t(\mathcal{H}^1 + \mathcal{H}^0 t)} \right)^2 \end{aligned} \right\}, \tag{25}$$

and

$$\mathcal{V}(\phi) = \left[\phi_0 t^{-3\mathcal{H}^1} e^{-3\mathcal{H}^0(t-1)} \left(\frac{\mathcal{H}^1}{t} + \mathcal{H}^0 \right)^{-1} \right] \left\{ \begin{aligned} & - 3(n + 5) \frac{\mathcal{H}^1}{t^2} + \frac{9(n^2 + 7n + 2)}{(n + 2)^2} \left(\frac{\mathcal{H}^1}{t} + \mathcal{H}^0 \right)^2 \\ & + \frac{2(\mathcal{H}^1)^2}{t^2(\mathcal{H}^1 + \mathcal{H}^0 t)^2} - \frac{2\mathcal{H}^1}{t^2(\mathcal{H}^1 + \mathcal{H}^0 t)} \end{aligned} \right\} + 8\pi(\rho - p), \tag{26}$$

Here, in order to determine the dynamical BD parameter and the self-interacting potential, we take into consideration a straightforward linear equation of state known as the equation of state of the unified dark fluid (UDF). Dark energy and dark matter, which are two separate concepts, are how the UDF explains how both dark sectors can come together. It is important to note here that there are several generalized equations of states in the literature that consider dark energy and dark matter as two different sides of the same cosmic fluid [26].

3. UNIFIED DARK FLUID

Undisputedly, exotic dark energy and non-baryonic matter are the main drivers of late-time cosmic acceleration. Recent Planck measurements show that the universe’s mass-energy budget is made up of 68.3% dark energy, 26.8% dark matter and 4.9% baryonic matter and that the dark sector, which comprises dark energy and dark matter, accounts for about 95% of that budget. The mysterious cosmic speed-up phenomenon in the late hours has several possible causes. Various theories and notions have been created to better understand the phenomenon. This could be accomplished by using a particular strategy that unifies dark energy and dark matter into a single UDF. After the generalized Chaplygin gas model (CGM) was successful in addressing concerns about the late-time cosmic acceleration and dark energy problem [27], a dark fluid model with a linear equation of state

$$p = \alpha (\rho - \rho_0), \tag{27}$$

was presented. Here, the UDF’s constant parameters α and ρ_0 are used. The adiabatic sound speed of the UDF is constant, $C_s^2 = \frac{dP}{d\rho} = \alpha$. Both hydrodynamically stable ($\alpha > 0$) and unstable ($\alpha < 0$) fluids are described by this non-homogeneous linear equation of state. The conservation equation is

$$\dot{\rho} + 3H(P + \rho) = 0, \tag{28}$$

by integrating equation (28),

$$\rho = \frac{\alpha}{(1 + \alpha)} \rho_0 + \frac{c_2}{(1 + \alpha)} \frac{1}{t^{3\mathcal{H}^1(1+\alpha)} e^{3\mathcal{H}^0 t(1+\alpha)}}, \tag{29}$$

where c_2 is an integrating constant.
From equations (27) and (29), we derive

$$p = \frac{-\alpha}{(1 + \alpha)}\rho_0 + \frac{c_2\alpha}{(1 + \alpha)} \frac{1}{t^{3\mathcal{H}^0(1+\alpha)}e^{3\mathcal{H}^0t(1+\alpha)}}, \tag{30}$$

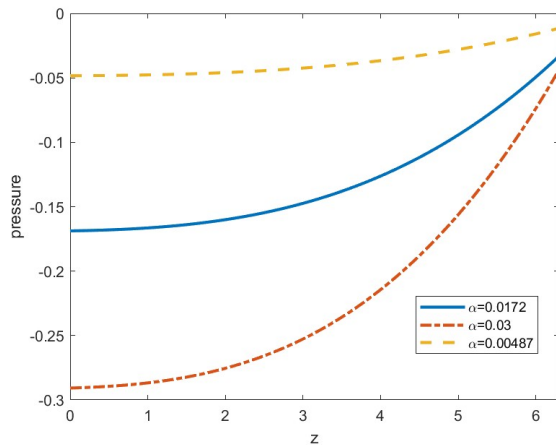


Figure 1. Study of pressure over the redshift parameter

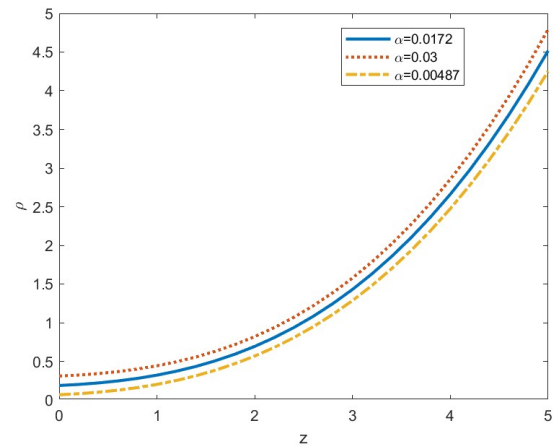


Figure 2. Analysis of density in terms of redshift parameter

The dark energy equation of state can be seized as the following when considering the redshift:

$$\omega_D = \frac{p}{\rho} = \alpha - \frac{\alpha(1 + \alpha)\rho_0}{(\alpha\rho_0 + c^1e^{-3\mathcal{H}^0(1+\alpha)}(1 + z)^{3(1+\alpha)})}, \tag{31}$$

where we have used the fact $1 + z = \frac{1}{a}$.

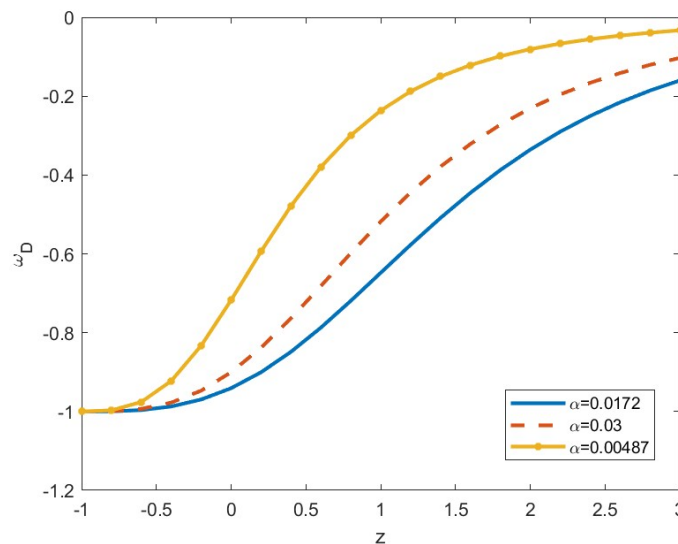


Figure 3. For three different values of α , the dark energy equation of state in terms of red shift.

Figure (3) depicts the dark energy equation of the state’s evolutionary behaviour for three different values of the limited adiabatic sound speed α . The dynamical behavior of a bouncing model has been discussed in the framework of the dark energy equation of state for UDF. Here, we fixed the values for constants $\mathcal{H}^0 = 0.55, c_2 = 0.1, \rho_0 = 10$ using various values of constants. A change in these values, as observed in this work, does not effect on ω_D ’s overall dynamical behaviour. In light of this, we used $\mathcal{H}^0 = 0.55, c_2 = 0.1, \rho_0 = 10$ to plot the figure in the current work. According to the illustration, the lower curve in the graphic reflects the value $\alpha = 0.0172$, the middle curve to the value $\alpha = 0.03$ and the higher curve to the value $\alpha = 0.00487$. Depending on various conditions, the dark energy equation of state can change in

a variety of ways. Consequently, affects the slope of ω_D . Regardless of the value of α , ω_D eventually develops to overlap with the Λ CDM model ($\omega_D = -1$).

3.1. Unified dark fluid in $\omega'_D - \omega_D$

In order to evaluate the quintessence scalar field, Caldwell and Linder [29,30] first developed the EoS plane to explain the areas of the expanding Universe. Two unique zones are characterised by the plane for varying values of ω_D and ω'_D . When $\omega'_D > 0$, $\omega_D < 0$, the plane is referred to as a thawing region and when $\omega'_D < 0$, $\omega_D < 0$, it is a freezing region. ω'_D is obtained for this model is,

$$\omega'_D = \frac{-3\alpha(1 + \alpha)^2 c^1 t^{-3\mathcal{H}^1(1+\alpha)} e^{-3\mathcal{H}^0 t(1+\alpha)} \left(\frac{\mathcal{H}^1}{t} + \mathcal{H}^0\right)}{[\alpha\rho_0 + c^1 t^{-3\mathcal{H}^1(1+\alpha)} e^{-3\mathcal{H}^0 t(1+\alpha)}]} . \tag{32}$$

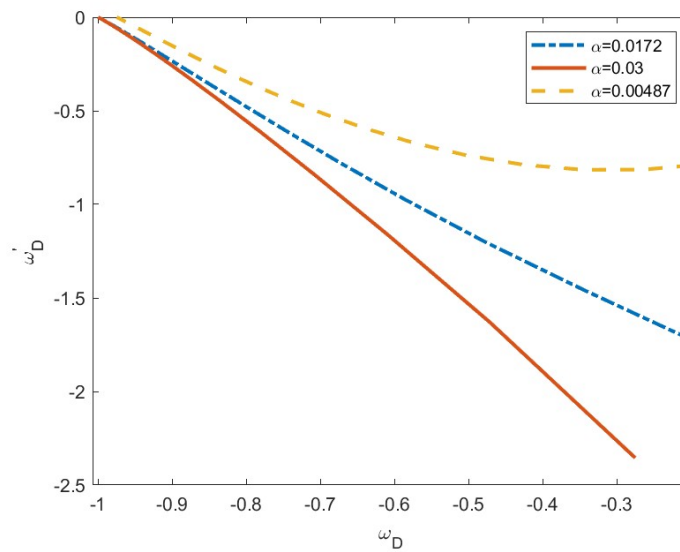


Figure 4. Overview of ω'_D against ω_D

The EoS plane ($\omega'_D - \omega_D$) for this cosmological model is shown in Figure (4) for various values of $\alpha = 0.0172$, $\alpha = 0.3$ and $\alpha = 0.00487$. As $\omega'_D < 0$, $\omega_D < 0$ for our model, it is seen that the model is in the freezing area. This shows that the universe is expanding faster than before.

4. PARAMETERS OF THE MODEL

- **Hubble Parameter:** Hubble’s parameter is

$$H = \frac{\dot{\mathcal{A}}}{\mathcal{A}} + 2\frac{\dot{\mathcal{B}}}{\mathcal{B}} = \frac{\mathcal{H}^1}{t} + \mathcal{H}^0. \tag{33}$$

- **Expansion scalar:**

$$\theta = 3H = 3 \left[\frac{\mathcal{H}^1}{t} + \mathcal{H}^0 \right]. \tag{34}$$

- **Shear scalar:**

$$\sigma^2 = \frac{1}{2} \left(\sum_{i=1}^3 H_i^2 - \frac{\theta^2}{3} \right) = \frac{(n-1)^2}{(n+2)^2} \left(\frac{\mathcal{H}^1}{t} + \mathcal{H}^0 \right)^2. \tag{35}$$

- **Anisotropic parameter:**

$$A_h = \frac{1}{3} \sum_{i=1}^3 \left(\frac{H_i - H}{H} \right)^2 = \frac{6(n^2 + 2n + 3)}{(n+2)^2}. \tag{36}$$

• **State-finder parameters:**

$$r = \frac{\ddot{a}}{aH^3} = \frac{1}{(\frac{\mathcal{H}^1}{t} + \mathcal{H}^0)^3} \left[\frac{\mathcal{H}^1(\mathcal{H}^1 - 1)(\mathcal{H}^2 - 2)}{t^3} + \frac{3\mathcal{H}^1\mathcal{H}^0(\mathcal{H}^1 - 1)}{t^2} + \frac{3\mathcal{H}^1\mathcal{H}^0}{t} + (\mathcal{H}^0)^3 \right], \tag{37}$$

and

$$s = \frac{r - 1}{3(q - \frac{1}{2})} = \frac{4\mathcal{H}^1}{(\mathcal{H}^1 + \mathcal{H}^0 t)(2\mathcal{H}^1 - 3(\mathcal{H}^1 + \mathcal{H}^0 t)^2)} - \frac{6\mathcal{H}^1}{(2\mathcal{H}^1 - 3(\mathcal{H}^1 + \mathcal{H}^0 t)^2)}. \tag{38}$$

• **Deceleration parameter:** The scale-factor $a(t)$ yields the following expression for the deceleration parameter $q(z)$:

$$q = \frac{-a\ddot{a}}{\dot{a}^2} = -1 + \frac{\mathcal{H}^1}{(\mathcal{H}^1 + \mathcal{H}^0 t)^2}. \tag{39}$$

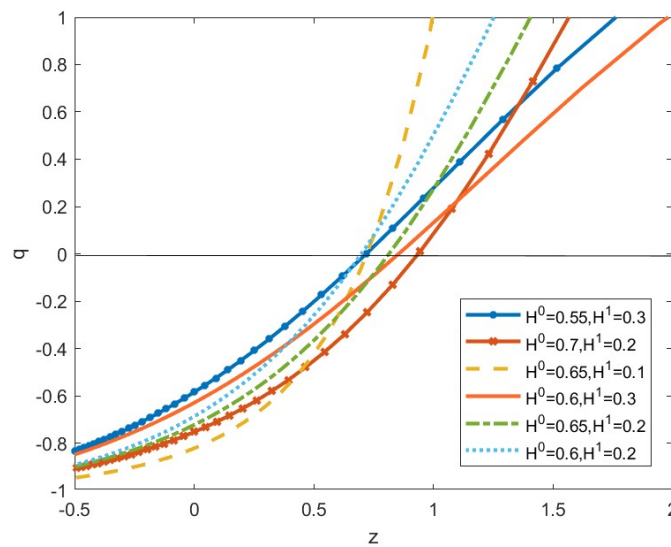


Figure 5. Study of deceleration parameter over z for various values of \mathcal{H}^0 and \mathcal{H}^1

The fluctuation of DP for the different sets of the HSF model parameters is shown in Figure (5). As illustrated in Table 1, we can see that $q(z)$ is an increasing function of redshift z and exhibits a signature-flipping (transition) point at z_a within the range $0.65 < z_a < 0.9$, where $q(z_a) = 0$ and $q(z) < 0$ for $z < z_a$ and $q(z) > 0$ for $z > z_a$, as well as $q(z) \rightarrow -1$ as $z \rightarrow -1$ and $q(z)$ tends to a finite positive value as $z \rightarrow \infty$.

Our universe is accelerating right now and decelerating in the early phases, which are quite close to the most recent observations, based on the behaviour of DP $q(z)$ over redshift z . As a result, in line with the most recent research evidence, our model’s derivation depicts a transit phase from a universe that is slowing down to one that is accelerating.

5. FLIPPING NATURE

Observations in the past indicate that the universe is growing more rapidly now than in earlier epochs. The idea that the cosmos may have changed from a decelerating to an accelerating phase is also held. The cosmic redshift at which this transition takes place is known as the transition redshift z_a . Inversion of the signature is implied.

The q ’s behaviour shifts from a positive value early in cosmic evolution to a negative value later. In the current work, we seek to construct a cosmological model that can both forecast how this universe will behave and offer a distinctive flipping of the deceleration parameter. Taking into account a hybrid scale factor equation (18).

This hybrid scale factor consists of two parts, one of which expands exponentially and the other of which expands power law-like. At the beginning of cosmic evolution, power law behaviour rules over cosmic dynamics, in contrast to the exponential factor’s supremacy at the end. The exponential law is recovered when $\mathcal{H}^1 = 0$, and a power law expansion is simulated by the scaling factor when $\mathcal{H}^0 = 0$. Power law and the exponential rule of expansion were previously employed by Tripathy et al. [24] to construct certain UDF models within the context of GBD theory. Both the power law and the exponential law of expansion produce a constant deceleration parameter. We suggest utilising a hybrid expansion law in which the deceleration parameter changes from positive to negative values early in cosmic history on account of

the behaviour of planetary transit. The deceleration parameter for this model is $q = -1 + \frac{\mathcal{H}^1}{(\mathcal{H}^0 t + \mathcal{H}^1)^2}$, while the Hubble parameter is $H = \mathcal{H}^0 + \frac{\mathcal{H}^1}{t}$. Mishra and Tripathy [31–36], in their recent publications, have addressed a number of issues relating to the late-time cosmic speed-up event within the context of GR and modified gravity, taking the HSF into mind. As $t \rightarrow 0$, the HSF deceleration parameter falls to $q \simeq -1 + \frac{1}{\mathcal{H}^1}$ and changes throughout cosmic time to become $q \simeq -1$ at the end of the culmination of cosmic evolution

The transit epoch correlates to a redshift called transit redshift z_a , which happens when the cosmos switches from a decelerated to an accelerated phase. This value has been constrained to be of the order of one based on several theoretical and empirical factors, i.e. $z_a \sim 1$. For instance, Busca [37] confined the redshift of the transition to be $z_a = 0.82 \pm 0.08$; and Capozziello et al. [38] succeeded in achieving a constraint on this parameter to be $z_a = 0.426^{+0.27}_{-0.089}$. According to Reiss et al. [39] calculated limitations of the transition redshift is $z_a = 0.69^{+0.23}_{-0.12}$. In contrast to Lu et al. [?] who got the constraint $z_a = 0.69^{+0.23}_{-0.12}$. The constraint was obtained by Moresco et al. [?] $z_a = 0.4 \pm 0.1$. The deceleration parameter vanishes at the transit redshift, corresponding to a geological time $t = -\frac{\mathcal{H}^1}{\mathcal{H}^0} \pm \frac{\sqrt{\mathcal{H}^1}}{\mathcal{H}^0}$. One may have the transition period as $t = \frac{\sqrt{\mathcal{H}^1} - \mathcal{H}^1}{\mathcal{H}^0}$ in the context of orthodox Big Bang cosmology with a positive time frame only. It obviously limits the value of the parameter \mathcal{H}^1 to the range $0 < \mathcal{H}^1 < 1$. Mishra and Tripathy [31] have attempted to restrict this parameter to the range $0 < \mathcal{H}^1 < \frac{1}{3}$. \mathcal{H}^0 is treated as a free parameter in that work. In contrast, \mathcal{H}^0 is restricted in later work to the range $0.075 \leq \mathcal{H}^0 \leq 0.1$ in accordance with the restrictions on the transition redshift $0.4 \leq z_a \leq 0.8$ [34]. Additionally, Mishra et al. [32] replicated the transition redshift of $z_a = 0.806$ using the precise values $\mathcal{H}^0 = 0.695$ and $\mathcal{H}^1 = 0.085$. HSF is unquestionably necessary to reproduce the deceleration parameter’s unique flipping behaviour. The value of \mathcal{H}^0 , one of the two HSF parameters, determines how quickly a decelerating world transitions to an accelerating one. The pace of transition is faster the higher the value of \mathcal{H}^0 . As a result, these parameters can be appropriately constrained using both the observed transit redshift values and the Hubble parameter data for various redshifts. In a recent study, we restricted the other parameters to achieve two specific values of the transition redshift, especially 0.8 and 0.5 [30] We also considered two specific values of \mathcal{H}^1 , specifically 0.2 and 0.3. The purpose of doing this was to restrict the HSF’s parameters.

It is undeniable that HSF is necessary to reproduce the deceleration parameter’s hallmark flipping behaviour. The value of \mathcal{H}^0 , one of the two HSF parameters, determines how quickly a decelerating world transitions to an accelerating one. The pace of transition is faster the higher the value of \mathcal{H}^0 . As a result, these parameters can be appropriately limited using both the Hubble parameter data at various redshifts and the observed transit redshift values. In a recent study, we took into consideration three specific values of \mathcal{H}^1 , particularly 0.1, 0.2 and 0.3, and confined the other parameter to obtain the interval of transition redshift in between $0.4 < z_a \leq 0.9$. Six alternative models—Set1, Set2, Set3, Set4, Set5 and Set6—have been produced as a result of this approach. Table I lists the model parameters that were produced. The built-in models fall comfortably within the permitted bounds of the observed value.

TABLE I: Using transition redshift data from figure (5), constrain model parameters for the hybrid scale factor.

HSF Models	\mathcal{H}^1	\mathcal{H}^0	z_a
Set1	0.3	0.55	0.7
Set2	0.2	0.7	0.88
Set3	0.1	0.65	0.7
Set4	0.3	0.6	0.84
Set5	0.2	0.65	0.8
Set6	0.2	0.6	0.687

6. DISCUSSION OF BRANS-DICKE SCALAR FIELD

The Brans-Dicke scalar field in this model is derived as,

$$\phi = \phi_0 t^{-3\mathcal{H}^1} e^{-3\mathcal{H}^0(t-1)} \left(\frac{\mathcal{H}^1}{t} + \mathcal{H}^0 \right)^{-1}, \tag{40}$$

where the BD scalar field’s value at the current epoch is ϕ_0 , in this case. The scale factor’s first derivative, together with both, affect the BD scalar field. The outcomes of Tripathy et al., [24] for an exponential and power law expansion of the scale factor can be retrieved from the BD scalar field calculation given above. The Hubble rate becomes constant for an exponential scale factor expansion, which causes the BD scalar field to be reduced to $\phi = \phi_0 a^3$.

Similar to how the BD scalar field changes with a power law expansion such as $a \sim t^{\mathcal{H}^1}$, it becomes a $\phi \sim t^{3\mathcal{H}^1-1}$.

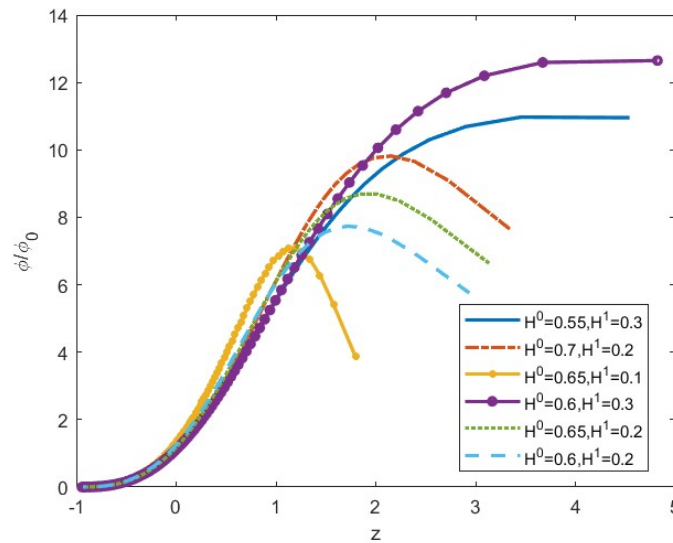


Figure 6. Evolution of the Brans-Dicke scalar field ϕ over the redshift z for six constraints.

The BD scalar field is shown in Fig:(6) for each model that has been constructed, transitioning from initially having some large values to currently having modest values. For the models with $\mathcal{H}^1 = 0.2$ and $\mathcal{H}^1 = 0.1$, however, ϕ first increases during the first phase to a specified maximum and subsequently decreases to the typical behaviour at a specific redshift. The HSF model performs the same at low redshift regardless the parameters of the model. Although behaves uniformly for all HSF models in the current epoch and those that follow, it's crucial to note that they exhibited fundamentally different behaviours at redshifts $z > 0.5$ during a prior cosmic phase. The behaviour of the models Set1 and Set4 appears to be smooth in terms of the development of the BD scalar field. Therefore, compared to the other four assumptions, these two approaches might be better suited for the cosmological study.

7. INVESTIGATION OF THE BRANS-DICKE PARAMETER

A prior work [24] used the built-in anisotropic models to compute the Brans-Dicke parameter while taking into consideration UDF within the context of the GBD theory and assuming either a power law or an exponential increase of the volume scale factor. The deceleration parameter is constant as a result of this assumption. It has been shown that in such cases the anisotropic parameter only influences the non-evolving part of the Bran-Dicke parameter. The hybrid expansion law we examined in this work, however, replicates the true transitory universe with early deceleration and late cosmic expansion.

The Brans-Dicke parameter is calculated in this work as,

$$\mathcal{W}(\phi) = \left[-3 \frac{(\mathcal{H}^1 + \mathcal{H}^0 t)}{t} + \frac{\mathcal{H}^1}{t(\mathcal{H}^1 + \mathcal{H}^0 t)} \right]^{-2} \left\{ \frac{8\pi c^1 (\mathcal{H}^1 + \mathcal{H}^0 t)}{t \phi_0 t^3 \mathcal{H}^1 \alpha e^{3\mathcal{H}^0 (at+1)}} - \frac{9(2n^2 + 3n + 5)(\mathcal{H}^1 + \mathcal{H}^0 t)^2}{(n + 2)^2 t^2} \right. \\ \left. - 2 \left(\frac{\mathcal{H}^1}{t(\mathcal{H}^1 + \mathcal{H}^0 t)} \right)^2 \right\}, \quad (41)$$

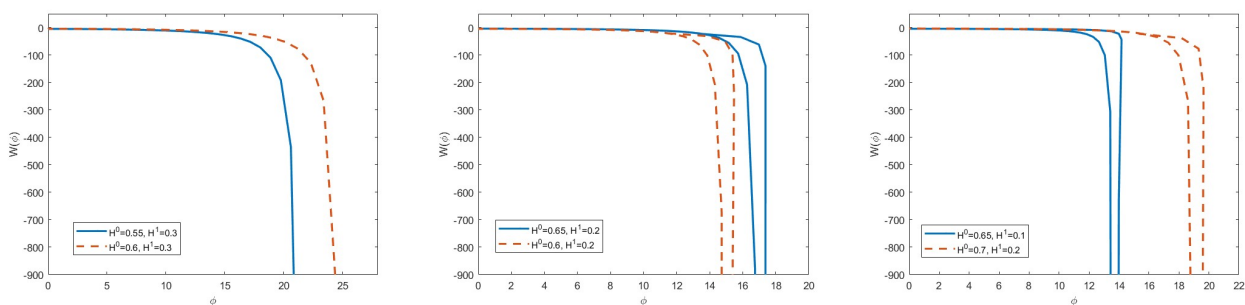


Figure 7. The Brans-Dicke parameter, $\mathcal{W}(\phi)$ for is shown over the scalar field ϕ for all \mathcal{H}^0 and \mathcal{H}^1 constraints.

Figures (7) (a), (b), and (c) show how the Brans-Dicke parameter has changed in relation to the BD scalar field . In each graph, the BD parameter is displayed for the two models. In Fig. (7)(a) \mathcal{H}^0 values are 0.55 and 0.6 with $\mathcal{H}^1 = 0.3$, in Fig. (7)(b) \mathcal{H}^0 values are 0.65 and 0.6 with $\mathcal{H}^1 = 0.2$, and in Fig. (7)(c) \mathcal{H}^0 values are 0.7 and 0.65 with $\mathcal{H}^1 = 0.2$ and 0.1 respectively. We took into account the value of $\alpha=0.0172$ in order to visualise the data.

The BD parameter frequently falls as the scalar field gets larger. However, it is noted that at the late stages of cosmic history, behaves consistently across all models generating a kind of loop structure in the cases that we presented in Fig.(7)(a) when $\mathcal{H}^1 = 0.3$. For the cases with $\mathcal{H}^1 = 0.1$ and 0.2 in Fig.(7)(b) and 8(c), at some early epochs, $\mathcal{W}(\phi)$ exhibits strange behaviour, forming a type of loop structure with the scalar field. This tendency may be a result of the peculiar behaviour of the BD scalar field for the set2, set3, set5, and set6 models, which shows decrease with z , a minimum at a particular z , and then grows as z grows further. As a result, set1 and set4 may be more appropriate models for cosmological studies than the others. Notably, the BD parameter eventually becomes a constant value irrespective of the HSF parameters chosen at a later stage of cosmic evolution. The quantitative estimation of the BD parameter remains a contentious topic. However, our research revealed that all models anticipate values that are essentially the same. This leads to the conclusion that the anisotropy in the expansion rates influences the value at a certain epoch.

8. SELF-INTERACTING POTENTIAL

The self interacting potential $\mathcal{V}(\phi)$ in this model is calculated as,

$$\mathcal{V}(\phi) = \left[\frac{\phi_0}{t^{3\mathcal{H}^1} e^{3\mathcal{H}^0(t-1)} \left(\frac{t^1}{t} + \mathcal{H}^0\right)} \right] \left\{ \begin{aligned} & \frac{9(n^2 + 7n + 2)}{(n + 2)^2} \left(\frac{\mathcal{H}^1}{t} + \mathcal{H}^0\right)^2 \\ & + \frac{2(\mathcal{H}^1)^2}{t^2(\mathcal{H}^1 + \mathcal{H}^0 t)^2} \\ & - \frac{3(n + 5)\mathcal{H}^1}{t^2} - \frac{2\mathcal{H}^1}{t^2(\mathcal{H}^1 + \mathcal{H}^0 t)} \end{aligned} \right\} + 8\pi \left(\frac{2\alpha\rho_0}{(1 + \alpha)} - \frac{c_2(1 - \alpha)}{(1 + \alpha)} \frac{1}{t^{3\mathcal{H}^1(1+\alpha)} e^{3\mathcal{H}^0 t(1+\alpha)}} \right), \tag{42}$$

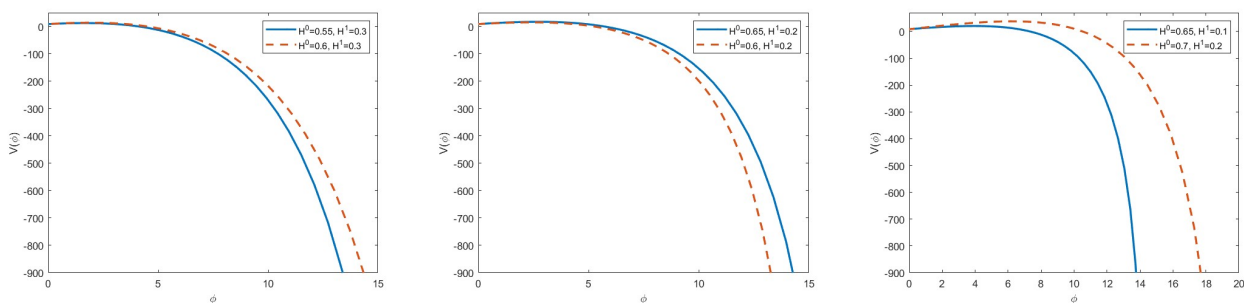


Figure 8. Study of the self interacting potential $\mathcal{V}(\phi)$ over the scalar field ϕ for all constraints of \mathcal{H}^0 and \mathcal{H}^1 .

Figures 9(a), 9(b), and 9(c) show the self-interacting potential $\mathcal{V}(\phi)$'s variation as a function of the BD scalar field. For the two models in each graph, the self-interacting potential nature is displayed. In Fig.9(a) \mathcal{H}^0 values are 0.55 and 0.6 with $\mathcal{H}^1 = 0.3$, in Fig.9(b) \mathcal{H}^0 values are 0.65 and 0.6 with $\mathcal{H}^1 = 0.2$, and in Fig.9(c) \mathcal{H}^0 values are 0.7 and 0.65 with $\mathcal{H}^1 = 0.2$ and 0.1 respectively. We took into account the value of $\alpha=0.0172$ to visualise the data.

The built-in HSF models have an attractive self-interacting potential that rises sharply from a significant negative value at an early epoch to virtually nothing at the end of evolution. The six models act in a manner that is comparable at the low redshift area, when the scalar field has a smaller magnitude. On the other hand, the six models split to act differently at the high redshift area with a big scalar field. At a late stage in the evolution of the universe, the self-interacting potential stops being reliant on HSF models and appears to be static about the BD scalar field.

9. NEWTONIAN GRAVITATIONAL CONSTANT G'S FLUCTUATION

The Newtonian gravitational constant $G(\phi)$ is described as follows in GBD theory:

$$G(\phi) = \frac{4 + 2\mathcal{W}(\phi)}{\phi(3 + 2\mathcal{W}(\phi))}, \tag{43}$$

so its variation of time is as

$$\frac{\dot{G}}{G} = \frac{-2\dot{\mathcal{W}}(\phi)}{(4 + 2\mathcal{W}(\phi))(3 + 2(\phi))} - \frac{\dot{\phi}}{\phi}. \tag{44}$$

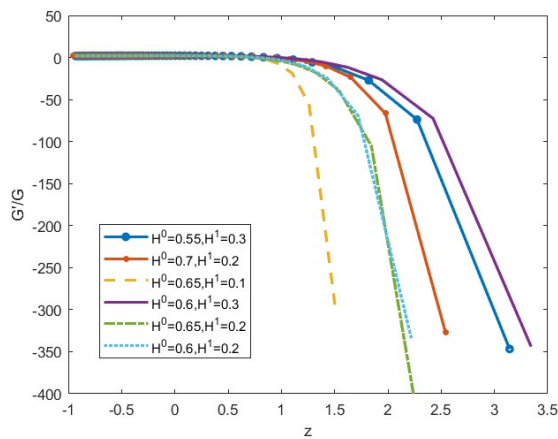


Figure 9. Study of $\frac{\dot{G}}{G}$ over the redshift z . Here we fixed the $\alpha = 0.0172$.

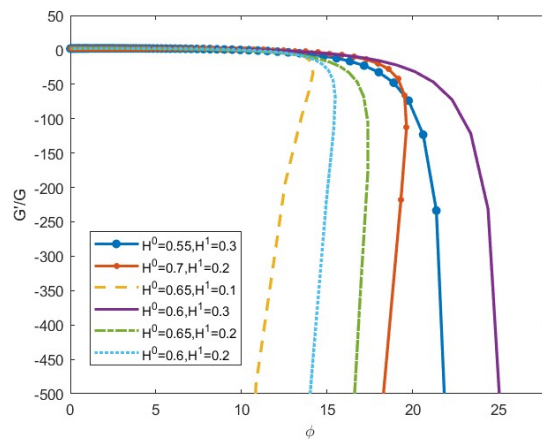


Figure 10. Study of $\frac{\dot{G}}{G}$ over the function ϕ . Here we fixed the $\alpha = 0.0172$.

In Figure (9) we display the G 's time variation for the six HSF models as a function of redshift. We have shown the G time variation as a function of redshift. The determining $\frac{\dot{G}}{G}$ climbs from a previously significant negative value and reached a high in the recent past. It then drops to a somewhat positive number. The $\frac{\dot{G}}{G}$ peaks for various models occur at various redshifts. For a fitted model, the z_{max} at which $\frac{\dot{G}}{G}$ peaks is determined by the values of z_a and \mathcal{H}^1 . For a specific \mathcal{H}^1 , higher z_a causes higher z_{max} . Similar to this, larger \mathcal{H}^1 values translate into higher z_{max} for a given z_a . The temporal variation of the Newtonian gravitational constant as a result of the BD scalar field is also shown in Figure (10). It is noted that the factor $\frac{\dot{G}}{G}$ initially increases with an increase in and then decreases after peaking at a particular value for all six HSF models. The particular HSF models and associated model parameters determine which BD scalar field hosts the peak of $\frac{\dot{G}}{G}$.

10. CONCLUSION

The dynamics of our cosmos are incredibly complex, according to numerous observable pieces of evidence. The history of the universe's expansion is shown using a variety of methods because it is unknown exactly what these enigmatic fluids are in their most basic form. One of the most widely accepted theories postulates that dark energy and dark matter develop independently of one another, with the dynamics of each dark fluid existing independently of the other. Furthermore, it's believed that these two black fluids are just two sides of a single fluid, posing as both dark fluids. In cosmological literature, the idea of a single dark fluid that displays two distinct dark sides of the cosmos is referred to as the "unified dark fluid." In the current work, we have concentrated on a unified dark fluid model. Using GBD, we have developed a few astronomical models that accelerate. We pick Bianchi type- V directional expansion rates that are anisotropic and homogeneous in space. The GBD theory postulates that the Brans-Dicke parameter fluctuates with the scalar field. The Brans-Dicke hypothesis modifies the GR by proposing that gravity is propagated by a dynamic scalar field. The late-time cosmic speed-up phenomenon has been verified by observations. We employ a unified dark fluid equation of state that combines the treatment of dark matter and dark energy into a single equation, allowing us to build accelerated simulations. The parameters of the unified dark fluid model have been subject to limitations generated from various observational data using different techniques. Observational constraints have been used to establish the operational range of the model. construct a workable cosmological model inside the GBD hypothesis. The universe is expanding faster and faster. It suggests that, at some point in time, the universe may have entered an acceleration phase after experiencing a period of deceleration. The deceleration parameter, which should be positive at some early point in cosmic history and negative at some late point, must flip as a signature for this behaviour. We employ a hybrid scale factor to roughly represent a deceleration parameter with clear switching behaviour. Two components comprise the HSF. One element is more prevalent in the early phases of cosmic evolution than the other element is in the later stages. The HSF could thus recreate an entire journey history, beginning with an early deceleration and concluding with a late-time acceleration. The HSF's parameters must be restricted to provide a testable accelerated cosmological model. The transition redshift, which marks the potential turning point from a decelerating to an expanding universe, is a crucial cosmological statistic. To constrain the HSF parameters, we studied the recently constrained transition redshift values. In particular, we employed six transition redshift values in our work, ranging from $z_a = 0.65$ to $z_a = 0.9$. For an accelerated model, six distinct models are set up. We looked into the scalar field evolution, Brans-Dicke parameter, self-interacting potential, and time variation of the Newtonian gravitational constant for these models. For each of the constructed models, the BD scalar field changes with time from initially having some large values to later having smaller values. The BD scalar fields of all HSF models react identically at a late stage of evolution. For the models Set4 and Set6, however, the redshift first increases during the

first phase to a specific maximum before declining to the typical behaviour at a specific low redshift. For the BD scalar field, the evolutionary behaviour of the other four models is a little bit smoother. This behaviour is consistent with the evolution of other parameters, such as the BD parameter and the fluctuation of the Newtonian gravitational constant. The BD parameter decreases along with the BD scalar field, which increases in every model that has been built. Because the BD parameter virtually becomes a constant amount at a later stage of evolution, the GBD theory may be convergent with the standard Brans-Dicke theory. A major negative value at an early epoch diminishes to ridiculously small values later in development, making the self-interacting potential of the built-in HSF models desirable by nature. The models behave similarly when the scalar field has a smaller amount at low redshift. In the large redshift sector with a big scalar field, however, all models split to act differently.

11. ACKNOWLEDGMENTS

M. Vijaya Santhi acknowledges Department of Science and Technology (DST), Govt of India, New Delhi for financial support to carry out the Research Project [No. EEQ/2021/000737, Dt. 07/03/2022].

ORCID

✉ M. Vijaya Santhi, <https://orcid.org/0000-0002-0050-3033>; ✉ K. SantoshRupa, <https://orcid.org/0009-0001-8996-8661>

REFERENCES

- [1] A.G. Riess, *et al.*, *Astron J.* **116**, 1009 (1998). <https://doi.org/10.1086/300499>
- [2] S. Perlmutter, *et al.*, *Nature*, **391**, 51 (1998). <https://doi.org/10.1038/34124>
- [3] C.L. Bennett, *et al.*, *Astrophys. J. suppl.* **148**, 1 (2003). <https://doi.org/10.1086/377253>
- [4] D.N. Spergel, *et al.*, *Astrophys. J. Suppl.* **148**, 175 (2003). <https://doi.org/10.1086/377226>
- [5] S.M. Carroll, *et al.*, *Living. Rev. Relativ.* **4**, 1 (2001). <https://doi.org/10.12942/lrr-2001-1>
- [6] T. Padmanabhan, *Phys. Rep.* **380**, 235 (2003). [https://doi.org/10.1016/S0370-1573\(03\)00120-0](https://doi.org/10.1016/S0370-1573(03)00120-0)
- [7] C.H. Brans, and R.H. Dicke, *Phys. Rev.* **124**, 925 (1961). <https://doi.org/10.1103/PhysRev.124.925>
- [8] C.M. Will, *Theory and Experiment in Gravitational Physics*, (Cambridge University, Cambridge, (1981).
- [9] C. Mathiazhagan and V.B. Johri, *Class. Quantum Grav.* **1**, L29 (1984). <https://doi.org/10.1088/0264-9381/1/2/005>
- [10] D. La, and P.J. Steinhardt, *Phys. Rev. Lett.* **62**, 376 (1989). <https://doi.org/10.1103/PhysRevLett.62.376>
- [11] N. Banerjee and D. Pavon, *Class. Quant. Grav.*, **18**, 593 (2001).
- [12] S. Sen and A.A. Sen, *Phys. Rev. D*, **63**, 124006 (2001).
- [13] D.F. Mota and J.D. Barrow, *Mon. Not. R. Astron. Soc.* **349**, 291 (2004).
- [14] D.F. Mota and J.D. Barrow, *Phys. Lett. B*, **581**, 141 (2004).
- [15] S. Das and N. Banerjee, *Phys. Rev. D*, **78**, 043512 (2008).
- [16] N. Banerjee and D. Pavon, *Phys. Rev. D*, **63**, 043504 (2001). <https://doi.org/10.1103/PhysRevD.63.043504>
- [17] K. Nordvedt (Jr), *Astrophys. J.* **161**, 1059 (1970). <https://doi.org/10.1086/150607>
- [18] J.P. Mimoso and A.M. Nunes, *Phys. Lett A*, **248**, 325 (1998). [https://doi.org/10.1016/S0375-9601\(98\)00724-5](https://doi.org/10.1016/S0375-9601(98)00724-5)
- [19] M.V. Santhi, *et al.*, *Canadian Journal of Physics*, **95**(2), 179 (2017). <https://doi.org/10.1139/cjp-2016-0628>
- [20] E.A. Hegazy, and F. Rahaman, *Indian Journal of Physics*, **94**(11), 1847 (2020). <https://doi.org/10.1007/s12648-019-01614-4>
- [21] Y. Aditya, *et al.*, *Indian Journal of Physics*, **95**, 383 (2021). <https://doi.org/10.1007/s12648-020-01722-6>
- [22] D. Chhajed, *et al.*, *Journal of Ultra Scientist of Physical Sciences-Section A. (Mathematics)*, **34**(4), (2022). <http://dx.doi.org/10.22147/jusps-B/340401>
- [23] S.K. Tripathy, *et al.*, *Physics of the Dark Universe* **30**, 100722 (2020). <https://doi.org/10.1016/j.dark.2020.100722>
- [24] S.K. Tripathy, *et al.*, *The European Physical Journal C*, **75**, 149 (2015). <https://doi.org/10.1140/epjc/s10052-015-3371-3>
- [25] C.B. Collins, *et al.*, *Gen. Relativ. Gravit.* **12**, 805, (1980). <https://doi.org/10.1007/BF00763057>
- [26] S. Capozziello, *et al.*, *Phys. Rev. D*, **73**, 043512 (2006), <https://doi.org/10.1103/PhysRevD.73.043512>
- [27] E. Babichev, *et al.*, *Clas. Quant. Grav.* **22**, 143 (2005). <https://doi.org/10.1088/0264-9381/22/1/010>
- [28] S.K. Tripathy, *et al.*, *Physics of the Dark Universe*, **30**, 100722 (2020). <https://doi.org/10.1016/j.dark.2020.100722>
- [29] R.R. Caldwell, *Phys. Lett. B*, **545**, 23 (2002). [https://doi.org/10.1016/S0370-2693\(02\)02589-3](https://doi.org/10.1016/S0370-2693(02)02589-3)
- [30] E.V. Linder, *Phys. Rev. Lett.* **90**, 091301 (2003). <https://doi.org/10.1103/PhysRevLett.90.091301>
- [31] B. Mishra and S.K. Tripathy, *Mod. Phys. Lett. A*, **30**, 1550175 (2015). <https://doi.org/10.1142/S0217732315501758>
- [32] B. Mishra, *et al.*, *Mod. Phys. Lett. A*, **33**, 1850052 (2018). <https://doi.org/10.1142/S0217732318500529>
- [33] B. Mishra, *et al.*, *Astrophys. Space Sci.* **363**, 86 (2018). <https://doi.org/10.1007/s10509-018-3313-2>

- [34] P.P. Ray, *et al.*, Int. J. Mod. Phys. D, **28**, 1950093 (2019). <https://doi.org/10.1142/S0218271819500937>
- [35] B. Mishra, *et al.*, Mod. Phys. Lett. A, **34**, 1950217 (2019). <https://doi.org/10.1142/S0217732319502171>
- [36] B. Mishra, *et al.*, Journal of Astrophysics and Astronomy, **42**, 2 (2021). <https://doi.org/10.1007/s12036-020-09655-6>
- [37] N.G. Busca, Astron. Astrophys. **552**, A96 (2013). <https://doi.org/10.1051/0004-6361/201220724>
- [38] S. Capozziello, *et al.*, (2014). <https://doi.org/10.48550/arXiv.1403.1421>
- [39] A.G. Reiss, *et al.*, Astrophys. J. **659**, 98 (2007). <https://doi.org/10.1086/510378>
- [40] J. Lu, *et al.*, Phys. Lett. B, **699**, 246 (2011). <https://doi.org/10.1016/j.physletb.2011.04.022>
- [41] M. Moresco, *et al.*, (2016). <https://doi.org/10.48550/arXiv.1601.01701>

ДОСЛІДЖЕННЯ КОСМОЛОГІЧНИХ МОДЕЛЕЙ АНІЗОТРОПНОЇ ТЕМНОЇ ЕНЕРГІЇ В УЗАГАЛЬНЕНІЙ ТЕОРІЇ БРАНСА-ДІКЕ

М. Віджая Санті, К. СантошРупа

Факультет прикладної математики, Університет Андхра, Вісакхапатнам 530003, Індія

У цій статті ми досліджували космологічну модель темної енергії в просторі-часі Б'янчі- $V I_0$, розглядаючи узагальнену теорію Бранса-Дікке, потенціал самовзаємодії та параметр динамічного зв'язку. Для цієї мети ми використали гібридний масштабний коефіцієнт для наближення динамічної поведінки параметра уповільнення. Параметр уповільнення повинен демонструвати характерну поведінку перевертання при перехідному червоному зсуві, оскільки вважається, що Всесвіт змінився з раннього уповільнення на пізні часове прискорення. Ми вивчили шість альтернативних моделей переходу темної енергії на основі спостережних обмежень на червоне зміщення переходу. Для кожної моделі досліджено поведінку динамічного скалярного поля, параметра Бранса-Дікке та потенціалу самовзаємодії. Крім того, ми використали узагальнену теорію Бранса-Дікке, щоб оцінити, як ньютонівська гравітаційна стала змінюється з часом.

Ключові слова: метрика типу Б'янчі- $V I_0$; узагальнена теорія Бранса-Дікке; гібридний масштабний коефіцієнт; параметр асиметрії; уніфікована темна рідина

SPECTRAL AND TIMING STUDY OF V404 CYGNI WITH *CHANDRA* OBSERVATIONS

✉ S. Rita Devi^{a*}, ✉ A. Seniorita Devi^b, ✉ Atri Deshamukhya^a

^aAssam University, Silchar, Assam, India

^bManipur University, Canchipur, Manipur, India

*Corresponding Author e-mail: sinamrita26@gmail.com

Received May 29, 2024; revised July 12, 2024; accepted August 15, 2024

We present the spectral and timing study of V404 Cygni from all its available Chandra observations and which recently come up in public domain of Chandra data archive. The data reduction and analysis were done using CIAO 4.14 and HEASOFT 6.30.1. The spectral analysis was done using spectral fitting package XSPEC version 12.12.1, available in the Heasoft package. The spectra of the source is fitted in the energy range 0.3–8.0 keV using two empirical spectral models - the absorbed power law and an absorbed disk-blackbody. The X-ray binary source V404 Cygni is found to be in the quiescent state having the X-ray luminosity in the range with few times 10^{32} erg s⁻¹. The source is found to be in the hard state and is well explained by power-law model with a powerlaw photon index $\Gamma \sim 2$ with n_H in the range $\sim (0.7-1.2) \times 10^{22}$ cm⁻². From timing analysis, Src-1 (V404 Cygni), in all the time bins- 0.5, 1 and 2 ks, the probability for the count rate to be constant is 0.17×10^{-33} in all the observations in the year 2021 and 2023 (ObsID 23421, ObsID 23422, ObsID 23423 & ObsID 28927). However, in the year 2017 observation it is found to be less variable. This clearly shows the presence of short-term variability in kilo-seconds time-scales with the currently available Chandra data. So, it is indicative that the binary source V404 Cygni is more likely to be variable source both in long-term (years) as well as short-term (kiloseconds) scales.

Keywords: Accretion, Accretion disks; X-rays; Binaries-stars:individual(V404 Cygni); Black holes

PACS: 97.10.Gz, 95.85.Nv, 97.80.-d : 97.80.Jp, 97.60.Lf

1. INTRODUCTION

Among the sky's brightest X-ray sources were X-ray binaries. X-ray binaries (XRBs) are the galaxy's principal X-ray sources. They include neutron star (NSXB) and black hole (BHXB) X-ray binaries, where wind-fed or Roche lobe overflow is responsible for the mass transfer from the companion to the compact star. Black hole X-ray binary (BHXB) is an interacting binary system consisting of a stellar-mass black hole accreting material from a companion star. Black hole X-ray binaries (BHXBs) are usually transient systems that undergo extended periods of (X-ray) quiescence interspersed with comparatively brief outbursts. The abrupt increase in the rate of accretion onto the compact object is what causes the outburst. Most likely, a disk instability is the reason for this increase. The quiescence phase and the outbursting phase are the two stages of a transient black hole candidate's (BHC) life cycle. They spend the most of their life in the quiescence phase, accreting small amounts of matter at low X-ray luminosities. The X-ray luminosity (L_x) during outburst, have been observed within a range of 10^{34-39} erg s⁻¹ at very high luminosities in the 0.5–10 keV band. The X-ray luminosity (L_x) during quiescence is mentioned to be ranging from $L_x \sim 10^{30-33}$ erg s⁻¹ [1]. The disc instability concept provides a comprehensive explanation for the quiescence to outburst cycle [2],[3]. According to the disc instability concept, which describes how accreting matter accumulates in the accretion disc during quiescence and is abruptly transported to the compact object during outburst. However, there is still debate over where the emission of X-rays from LMXBs during quiescence originates.

Black hole binaries (BHBs) show different X-ray spectral states as they accrete gas during transient outburst episodes [4]. The two primary spectral states are the hard state and the soft state, traditionally known as the low-hard state (LHS) and the high-soft state (HSS), respectively [5]. X-ray binaries within the Milky Way have been extensively studied and are an important benchmark in studying ULXs [6]. Furthermore, X-ray binaries are very helpful in comprehending the nature of compact objects and the physical mechanism of accretion. Also timing study of X-ray binaries will comprehend the nature of compact objects even the presence of temporal variability across a range of timescales will enhance the physical mechanism of accretion. The X-ray light curves of blackhole binaries can be variable over a broad timescale, ranging from milliseconds to years [7],[8].

One of the most researched black hole X-ray binary systems is V404 Cygni. V404 Cygni, a binary system comprising a black hole and a companion star, has been a subject of astronomical interest due to its notable outbursts in both optical and X-ray wavelengths. V404 Cyg, also referred to as GS 2023+338, was discovered on May 22, 1989, by the all-sky monitor aboard the Ginga satellite [9]. It is the most luminous of the quiescent black hole low-mass X-ray binaries (BH LMXBs), with an X-ray luminosity of about 7×10^{32} erg s⁻¹ at a distance of 2.39 kpc [10]. In 1938, it was initially recognized as an optical nova. In 1956, there was another recorded nova outburst observed within this particular system [11]. Comparing

V404 Cyg's X-ray outburst behavior to the other BH transients, it is extremely unusual. In 1989, V404 Cygni experienced another outburst [12]. After remaining in a quiescent state for approximately 26 years, V404 Cygni underwent a brief yet intense outburst on June 15, 2015 [13],[14],[15] and again another short-lived burst of activity was observed in December 2015 [16],[17]. V404 Cygni harbors a black hole with a mass of $9.0^{+0.6}_{-0.2} M_{\odot}$ and a binary inclination of $67^{+3}_{-1}^{\circ}$ [18]. We adopt the distance of V404 Cygni is 2.39 kpc [10].

In this paper, we present the spectral and timing study of V404 Cygni from all its available *Chandra* observations and which recently come up in public domain of Chandra data archive. The observation and data analysis are described in Section 2. Results and discussion are presented in Section 3. Section 4 represents the timing analysis of X-ray binary source V404 Cygni and summarized in Section 5.

2. OBSERVATION AND DATA ANALYSIS

In the present work, we have carried out spectral and timing analysis of V404 Cygni as detected by *Chandra* ACIS-S detector. V404 Cygni has been observed by *Chandra* ACIS-S detector five times - first in the year 2017 (ObsID 19000) and three times in the year 2021 (ObsID 23421, ObsID 23422 and ObsID 23423) and then in the year 2023 (ObsID 28927). The detail Chandra observational log of V404 Cygni is given in Table 1.

Table 1. Chandra ACIS-S Observation log for V404 Cygni

Source	Distance (Kpc)	ObsID*	Exposure (ks)	Observation Year	References for distance
V404 Cygni	2.39	19000	49.00	2017-08-11	Miller-Jones et al. 2009
		23421	22.00	2021-01-23	
		23422	22.00	2021-02-06	
		23423	22.00	2021-02-21	
		28927	15.00	2023-10-14	

*ObsID - *Chandra* Observation ID

The data reduction and analysis were done using CIAO 4.14 and HEASOFT 6.30.1. X-ray point source was extracted from the level 2 event lists by using the CIAO source detection tool *Wavdetect*. Using a combination of CIAO tools and calibration data, the source (and background) spectrum were extracted. Spectra were grouped and rebinned so that each bin had a minimum of 30 counts. As adopted by Devi et al.2007 [19], a conservative threshold of the count rate ≥ 0.05 counts s^{-1} is considered as pileup affected, however in our present study it is found that all the sources are not pileup affected as the count rates were all ≤ 0.04 counts s^{-1} .

The spectral analysis was done using spectral fitting package XSPEC version 12.12.1, available in the Heasoft package. The spectra of the two sources are fitted in the energy range 0.3 -8.0 keV using two empirical spectral models - the absorbed power law and an absorbed disk-blackbody. XSPEC model *-phabs* was used to take into account the absorption in the spectrum. A measure of the goodness of fit is determined by $\chi^2/(\text{degrees of freedom}(\text{dof}))$, which should be approximately one. Taking care of the possibility of many local minima in the discerning statistic space while fitting low-count data with a two parameter (plus normalization) model, we compute the χ^2 statistics for a range of parameter values (using the XSPEC command *steppar*) and find the global minimum instead of fitting the data using the XSPEC minimization routine. Finally, from the model parameters obtained from the spectral fitting, the corresponding luminosity of the point sources are estimated.

For the disk blackbody model, the bolometric luminosity is defined as $L_{bol} = 4\pi R_{in}^2 \sigma T_{in}^4$, where R_{in} , the inner disk radius from where the X-rays are emitted, is given by $R_{in} = (\sqrt{\text{Normalisation}} \times \text{Distance}_{10kpc}) / \sqrt{\cos \theta}$ km; θ is the viewing angle, T_{in} is the inner disk temperature & σ is the Stefan Boltzmann constant. However, for the powerlaw model, considering *Chandra*'s energy sensitivity range, only the luminosity in the 0.3-8.0 keV range is estimated for the present work.

3. RESULTS AND DISCUSSION

The details of the V404 cygni source is tabulated in Table 2. Spectral properties of the source V404 Cygni is given in Table 3. The observed normalized net count distribution of V404 Cygni source fitted with powerlaw model and disk

blackbody model is shown in Figure 1 and Figure 2 respectively. The detail study and findings of V404 Cygni is discussed below.

Table 2. Details of the V404 Cygni X-ray source

Source name	R.A.*	Decl.**	ObsId	Net count rate
Src-1	+20:24:03.82	+33:52:01.90	19000	0.015
			23421	0.018
			23422	0.020
			23423	0.016
			28927	0.042

*R.A - in (hours, minutes and seconds); **Decl. in (degrees, arcminutes and arcseconds)

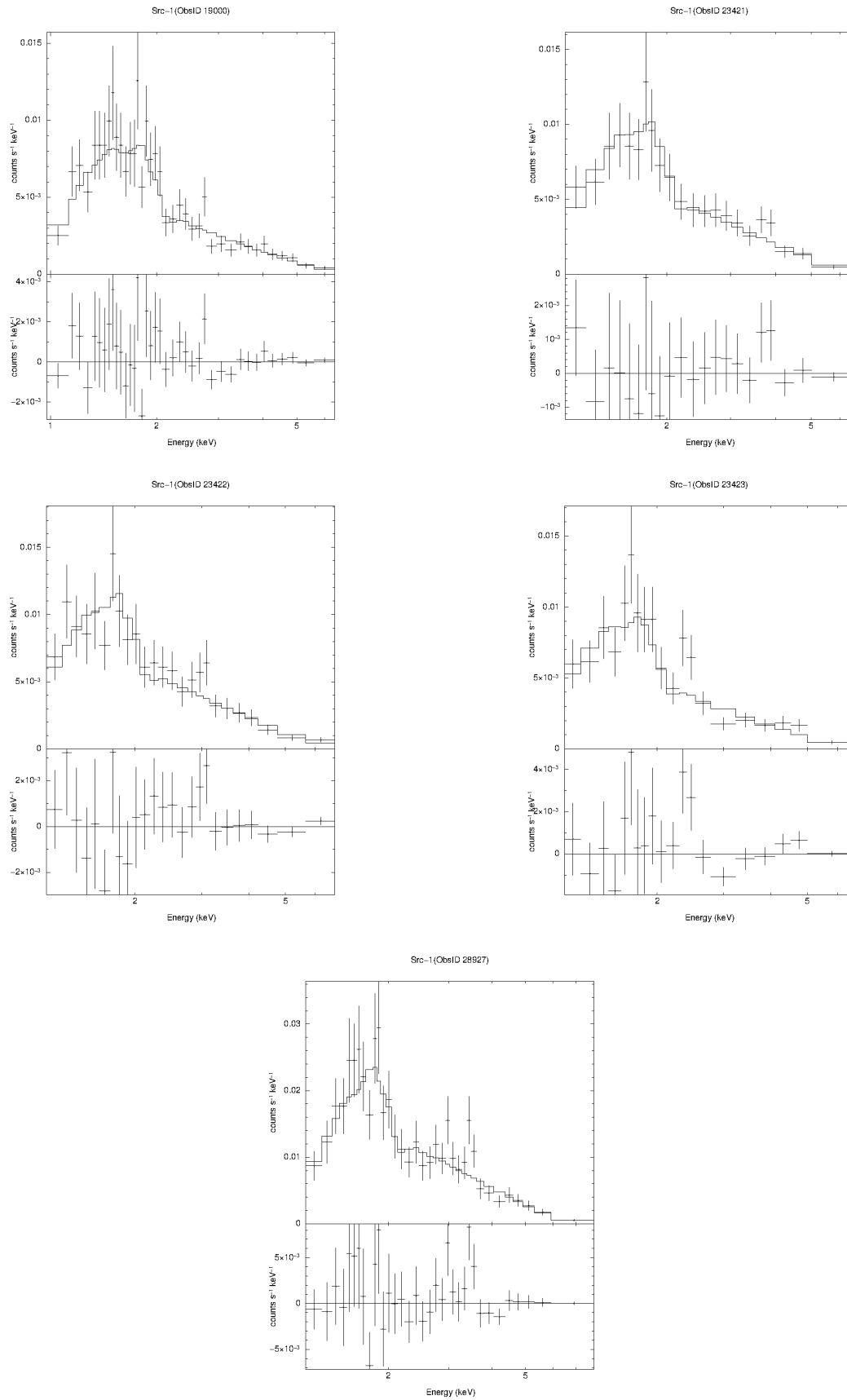
Table 3. Spectral properties of the V404 Cygni X-ray source

Source	Obs Id.	Powerlaw				Disk-blackbody			
		n_H (10^{22}cm^{-2})	Γ	$\log(L_x)$ (ergs s^{-1})	χ^2/dof	n_H (10^{22}cm^{-2})	KT_{in} keV	$\log(L_x)$ (ergs s^{-1})	χ^2/dof
(1)	(2)	(3)	(4)	(5)	(6)	(7)	(8)	(9)	(10)
Src-1	19000	$0.94^{+0.24}_{-0.27}$	$2.19^{+0.32}_{-0.22}$	$32.55^{+0.15}_{-0.10}$	30.66/36	$0.38^{+0.17}_{-0.17}$	$1.40^{+0.22}_{-0.16}$	$32.57^{+0.02}_{-0.02}$	39.08/36
	23421	$0.75^{+0.49}_{-0.41}$	$2.12^{+0.44}_{-0.39}$	$32.43^{+0.23}_{-0.14}$	8.87/21	$0.21^{+0.30}_{-0.19}$	$1.46^{+0.38}_{-0.25}$	$32.48^{+0.04}_{-0.04}$	6.69/21
	23422	$0.96^{+0.39}_{-0.42}$	$2.19^{+0.32}_{-0.33}$	$32.69^{+0.18}_{-0.14}$	17.52/22	$0.27^{+0.33}_{-0.25}$	$1.51^{+0.43}_{-0.28}$	$32.71^{+0.04}_{-0.04}$	18.25/22
	23423	$1.01^{+0.41}_{-0.50}$	$2.41^{+0.43}_{-0.44}$	$32.67^{+0.26}_{-0.21}$	22.89/17	$0.21^{+0.37}_{-0.18}$	$1.39^{+0.37}_{-0.26}$	$32.58^{+0.05}_{-0.04}$	26.70/17
	28927	$1.29^{+0.33}_{-0.37}$	$2.29^{+0.33}_{-0.22}$	$32.98^{+0.18}_{-0.12}$	31.05/32	$0.51^{+0.26}_{-0.28}$	$1.47^{+0.27}_{-0.17}$	$32.95^{+0.03}_{-0.03}$	33.0/32

Columns: (1): Source (2): Observation ID. (3): n_H , equivalent hydrogen column density. (4): Γ , the powerlaw photon index. (5): (L_x) , X-ray luminosity in the 0.3 -8.0 keV energy range, (6): $\chi^2/\text{Degrees of freedom}$. (7): n_H , equivalent hydrogen column density. (8): KT_{in} , the inner disk temperature. (9): (L_x) , bolometric X-ray luminosity. (10): $\chi^2/\text{Degrees of freedom}$.

In the present study, the binary source, Src-1 (V404 Cygni) is found to be in the quiescent state having the X-ray luminosity in the range with few times $10^{32} \text{ erg s}^{-1}$ in all the observations. In all the observations, the binary source V404 Cygni is found to be spectrally hard with powerlaw photon index, $\Gamma \sim 2$ as explained by the powerlaw model and an inner disk temperature, $kT_{in} \sim 1 \text{ keV}$ as explained by the disk blackbody model. The source is well explained by power-law model with a powerlaw photon index $\Gamma \sim 2$ with n_H in the range $\sim (0.7 - 1.2) \times 10^{22} \text{ cm}^{-2}$. In the year 20017 observation having ObsID 19000, the binary source Src-1 (V404 Cygni) is found to be having the X-ray luminosity with $\sim 3.54 \times 10^{32} \text{ erg s}^{-1}$ fitted with powerlaw model. But in the year 2021 observations, the source is found to be $\sim 2.69 \times 10^{32} \text{ erg s}^{-1}$ in one observation having ObsID 23421, however, in two observations having ObsID 23422 and ObsID 23423, it is found to be $\sim 4 \times 10^{32} \text{ erg s}^{-1}$. The source luminosity is found to be a slight increase to $\sim 9 \times 10^{32} \text{ erg s}^{-1}$ in the latest observation of 2023 having ObsID 28927. This clearly shows the presence of long-term variability (years) with the currently available Chandra data.

This result is in agreement with many other earlier works. Wagner et al.(1994)[20] estimated the luminosity of the source to be $8 \times 10^{33} \text{ erg s}^{-1}$ at a distance 3.5 kpc by Rosat observational data. Also, Narayan et al. 1997 [21], Kong et al. 2002 [22] and Bradley et al. 2007 [23] found this source to have a luminosity of $\sim 1.0 \times 10^{33} \text{ erg s}^{-1}$ and its spectrum is well fitted by a simple power-law model with photon index $\Gamma \sim 2$ with n_H in the range $\sim (0.7 - 2.3) \times 10^{22} \text{ cm}^{-2}$. The quiescent X-ray spectrum has a power-law photon index $\Gamma \sim 2$ seen through a total column density of $n_H = (1.0 \pm 0.1) \times 10^{22} \text{ cm}^{-2}$ [24]. However, in latter observations the source seems to get dimmer such as- luminosity approaches several times $10^{32} \text{ erg s}^{-1}$ [25]. Rana et al. 2016 [26] reported the quiescent luminosity of this source is $8.9 \times 10^{32} \text{ erg s}^{-1}$ for a distance of 2.4 kpc at energies (0.3-30keV) using NuStar observation. This later observations seem to agree well with the present finding of X-ray luminosity around $10^{32} \text{ erg s}^{-1}$ in the 0.3-8.0 keV by using the latest Chandra observational data of the year 2017, 2021 & 2023.

**Figure 1.** Powerlaw Spectra of the V404 Cygni X-ray Binary Source

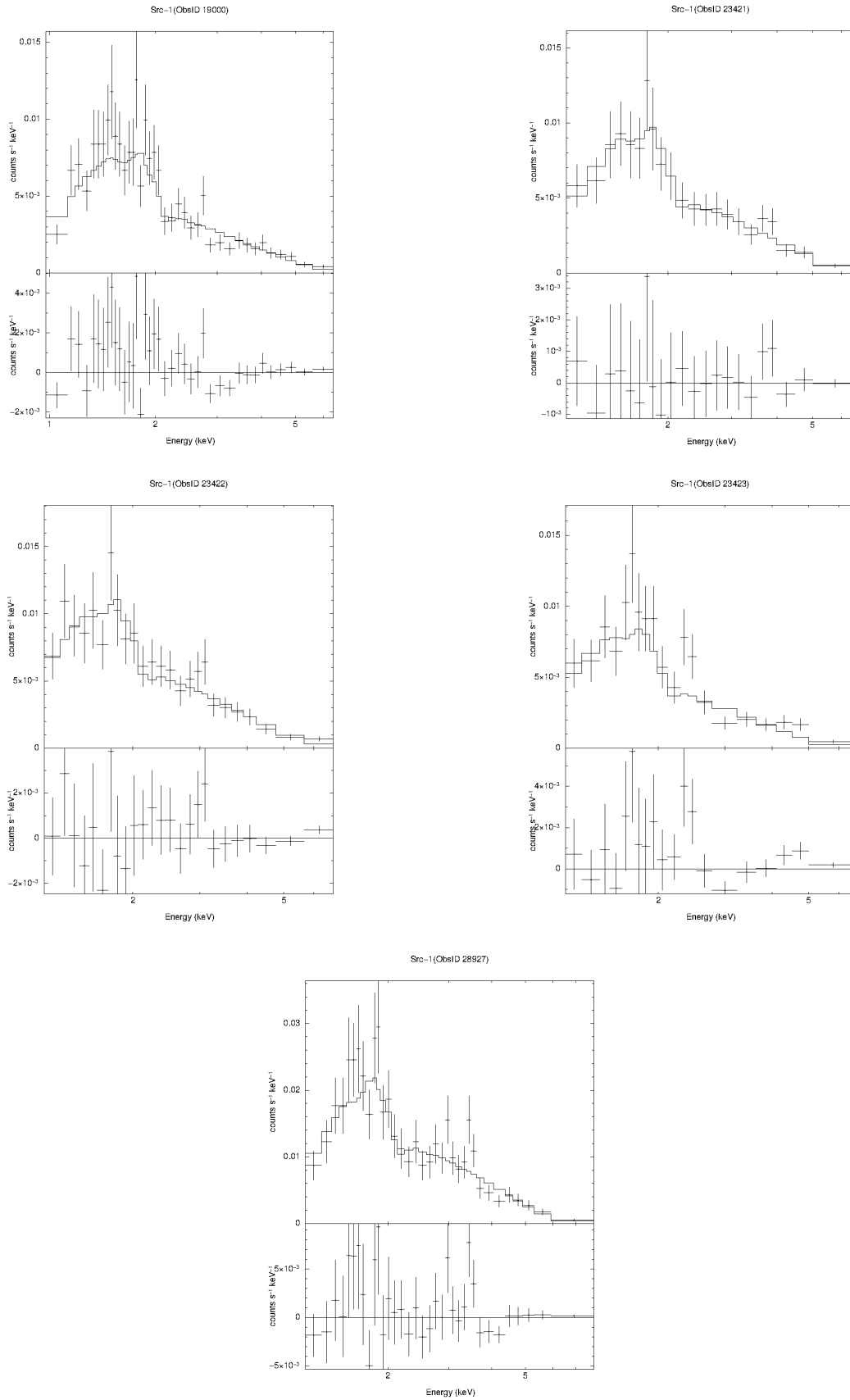


Figure 2. Disk blackbody Spectra of the V404 Cygni X-ray Binary Source

4. TEMPORAL PROPERTY OF THE BINARY SOURCE V404 CYGNI

To check the presence of any short-term/kiloseconds variability for V404 Cygni X-ray binary source detected in the present study, temporal analysis was carried out. The lightcurve of V404 Cygni binned over 0.5, 1, 2 ks for the *Chandra* observations is shown in Figure 3.

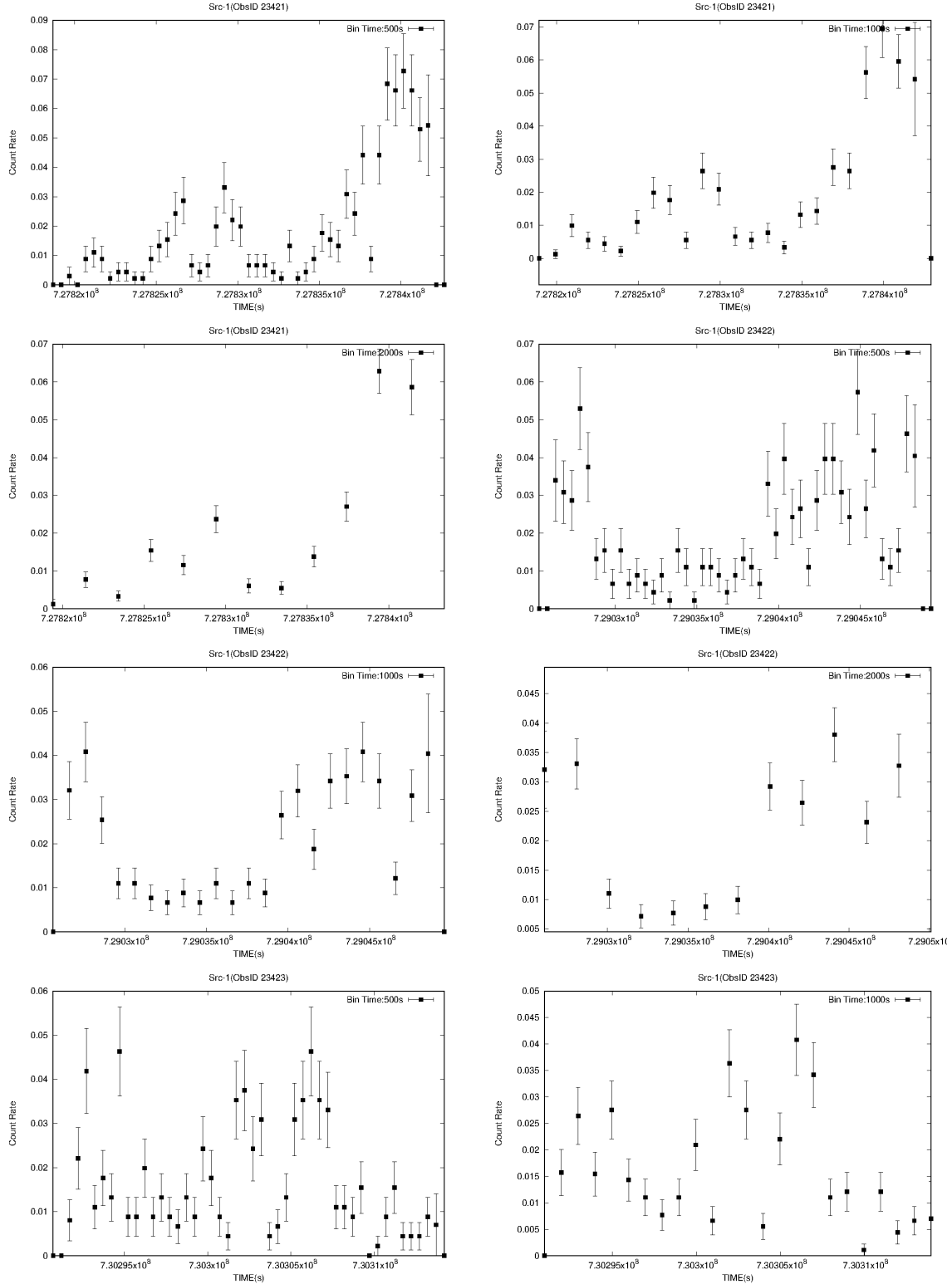
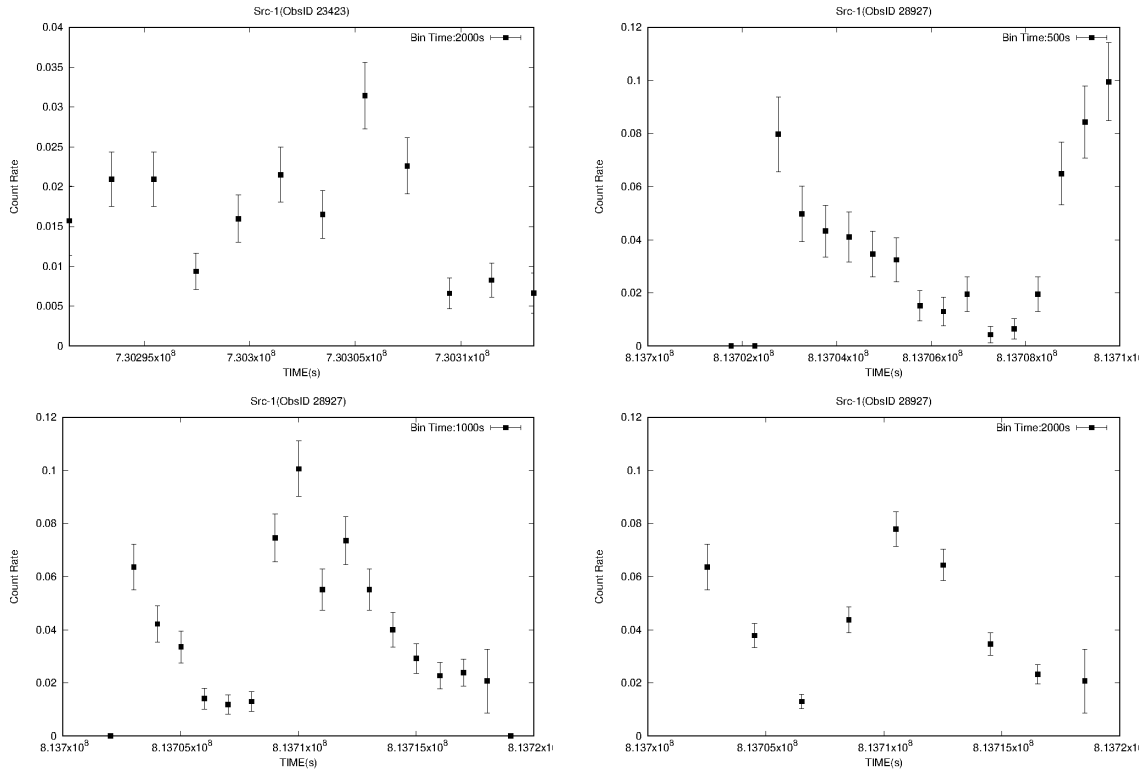


Figure 3. Lightcurve of V404 Cygni in its observations - ObsID 23421, ObsID 23422, ObsID 23423 and ObsId 28927, in different time bins (500 s, 1000 s, 2000 s)

Figure 3 continued



In our analysis, Src-1 (V404 Cyg), in all the time bins- 0.5, 1 and 2 ks, the probability for the count rate to be constant is 0.17×10^{-33} in all the observations in the year 2021 and 2023 (ObsID 23421, ObsID 23422, ObsID 23423 & ObsID 28927). However, in the year 2017 observation it is found to be less variable. Previous studies have found significant variations in the quiescent X-ray flux of V404 Cyg over a few-year timescale. It is evident from the light curve that the source's flaring activity causes significant variability. Over the course of the XMM-Newton observation, the count rate varies by a factor of 4-5 over a few-hour timescale. Hence, V404 Cyg exhibits distinct variability in the form of several flares on short timescales (one to two hours) in the radio, soft X-ray, and hard X-ray bands [26]. This clearly shows the presence of short-term variability in kilo-seconds time-scales with the currently available Chandra data. So, it is indicative that the binary source V404 Cygni is more likely to be variable source both in long-term (years) as well as short-term (kiloseconds) scales.

However, due to limited timing capabilities of many sensitive X-ray instruments aboard X-ray satellites, the transient nature of BH binaries of many variable sources have eluded detections. So, a more detail future work with high quality data from other missions may enable us to ascertain the real physical nature of this binary in more details.

5. CONCLUSION

We present the results of spectral and timing analysis of V404Cygni X-ray binary which has been observed by *Chandra* and which recently come up in the public domain of Chandra archive. The spectra of the binary source V404 Cygni was fitted with two empirical models - the absorbed power law and an absorbed disk black-body. The binary source V404 Cygni, was observed in three *Chandra* observational epochs. In all the epochs, the binary source, Src-1 (V404 Cygni) is found to be in the quiescent state having the X-ray luminosity in the range with few times 10^{32} erg s^{-1} . In all the observations, the binary source V404 Cygni is found to be spectrally hard with powerlaw photon index, $\Gamma \sim 2$ as explained by the powerlaw model and an inner disk temperature, $kT_{in} \sim 1$ keV as explained by the disk blackbody model. The source is well explained by power-law model with a powerlaw photon index $\Gamma \sim 2$ with n_H in the range $\sim (0.7 - 1.2) \times 10^{22}$ cm^{-2} . In the year 20017 observation having ObsID 19000, the binary source Src-1 (V404 Cygni) is found to be having the X-ray luminosity with $\sim 3.54 \times 10^{32}$ erg s^{-1} fitted with powerlaw model. But in the year 2021 observations, the source is found to be $\sim 2.69 \times 10^{32}$ erg s^{-1} in one observation having ObsID 23421, however, in two observations having ObsID 23422 and ObsID 23423, it is found to be $\sim 4 \times 10^{32}$ erg s^{-1} . The source luminosity is found to be a slight increase to $\sim 9 \times 10^{32}$ erg s^{-1} in the latest observation of 2023 having ObsID 28927. Timing analysis of Src-1 (V404 Cyg), in all the time bins- 0.5, 1 and 2 ks, the probability for the count rate to be constant is 0.17×10^{-33} in all the observations in the year 2021 and 2023 (ObsID 23421, ObsID 23422, ObsID 23423 & ObsID 28927). However, in the year 2017 observation

it is found to be less variable. This clearly shows the presence of short-term variability in kilo-seconds time-scales with the currently available Chandra data. So, it is indicative that the binary source V404 Cygni is more likely to be variable source both in long-term (years) as well as short-term (kiloseconds) scales. However, due to limited timing capabilities of many sensitive X-ray instruments aboard X-ray satellites, the transient nature of BH binaries of many variable sources have eluded detections. So, a more detail future work with high quality data from other missions may enable us to ascertain the real physical nature of this binary in more details.

Acknowledgment

The authors would like to thank Chandra X-ray Center (CXC) archive for its resources of data that are used in the present work.

ORCID

 S. Rita Devi, <https://orcid.org/0000-0002-0663-1538>;  A. Seniorita Devi, <https://orcid.org/0000-0001-9971-4262>;  Atri Deshamukhya, <https://orcid.org/0000-0003-4350-6645>

REFERENCES

- [1] J.E. McClintock, and R.A. Remillard, *Compact Stellar X-ray Sources*, edited by W.H.G. Lewin, and M. van der Klis, (Cambridge University Press, 2006).
- [2] J.K. Cannizzo, *Astrophysical Journal*, **419**, 318 (1993).
- [3] J.P. Lasota, *New Astron Review*, **45**, 449 (2001). [https://doi.org/10.1016/S1387-6473\(01\)00112-9](https://doi.org/10.1016/S1387-6473(01)00112-9)
- [4] T.M. Belloni, and S.E. Motta, in: *Astrophysics of Black Holes: From Fundamental Aspects to Latest Developments*, edited by C. Bambi, *Astrophys. Space Sci. Libr.* **440**, (Springer, Berlin, Heidelberg, 2016). pp. 61-67. https://doi.org/10.1007/978-3-662-52859-4_2
- [5] H. Tananbaum, H. Gursky, E. Kellogg, R. Giacconi, and C. Jones, *ApJ*, **177**, L5 (1972). <https://doi.org/10.1086/181042>
- [6] R.A. Remillard, and J.E. McClintock, *Ann. Rev. A & A*, **44**, 49 (2006). <https://doi.org/10.1146/annurev.astro.44.051905.092532>
- [7] T.M. Belloni, and L. Stella, *Space Science Review*, **183**, 43 (2014). <https://doi.org/10.1007/s11214-014-0076-0>
- [8] A.R. Ingram, and S.E. Motta, *New Astron. Rev.* **85**, 101524 (2019). <https://doi.org/10.1016/j.newar.2020.101524>
- [9] F. Makino, *IAUC*, 4782, 1 (1989).
- [10] J.C.A. Miller-Jones, P.G. Jonker, V. Dhawan, W. Briskin, M.P. Rupen, G. Nelemans, and E. Gallo, *ApJ*, **706**, L230 (2009). <https://doi.org/10.1088/0004-637X/706/2/L230>
- [11] A. Jana, J.-R. Shang, D. Debnath, S.K. Chakrabarti, D. Chatterjee, and H.-K. Chang, *Galaxies*, **9**, 39 (2021). <https://doi.org/10.3390/galaxies9020039>
- [12] Y. Tanaka, in: *Proc. 23rd ESLAB Symp. On Two-Topics in X-ray Astronomy, ESA SP-296*, **1**, edited by J. Hunt, and B. Battrick, (ESA, Paris, 1989).
- [13] J. Rodriguez, M.Cadolle Bel, J. Alfonso-Garzón, *et al.*, *A & A*, **581**, L9 (2015). <https://doi.org/10.1051/0004-6361/201527043>
- [14] J.P. Roques, E. Jourdain, A. Bazzano, *et al.*, *ApJ*, **813**, L22 (2015). <https://doi.org/10.1088/2041-8205/813/1/L22>
- [15] P.A. Jenke, C.A. Wilson-Hodge, H. Jeroen, *et al.*, *ApJ*, **826** 37 (2016). <https://doi.org/10.3847/0004-637X/826/1/37>
- [16] T. Munoz-Darias, J. Casares, M.D. Sánchez, *et al.*, *MNRAS: Letters*, **465**, L124 (2017). <https://doi.org/10.1093/mnrasl/slw222>
- [17] J.J.E. Kajava, S.E. Motta, *et al.*, *A & A*, **616**, A129 (2018). <https://doi.org/10.1051/0004-6361/201731768>
- [18] J. Khargharia, C.S. Froning, and E.L. Robinson, *ApJ*, **716**, 1105 (2010). <https://doi.org/10.1088/0004-637X/716/2/1105>
- [19] A.S. Devi, R. Misra, V.K. Agrawal, and K.Y. Singh, *ApJ*, **664**, 458 (2007). <https://doi.org/10.1086/518533>
- [20] R.M. Wagner, S.G. Starrfield, R.M. Hjellming, S.B. Howell, and T.J. Kreidl, *ApJL*, **429**, L25 (1994). <https://doi.org/10.1086/187404>
- [21] R. Narayan, D. Barret, and J.E. McClintock, *ApJ*, **482**, 448 (1997). <https://doi.org/10.1086/304134>
- [22] A.K.H. Kong, J.E. McClintock, M.R. Garcia, S.S. Murray, and D. Barret, *ApJ*, **570**, 277 (2002). <https://doi.org/10.1086/339501>
- [23] C.K. Bradley, R.I. Hynes, A.K.H. Kong, *et al.*, *ApJ*, **667**, 427 (2007). <https://doi.org/10.1086/520323>
- [24] M.T. Reynolds, R.C. Reis, J.M. Miller, E.M. Cackett, and N. Degenaar, *MNRAS*, **441**, 3656 (2014). <https://doi.org/10.1093/mnras/stu832>
- [25] J. Martí, P.L. Luque-Escamilla, and M.T. García-Hernández, *A & A*, **586**, A58 (2016). <https://doi.org/10.1051/0004-6361/201527239>
- [26] V. Rana, A. Loh, S. Corbel, *et al.*, *ApJ*, **821**, 103 (2016). <https://doi.org/10.3847/0004-637X/821/2/103>

СПЕКТРАЛЬНІ ТА ЧАСОВІ ДОСЛІДЖЕННЯ V404 Cygni ЗА ДОПОМОГОЮ CHANDRA
СПОСТЕРЕЖЕНЬС. Ріта Деві^a, А. Сеньорита Деві^b, Атрі Дешамукх'я^a^a Ассамський університет, Сілчар, Ассам, Індія^b Маніпурський університет, Канчіпур, Маніпур, Індія

Ми представляємо спектральне та часове дослідження V404 Cygni з усіх доступних спостережень Chandra, які нещодавно опубліковані в архіві даних Chandra. Обробку та аналіз даних проводили за допомогою CIAO 4.14 і HEASOFT 6.30.1. Спектральний аналіз проводився за допомогою пакета спектрального підбору XSPEC версії 12.12.1, доступного в пакеті Heasoft. Спектр джерела встановлюється в діапазоні енергій 0,3-8,0 кеВ з використанням двох емпіричних спектральних моделей - поглиненого степеневому закону та поглиненого диска-чорного тіла. Встановлено, що подвійне джерело рентгенівського випромінювання V404 Cygni знаходиться в стані спокою, його рентгенівська світність у кілька разів перевищує 10^{32} ерг с^{-1} . Виявлено, що джерело перебуває у жорсткому стані та добре пояснюється степеневою моделлю зі степеневим індексом фотона $\Gamma \sim 2$ з n_H у діапазоні $\sim (0,7 - 1,2) \times 10^{22} \text{ см}^{-2}$. Згідно з аналізом часу, Src-1 (V404 Cygni), у всіх інтервалах часу - 0,5, 1 і 2 кс, ймовірність того, що швидкість рахунку буде постійною, становить $0,17 \times 10^{-33}$ у всіх спостереженнях у 2021 та 2023 роках (ObsID 23421, ObsID 23422, ObsID 23423 & ObsID 28927). Однак у спостереженнях за 2017 рік він виявився менш мінливим. Це чітко демонструє наявність короткочасної мінливості в кілосекундних масштабах часу з доступними на даний момент даними Chandra. Отже, показово, що бінарне джерело V404 Cygni, швидше за все, буде змінним джерелом як у довгостроковому (роки), так і в короткостроковому (кілосекунди) масштабах.

Ключові слова: акреція, акреційні диски; рентгенівські промені; подвійні зірки: індивідуальні (V404 Cygni); чорні діри

ON THE STABILITY OF PLANETARY MOTIONS DURING STELLAR APPROACHES

A.G. Mammadli^{a*}, R.T. Mammadov^{a,b}, U.S. Valiyev^a

^a*Batabat Astrophysics Observatory, Ministry of Science and Education of the Republic of Azerbaijan, Nakhchivan, AZ-7000, Azerbaijan*

^b*Nakhchivan State University, Nakhchivan, AZ-7012, Azerbaijan*

*Corresponding Author e-mail: azad_mammadli@yahoo.com

Received June 26, 2024; revised July 13, 2024; accepted August 15, 2024

The problem of the spatial motion of a passively gravitating body during an to the central body of a perturbing body – a test star – is considered. Using the exact expression of the force function, an integral invariant relationship – a quasi-integral – was found. Due to the quasi-integral, the regions of possible motion of the passively gravitating body, the surfaces of minimal energy (a generalization of the zero velocity surfaces), and the singular points of these surfaces were determined. The stability of planetary motion according to Hill during the approach of a test star to the Solar System was investigated. Criteria for the possibility, as well as the impossibility of capturing the passively gravitating body by the test star, were established. According to the Hill stability criteria, critical values of the orbital parameters of the test star were established, at which the planets of the Solar System either become satellites of the test star or leave the bounds of the Solar System.

Keywords: *Celestial mechanics; Restricted three-body problem; Jacobi function analog; Quasi-integral; Law of energy conservation; Surfaces of minimal energy; Singular points; Hill stability*

PACS: 95.10.-a; 95.10.Ce; 96.10.+i

1. PROBLEM FORMULATION. AN ANALOGUE OF JACOBIAN FUNCTION

In the works of A.G. Mamedov [4, 5, 6], the evolution of planetary orbits during stellar approaches to the Solar System is explored within the framework of the planar averaged parabolic three-body problem. It has been shown that with a moderate approach of the perturbing body to the central body, the size and shape of the orbit of the perturbed body remain constant, with only its orientation changing. A test star of solar mass was used as the perturbing body, and the orbits of the planets during its approach to the Sun at a distance of 50 au were studied. The results are presented in the form of figures and tables.

In the work of Kholoshevnikov and Mishchuk [13], the restricted hyperbolic three-body problem was considered, and an assessment was made of the influence of a test star of solar mass on the orbits of the planets during its approach to the Sun from a distance of 100 au. to 1152 au. It has been shown that during a moderate approach of such a star to the Sun, the sizes of the planetary orbits do not undergo any changes. When the test star approaches the Sun to a distance of 100 au, the inclination, eccentricity, longitude of ascending node, and argument of pericenter change very little.

In this study, the motion of the passively gravitating body M is examined in a rotating and pulsating coordinate system [1,2] within the framework of the restricted three-body problem. The actively gravitating bodies are: the central body M_0 with mass m_0 , and the perturbing body M' with mass m' , where $m_0 \leq m'$. In this coordinate system, the origin coincides with the barycenter G_0 of the actively gravitating bodies, the G_0xy plane aligns with the plane of motion of these bodies, and the G_0x axis aligns with the line connecting bodies M_0 and M' . The true anomaly of the perturbing body v' is used as the independent variable. Consequently, the equations of motion for body M in this coordinate system take a simple form [1,2].

$$\frac{d^2x}{dv'^2} - 2\frac{dy}{dv'} = \frac{\partial\Omega}{\partial x}, \quad \frac{d^2y}{dv'^2} + 2\frac{dx}{dv'} = \frac{\partial\Omega}{\partial y}, \quad \frac{d^2z}{dv'^2} = \frac{\partial\Omega}{\partial z} \quad (1)$$

We will refer to equation system (1) as SHAPNER's equations - an acronym formed from the surnames Scheibner [9], Petr and Nechvil [10, 11 and Rein 12]. In equation system (1), the force function $\Omega = \Omega(v', x, y, z)$ is analogous to the Jacobi function in the circular problem and is defined by equality

$$\Omega = \rho' \left[\frac{1}{2}(x^2 + y^2 - e'z^2 \cos v') + p'^3 \left(\frac{\mu}{r_1} + \frac{1-\mu}{r_2} \right) \right]. \quad (2)$$

Here, the dimensionless quantity ρ' is defined below, e' and p' are the eccentricity and the focal parameter of the perturbing body M' orbit relative to the central M_0 , and $1-\mu$ and μ are the relative masses of the main bodies M' and M_0 :

$$1 - \mu = \frac{m'}{m_0 + m'}, \quad \mu = \frac{m_0}{m_0 + m'} \quad \left(\mu < \frac{1}{2} \right) \tag{3}$$

respectively. The distances of the passively gravitating body from the main bodies r_1 and r_2 are determined by equalities

$$r_1^2 = (x - p'\mu + p')^2 + y^2 + z^2, \quad r_2^2 = (x - p'\mu)^2 + y^2 + z^2. \tag{4}$$

In this context, the distance between the main bodies r' equals

$$r' = p'\rho', \quad \rho' = \frac{1}{1 + e' \cos v'}, \quad p' = q'(1 + e'), \tag{5}$$

where q' is the minimum distance (perihelion distance in the Solar System) of the perturbing body from the central one. The equality in (5) for r' practically defines the orbit of the perturbing body: for $e' < 1$ it is an elliptical orbit, for $e' > 1$ it is a hyperbolic orbit, and for $e' = 1$ it is a parabolic orbit. Additionally, the range of variation of the true anomaly is assumed to be

$$-\pi \leq v' \leq \pi, \quad (e' \leq 1), \quad \pi - \arccos\left(\frac{1}{e'}\right) < v' < \pi + \arccos\left(\frac{1}{e'}\right), \quad (e' > 1), \tag{6}$$

where the first interval corresponds to changes in v' during elliptical and parabolic motions of the perturbing body, and the second interval corresponds to hyperbolic motion.

REMARK 1. The Jacobian function analog defined by equality (2) corresponds to the case where $m_0 < m'$. If $m_0 > m'$, then the Jacobian function analog, the relative masses μ and $1 - \mu$, as well as the distances r_1 and r_2 should be determined by equalities

$$\Omega = \rho' \left[\frac{1}{2} (x^2 + y^2 - e'z^2 \cos v') + p'^3 \left(\frac{1 - \mu}{r_1} + \frac{\mu}{r_2} \right) \right], \tag{7}$$

$$\mu = \frac{m'}{m_0 + m'}, \quad 1 - \mu = \frac{m_0}{m_0 + m'} \quad \left(\mu < \frac{1}{2} \right), \tag{8}$$

$$r_1^2 = (x + p'\mu)^2 + y^2 + z^2, \quad r_2^2 = (x + p'\mu - p')^2 + y^2 + z^2. \tag{9}$$

2. QUASI-INTEGRAL AND THE LAW OF ENERGY CONSERVATION.

In the restricted circular ($e' = 0$) three-body problem, the equations of motion (1) for SHAPNER admit a Jacobi integral

$$V^2 - 2\Omega = 2C, \quad 2C = V_0^2 - 2\Omega_0 = const, \tag{10}$$

where the zero subscript denotes the values of the velocity V of the passively-gravitating body and the Jacobian function Ω at some initial value of the true anomaly v'_0 , and C is the constant of the Jacobi integral.

It is clear that in the non-circular ($e' \neq 0$) restricted three-body problem, such a first integral as the Jacobi integral (10) does not exist. This is due to the fact that the force function Ω explicitly depends on the independent variable v' . Indeed, if we multiply the first equation of system (1) by dx/dv' , the second by dy/dv' , and the third by dz/dv' , summing the resulting equations and integrating over v' , we obtain

$$\frac{V^2}{2} - \frac{V_0^2}{2} = \int_{v'_0}^{v'} \left(\frac{\partial \Omega}{\partial x} \frac{dx}{dv'} + \frac{\partial \Omega}{\partial y} \frac{dy}{dv'} + \frac{\partial \Omega}{\partial z} \frac{dz}{dv'} \right) dv' = \int_{v'_0}^{v'} \left(\frac{d\Omega}{dv'} - \frac{\partial \Omega}{\partial v'} \right) dv', \tag{11}$$

or

$$\frac{V^2}{2} - \Omega = \frac{V_0^2}{2} - \Omega_0 - \int_{v'_0}^{v'} \frac{\partial \Omega}{\partial v'} dv'. \tag{12}$$

The relation obtained (12) is not a first integral of the motion equations (1): it should be considered as an integral invariant relation, or quasi-integral [2]. This can be rewritten in the form of

$$\frac{V^2}{2} - \Omega + u(v') = h, \quad h = \frac{V_0^2}{2} - \Omega_0 + u(v'_0), \quad (13)$$

if an unknown antiderivative function $u(v')$:

$$u(v') - u(v'_0) = \int_{v'_0}^{v'} \frac{\partial \Omega}{\partial v'} dv', \quad (14)$$

is introduced. In the quasi-integral (13), h represents a constant energy and depends on the value of the unknown function $u(v'_0)$, i.e., it takes different values on different trajectories of motion.

Note that the quasi-integral (13) in the case of circular motion $e' = 0$ of the perturbing body transforms into the Jacobi integral (10), since in this case $\partial \Omega / \partial v' = 0$, i.e. $u(v') \equiv 0$. Thus, the obtained quasi-integral (13) in the non-circular ($e' \neq 0$) restricted three-body problem represents the law of conservation of energy of the passively gravitating body: the total energy of the body M , consisting of the Jacobi energy $V^2 / 2 - \Omega$ and the additional energy $u(v')$, is a constant quantity, depending only on the initial values of the coordinates and velocities of the body M . The quantity h can be considered as the constant energy, having its specific value on each trajectory [2]. Additionally, the Jacobi energy $V^2 / 2 - \Omega$ reaches its maximum value at the pericenter of the orbits of the main bodies M_0 and M' , and its minimum value at the apocenter. Therefore, during $0 \leq v' \leq \pi$, the double inequality

$$\frac{V_a^2}{2} - \Omega_a \leq \frac{V^2}{2} - \Omega \leq \frac{V_p^2}{2} - \Omega_p, \quad (15)$$

holds, where the indices "a" and "p" correspond to apocenter and pericenter. Moreover, the additional energy $u(v')$ monotonically increases as the main bodies M_0 and M' move away from the pericenter, and the passively gravitating body M gains additional (potential) energy from them. Conversely, as the main bodies move towards the pericenter, the additional energy $u(v')$ decreases, and the body M transfers energy to the main bodies [2].

Note that the law of conservation of energy (13) at the moment the primary bodies pass through the periaapses of their orbits can be represented as

$$\frac{V^2}{2} - \Omega + u(v') = h_p, \quad h_p = \frac{V_p^2}{2} - \Omega_p + \frac{\tilde{\Omega}_{\min}}{1 + e'}, \quad (16)$$

where the index "p" signifies the values of the Jacobian function analog Ω and the velocity V of the passively gravitating body, calculated at the moment the perturbing body passes through the pericenter, i.e. at $v' = 0$. Furthermore, $\tilde{\Omega}_{\min}$ denotes the minimum value of the function

$$\tilde{\Omega} = \frac{1}{2}(x^2 + y^2 + z^2) + p'^3 \left(\frac{\mu}{r_1} + \frac{1 - \mu}{r_2} \right) \geq 0, \quad (17)$$

which is related to the Jacobian function analog Ω by equality [2]

$$\frac{\partial \Omega}{\partial v'} = \tilde{\Omega} \frac{e' \sin v'}{(1 + e' \cos v')^2} = \tilde{\Omega} \frac{d\rho'}{dv'}. \quad (18)$$

Such a value of the function $\tilde{\Omega}$ exists on the circle [2]

$$x = -\frac{p'}{2}(1 - 2\mu), \quad y^2 + z^2 = \frac{3p'^2}{4}, \quad (19)$$

and is equal to

$$\tilde{\Omega}_{\min} = \frac{p'^2}{2}(3 - \mu + \mu^2). \quad (20)$$

3. REGIONS OF POSSIBLE MOTION. SURFACES OF MINIMUM ENERGY AND THEIR CRITICAL POINTS

The conservation of energy at the pericenter (16) can be rewritten in the form

$$V^2 + 2u(v') - 2\tilde{\Omega}_{\min} \cdot \rho' = 2\Omega - 2\tilde{\Omega}_{\min} \cdot \rho' + 2h_p \geq 0, \quad (21)$$

from which we can identify the regions of possible motion

$$2\Omega - 2\tilde{\Omega}_{\min} \cdot \rho' \geq C, \quad C = -2h_p = 2\Omega_p - V_p^2 - \frac{2\tilde{\Omega}_{\min}}{1+e'}, \quad (22)$$

where C is the equivalent of the Jacobi constant, and $\tilde{\Omega}_{\min}$ has been defined previously. The boundary of the region (22)

$$2\Omega - 2\rho'\tilde{\Omega}_{\min} \geq C, \quad (23)$$

is referred to as surfaces of minimum energy, the equation of which we write in the form [2]

$$H \equiv x^2 + y^2 - e'z^2 \cos v' + 2p'^3 \left(\frac{\mu}{r_1} + \frac{1-\mu}{r_2} \right) - 2\tilde{\Omega}_{\min} = C(1 + e' \cos v'). \quad (24)$$

It's clear that the function $H \equiv H(x, y, z, p', e', v', \mu, C)$, meaning the family of surfaces of minimum energy (24) depends not only on the coordinates x, y, z but also on five parameters: p', e', v', μ, C . The Jacobi constant equivalent C characterizes the energy of the passively-gravitating body M , and the focal parameter p' represents the linear scale of the surfaces. With given values of these parameters p', e', v', μ and C , the body M cannot move beyond the surface defined by equation (24). When $e' = 0$, the surfaces of minimum energy (24) transform into the zero velocity surfaces of the restricted circular three-body problem. Moreover, from equation (24), it follows that the family of minimum energy surfaces given values of the parameters p', e', μ and C for all true anomaly values v' within the range $[-v_a, v_a]$ is located between two surfaces [2]

$$x^2 + y^2 - e'z^2 \cos v' + 2p'^3 \left(\frac{\mu}{r_1} + \frac{1-\mu}{r_2} \right) - 2\tilde{\Omega}_{\min} = C(1 + e'), \quad (25)$$

and

$$x^2 + y^2 - e'z^2 \cos v_a + 2p'^3 \left(\frac{\mu}{r_1} + \frac{1-\mu}{r_2} \right) - 2\tilde{\Omega}_{\min} = C(1 + e' \cos v_a), \quad (26)$$

Furthermore, the singular points of the family (24) at fixed values of the parameters p', e', v' and μ are the points where it is impossible to construct a unique tangent plane. Therefore, the singular points of the family (24) are determined by algebraic equations

$$\begin{aligned} \frac{\partial H}{\partial x} &= 2 \left[x - p'^3 \frac{\mu}{r_1^3} (x + p' - p'\mu) - p'^3 \frac{1-\mu}{r_2^3} (x - p'\mu) \right] = 0, \\ \frac{\partial H}{\partial y} &= 2y \left(1 - p'^3 \frac{\mu}{r_1^3} - p'^3 \frac{1-\mu}{r_2^3} \right) = 0, \\ \frac{\partial H}{\partial z} &= -2z \left(e' \cos v' + p'^3 \frac{\mu}{r_1^3} + p'^3 \frac{1-\mu}{r_2^3} \right) = 0, \end{aligned} \quad (27)$$

which coincide with the same equations used to determine libration points in the restricted three-body problem [1,2].

The solutions to the algebraic equations (27) are the collinear singular points $L_1 = L_1(x_1, 0, 0)$, $L_2 = L_2(x_2, 0, 0)$, $L_3 = L_3(x_3, 0, 0)$ and two pairs of coplanar (triangular) singular points: $L_4 = L_4(x_4, y_4, 0)$, $L_5 = L_5(x_4, -y_4, 0)$ in the plane $z = 0$ and $L_6 = L_6(x_6, 0, z_6)$, $L_7 = L_7(x_6, 0, -z_6)$ in the plane $y = 0$ (see below). The collinear singular point L_1 is located to the left of the main body M_0 of lesser mass, i.e., $x_1 < \bar{x}_1 = -p'(1-\mu) < 0$, L_2 is located between the main bodies, i.e., $\bar{x}_1 < x_2 < 0 < \bar{x}_2 = p'\mu$, and L_3 is to the right of the main body M' of greater mass, i.e., $x_3 > \bar{x}_2$. The triangular singular points L_4 and L_5 are located in the left half-plane $x < 0$, closer to the main body M_0 of lesser mass and for them $x_4 < 0$. Furthermore, if the masses of the main bodies are equal $m_0 = m'$, then $\mu = 1/2$ and the singular point L_2 will be located at the center of mass of the main bodies – at the origin, i.e., $x_2 = 0$.

Now, let's determine the triangular singular points L_4 and L_5 , in the plane $z = 0$ from the system of algebraic equations (27), in which the third equation is absent, and the first equation is rewritten in another form:

$$\begin{aligned} x \left[1 - p'^3 \frac{\mu}{r_1^3} - p'^3 \frac{1-\mu}{r_2^3} \right] - p'^4 \mu (1-\mu) \left(\frac{1}{r_1^3} - \frac{1}{r_2^3} \right) &= 0, \\ y \left(1 - p'^3 \frac{\mu}{r_1^3} - p'^3 \frac{1-\mu}{r_2^3} \right) &= 0. \end{aligned} \quad (28)$$

It is evident that the system (28) is consistent only when $r_1 = r_2$. Therefore, there exists a unique real analytical solution at $y \neq 0$ in the form of $r_1 = r_2 = p'$. Let's express the found solution in coordinates x and y , where in the expression (4) for r_1 and r_2 , $z = 0$ should be set. This gives us

$$x = x_4 = -\frac{p'}{2} + p'\mu, \quad y = y_4 = \frac{\sqrt{3}}{2} p', \quad z = 0. \quad (29)$$

It is clear that the x_4 -coordinate (x_4) of the singular point L_4 or L_5 depends on the focal parameter p' of the test star's orbit and its mass through μ , while the y_4 -coordinate (y_4) depends only on p' .

Next, from the system of equations (27) with $y = 0$, i.e., from the system of two equations

$$\begin{aligned} x \left[1 - p'^3 \frac{\mu}{r_1^3} - p'^3 \frac{1-\mu}{r_2^3} \right] - p'^4 \mu (1-\mu) \left(\frac{1}{r_1^3} - \frac{1}{r_2^3} \right) &= 0 \\ z \left(e' \cos v' + p'^3 \frac{\mu}{r_1^3} + p'^3 \frac{1-\mu}{r_2^3} \right) &= 0, \end{aligned} \quad (30)$$

we find two symmetric coplanar solutions $L_6 = L_6(x_6, 0, z_6)$ and $L_7 = L_7(x_6, 0, -z_6)$ relative to the x -axis. It is clear that $x_6 = x_6(v')$ and $z_6 = z_6(v')$, and from the second equation of the system (30), it follows that real solutions L_6 and L_7 can only exist when $\cos v' < 0$. It should be noted that at $v' = \pm \frac{\pi}{2}$, the coplanar singular points will also include two infinitely distant singular points $L_8 = L_8(0, 0, +\infty)$ and $L_9 = L_9(0, 0, -\infty)$, known for the circular problem [2]. At $e' \rightarrow 0$, the infinitely distant libration points tend towards the infinitely distant singular points. Moreover, the equations (30) also have an analytical solution in the plane $y = 0$ for parabolic motion ($e' = 1$) of the test star and $\cos v' = -1$. This solution also has the form $r_1 = r_2 = p'$ and in coordinates, similar to (29), is written as follows:

$$x = x_6 = -\frac{p'}{2} + p'\mu, \quad y = 0, \quad z = z_6 = \frac{\sqrt{3}}{2} p' \quad (\cos v' = -1, e' = 1). \quad (31)$$

Therefore, in the parabolic motion of the test star and at $\cos v' = -1$, the x -coordinate of the singular point L_6 or L_7 depends on the focal parameter p' of the orbit of the test star and its mass through μ , while the z -coordinate z_6 depends only on p' . In other cases, the coordinates of the coplanar singular points L_6 or L_7 are determined only numerically.

Thus, in the restricted circular three-body problem, there are a total of seven libration points including the infinitely distant ones, whereas in the non-circular problem we are considering, the number of singular points is greater.

In conclusion, let us note some differences between singular points and libration points. In each singular point, there is a bifurcation of the minimum energy surfaces, i.e., a transition from one state to another. Bifurcation also occurs at the values of the true anomaly $v' = \pm \frac{\pi}{2}$ [2]. Unlike the coordinates of libration points, the coordinates of coplanar

singular points are not stationary particular solutions of the SHAPNER equations (1), as they do not satisfy these equations. Libration points are conical singular points, while coplanar points are singular points of the "center" type.

REMARK 2. The existence of a Jacobian integral analogue in the restricted elliptical, parabolic, and hyperbolic three-body problems was denied. However, work [2] has proven that such an analogue – a quasi-integral does exist. From this discovered quasi-integral, an analogue of zero-velocity surfaces – minimum energy surfaces – is derived. These surfaces also allow for the existence of satellite-type motions, i.e., there is Hill stability at certain parameter values, which will be discussed in the next section.

4. CRITERIA FOR HILL STABILITY OF MOTION.

In the restricted three-body problem, the motion of a passively gravitating body is considered Hill stable if it remains confined within a certain closed region around one of the primary bodies. In other words, if the passively gravitating body, at any values of the true anomaly v' , maintains a satellite-type motion around one of the primary bodies and remains within a restricted area, its motion is deemed Hill stable. The concept of Hill stability is intimately linked to the value of the Jacobian constant analog C , calculated at the special point L_2 , which lies between the primary bodies M_0 and M' and corresponds to a satellite-type motion. The value of the Jacobian constant analog from the family of minimal energy surfaces corresponding to the special point $L_2(x_2, 0, 0)$ is denoted by C_2 , i.e., from equation (24) we set

$$C_2 = H(x_2, 0, 0) = x_2^2 + 2p'^3 \left(\frac{\mu}{\sqrt{(x_2 + p' - p'\mu)^2}} + \frac{1 - \mu}{\sqrt{(x_2 - p'\mu)^2}} \right) - p'^2(3 - \mu + \mu^2). \tag{32}$$

Then, for any values of the true anomaly v' , chosen as the independent variable, the inequality

$$C = 2\Omega_p - V_p^2 - \frac{2\tilde{\Omega}_{\min}}{1 + e' \cos v'} \geq \frac{C_2}{1 + e' \cos v'}, \tag{33}$$

where Ω_p, V_p^2 and $\tilde{\Omega}_{\min}$ are defined earlier, is satisfied.

Using inequality (33), the criteria for stability, instability, and conditional stability of the motion of a small mass body are determined in the restricted elliptical, hyperbolic, and parabolic three-body problems.

In the case of the restricted elliptical three-body problem, the sufficient condition – a criterion for Hill stability of the motion of a small mass body M – takes the form of equation in reference [2],

$$C \geq \frac{C_2}{1 - e'}, \tag{34}$$

where the values of the Jacobian constant analog C_2 and C are determined by equations (32) and (33).

The opposite inequality (34)

$$C < \frac{C_2}{1 - e'} \tag{35}$$

defines the criterion for the instability of the motion of the body M according to Hill. In this case, there will be values of v' for which the inequality $C < C_2$ will hold.

For the parabolic or hyperbolic restricted three-body problem, one should use the inequality

$$\frac{1}{1 + e' \cos v'} < \infty,$$

from which it follows that the criterion for the stability of the motion of body M according to Hill is asymptotically fulfilled, i.e., when $C \rightarrow \infty$. Therefore, stability of the motion of body M according to Hill in the restricted parabolic and hyperbolic three-body problems can never be achieved. Indeed, for any arbitrarily chosen C , there will be a positive value of the true anomaly $v'_p \rightarrow 0$ such that for any $|v'| > v'_p$, the inequality $C < C_2$ will hold.

When the instability criterion (35) is satisfied, there will be such a value of $v'_p > 0$ that for any $|v'| \leq v'_p$ the inequality $C \geq C_2$ is met. In such cases, the motion of the passively gravitating body is referred to as conditionally stable according to Hill [2].

In the case of the restricted elliptical three-body problem, the criterion for conditional stability of the motion of body M according to Hill is the fulfillment of the double inequality

$$\frac{C_2}{1 + e'} \leq C < \frac{C_2}{1 - e'} \tag{36}$$

and for the parabolic and hyperbolic restricted three-body problems, conditional stability of the motion of body M according to Hill is achieved under condition

$$\frac{C_2}{1 + e'} \leq C < \infty. \tag{37}$$

It should be noted that conditional stability of the motion of a small mass body M according to Hill occurs when the instability criterion (35) and inequality [2]

$$\cos v' \geq \cos v'_a = \frac{1}{e'} \left(\frac{C_2}{C} - 1 \right), \quad |v'| \leq v'_a, \quad (38)$$

are met.

The criterion for absolute instability of the motion of body M according to Hill is the inequality

$$C < \frac{C_2}{1+e'}, \quad (39)$$

which ensures that the inequality $C < C_2$ is satisfied at any v' .

The criterion for stability of the motion of a passively gravitating body in the restricted elliptical three-body problem according to Hill within a certain bounded area encompassing both primary bodies is the fulfillment of inequality

$$C \geq \frac{C_3}{1-e'}, \quad \left(\frac{C_3}{1+e'} \leq C < \frac{C_3}{1-e'} \right). \quad (40)$$

Here $C_3 = H(x_3, 0, 0)$ is the value from the family of minimal energy surfaces corresponding to the special point $L_3(x_3, 0, 0)$, located to the right of the primary body of greater mass M' . Additionally, the brackets indicate the criterion for conditional stability according to Hill for motion in this area. The inequality opposite to (40) represents the criterion for instability of the motion of body M in this area.

For brevity, the stability of motion according to Hill, associated with the value C_2 of the Jacobian constant analogue, i.e., meeting criterion (34), will be referred to as *first-type stability*, while the stability of motion according to Hill when criterion (40) with the value C_3 is met will be referred to as *second-type stability*.

Similarly, criteria for stability, conditional stability, instability, and absolute instability according to Hill for the motion of a passively-gravitating body in the restricted elliptical three-body problem associated with other special points can be established. For brevity, these criteria are not presented here.

5. SATELLITE EXCHANGE BETWEEN PRIMARY BODIES

Let us now consider the problem of exchanging a satellite between the primary bodies M_0 and M' , which are approaching each other along elliptical, hyperbolic, and parabolic orbits. The theory outlined above regarding the criteria for the stability of the motion of body M by Hill [2] allows us to establish: a) the necessary condition for the exchange or capture to take place, b) the sufficient condition for the impossibility of exchange, c) the range of values of the true anomaly v' during which a satellite exchange is possible.

Let's first consider the restricted elliptical three-body problem. When inequality (34) – the condition for the stability of the motion of body M by Hill – is met, an exchange of satellites between the primary bodies in elliptical motion is not possible. Therefore, inequality (34) can be considered as a sufficient condition for the impossibility of satellite exchange in the case of elliptical motion, as the energy of the satellite in this case is so low that it cannot detach from its parent body. However, the necessary condition for satellite exchange in elliptical motion is the fulfillment of the instability criterion by Hill, i.e., inequality (35). This inequality, along with the surfaces of minimal energy, facilitates the numerical search for the satellite's trajectory during exchange. Thus, when inequality (35) is met and the initial conditions are appropriately chosen, the satellite may either leave the vicinity of its parent body and become the satellite of the second body (exchange), transform into an independent celestial body (ejection), or remain the satellite of its parent body. Furthermore, when the criterion for conditional stability (36) is met, the conditions for the possibility of satellite exchange in elliptical motion should be clarified. The exchange can then only occur in interval $|v'| > v'_a$, i.e., in the vicinity of the most distant point of the primary bodies' orbit. It is precisely in this interval of true anomaly values, according to inequality (38), that the loss of conditional stability by Hill occurs.

In the case of parabolic and hyperbolic motion of the primary bodies, the necessary condition for exchange, i.e., the instability criterion (35) for the motion of body M by Hill, is always met. In this case, instability by Hill occurs at any energy level when $|v'|$ is sufficiently large. Furthermore, in the case of violation of the conditions for conditional stability (38) by Hill, i.e., in interval $|v'| > v'_a$, satellite exchange can occur in both elliptical and in parabolic and hyperbolic motions of the primary bodies.

Under the criterion of absolute instability (39), satellite exchange is theoretically possible at any value of the true anomaly v' . It is worth noting that such conditions were previously unknown, and the possibility or impossibility of satellite exchange was checked by intuitively selecting initial conditions and parameters [2].

For example, Hill [8], within the framework of the restricted circular three-body problem of the Sun-Earth-Moon, established that the satellite motion of the Moon relative to Earth is stable according to Hill, as the sufficient condition – inequality (34) is met when $e' = 0: C = 2.2544 > C_2 = 2.00092$. As shown in the study [2], the Moon's motion remains stable according to Hill in the restricted elliptical three-body problem as well – the condition $C = 2.2544 > C_2 / (1 - e') = 2.03501$ is met, where $e' = 0.016751$ is the eccentricity of Earth's orbit. If e' were seven times larger, then the motion of the Moon would become conditionally stable according to Hill, i.e., inequality (38) would be met: $C = 2.2544 > C_2 / (1 + 7e') = 1.7909$, and inequality (34) would not be satisfied: $C = 2.2544 < C_2 / (1 - 7e') = 2.2667$.

6. ON SOME APPLICATIONS OF THE RESTRICTED THREE-BODY PROBLEM TO ASTRONOMICAL OBJECTS

In the study [3], within the framework of the restricted three-body problem, the motion of a star in a close binary system (CBS) with conservative mass transfer was investigated. Unlike the well-known Paczynski-Huang model, a new model defining the relative motion of the star in the CBS along an elliptical orbit was used. The third body in this scenario is the mass stream flowing from the donor star to the accretor star. The elliptical motion of the star takes into account the mutual attraction of the stars, reactive forces, and the gravitational force of the stars on the flowing stream. Changes in the semi-major axis and eccentricity of the second star were identified, showing that CBS does not form a closed mechanical system, i.e., a system that allows for the conservation of linear momentum and angular momentum. Moreover, the classical law of conservation of energy does not apply, but there exists an analogue of the conservation law in the form of a quasi-integral. This can be confirmed based on the general equations of motion by Meshcherskiy for a two-body problem with variable masses. Therefore, the use of the Paczynski-Huang model, which assumes that CBS forms a closed mechanical system, is not appropriate for this problem. The model proposed in the study [3] was subsequently named the Luk'yanov's model.

In the work [7], the problem of the motion of a rotating star in a close binary system (CBS) with conservative mass transfer was considered. Using the Luk'yanov's model [3], the relative motion of the star in close binary systems along an elliptical orbit was determined. The elliptical motion of the star accounts for the mutual attraction of the stars, reactive forces, the gravitational force of the stars on the flowing stream, and disturbances from the rotational movement of the accretor star. Changes in the semi-major axis, eccentricity, and angular velocity of the accretor star's orbit were defined depending on the parameter q – the mass ratio of the stars. The results were applied to the star system BF Aurigae (in the constellation Auriga) and presented in the form of diagrams. The Luk'yanov model is also applicable in studying the motion of stars in CBS with non-conservative mass exchange.

In the study [14], the problem of the stability of a planet's satellite motion was considered. Within the general three-body problem (Sun-planet-satellite), "Sundman surfaces" were constructed, based on which the concept of "stability by Sundman" was formulated. Special points of these surfaces were identified, possible motion regions were defined, and the stability of the special points by Sundman was established. The stability of the motion of all known natural satellites of planets was investigated, and it was shown that the motion of a number of natural satellites, stable by Hill, as well as some planet satellites stable by the Golubev method, turn out to be unstable by Sundman.

In work [15], within the framework of the restricted elliptical three-body problem, the criterion for stability by Hill was established. By virtue of this criterion, the stability of four exoplanets outside the solar system in a binary star system: CepheiAb, Gliese 86 Ab, HD 41004 Ab, and HD 41004 Bb was investigated.

7. INVESTIGATION OF HILL'S STABILITY OF PLANETARY MOTIONS DURING STELLAR APPROACHES

To investigate the stability of planetary motion in the Hill frame during the approach of a test star to the Solar System, moving along a hyperbolic (parabolic or elliptical) orbit, it is necessary to know its mass and orbital parameters. As an example, let us take a test star with mass m' , heliocentric distance q' (in astronomical units), and eccentricity e' , varying within the range

$$M_{\odot} \leq m' \leq 5M_{\odot}, \quad 50 \leq q' \leq 100, \quad 1 \leq e' \leq 5, \quad (0.1 \leq e' \leq 0.9), \quad (41)$$

where M_{\odot} is the mass of the Sun, $e' = 1$ corresponds to parabolic motion of the test star, and the values of the eccentricity of its orbit are indicated in parentheses for elliptical motion. It should be noted that the relationship between the time t and the true anomaly ν' of the test star depends on the type of its orbit. Thus, in the case of elliptical motion of the test star with orbit parameters $e' = 0.2$, $q' = 50$ au, and $m' = 3M_{\odot}$, the change in ν' in interval $[0, 3\pi/4]$ corresponds to a change in time in the interval $[0, 80.26]$ years. For the same values of eccentricity and mass of the test star, but at $q' = 75$ au, this interval of changes in ν' corresponds to the interval $[0, 147.45]$ years, and at $e' = 0.2$, $q' = 75$ au, and $m' = 5M_{\odot}$, it corresponds to $[0, 120.39]$ years.

In the case of parabolic motion ($e' = 1$) of the test star at $q' = 50$ au and $m' = 3 M_{\odot}$, the interval of changes $[0, 3\pi/4]$ in the true anomaly ν' corresponds to the time interval $[0, 799.53]$ years, at $q' = 75$ au and $m' = 3 M_{\odot} - [0, 1468.83]$ years, and at $q' = 75$ au and $m' = 5 M_{\odot} - [0, 1199.29]$ years.

Finally, in the case of hyperbolic motion with $e' = 1.15$, $q' = 50$ au, and $m' = 3 M_{\odot}$, the interval $[0, 3\pi/4]$ of changes in ν' corresponds to the time interval $[0, 466.49]$ years, at $q' = 75$ au and $m' = 3 M_{\odot} - [0, 857.0]$ years, and at $q' = 75$ au and $m' = 5 M_{\odot} - [0, 699.74]$ years.

Table 1 presents the results of the study of Hill stability motion of three planets (Earth, Jupiter, and Saturn) depending on the focal parameter p' of the star's orbit and its mass m' during hyperbolic orbits, and in Table 2 - during parabolic orbits of the star. In these tables, C_p denotes the value of the analogue of the Jacobi constant when $\nu' = 0$, and C_2 denotes its value computed at the special point L2. It turned out that in the case of a parabolic or hyperbolic star orbit, only conditional stability of planetary motion in the Hill frame occurs.

Table 1. The Hill stability of planetary motion in the restricted hyperbolic three-body problem: planet – Sun – star

Planets	p' (au)	m'	C_p	$\frac{C_2}{1+e'}$	Stability
Earth	107.5	M_{\odot}	11223.63801	6718.7500	Conditional
		$3M_{\odot}$	25583.32507	5687.60356	
		$5M_{\odot}$	47022.20069	4772.35271	
	161.25	M_{\odot}	20191.97684	15117.18750	
		$3M_{\odot}$	61105.18565	12797.10802	
		$5M_{\odot}$	95570.33302	10737.79359	
	215	M_{\odot}	33270.29723	26875.0	
		$3M_{\odot}$	112264.5806	22750.41426	
		$5M_{\odot}$	165109.6349	19089.41084	
Jupiter	107.5	M_{\odot}	13331.70751	6718.7500	stability
		$3M_{\odot}$	24861.51172	5687.60356	
		$5M_{\odot}$	49624.43491	4772.35271	
	161.25	M_{\odot}	21467.26449	15117.18750	
		$3M_{\odot}$	60262.03232	12797.10802	
		$5M_{\odot}$	95683.01105	10737.79359	
	215	M_{\odot}	33930.418233	26875.0	
		$3M_{\odot}$	111454.2512	22750.41426	
		$5M_{\odot}$	164324.6482	19089.41084	
Saturn	107.5	M_{\odot}	8727.26427	6718.7500	stability
		$3M_{\odot}$	27513.53878	5687.60356	
		$5M_{\odot}$	42004.00334	4772.35271	
	161.25	M_{\odot}	18716.70519	15117.18750	
		$3M_{\odot}$	63492.14497	12797.10802	
		$5M_{\odot}$	92061.73155	10737.79359	
	215	M_{\odot}	32919.55202	26875.0	
		$3M_{\odot}$	115125.8691	22750.41426	
		$5M_{\odot}$	162201.6013	19089.41084	

Table 2. The Hill stability of planetary motion in the restricted parabolic three-body problem: planet – Sun – star

Planets	p' (au)	m'	C_p	$\frac{C_2}{1+e'}$	Stability
Earth	100	M_{\odot}	11219.60303	6250.0	Conditional
		$3M_{\odot}$	23482.33868	5290.79401	
		$5M_{\odot}$	44605.58035	4439.39787	
	150	M_{\odot}	19471.08396	14062.50	
		$3M_{\odot}$	56332.99884	11904.28652	
		$5M_{\odot}$	88706.78297	9988.64521	
	200	M_{\odot}	31408.15909	25000.0	
		$3M_{\odot}$	103775.4097	21163.17606	
		$5M_{\odot}$	152887.0666	17757.59148	
Jupiter	100	M_{\odot}	13530.15606	6250.0	stability
		$3M_{\odot}$	22763.67615	5290.79401	
		$5M_{\odot}$	48838.76295	4439.39787	
	150	M_{\odot}	20865.61324	14062.50	
		$3M_{\odot}$	55415.29318	11904.28652	
		$5M_{\odot}$	90292.22156	9988.64521	
	200	M_{\odot}	32241.85212	25000.0	
		$3M_{\odot}$	102759.3469	21163.17606	
		$5M_{\odot}$	153761.1559	17757.59148	
Saturn	100	M_{\odot}	94538.09535	6250.0	stability
		$3M_{\odot}$	169050.8402	5290.79401	
		$5M_{\odot}$	235037.3713	4439.39787	
	150	M_{\odot}	136655.9248	14062.50	
		$3M_{\odot}$	246167.2023	11904.28652	
		$5M_{\odot}$	337912.9926	9988.64521	
	200	M_{\odot}	186559.9802	25000.0	
		$3M_{\odot}$	337870.9594	21163.17606	
		$5M_{\odot}$	459756.0501	17757.59148	

8. CONCLUSION

The problem of the spatial motion of a passive-gravitating body during approach to the central body of a test star – the perturbing body, has been considered. The perturbing body - the star - may move along an elliptical, parabolic, or hyperbolic orbit. An exact expression of the force function without expansion into a series has been used. An integral

invariant relationship - a quasi-integral, has been found. Due to the quasi-integral, regions of possible motion of the passive-gravitating body, surfaces of minimum energy, which generalize the surfaces of zero velocity, and the special points of these surfaces have been determined. The necessary condition has been established - the fulfillment of the Hill instability criterion for satellite exchange in the restricted elliptical three-body problem. It has been shown that in the case of parabolic or hyperbolic motion of the principal bodies, the necessary condition for satellite exchange is always satisfied. In the region of instability loss of Hill motion, satellite exchange can occur in both elliptical and parabolic or hyperbolic motions of the principal bodies. Exchange can only occur in the vicinity of the farthest point of the principal bodies' orbits. When the instability criterion is met and the initial conditions of the satellite are properly chosen, the satellite may either leave the vicinity of the parent body and become a satellite of the second body (exchange), or transform into an independent celestial body (ejection), or remain a satellite of the parent body.

To illustrate the obtained results, restricted hyperbolic, parabolic, and elliptical three-body problems have been considered as an example: Sun-planet-test star. In this case, the heliocentric distance q' of the test star and its mass m' oscillate within the range of 50 to 100 au and from one to five solar masses, respectively. According to the stability criteria of the first and second types, critical values of the orbit parameters of the test star have been established, at which the planets of the Solar System either become satellites of the test star or leave the boundaries of the Solar System.

ORCID

©Ruslan Mammadov, <https://orcid.org/0000-0001-5879-1368>

REFERENCES

- [1] G.N. Duboshin, *Celestial mechanics: Analytical and qualitative methods*, 2nd edition, (Izdatel'stvo Nauka, Moscow, 1978). <https://ui.adsabs.harvard.edu/abs/1978MoIzN....Q...D/abstract> (in Russian)
- [2] L.G. Luk'yanov, "Analog of the surfaces of zero velocity in the restricted elliptic, parabolic, and hyperbolic three-body problem," *Astronomy Letters*, **36**, 823-833 (2010). <https://doi.org/10.1134/S1063773710110083>
- [3] L.G. Luk'yanov, and S.A. Gasanov, "Elliptical motions of stars in close binary systems," *Astronomy Reports*, **55** (8), 733-741. (2011). <https://doi.org/10.1134/S106377291108004X>
- [4] A.G. Mamedov, "A twice-averaged parabolic restricted three-body problem," *Tr. Gos. Astr. Inst. im. Sternberga*, **61**, 79-86 (1989). <https://ui.adsabs.harvard.edu/abs/1989TrSht..61...79M/abstract> (in Russian)
- [5] A.G. Mamedov, "Secular perturbations of elements in the restricted parabolic three-body problem," *Astronomicheskii Zhurnal*, **68**, 1323-1327 (1991). <https://ui.adsabs.harvard.edu/abs/1991AZh....68.1323M/abstract> (in Russian)
- [6] A.G. Mammadli, "The limiting case of the double-averaged parabolic restricted three-body problem," *Solar System Research*, **41**(2), 171-173 (2007). <https://doi.org/10.1134/S0038094607020104>
- [7] A.A. Medvedeva, and S.A. Gasanov, "Elliptical motion of a star in a close binary system," *Astronomy Reports*, **58**(8), 554-562 (2014). <https://doi.org/10.1134/S1063772914080046>
- [8] G.W. Hill, "Researches on the Lunar theory," *Am. J. of Math.* **1**, 5-26 (1878). <https://doi.org/10.2307/2369430>
- [9] W. Scheibner, "Satz aus der störungstheorie," *Reine Angew. Math.* **65**, 291 (1866). <https://doi.org/10.1515/crll.1866.65.291>
- [10] K. Petr, and M.V. Nechvil, "Two remarks to a special case of three bodies problem," *Casopis Pestovani Mat. Fys. (Praha)*, **47**, 268-273 (1918). <https://iopscience.iop.org/article/10.3847/1538-4357/acc573/meta#fnref-apjacc573bib30>
- [11] M.V. Nechvil, "Sur une nouvelle forme des equations differentielles du probleme restreint elliptique," *Compte. Rendue*, **182**, 310-314 (1926). <https://iopscience.iop.org/article/10.3847/1538-4357/acc573/meta#fnref-apjacc573bib29>
- [12] N. Rein, "Note sur l'article de M.V. Nechvil, "Sur une nouvelle forme des equations differentielles du probleme restreint elliptique," *Tr. Gos. Astron. Inst. im. P.K. Shternberga*, **14**, 85-87 (1940). <https://ui.adsabs.harvard.edu/abs/1940TrSht..14...85R/abstract> (in Russian)
- [13] K.V. Khol'shevnikov, and Yu.F. Mishchuk, "The effect of stellar encounters on planetary orbits," *Vestn. Leningr. Univ.* **2**, 72-81 (1983). <https://ui.adsabs.harvard.edu/abs/1983VeLen...2...72K/abstract> (in Russian)
- [14] L.G. Luk'yanov, and V.S. Uralskaya, "Sunman stability of natural planet satellites," *Mon. Notic. Roy. Astron. Soc. (MNRAS)*, **421**(3), 2316-2324 (2012). <https://doi.org/10.1111/j.1365-2966.2012.20457.x>
- [15] F. Szenkovits, and Z. Makó, "About the Hill stability of extrasolar planets in stellar binary Systems," *Celest. Mech. Dyn. Astron.* **101**, 273-287 (2008). <https://doi.org/10.1007/s10569-008-9144-7>

ПРО СТІЙКІСТЬ РУХІВ ПЛАНЕТ ПІД ЧАС ЗБЛИЖЕННЯ ЗІР

А.Г. Мамедлі^а, Р.Т. Мамедов^{а,б}, У.С. Валієв^а

^аБатабатська Астрофізична Обсерваторія Міністерства Науки і Освіти Азербайджанської Республіки,

Нахічевань, AZ-7000, Азербайджан

^бНахічеванський Державний Університет, Нахічевань, AZ-7012, Азербайджан

Розглянуто задачу про просторовий рух пасивно гравітаційного тіла під час наближення до центрального тіла збурюючого тіла – пробної зірки. Використовуючи точний вираз силової функції, знайдено інтегральне інваріантне співвідношення – квазіінтеграл. За допомогою квазіінтеграла визначено області можливого руху пасивно гравітаційного тіла, поверхні мінімальної енергії (узагальнення поверхонь нульової швидкості) та особливі точки цих поверхонь. Досліджено стабільність руху планет за Хіллом під час наближення пробної зірки до Сонячної системи. Встановлено критерії можливості, а також неможливості захоплення тестовою зіркою пасивно гравітаційного тіла. Відповідно до критеріїв стійкості Хілла були встановлені критичні значення параметрів орбіти досліджуваної зірки, при яких планети Сонячної системи або стають супутниками досліджуваної зірки, або залишають межі Сонячної системи.

Ключові слова: небесна механіка; обмежена задача трьох тіл; аналог функції Якобі; квазіінтеграл; закон збереження енергії; поверхні мінімальної енергії; особливі точки; стійкість Хілла

HIGH-ORDER B-SPLINE FINITE DIFFERENCE APPROACH FOR SCHRODINGER EQUATION IN QUANTUM MECHANICS

 Archana Senapati,  Balaji Padhy*,  Shashikant Das

Centurion University of Technology and Management, Odisha, India.

*Corresponding Author e-mail: balaji.padhy11@gmail.com

Received May 7, 2024; revised July 9, 2024; accepted July 19, 2024

This paper presents a new numerical method for solving the quantum mechanical complex-valued Schrodinger equation (CSE). The technique combines a second-order Crank-Nicolson scheme based on the finite element method (FEM) for temporal discretisation with nonic B-spline functions for spatial discretisation. This method is unconditionally stable with the help of Von-Neumann stability analysis. To verify our methodology, we examined an experiment utilising a range of error norms to compare experimental outcomes with analytical solutions. Our investigation verifies that the suggested approach works better than current methods, providing better accuracy and efficiency in quantum mechanical error analysis.

Keywords: Crank-Nicolson Method; Finite element scream; Von-Neumann stability assessment; Nonic B-spline

PACS: 02.90.p, 03.65.w, 47.11.Fg, 02.30.Jr

1. INTRODUCTION

Differential equations (DEs) are fundamental tools for analysing dynamic phenomena across various fields and are indispensable in mathematically representing physical systems. They find extensive application in simulating diverse physical problems such as fluid dynamics, signal processing, and electrical engineering. Dynamic systems with measurement errors often necessitate numerical treatment due to the complexity of obtaining analytical solutions.

The Schrodinger equation (SE), formulated by Austrian physicist Erwin Schrodinger in 1926, stands as a cornerstone in quantum theory and mechanics, governing sub-microscopic events. And the probabilistic nature of wave functions. Its significance permeates through atomic, nuclear, and solid-state physics. Schrodinger's experimental validation of SE, particularly with the hydrogen atom, underscored its efficacy in describing quantum phenomena.

SE exists in two primary forms: the time-dependent Schrodinger wave equation, portraying wave function evolution over time, and the time-independent Schrödinger equation, elucidating stationary states. While the former characterises progressive waves pertinent to free particle motion, the latter describes standing waves, especially when the particle's potential energy is independent of time and solely dependent on position.

The solutions to the time-dependent Schrodinger equation mirror the dynamic properties of particles, analogous to Newton's force definition ($F = ma$) in classical physics. Furthermore, nonlinear Schrodinger equations find applications in various fields, such as plasma physics[2], nonlinear optics [19], and water waves [26].

Recent research delves into specialised solutions and applications of SE variants, including Haar wavelet and finite difference method [1], quantic Hermite collocation method [3], differential quadrature method (DQM) [4], quadratic B-Spline FEM [6], reverse-time SE [9], cubic spline technique [17]. Additionally, studies explore specific solutions and phenomena like breather-type solutions and rogue waves in generalised nonlinear SE formulations [5], highlighting the versatility and ongoing research interest in SE and its extensions.

Many approaches have been used with finite differences [18], and the finite element method [21] is designed specifically for fractional Schrodinger equations with trigonometric B-splines [8]. It has also been investigated to analyse the superconvergence of linearised MFEM for nonlinear Schrödinger equations [24]. Additionally, specialised methods have addressed time-dependent singly perturbed convection-diffusion equations, such as the Crank-Nicolson finite difference approach with a midpoint upwind scheme on non-uniform meshes [12].

Numerous numerical methods have been studied to solve the coupled nonlinear Schrödinger equation using cubic B-spline Galerkin methods [10]. Furthermore, to approximate solutions to Equation (1), multistep and hybrid approaches [25] and two-step hybrid methods [15] have been proposed. Other techniques include B-Spline collocation technique [11], [7] improvised cubic B-spline collocation [13], Crank-Nicolson scheme [14], homotopy analysis method [20], BFRK scheme [22], septic B-Spline collocation [23] and numerical quadrature schemes, which have also been applied. Despite exploring several ways, difficulties in delivering comprehensive computations for these techniques continue to arise. For example, Lehtovaara *et al.*, by the time propagation method [16], presents viable approaches to solve equation (1), but the computation details are still elusive.

Adopting the nonic B-spline collocation methodology is a significant step forward in tackling complicated problems like the Schrödinger equation by surpassing the drawbacks of the previous numerical methods. Using this technology, researchers can reduce problems associated with excessive computing complexity, poor precision, and programming difficulties.

Researchers can effectively handle the complex computations needed to approximate solutions using MATLAB and MATHEMATICA for computing. Compared to more conventional approaches, this one simplifies computation, improves accuracy, and simplifies implementation.

Furthermore, this effort offers scholars essential insights into the effectiveness of complex analysis as a physics tool by integrating these techniques within the quantum mechanics curriculum. Comprehending complex analysis broadens researchers' understanding and gives them an advantage when addressing other physics problems requiring advanced mathematical techniques. Using the finite element method in conjunction with the B-spline collocation method promotes a catalytic approach to quantum mechanics research advancement. This work opens the door for revolutionary developments in the discipline by proposing novel approaches and encouraging multidisciplinary collaboration.

The primary goal of the scheme that we suggest in this study is to improve the accuracy of approximate solutions for quantum-mechanical energy, similar to Schrödinger's original answer. Our goal is to show that the nonic B-spline collocation approach, in combination with the finite element method (FEM) and Crank-Nicolson scheme, can be a valuable tool for the efficient implementation of intermediate-level complex analysis of the Schrödinger equation.

The Schrödinger equation is converted into an algebraic system of equations at each step of the procedure, making a numerical solution easier, more dependable, and more effective than other approaches. Optical soliton solutions require managing the complex function's real and imaginary parts.

The Crank-Nicolson method, initially proposed by Crank and Phyllis Nicolson in 1947 for the numerical solution of partial differential equations, emerges as an elegant solution for our purposes. This method is known for its convergence and stability properties across finite values of the Courant number ω , defined as $(\frac{\Delta t}{h^2}) = \omega$. Implementing the Crank-Nicolson method offers an efficient solution to the time-dependent Schrödinger equation, a fundamental tool with extensive utility in various fields of physics such as acoustics and optics. By employing this comprehensive approach, we aim to provide researchers with a robust framework for tackling complex quantum-mechanical problems while shedding light on the practical applications of the Schrödinger equation in diverse physical phenomena.

The non-dimensionalized form of the equation can be written as

$$iv_t + \gamma v_{xx} + p|v|^2v = 0, \tag{1}$$

with the initial conditions

$$v(x, 0) = f(x), \quad a \leq x \leq b, \tag{2}$$

and the boundary conditions

$$\begin{aligned} v(a, t) &= v(b, t) = 0 \\ v_{5x}(a, t) &= v_{5x}(b, t) = v_{6x}(a, t) = v_{6x}(b, t) = 0 \\ v_{7x}(a, t) &= v_{7x}(b, t) = v_{8x}(a, t) = v_{8x}(b, t) = 0, \quad t \in [0, T]. \end{aligned} \tag{3}$$

Here, $\gamma \neq 0$ and $i^2 = -1$ is an imaginary unit, and $f(x)$ is a smooth function.

If $\gamma = -1$ and $p = 0$, then equation (1) becomes

$$iv_t - v_{xx} = 0 \tag{4}$$

The current work is organised as follows: Section 2 suggests and constructs the nonic B-spline. The nonic B-spline is implemented in Section 3. The Section 4 is reported with linear stability analysis. Section 5 discusses numerical examples, and corresponding results are reported in the table and surfed in figures. Section 6 contains a portion of the conclusions.

2. B-SPLINE OF ORDER NINE

Let's find the step length $h = x_{m+1} - x_m, m = 0, 1, \dots, N$, where $m=0, 1, \dots, N$, and divide the interval $[a, b]$ into N equally spaced points x_n such that $a = x_0 < x_1 < \dots < x_N = b$. Next, at the knots x_m , the nonic B-splines $B_m(x), m = -4(1)N + 4$ are provided by:

$$B_m(x) = \frac{1}{h^9} \begin{cases} d_1^9 & x \in I_1 \\ d_1^9 - \binom{10}{1} d_2^9 & x \in I_2 \\ d_1^9 - \binom{10}{1} d_2^9 + \binom{10}{2} d_3^9 & x \in I_3 \\ d_1^9 - \binom{10}{1} d_2^9 + \binom{10}{2} d_3^9 - \binom{10}{3} d_4^9 & x \in I_4 \\ d_1^9 - \binom{10}{1} d_2^9 + \binom{10}{2} d_3^9 - \binom{10}{3} d_4^9 + \binom{10}{4} d_5^9 & x \in I_5 \\ d_6^9 - \binom{10}{1} d_7^9 + \binom{10}{2} d_8^9 - \binom{10}{3} d_9^9 + \binom{10}{4} d_{10}^9 & x \in I_6 \\ d_6^9 - \binom{10}{1} d_7^9 + \binom{10}{2} d_8^9 - \binom{10}{3} d_9^9 & x \in I_7 \\ d_6^9 - \binom{10}{1} d_7^9 + \binom{10}{2} d_8^9 & x \in I_8 \\ d_6^9 - \binom{10}{1} d_7^9 & x \in I_9 \\ d_{10}^9 & x \in I_{10} \\ 0 & otherwise \end{cases} \tag{5}$$

where

$$d_1 = (x - x_{m-5}), d_2 = (x - x_{m-4}), d_3 = (x - x_{m-3}), d_4 = (x - x_{m-2}), d_5 = (x - x_{m-1}), d_6 = (x_{m+5} - x),$$

$$d_7 = (x_{m+4} - x), d_8 = (x_{m+3} - x), d_9 = (x_{m+2} - x), d_{10} = (x_{m+1} - x),$$

$$I_1 = [x_{m-5}, x_{m-4}), I_2 = [x_{m-4}, x_{m-3}), I_3 = [x_{m-3}, x_{m-2}), I_4 = [x_{m-2}, x_{m-1}), I_5 = [x_{m-1}, x_m), I_6 = [x_m, x_{m+1}),$$

$$I_7 = [x_{m+1}, x_{m+2}), I_8 = [x_{m+2}, x_{m+3}), I_9 = [x_{m+3}, x_{m+4}), I_{10} = [x_{m+4}, x_{m+5})$$

The nonic B-splines $B_{-4}, B_{-3}, \dots, B_{N+4}$ constitute a basis over the area of space $[a, b]$. The solution $u(x, t)$, approximating the exact solution $v(x, t)$ of equation (1), is expressed as:

$$u(x, t) = \sum_{m=-4}^{N+4} c_m(t) B_m(x) \tag{6}$$

At each time level, the parameters c_m and $B_m(x)$ are the temporal quantities to be found.

At the mesh points x_m , the nodal values of u_m and its higher-order derivatives were acquired using equations (5) and (6), which are as follows:

$$u_m = c_{m-4} + 502c_{m-3} + 14608c_{m-2} + 88234c_{m-1} + 156190c_m + 88234c_{m+1} + 4608c_{m+2} + 502c_{m+3} + c_{m+4}$$

$$u'_m = \frac{9}{h} (-c_{m-4} - 246c_{m-3} - 4046c_{m-2} - 11326c_{m-1} + 11326c_{m+1} + 4046c_{m+2} + 246c_{m+3} + c_{m+4})$$

$$u''_m = \frac{72}{h^2} (c_{m-4} + 118c_{m-3} + 952c_{m-2} + 154c_{m-1} - 2450c_m + 154c_{m+1} + 952c_{m+2} + 118c_{m+3} + c_{m+4})$$

$$u'''_m = \frac{504}{h^3} (-c_{m-4} - 54c_{m-3} - 134c_{m-2} + 434c_{m-1} - 434c_{m+1} + 134c_{m+2} + 54c_{m+3} + c_{m+4})$$

$$u^{iv}_m = \frac{3024}{h^4} (c_{m-4} + 22c_{m-3} - 32c_{m-2} - 86c_{m-1} + 190c_m - 86c_{m+1} - 32c_{m+2} + 22c_{m+3} + c_{m+4})$$

$$u^v_m = \frac{15120}{h^5} (-c_{m-4} - 6c_{m-3} + 34c_{m-2} - 46c_{m-1} + 46c_{m+1} - 34c_{m+2} + 6c_{m+3} + c_{m+4})$$

$$u^{vi}_m = \frac{60480}{h^6} (c_{m-4} - 2c_{m-3} - 8c_{m-2} + 34c_{m-1} - 50c_m + 34c_{m+1} - 8c_{m+2} - 2c_{m+3} + c_{m+4})$$

$$u^{vii}_m = \frac{181440}{h^7} (-c_{m-4} + 6c_{m-3} - 14c_{m-2} + 14c_{m-1} - 14c_{m+1} + 14c_{m+2} - 6c_{m+3} + c_{m+4})$$

$$u^{viii}_m = \frac{362880}{h^8} (c_{m-4} - 8c_{m-3} + 28c_{m-2} - 56c_{m-1} + 70c_m - 56c_{m+1} + 28c_{m+2} - 8c_{m+3} + c_{m+4}). \tag{7}$$

The continuity of nonic B-splines and their first eight derivatives is ensured.

3. EXECUTION

The current implementation strategy revolves around leveraging a hybrid numerical approach to approximate the equation's solution. The temporal derivatives within the equation are discretised using the forward finite difference method. This method, known for its simplicity and ease of implementation, involves approximating the derivatives by the difference between neighbouring points in time. Discretizing the time derivatives transforms the continuous-time problem into a discrete-time one, enabling numerical computation using iterative techniques.

$$i \frac{(v^{n+1}) - (v^n)}{\Delta t} = \frac{(v_{xx}^{n+1}) + (v_{xx}^n)}{2} \tag{8}$$

With equation (8) established, we derive the recurrence relation (9) through a systematic analysis of the simplified system's behaviour. This involves identifying recurring patterns or dependencies among the system's variables across consecutive time steps, which can be expressed using a recursive formula.

$$\begin{aligned} &\delta_{m,1}c_{m-4}^{n+1} + \delta_{m,2}c_{m-3}^{n+1} + \delta_{m,3}c_{m-2}^{n+1} + \delta_{m,4}c_{m-1}^{n+1} + \delta_{m,5}c_m^{n+1} + \delta_{m,6}c_{m+1}^{n+1} + \delta_{m,7}c_{m+2}^{n+1} + \delta_{m,8}c_{m+3}^{n+1} + \delta_{m,9}c_{m+4}^{n+1} \\ &= \delta_{m,6}c_{m-4}^n + \delta_{m,7}c_{m-3}^n + \delta_{m,8}c_{m-2}^n + \delta_{m,9}c_{m-1}^n + \delta_{m,10}c_m^n + \delta_{m,9}c_{m+1}^n + \delta_{m,8}c_{m+2}^n + \delta_{m,7}c_{m+3}^n + \delta_{m,6}c_{m+4}^n, \end{aligned} \quad (9)$$

where $m = 0, 1, \dots, N$ and i is an imaginary unit.

$$\begin{aligned} \delta_{m,1} &= 2ih^2 - 72\Delta t & \delta_{m,2} &= 1004ih^2 - 8496\Delta t \\ \delta_{m,3} &= 29216ih^2 - 68544\Delta t & \delta_{m,4} &= 176468ih^2 - 11088\Delta t \\ \delta_{m,5} &= 312380ih^2 + 176400\Delta t & \delta_{m,6} &= 2ih^2 + 72\Delta t \\ \delta_{m,7} &= 1004ih^2 + 8496\Delta t & \delta_{m,8} &= 29216ih^2 + 68544\Delta t \\ \delta_{m,9} &= 176468ih^2 + 11088\Delta t & \delta_{m,10} &= 312380ih^2 - 176400\Delta t \end{aligned}$$

Consequently, with the aid of MATLAB, the augmented system (9) is efficiently formulated, incorporating the additional equations derived from the boundary conditions(3). This expanded system now consists of (N+9) equations, precisely matching the number of unknowns, thereby enabling a comprehensive solution. MATLAB's robust numerical solvers facilitate the exploration of the solution space, allowing for accurate and reliable results to be obtained with minimal effort.

$$A_1 \bar{\alpha}^{n+1} = A_2(\alpha^n) \quad (10)$$

where, $\bar{\alpha}^{n+1} = [c_{-4}^{n+1} \ c_{-3}^{n+1} \ \dots \ c_{N+4}^{n+1}]^T$, A_1, A_2 are $(N + 9) \times (N + 9)$ and $(N + 9) \times 1$ matrix respectively.

$$A_1 = \begin{pmatrix} 1 & 502 & 14608 & 88234 & 156190 & 88234 & 14608 & 502 & 1 \\ -1 & -54 & -134 & 434 & 0 & -434 & 134 & 54 & 1 \\ -1 & -6 & 34 & -46 & 0 & 46 & -34 & 6 & 1 \\ -1 & 6 & -14 & 14 & 0 & -14 & 14 & -6 & 1 \\ \delta_{0,1} & \delta_{0,2} & \delta_{0,3} & \delta_{0,4} & \delta_{0,5} & \delta_{0,4} & \delta_{0,3} & \delta_{0,2} & \delta_{0,1} \\ & \delta_{1,1} & \delta_{1,2} & \delta_{1,3} & \delta_{1,4} & \delta_{1,5} & \delta_{1,4} & \delta_{1,3} & \delta_{1,2} & \delta_{1,1} \\ & & - & - & - & - & - & - & - & - \\ & & & \delta_{N-1,1} & \delta_{N-1,2} & \delta_{N-1,3} & \delta_{N-1,4} & \delta_{N-1,5} & \delta_{N-1,4} & \delta_{N-1,3} & \delta_{N-1,2} & \delta_{N-1,1} \\ & & & & \delta_{N,1} & \delta_{N,2} & \delta_{N,3} & \delta_{N,4} & \delta_{N,5} & \delta_{N,4} & \delta_{N,3} & \delta_{N,2} & \delta_{N,1} \\ & & & & & 1 & 502 & 14608 & 88234 & 156190 & 88234 & 14608 & 502 & 1 \\ & & & & & & -1 & -54 & -134 & 434 & 0 & -434 & 134 & 54 & 1 \\ & & & & & & -1 & -6 & 34 & -46 & 0 & 46 & -34 & 6 & 1 \\ & & & & & & & -1 & 6 & -14 & 14 & 0 & -14 & 14 & -6 & 1 \end{pmatrix}$$

Initial state

To evaluate the initial vector α^0 and the solution space $u(x, t)$ is decomposed into complex form as follows:

$$u(x, t) = X(x, t) + iY(x, t). \quad (11)$$

Here, X and Y are real coefficients. We derive the associated coupled pair of real differential equations by substituting equation (11) into equation (4).

$$X_t - Y_{xx} = 0 \quad \text{and} \quad X_t + Y_{xx} = 0 \quad (12)$$

In the collocation method implementation, loops are recognised as collocation sites for systems. (11) and (12). The nonic B-splines $B_m(x)$ provide solutions for global approximation by expressing $X(x, t)$ and $Y(x, t)$ as expansions:

$$X_N(x, t) = \sum_{m=-4}^{N+4} \alpha_m(t)B_m(x), \quad \text{and} \quad Y_N(x, t) = \sum_{m=-4}^{N+4} \beta_m(t)B_m(x) \quad (13)$$

In this case, the parameters η_i and ζ_i must be found gradually. equation (12) and the B-splines found in equation (5) are used to estimate the solution of equation (4) by obtaining the initial parameters, α_m^0 and β_m^0 . This leads to a system of $(2N+18)$ equations containing $2N$ unknowns. equation (3) yields the subsequent equations derived from boundary conditions.

$$\begin{aligned}
 X_N^v(a, 0) &= (-\alpha_{-4}^0 - 6\alpha_{-3}^0 + 34\alpha_{-2}^0 - 46\alpha_{-1}^0 + 46\alpha_1^0 - 34\alpha_2^0 + 6\alpha_3^0 + \alpha_4^0) = 0 \\
 X_N^{vi}(a, 0) &= (\alpha_{-4}^0 - 2\alpha_{-3}^0 - 8\alpha_{-2}^0 + 34\alpha_{-1}^0 - 50\alpha_0^0 + 34\alpha_1^0 - 8\alpha_2^0 - 2\alpha_3^0 + \alpha_4^0) = 0 \\
 X_N^{vii}(a, 0) &= (-\alpha_{-4}^0 + 6\alpha_{-3}^0 - 14\alpha_{-2}^0 + 14\alpha_{-1}^0 - 14\alpha_1^0 + 14\alpha_2^0 - 6\alpha_3^0 + \alpha_4^0) = 0 \\
 X_N^{viii}(a, 0) &= (\alpha_{-4}^0 - 8\alpha_{-3}^0 + 28\alpha_{-2}^0 - 56\alpha_{-1}^0 + 70\alpha_0^0 - 56\alpha_1^0 + 28\alpha_2^0 - 8\alpha_3^0 + \alpha_4^0) = 0 \\
 X_N(x, 0) &= (\alpha_{m-4}^0 + 502\alpha_{m-3}^0 + 14608\alpha_{m-2}^0 + 88234\alpha_{m-1}^0 + 156190\alpha_m^0 + 88234\alpha_{m+1}^0 + 4608\alpha_{m+2}^0 + 502\alpha_{m+3}^0 + \alpha_{m+4}^0) \\
 &= X(x_m, 0) \\
 X_N^v(b, 0) &= (-\beta_{N-4}^0 - 6\beta_{N-3}^0 + 34\beta_{N-2}^0 - 46\beta_{N-1}^0 + 46\beta_{N+1}^0 - 34\beta_{N+2}^0 + 6\beta_{N+3}^0 + \beta_{N+4}^0) = 0 \\
 X_N^{vi}(b, 0) &= (\beta_{N-4}^0 - 2\beta_{N-3}^0 - 8\beta_{N-2}^0 + 34\beta_{N-1}^0 - 50\beta_N^0 + 34\beta_{N+1}^0 - 8\beta_{N+2}^0 - 2\beta_{N+3}^0 + \beta_{N+4}^0) = 0 \\
 X_N^{vii}(b, 0) &= (-\beta_{N-4}^0 + 6\beta_{N-3}^0 - 14\beta_{N-2}^0 + 14\beta_{N-1}^0 - 14\beta_{N+1}^0 + 14\beta_{N+2}^0 - 6\beta_{N+3}^0 + \beta_{N+4}^0) = 0 \\
 X_N^{viii}(b, 0) &= (\beta_{N-4}^0 - 8\beta_{N-3}^0 + 28\beta_{N-2}^0 - 56\beta_{N-1}^0 + 70\beta_N^0 - 56\beta_{N+1}^0 + 28\beta_{N+2}^0 - 8\beta_{N+3}^0 + \beta_{N+4}^0) = 0.
 \end{aligned}
 \tag{14}$$

Analogously, $Y_N(x, t)$ may be derived. The initial vector c_m^0 is computed as $c_m^0 = \alpha_m^0 + i\beta_m^0$, where i denotes the imaginary unit.

4. STUDY OF STABILITY

Examining the robustness of a methodology includes pinpointing the scenarios in which the divergence between theoretical expectations and numerical approximations remains limited with successive temporal iterations. Utilising the Von-Neumann technique aids in validating the stability of the method.

Consider

$$\phi_i^n = E\phi^n e^{i\varphi Kh}, \tag{15}$$

where $i = \sqrt{-1}$ represents an imaginary unit, E represents the amplitude, ϕ is the amplification factor, h represents the spatial step length, and φ is the mode number.

Now, applying equation (15) in the equation (9) and after simplification, we obtained

$$\begin{aligned}
 \phi^{n+1}[a_1 e^{-4i\varphi h} + a_2 e^{-3i\varphi h} + a_3 e^{-2i\varphi h} + a_4 e^{-i\varphi h} + a_5 + a_6 e^{i\varphi h} + a_7 e^{2i\varphi h} + a_8 e^{3i\varphi h} + a_9 e^{4i\varphi h}] = \\
 \phi^n [b_1 e^{-4i\varphi h} + b_2 e^{-3i\varphi h} + b_3 e^{-2i\varphi h} + b_4 e^{-i\varphi h} + b_5 + b_6 e^{i\varphi h} + b_7 e^{2i\varphi h} + b_8 e^{3i\varphi h} + b_9 e^{4i\varphi h}]
 \end{aligned}
 \tag{16}$$

Applying Euler's formula $e^{\pm i\varphi h} = \cos(\varphi h) \pm i(\sin(\varphi h))$ to equation (16)

$$\frac{\phi^{n+1}}{\phi^n} = \frac{B_1 + iC_1}{B_2 - iC_2}, \tag{17}$$

where

$$\begin{aligned}
 B_1 &= (b_1 + b_9)\cos(4\varphi h) + (b_2 + b_8)\cos(3\varphi h) + (b_3 + b_7)\cos(2\varphi h) + (b_4 + b_6)\cos(\varphi h) + b_5 \\
 C_1 &= (b_1 - b_9)\sin(4\varphi h) + (b_2 - b_8)\sin(3\varphi h) + (b_3 - b_7)\sin(2\varphi h) + (b_4 - b_6)\sin(\varphi h) \\
 B_2 &= (a_1 + a_9)\cos(4\varphi h) + (a_2 + a_8)\cos(3\varphi h) + (a_3 + a_7)\cos(2\varphi h) + (a_4 + a_6)\cos(\varphi h) + a_5 \\
 C_2 &= (a_1 - a_9)\sin(4\varphi h) + (a_2 - a_8)\sin(3\varphi h) + (a_3 - a_7)\sin(2\varphi h) + (a_4 - a_6)\sin(\varphi h).
 \end{aligned}
 \tag{18}$$

Check the stability condition $|\frac{\phi^{n+1}}{\phi^n}| \leq 1$, we get

$$B_1^2 + C_1^2 - B_2^2 - C_2^2 \leq 1. \tag{19}$$

Consequently, the proposed scheme exhibits unconditional stability.

5. NUMERICAL ILLUSTRATIONS AND CONVERSATIONS

Three test problems are examined to assess the present study's efficiency and accuracy. The accuracy of the methods is evaluated in this section by computing the error norms L_2 and the maximum absolute error norm L_∞ , defined as follows:

By computing both the L_2 and L_∞ , error norms for each test problem, the study can effectively evaluate the accuracy of the methods across different scenarios and provide a comprehensive assessment of their performance. These error norms serve as valuable metrics for quantifying the discrepancy between computed and exact solutions, thereby informing decisions regarding the suitability and reliability of the computational methods employed in the study.

$$L_\infty = \max_{0 \leq m \leq N} |u_m - v_m|$$

$$L_2 = \sqrt{h \sum_{m=0}^N |(u_m - v_m)^2|}$$

Where u_m and v_m represent the exact and numerical solutions, respectively. MATLAB R2019 and MATHEMATICA software were utilised for numerical simulations.

Example-1. Solve the equation (4) commencing with the exact solution within the domain

$$v(x, t) = e^{\frac{-it+x}{2}}, \quad x \in [0, \pi]$$

followed by the initial condition $v(x, 0) = e^{\frac{x}{2}}$ and boundary conditions

$$v(-\pi, t) = v(\pi, t) = v_{5x}(-\pi, t) = v_{5x}(\pi, t) = v_{6x}(-\pi, t) = v_{6x}(\pi, t) = v_{7x}(-\pi, t) = v_{7x}(\pi, t) = v_{8x}(-\pi, t) = v_{8x}(\pi, t) = 0, \quad t \in [0, T].$$

Solution.

The numerical solution, along with error norms L_2 and L_∞ , incorporating absolute error at parameters $\Delta t = 0.01$, $h = 0.05$, $x \in [0, \pi]$, and $x \in [0, \pi]$ fo or various time steps t is as follows:

Observations from Table 1.

- As time progresses, the absolute errors in the numerical solution tend to increase. This indicates that the accuracy of the numerical solution decreases over time.
- Conversely, the error norms L_2 and L_∞ decrease as time advances from $t = 2$ to $t = 4$. This implies that, although the absolute errors increase, the overall discrepancy between the numerical and exact solutions decreases.

Table 1. Numerical solution with error norms at the parameters $\Delta t = 0.01, h = 0.05, x \in [0, \pi]$ for Example-1.

x	t = 1			t = 4		
	Numerical	Exact	Absolute Error	Numerical	Exact	Absolute Error
0.20	0.329963 - 0.513877i	0.329963 - 0.513887i	9.712170e - 06	-0.399172 + 0.462174i	-0.399181 + 0.462180i	9.841173e - 06
0.30	0.364670 - 0.567915i	0.364665 - 0.567933i	1.843042e - 05	-0.441153 + 0.51078i	-0.441163 + 0.510788i	1.172312e - 05
0.50	0.445413 - 0.693649i	0.445403 - 0.693675i	2.800452e - 05	-0.538829 + 0.623867i	-0.538838 + 0.623878i	1.364284e - 05
0.60	0.492253 - 0.766603i	0.492247 - 0.766630i	2.672546e - 05	-0.595497 + 0.689477i	-0.595508 + 0.689492i	1.795372e - 05
1.20	0.896940 - 1.396860i	0.896933 - 1.396891i	3.129149e - 05	-1.085095 + 1.256315i	-1.085086 + 1.256336i	2.239132e - 05
1.50	1.210741 - 1.885569i	1.210733 - 1.885605i	3.741733e - 05	-1.464716 + 1.695852i	-1.464713 + 1.695876i	2.402096e - 05
1.60	1.338075 - 2.083884i	1.338067 - 2.083916i	3.310374e - 05	-1.618761 + 1.874208i	-1.618759 + 1.874233i	2.529512e - 05
1.70	1.478800 - 2.303052i	1.478793 - 2.303083i	3.227069e - 05	-1.789007 + 2.071320i	-1.789005 + 2.071348i	2.837233e-05
2.50	3.291092 - 5.125581i	3.291114 - 5.125607i	3.435566e - 05	-3.981497 + 4.609828i	-3.981504 + 4.609870i	4.318684e - 05
3.10	5.996802 - 9.339465i	5.996802 - 9.339465i	8.881784e - 16	-7.254774 + 8.399732i	-7.254774 + 8.399732i	1.776356e - 15
L_2	5.0676e - 05			4.8695e - 05		
L_∞	2.7220e - 05			2.6560e - 05		

Plotting Numerical Solution vs. Exact Solutions.

Figure 1 illustrates the natural part, and Figure 2 depicts the imaginary part of the numerical solutions compared to the exact solutions. The curves in these plots overlap closely, indicating that the numerical solutions are approximately equal to the analytical solution.

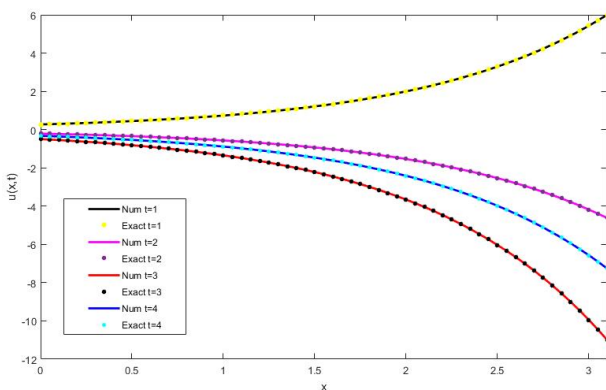


Figure 1. Comparison of numerical solution with exact solution (Real) of Example-1

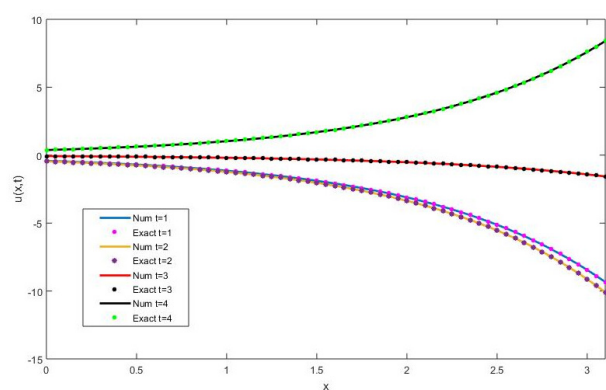


Figure 2. Comparison of numerical solution with analytical solution (Imaginary) of Example 1

3D Comparison of Numerical Solutions and Analytical Solutions:

Figures 3 and 4 present 3D plots comparing the numerical and analytical solutions. These plots, at parameters $h = \Delta t = 0.1$, $t = 4$, $x \in [0, \pi]$, demonstrate the approximate nature of the numerical solutions. The close alignment between the surfaces suggests that the numerical solutions closely resemble the analytical solutions.

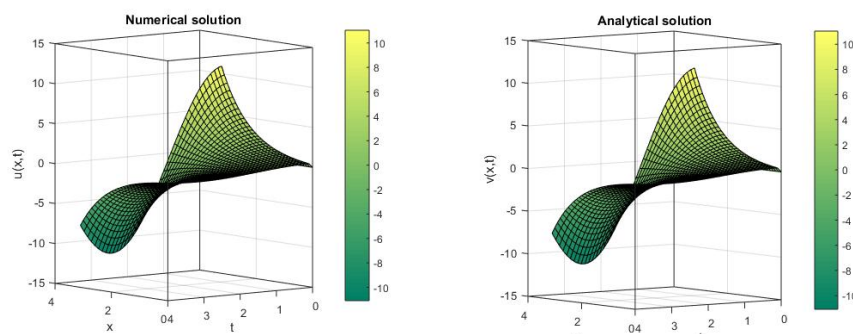


Figure 3. 3D plot of comparison of numerical with analytical solution (Real) of Example 1

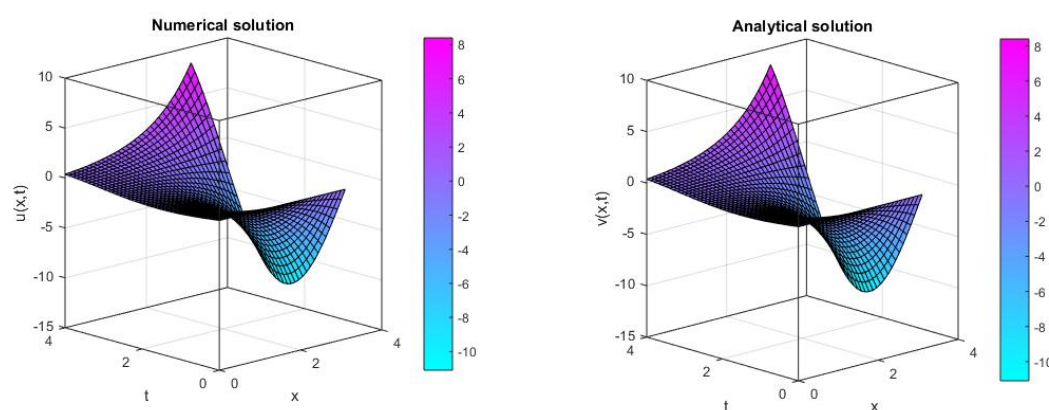


Figure 4. 3D plot of comparison of numerical with analytical solution (Imaginary) of Example 1
The 3D plot of the numerical solution of (a) real and (b) imaginary at $h = \Delta t = 0.1$, $t = 4$, $x \in [0, \pi]$.

6. CONCLUSION

This study provides a comprehensive approach to approximate solutions to the Schrödinger equation in quantum mechanics using the nonic B-spline technique. An intermediate level of knowledge in complex analysis is necessary for this strategy, especially when defining and applying B-spline collocation techniques. We stress that the B-spline collocation method can solve a broad range of analytically solvable quantum mechanical problems, not just the Schrödinger equation. We provide a reliable framework for solving the Schrödinger equation quickly by fusing the finite element method (FEM) with the nonic B-spline collocation method. We have thoroughly evaluated inaccuracy, stability, and convergence to verify the suggested plan's efficacy. We look into the three conservation constants' approximations and assess them.

ORCID

Archana Senapati, <https://orcid.org/0009-0001-7180-5194>; Balaji Padhy, <https://orcid.org/0000-0002-3447-2917>
Shashikant Das, <https://orcid.org/0000-0002-8568-5082>

REFERENCES

- [1] M. Ahsan, I. Ahmad, M. Ahmad, and I. Hussian, "A numerical Haar wavelet-finite difference hybrid method for linear and non-linear Schrodinger equation," *Mathematics and Computers in Simulation*, **165**, 13-25 (2019). <https://doi.org/10.1016/j.matcom.2019.02.011>
- [2] M.A. Akbar, N.H.M. Ali, and R. Roy, "Closed-form solutions of two-time fractional nonlinear wave equations," *Results in Physics*, **9**, 1031-1039 (2018). <https://doi.org/10.1016/j.rinp.2018.03.059>
- [3] S. Arora, and I. Kaur, "Applications of quintic Hermite collocation with time discretisation to singularly perturbed problems," *Applied Mathematics and Computation*, **316**, 409-421 (2018). <https://doi.org/10.1016/j.amc.2017.08.040>
- [4] A. Başhan, "A mixed methods approach to Schrodinger equation: Finite difference method and quartic B-spline based differential quadrature method," *An International Journal of Optimization and Control: Theories & Applications*, **9**(2), 223-235 (2019). <https://doi.org/10.11121/ijocta.01.2019.00709>
- [5] L. Cheng, and Y. Zhang, "Breather-type solutions and rogue waves to a generalised (2++1)-dimensional nonlinear Schrodinger equation," *Pramana – J. Phys.* **96**, 52 (2022). <https://doi.org/10.1007/s12043-022-02293-3>

- [6] A. Esen, and O. Tasbozan, "Numerical solution of time-fractional Schrodinger equation by using quadratic B-spline finite elements," In *Annales Mathematicae Silesianae*, **31**(1), 83-98 (2017). <https://eudml.org/doc/288345>
- [7] D. Fyfe, "The use of cubic splines in the solution of two-point boundary value problems," *The computer journal*, **12**(2), 188-192 (1969). <https://doi.org/10.1093/comjnl/12.2.188>
- [8] A.R. Hadhoud, A.A. Rageh, and T. Radwan, "Computational solution of the time-fractional Schrodinger equation by using trigonometric B-spline collocation method," *Fractal and Fractional*, **6**(3), 127 (2022). <https://doi.org/10.3390/fractalfract6030127>
- [9] Q. Huang, C. Ruan, Z. Huang, and J. Huang, "Soliton solutions to a reverse-time non-local nonlinear Schrodinger differential equation," *Pramana – J. Phys.* **97**, 14 (2023). <https://doi.org/10.1007/s12043-022-02491-z>
- [10] A. Iqbal, N.N. Abd Hamid, and A.I.M. Ismail, "Cubic B-spline Galerkin method for numerical solution of the coupled nonlinear Schrodinger equation," *Mathematics and Computers in Simulation*, **174**, 32-44 (2020). <https://doi.org/10.1016/j.matcom.2020.02.017>
- [11] S.R. Jena, A. Senapati, and G.S. Gebremedhin, "Approximate solution of MRLW equation in B-spline environment," *Mathematical Sciences*, **14**(4), 345-357 (2020). <https://doi.org/10.1007/s40096-020-00345-6>
- [12] M.K. Kadalbajoo, and A. Awasthi, "Crank–Nicolson finite difference method based on a midpoint upwind scheme on a non-uniform mesh for time-dependent singularly perturbed convection-diffusion equations," *International Journal of Computer Mathematics*, **85**(5), 771-790 (2008). <https://doi.org/10.1080/00207160701459672>
- [13] S.R. Jena, and A. Senapati, "One-dimensional heat and advection-diffusion equation is based on improvised cubic B-spline collocation, the finite element method, and the Crank-Nicolson technique," *International Communications in Heat and Mass Transfer*, **147**, 106958 (2023). <https://doi.org/10.1016/j.icheatmasstransfer.2023.106958>
- [14] A. Khan, M. Ahsan, E. Bonyah, R. Jan, M. Nisar, A.H. Abdel-Aty, and I.S. Yahia, "Numerical Solution of Schrodinger Equation by Crank–Nicolson Method," *Mathematical Problems in Engineering*, **2022**, 991067 (2022). <https://doi.org/10.1155/2022/6991067>
- [15] A. Konguetsof, "A new two-step hybrid method for the numerical solution of the Schrodinger equation," *Journal of mathematical chemistry*, **47**(2), 871-890 (2010). <https://doi.org/10.1007/s10910-009-9606-5>
- [16] L. Lehtovaara, J. Toivanen, and J. Eloranta, "Solution of time-independent Schrodinger equation by the imaginary time propagation method," *Journal of Computational Physics*, **221**(1), 148-157 (2007). <https://doi.org/10.1016/j.jcp.2006.06.006>
- [17] T.R. Lucas, "Error bounds for interpolating cubic splines under various end conditions," *SIAM Journal on Numerical Analysis*, **11**(3), 569-584 (1974). <https://doi.org/10.1137/0711049>
- [18] M. Modanli, and F. Ozbag, "Stability of finite difference schemes for two-space dimensional telegraph equation," *Pramana – J. Phys.* **96**, 228 (2022). <https://doi.org/10.1007/s12043-022-02474-0>
- [19] Y.S. Ozkan, E. Yaşar, and A.R. Seadawy, "A third-order nonlinear Schrodinger equation: the exact solutions, group-invariant solutions and conservation laws," *Journal of Taibah University for Science*, **14**(1), 585-597 (2020). <https://doi.org/10.1080/16583655.2020.1760513>
- [20] J. Rana, and S. Liao, "On-time independent Schrodinger equations in quantum mechanics by the homotopy analysis method," *Theoretical and Applied Mechanics Letters*, **9**(6), 376-381 (2019). <https://doi.org/10.1016/j.taml.2019.05.006>
- [21] B. Saka, "A quintic B-spline finite-element method for solving the nonlinear Schrodinger equation," *Physics of Wave Phenomena*, **20**(2), 107-117 (2012). <http://doi.org/10.3103/s1541308x12020033>
- [22] A. Senapati, and S.R. Jena, "Generalized Rosenau-RLW equation in B-spline scheme via BFRK approach," *Nonlinear Studies*, **30**(1), 73-85 (2023).
- [23] A. Senapati, and S.R. Jena, "A computational scheme for fifth-order boundary value problems," *International Journal of Information Technology*, **14**(3), 1397-1404 (2022). <https://doi.org/10.1007/s41870-022-00871-7>
- [24] D.Y. Shi, and H.J. Yang, "Superconvergence analysis of a new linearised MFEM for nonlinear Schrodinger equation," *International Journal of Computer Mathematics*, **96**(7), 1514–1531 (2018). <https://doi.org/10.1080/00207160.2018.1527909>
- [25] T.E. Simos, "A new Numerov-type method for the numerical solution of the Schrodinger equation," *Journal of mathematical chemistry*, **46**(3), 981-1007 (2009). <https://doi.org/10.1007/s10910-009-9553-1>
- [26] T.A. Sulaiman, A. Yusuf, and M. Alquran, "Dynamics of optical solitons and non-autonomous complex wave solutions to the nonlinear Schrodinger equation with variable coefficients," *Nonlinear Dynamics*, **104**, 639-648 (2021). <https://doi.org/10.1007/s11071-021-06284-8>

СКІНЧЕННО-РІЗНИЦЕВИЙ ПІДХІД ВИЩОГО ПОРЯДКУ В-СПЛАЙНА ДЛЯ РІВНЯННЯ ШРЕДІНГЕРА У КВАНТОВІЙ МЕХАНІЦІ

Арчана Сенapati, Баладжі Падхі, Шашікант Дас

Університет технологій та менеджменту Центуріон, Одіша, Індія

У цій статті представлено новий чисельний метод розв'язування квантово-механічного комплексного рівняння Шредінгера (CSE). Методика поєднує схему Кренка-Ніколсона другого порядку, засновану на методі скінченних елементів (FEM) для часової дискретизації з неничними В-сплайновими функціями для просторової дискретизації. Цей метод є безумовно стійким за допомогою аналізу стабільності фон-Неймана. Щоб перевірити нашу методологію, ми перевірили експеримент, використовуючи низку норм помилок, щоб порівняти експериментальні результати з аналітичними рішеннями. Наше дослідження підтверджує, що запропонований підхід працює краще, ніж поточні методи, забезпечуючи кращу точність і ефективність квантово-механічного аналізу помилок.

Ключові слова: метод Кренка-Ніколсона; *finite element method*; оцінка стійкості за фон-Нейманом; В-сплайн

IMPACT OF ION PRESSURE ANISOTROPY IN COLLISIONAL QUANTUM MAGNETO-PLASMA WITH HEAVY AND LIGHT IONS

 Deepsikha Mahanta^a,  Swarniv Chandra^b,  Jnanjyoti Sarma^c

^aDepartment of Mathematics, Gauhati University, Guwahati 781014, India

^bDepartment of Physics, Govt. General Degree College at Kushmandi, Dakshin Dinajpur, 733121, India;
Institute of Natural Sciences and Applied Technology, Kolkata 700032, India

^cDepartment of Mathematics, Radha Govinda Baruah College, Guwahati 781025, India

*Corresponding Author e-mail: mahanta2017@gmail.com

Received May 25, 2024; revised July 16, 2024; in final form August 4, 2024; accepted August 12, 2024

We have examined collisional degenerate plasma composed of charged state of heavy positive ion and light positive as well as negative ion. Employing the reductive perturbation method, we derived the damped Korteweg-de Vries-Burgers (dKdV-B) equation and by using its standard solution we analyze the characteristics of the solitary-shock profile under varying parameters. Furthermore, with the application of planar dynamical systems bifurcation theory, the phase portraits have been analyzed. This dynamical system analysis allowed us to extract important information on the stability of these structures as represented by the dKdV-B equation.

Keywords: *dKdV-B Equation; Quantum Plasma; Dynamical System; Reductive perturbation method; Pressure Anisotropy*

PACS: 02.30.Jr, 52.30-q, 45.30.+s, 52.27Lw

1. INTRODUCTION

The physics of quantum plasmas comprising both positive and negative ions, particularly multi-ion plasmas have garnered significant attention recently due to its obligatory presence from laboratory to astrophysical plasma environments [1–4]. The constituents of the degenerate quantum plasma includes electrons, heavy ions with positive charges, and light ions [5]. Electrons, positive ions, and negative ions are all present in negative ion plasma. A portion of the electrons in these kinds of plasmas are bound to negative ions. Negative ion plasma can be created in a laboratory and is a naturally occurring phenomenon in space and astrophysical surroundings. Examples of plasma systems containing negative ions are plasma processing reactors, the Sun's photosphere, the D region of the ionosphere, and neutral beam sources. Both theoretical and practical research has shown that the presence of these negative ions dramatically changes a number of distinctive plasma phenomena. Electronic behavior and the plasma potential are altered by negative ions. It is also commonly known that negative ions exist in the comet Halley's comet [6] and the Earth's ionosphere [7]. Positive-negative ion plasmas have also been discovered to exist in a variety of settings, including neutral beam sources [8], low-temperature laboratory studies [9], reactors for plasma processing [10], etc. Numerous authors [4, 11–14] used positively charged heavy and light ions in quantum plasmas to study nonlinear waves. Akhtar and Hussain [15] investigated ion acoustic shock waves in degenerate plasma with negative ions, They found that quantum parameters, temperature of positive and negative ions have significant impact on shock wave structure in negative ion degenerate plasma. Hussain and Akhtar [16] studied collisional effects in negative ion plasmas in the presence of degenerate electrons. Mohsenpour et al [17] studied ion acoustic solitons in negative ion degenerate plasma. they found that negative ion parameters have influence on width and amplitude of the soliton.

In the presence of elevated magnetic fields, the plasma ion pressure exhibits anisotropic behavior, and the plasma behaves differently in parallel and perpendicular directions relative to the external magnetic field [18]. So, to consider the effect of ionic pressure anisotropy pressure i.e., the parallel (P_{\parallel}) and perpendicular (P_{\perp}) ion pressure become very important. Numerous studies have been reported on the impact of pressure anisotropy on the propagation of solitary and shock waves in different plasma regimes [19, 20]. For example, Almas et al. [21] investigated the properties of ion-acoustic solitary waves composed of anisotropic pressure of electron-positron-ion (e-p-i) plasma and found that the characteristics of such waves are more sensitive to parallel ion pressure than perpendicular ion pressure. Khalid et al. [22] also studied the propagation of ion-acoustic electrostatic waves in a magnetized electron-ion plasma with pressure anisotropy. Mahmood et al. [23] studied the properties of non-linear electrostatic structure in anisotropic pressure plasma and found that only the width of the soliton depends on the perpendicular pressure (P_{\perp}), however, an increase in the parallel pressure (P_{\parallel}) decreases both the amplitude as well as the width of the soliton. Manesh et al. [24] studied the properties of solitary waves in an anisotropic plasma with lighter and heavier ions and found that the light ion's pressure anisotropy determines the polarity of solitary waves, and it is rarefactive for anisotropic lighter ion whereas compressive for the isotropic lighter ion. Khan et al. [25] studied the properties of soliton and cnoidal wave in an anisotropic superthermal electron-positron-ion plasma and found that the wavelength of the cnoidal wave structure is reduced on increasing the parallel and perpendicular

anisotropy of ion. Khalid and Rahman [26] studied the ion pressure anisotropy of the ion acoustic non-linear periodic waves in a magnetized plasma. They reported that the increase of parallel pressure of ions decreases the amplitude and width of the ion-acoustic periodic waves and the ion-acoustic waves behave differently than ion-acoustic periodic (cnoidal) waves in anisotropic plasmas.

Apart from classical plasmas, the effect of pressure anisotropy has been widely investigated in dense quantum magnetized plasmas. For example, Bordbar and Karami [27] studied the structural properties of an anisotropic dense neutron star and analyzed the compactness, redshift, etc. of such a dense matter as a function strong magnetic field of the order of 10^{17} Gauss which creates the anisotropy. Patidar and Sharma [28] explored the MHD wave modes in anisotropic relativistic degenerate plasma and found fast and slow wave modes propagating under the combined influence of various forces such as pressure anisotropy, exchange potential, Bohm force, and magnetic field. Irfan et al. [29] observed a strong modification of amplitude and width of weakly nonlinear ion-acoustic waves considering the pressure anisotropy of positive ions and electron trapping effects in a dense quantum magneto-plasma. Moreover, in the non-relativistic and ultra-relativistic regimes, the anisotropic ion pressure also affects the stability of solitary waves.

Various nonlinear waves, such as shock, solitary, rogue, etc., present in our environment are addressed using different mathematical nonlinear equations like Zakharov-Kuznetsov Burger (ZKB) equation, Korteweg-de-Vries (KdV) equation, Non-linear Schrodinger (NLSE) equation, Burgers equation etc [30–33]. In plasma, damping of various types of nonlinear waves can occur due to collisions between plasma species, elevated temperature of the inertial providing fluid, fluid viscosity, nonlinear Landau damping, among other factors. Most of the natural systems are not in perfect equilibrium, nearly all plasma waves experience some degree of damping [34–46]. The propagation of nonlinear waves is significantly influenced by particle collisions. Findings revealed that the effect of collision between charged particles may have a substantial impact on the wave’s characteristics [47, 48].

Phase plane analysis is an effective technique for exploring the qualitative behavior of dynamical systems, a graphical approach specifically designed for examining second-order systems concerning their initial condition. Geometrically, in a phase plane, the trajectory of a dynamical system for a given initial condition is represented by a curve or point. Additionally, this technique allows us to get information about the stability of the system and gain further insight into the existence of solutions [49]. The significance of phase plane analysis in understanding the qualitative solutions of plasma systems is commonly acknowledged and used by researchers [50–53]. Recently, in various plasma systems, researchers have examined the bifurcation features of small-amplitude nonlinear waves within the framework of equations such as the Burgers equation [54], ZK equation [55], etc. [56, 57]

The objective of the present paper is to study the solitary-shock wave propagation in collisional quantum magneto-plasma considering the ionic pressure anisotropy as well as anisotropic viscosities. The damped Korteweg-de Vries Burger (dKdV-B) equation is derived using the RPT to study the shock wave nature in such plasma. These plasmas are believed to exist in white dwarfs and neutron stars. The results obtained here may be useful for laboratory as well as space astrophysical plasma environments wherein such plasma environments are prevalent. The manuscript is arranged as follows, Section 2 contains the detail theoretical formulation, Section 3 contains methodologies as well as detail derivations of dKdV-B Equation, Section 4 contains the results and discussion part, Section 5 contains the Dynamical system analysis and overall conclusion is presented in Section 6.

2. THEORETICAL FORMULATION

We consider a collisional plasma composed of charged state of heavy positive ion and light positive as well as negative ion. The normalized set of governing equations is given by [58]:

$$\frac{\partial N_{ln,lp}}{\partial T} + \frac{\partial(N_{ln,lp}V_{ln,lp_x})}{\partial x} + \frac{\partial(N_{ln,lp}V_{ln,lp_y})}{\partial y} + \frac{\partial(N_{ln,lp}V_{ln,lp_z})}{\partial z} = 0 \tag{1}$$

$$\frac{\partial V_{lnx}}{\partial T} + \left(V_{lnx} \frac{\partial}{\partial x} + V_{lny} \frac{\partial}{\partial y} + V_{lnz} \frac{\partial}{\partial z} \right) V_{lnx} = \vartheta \frac{\partial \Phi}{\partial x} + \eta_{ln\parallel} \frac{\partial^2 V_{lnx}}{\partial x^2} - P_{ln\parallel} N_{ln} \frac{\partial N_{ln}}{\partial x} - \nu_{ln} V_{lnx} \tag{2}$$

$$\frac{\partial V_{lny}}{\partial T} + \left(V_{lnx} \frac{\partial}{\partial x} + V_{lny} \frac{\partial}{\partial y} + V_{lnz} \frac{\partial}{\partial z} \right) V_{lny} = \vartheta \frac{\partial \Phi}{\partial y} + \eta_{ln\perp} \frac{\partial^2 V_{lny}}{\partial y^2} + V_{lnz} \Omega_{ln} - P_{ln\perp} \frac{1}{N_{ln}} \frac{\partial N_{ln}}{\partial y} - \nu_{ln} V_{lny} \tag{3}$$

$$\frac{\partial V_{lnz}}{\partial T} + \left(V_{lnx} \frac{\partial}{\partial x} + V_{lny} \frac{\partial}{\partial y} + V_{lnz} \frac{\partial}{\partial z} \right) V_{lnz} = \vartheta \frac{\partial \Phi}{\partial z} + \eta_{ln\perp} \frac{\partial^2 V_{lnz}}{\partial z^2} + V_{lny} \Omega_{ln} - P_{ln\perp} \frac{1}{N_{ln}} \frac{\partial N_{ln}}{\partial z} - \nu_{ln} V_{lnz} \tag{4}$$

$$\frac{\partial V_{lp_x}}{\partial T} + \left(V_{lp_x} \frac{\partial}{\partial x} + V_{lp_y} \frac{\partial}{\partial y} + V_{lp_z} \frac{\partial}{\partial z} \right) V_{lp_x} = -\frac{\partial \Phi}{\partial x} + \eta_{lp\parallel} \frac{\partial^2 V_{lp_x}}{\partial x^2} - P_{lp\parallel} N_{lp} \frac{\partial N_{lp}}{\partial x} - \nu_{lp} V_{lp_x} \tag{5}$$

$$\frac{\partial V_{lp_y}}{\partial T} + \left(V_{lp_x} \frac{\partial}{\partial x} + V_{lp_y} \frac{\partial}{\partial y} + V_{lp_z} \frac{\partial}{\partial z} \right) V_{lp_y} = -\frac{\partial \Phi}{\partial y} + \eta_{lp\perp} \frac{\partial^2 V_{lp_y}}{\partial y^2} + V_{lp_z} \Omega_{lp} - P_{lp\perp} \frac{1}{N_{lp}} \frac{\partial N_{lp}}{\partial y} - \nu_{lp} V_{lp_y} \tag{6}$$

$$\frac{\partial V_{lpz}}{\partial T} + \left(V_{lpz} \frac{\partial}{\partial x} + V_{lpy} \frac{\partial}{\partial y} + V_{lpz} \frac{\partial}{\partial z} \right) V_{lpz} = -\frac{\partial \Phi}{\partial z} + \eta_{lp\perp} \frac{\partial^2 V_{lpz}}{\partial z^2} + V_{lpy} \Omega_{lp} - P_{lp\perp} \frac{1}{N_{lp}} \frac{\partial N_{lp}}{\partial z} - \nu_{lp} V_{lpz} \quad (7)$$

$$\frac{\partial^2 \phi}{\partial x^2} + \frac{\partial^2 \phi}{\partial y^2} + \frac{\partial^2 \phi}{\partial z^2} = N_e [1 + Z_{hp} \mu_{hp} + \alpha_p - \mu_{ln}] + N_{ln} \mu_{ln} - Z_{hp} \mu_{hp} - N_{lp} - N_p [\alpha_e + \mu_{ln} - 1 - Z_{hp} \mu_{hp}] \quad (8)$$

Here $\Omega_{lp,ln} = \omega_{clp,ln} / \omega_{ph}$, $\vartheta = \frac{m_{lp} Z_{ln}}{Z_{lp} m_{ln}}$, $\nu_{ln(lp)} = \frac{\mu_{ln(lp)}}{m_{ln(lp)} n_{ln(lp)}}$ where $\mu_{ln(lp)}$ is the dynamic viscosity which is given by $\mu_{ln(lp)} = 2.21 \times 10^{-15} \frac{T_{ln(lp)}^{5/2} A_{ln(lp)}^{1/2}}{Z_{ln(lp)}^4 \ln(lp) \Lambda}$; $\ln \Lambda$ is the logarithm of Coulomb parameter, $A_{ln(lp)}$ is the atomic weight of heavy positive ion, Z_{hp} is the charged state of heavy positive ions, $Z_{lp(ln)}$ is the charged state of light positive (negative) ions, ϕ is the normalized electrostatic potential, $\eta_{lp(ln)}$ is the normalized viscosity for light positive (negative) ion, $\nu_{lp(ln)}$ collisional frequency of light positive (negative) ion. $P_{lp(ln)\parallel}$ and $P_{lp(ln)\perp}$ are the parallel and perpendicular pressure of light positive (negative) ion. The pressure equations for the anisotropic and adiabatic system are given by Chew–Goldberger–Law popularly known as (CGL) or double adiabatic theory [59–61], according to which $\frac{d}{dt} (P_{i\parallel} B^2 / n_i^3) = 0$ and $\frac{d}{dt} (P_{i\perp} / n_i B) = 0$. In the case of electrostatic waves in a magnetized plasma, the ambient magnetic field $B = B_0$ is constant with time, i.e. $\frac{d}{dt} (B) = 0$ where B_0 is the magnetic field at equilibrium. Moreover, the normalized parallel and perpendicular ion pressures obtained from the CGL theory are given as $P_{i\parallel} = 3P_{i\parallel 0} / n_{i0} \varepsilon_{Fe}$ and $P_{i\perp} = P_{i\perp 0} / n_{i0} \varepsilon_{Fe}$ where $P_{i\parallel 0} = n_{i0} T_{i\parallel}$ and $P_{i\perp 0} = n_{i0} T_{i\perp}$ are the equilibrium values of parallel and perpendicular pressure functions respectively, and n_{i0} is the unperturbed ion density. [18, 60, 62] The variations in the ambient magnetic field alter the ionic temperatures in parallel and perpendicular directions to the magnetic field, i.e., $T_{i\parallel} \propto B_0$ and $T_{i\perp} \propto \left(\frac{n_{i0}}{B_0}\right)^2$ respectively [62, 63].

The other plasma parameters are normalized as follows:

$\Phi = \frac{\varepsilon_{Fe}}{e}$, $t = T \omega_p^{-1}$, $x = X \times \lambda_{Fe}$, $N_j = \frac{n_j}{n_{j0}}$, $\lambda_{Fe} = \frac{C_s}{\omega_s}$, $\varepsilon_{Fe} = \left(\frac{\hbar}{2m_e}\right) \left(\frac{3\pi^2}{n_{e0}}\right)^{2/3}$ Where, λ_{Fe} is the Thomas-Fermi length, C_s is the Fermi ion sound velocity, ω_{ph} is the plasma frequency, $m_{lp(ln)}$ is the mass of light negative (light positive) ions

3. DERIVATION OF DKDV-B EQUATION

To derive the evolution equation we employed the reductive perturbation technique. The stretched coordinates [18] used here are given by:

$$\xi = \varepsilon^{1/2} (I_x x + I_y y + I_z z - MT), \eta_{ln(lp)\parallel} = \varepsilon^{1/2} \eta_{ln(lp)\parallel 0}, \quad (9)$$

$$\eta_{ln(lp)\perp} = \varepsilon^{1/2} \eta_{ln(lp)\perp 0}, \nu_{ln(lp)} = \varepsilon^{3/2} \nu_{ln0(lp0)}$$

Where, M is the phase velocity (Mach number) and ε is a small nonzero constant measuring the strength of dispersion. In terms of the expansion parameter ε , the physical variables in equations are expanded in a power series as

$$\left. \begin{aligned} N_j &= 1 + \varepsilon N_j^{(1)} + \varepsilon^2 N_j^{(2)} + \varepsilon^3 N_j^{(3)} + \dots \\ V_{ix} &= \varepsilon V_{ix}^{(1)} + \varepsilon^2 V_{ix}^{(2)} + \varepsilon^3 V_{ix}^{(3)} + \dots \\ V_{jy,z} &= \varepsilon^{3/2} V_{jy,z}^{(1)} + \varepsilon^2 V_{jy,z}^{(2)} + \varepsilon^{5/2} V_{jy,z}^{(3)} + \dots \\ \phi &= \varepsilon \phi^{(1)} + \varepsilon^2 \phi^{(2)} + \varepsilon^3 \phi^{(3)} + \dots \end{aligned} \right\} \quad (10)$$

Substituting the above stretched coordinates from Eq.(8) and the respective expansions from Eq. (10) in the Eqs.(1)-(8), and then collecting the terms appearing in the lowest order of ε gives the following relations which gives the phase velocity as

$$M = \pm \sqrt{\frac{b \pm \sqrt{b^2 - 4ac}}{2a}} \quad (11)$$

$$a = (\mu_e \alpha_1 - \mu_p \Upsilon_1)$$

Where $b = I_x^2 (\mu_e \alpha_1 (P_{ln\parallel} + P_{lp\parallel}) - (1 - \vartheta \mu_{ln}) + \mu_p \Upsilon_1 (P_{ln\parallel} + P_{lp\parallel}))$

$$c = I_x^4 (\mu_e \alpha_1 P_{ln\parallel} P_{lp\parallel} + P_{ln\parallel} - \vartheta \mu_{ln} P_{lp\parallel} - \mu_p \Upsilon_1 P_{ln\parallel} P_{lp\parallel})$$

Using standard procedure we obtain the following equation

$$p \frac{\partial \phi^{(1)}}{\partial \tau} + q \phi^{(1)} \frac{\partial \phi^{(1)}}{\partial \xi} + r \frac{\partial^3 \phi^{(1)}}{\partial \xi^3} - s \frac{\partial^2 \phi^{(1)}}{\partial \xi^2} + t \phi^{(1)} = 0 \quad (12)$$

Where

$$\begin{aligned}
 p &= \left(\frac{\mu_{in} 2 \vartheta M I_x^2}{(M^2 - P_{In\parallel} I_x^2)^2} + \frac{2 M I_x^2}{(M^2 - P_{Ip\parallel} I_x^2)^2} \right) \\
 q &= \left(2 \mu_p \Upsilon_2 - 2 \mu_e \alpha_2 - \frac{\mu_{in} \vartheta^2 M^2 I_x^2 \left(3 I_x^2 + P_{In\parallel} \frac{I_x^4}{M^2} \right)}{(M^2 - P_{In\parallel} I_x^2)^3} + \frac{M^2 I_x^2 \left(3 I_x^2 + P_{Ip\parallel} \frac{I_x^4}{M^2} \right)}{(M^2 - P_{Ip\parallel} I_x^2)^3} \right) \\
 r &= \left(1 - \left((I_x^2 P_{In\perp} + 1) \frac{(1 - I_x^2) \mu_{in} \vartheta M^2}{(M^2 - P_{In\parallel} I_x^2)^2 \Omega_{In}^2} + (I_x^2 P_{Ip\perp} + 1) \frac{(1 - I_x^2) M^2}{(M^2 - P_{Ip\parallel} I_x^2)^2 \Omega_{In}^2} \right) \right) \\
 s &= \left(\frac{\vartheta \mu_{in} M \eta_{In\parallel 0} I_x^4}{(M^2 - P_{In\parallel} I_x^2)^2} + \frac{M \eta_{Ip\parallel 0} I_x^4}{(M^2 - P_{Ip\parallel} I_x^2)^2} \right) \\
 t &= \frac{\vartheta \mu_{in} I_x^2 M \nu_{In}}{(M^2 - I_x^2 P_{In\parallel})} + \frac{M \nu_{Ip} I_x^2}{(M^2 - I_x^2 P_{Ip\parallel})}
 \end{aligned}$$

Finally, the dKdV-B equation can be extracted as

$$\frac{\partial \phi^{(1)}}{\partial \tau} + A \phi^{(1)} \frac{\partial \phi^{(1)}}{\partial \xi} + B \frac{\partial^3 \phi^{(1)}}{\partial \xi^3} - C \frac{\partial^2 \phi^{(1)}}{\partial \xi^2} + D \phi^{(1)} = 0 \tag{13}$$

Where

$$A = \frac{q}{p}, \quad B = \frac{r}{p}, \quad C = \frac{s}{p}, \quad D = \frac{t}{p}$$

To obtain the solution of Eq. (13), the authors consider the new variable $\chi = \xi - U\tau$ where χ is the transformed coordinate with respect to a frame moving with velocity U. By taking $\phi^{(1)} = \phi$, Eq.(13) becomes

$$-U \frac{d\phi}{d\chi} + A \phi \frac{d\phi}{d\chi} + B \frac{d^3 \phi}{d\chi^3} - C \frac{d^2 \phi}{d\chi^2} + D \phi = 0 \tag{14}$$

Now, employing the method used in [64] results the solution of equation(14) as

$$\phi = \frac{2(144BC + 12CU + BD + 2UD)}{6A(4C - D)} + \left(\frac{2(-6C - D)}{5A} \right) \tanh(\chi) - \frac{12B}{A} \tanh^2(\chi) \tag{15}$$

4. RESULTS AND DISCUSSION

We have obtained the asymptotic solution of the dKdV-B equation in equ.(15). Now we find that the solution has got a solitary wave structure composed with a shock. Additionally due to damping the shock amplitude is affected and there is a constant part. We now take the parameters and study their effect on the nature and properties of these solitary-shock profiles. The tuning parameters are: Charged state of heavy positive ions (Z_{hp}), viscosity for light positive ion in parallel direction ($\eta_{Ip\parallel 0}$), viscosity for light negative ion in parallel direction ($\eta_{In\parallel 0}$), parallel pressure of light positive ion ($P_{Ip\parallel}$), parallel pressure of light negative ion ($P_{In\parallel}$) and perpendicular pressure of light positive ion ($P_{Ip\perp}$), perpendicular pressure of light negative ion ($P_{In\perp}$) respectively.

Now by taking combinations of other parameters and tuning one we obtain a series of figures which we discuss below.

In Figure 1 we take different pressure combination of light negative and positive ions. We plot curves for different charge density of heavy positive ion (Z_{hp}). Both the light negative and positive ions in subfigure (i) have different parallel and perpendicular pressure values, indicating that they are anisotropic. Light negative ions are anisotropic in subfigure (ii), but light positive ions are isotropic. Light positive ions are anisotropic in subfigure (iii), but light negative ions are isotropic. Comparing sub Figure (i),(ii) and (iii) we conclude that as the perpendicular pressure component for light positive ion ($P_{Ip\perp}$) causes the overall value of the solitary structure gets an upward lift. In subfigure(i) the left base of the potential profile was at 0.3, the peak is 0.4 and the right base at 0.365. However as perpendicular pressure component for light positive ion ($P_{Ip\perp}$) increases for 0.2 to 0.5 in subfig(ii) the left base jumps to 0.48 and the peak at 0.6 as the right base at 0.55. Additionally the separation between plots for different Z_{hp} gets widened. Now comparing subfig (i) and (ii) we see that as $P_{In\perp}$ increases from 0.2 to 0.5 an upward potential shift is there but not as prominent as for a change in $P_{Ip\perp}$. It may be inferred that pressure anisotropy due to light negative ion is causing a slight increase in the potential compared to that of positive light ion, which can be attributed to the repulsion of electrons by the negative light ions causing a lesser shift of potential profile. The light positive ion on the other hand exerts more nonlinear effects when compared to their negative counterparts.

In Figure 2, the light positive and light negative ions are anisotropic ($P_{Ip\parallel} > P_{Ip\perp}$) and isotropic respectively, in subfigure (i). In subfigure (ii), both ions are isotropic while in the subfigure (iii), both ions are anisotropic ($P_{Ip\parallel} > P_{Ip\perp}, P_{In\parallel} < P_{In\perp}$). Comparing subfigures (i) and (ii) we see that as $P_{Ip\perp}$ increases from 0.2 to 0.5 the base level of the shock jumps abruptly manifold from -0.04 to 0.04 (approx). Also the relative value of the potential (ϕ) for different values of Z_{hp} also changes. A deep introspection shows that when for $\chi < 0$ the green curve was below the red, it suddenly comes

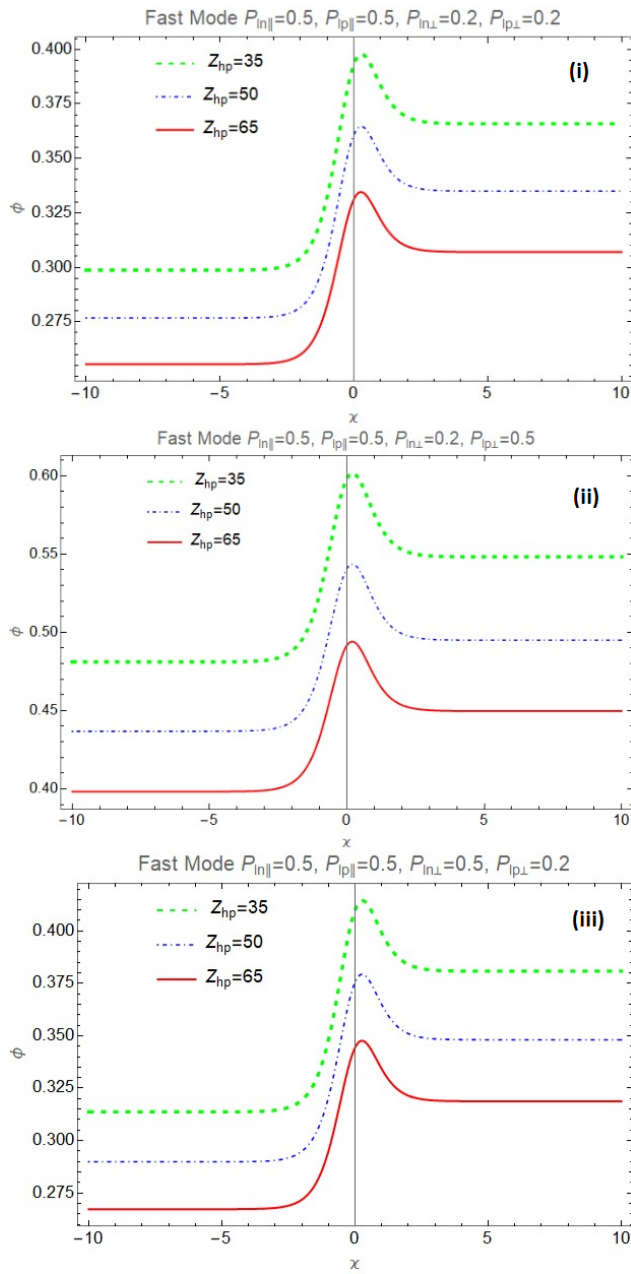


Figure 1. Variation of solitary-shock wave potential profile with different pressure combination of ions for different values of heavy positive ions

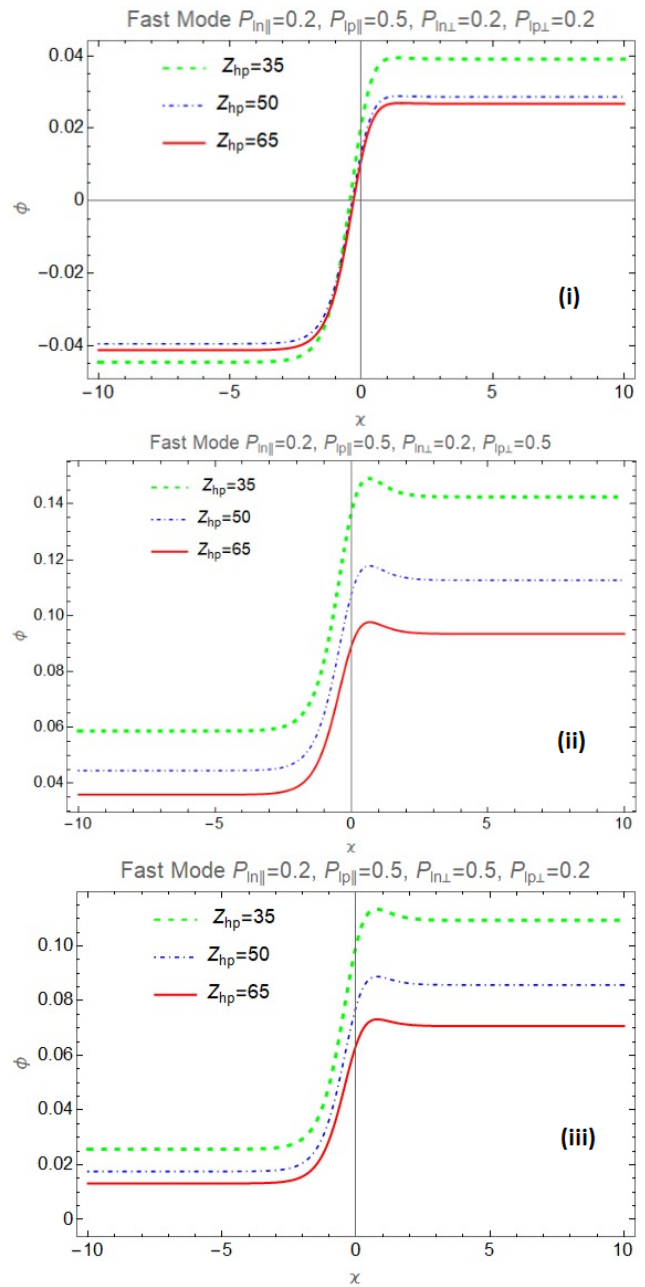


Figure 2. Variation of solitary-shock wave potential profile with different pressure combination of ions for different values of heavy positive ions

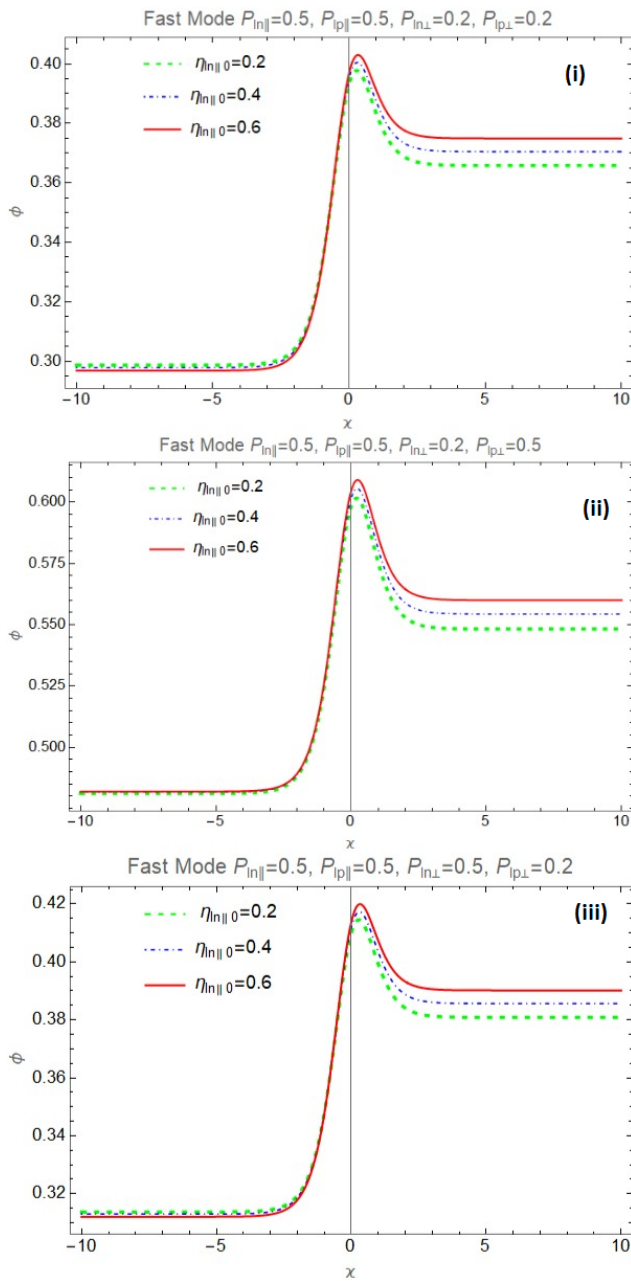


Figure 3. Variation of solitary-shock wave potential profile with different pressure combination of ions for different values of viscosity(parallel) of light negative ions

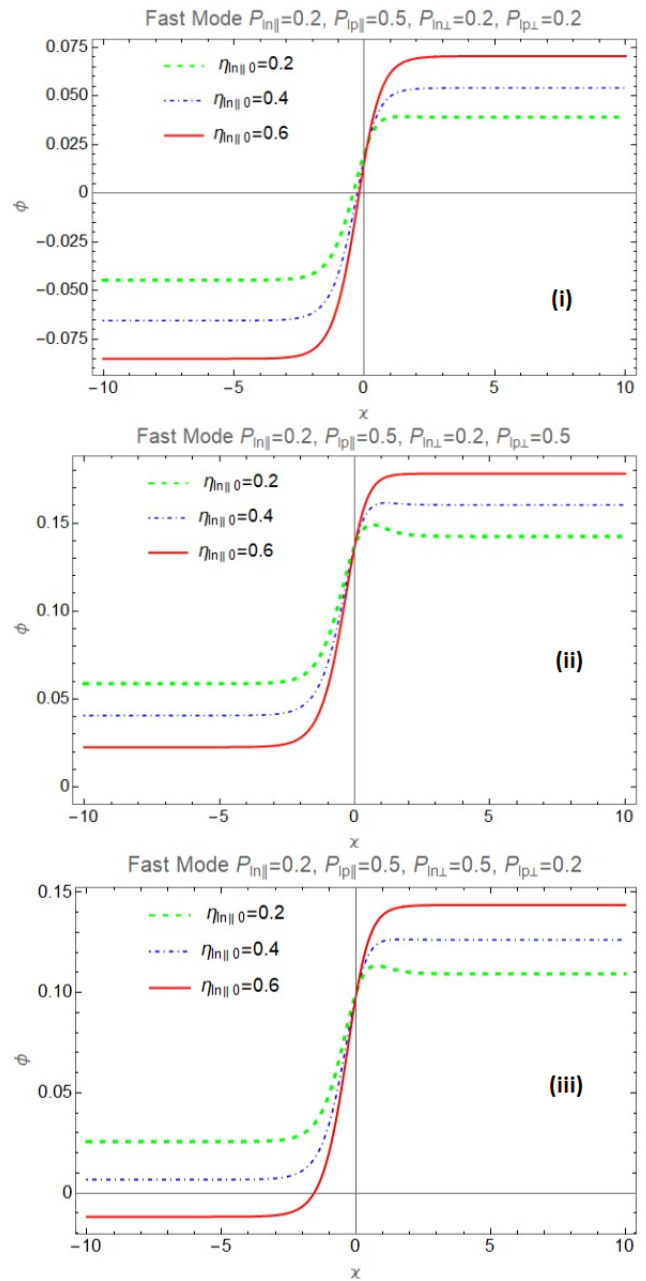


Figure 4. Variation of solitary-shock wave potential profile with different pressure combination of ions for different values of viscosity(parallel) of light negative ions

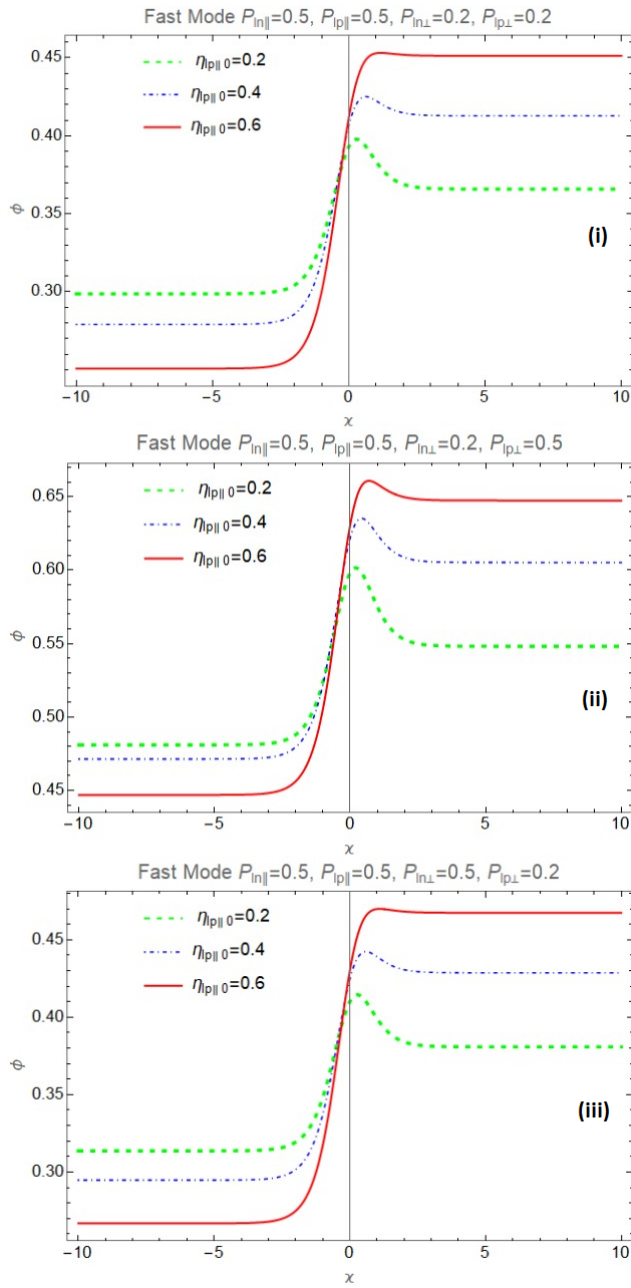


Figure 5. Variation of solitary-shock wave potential profile with different pressure combination of ions for different values of viscosity(parallel) of light positive ions

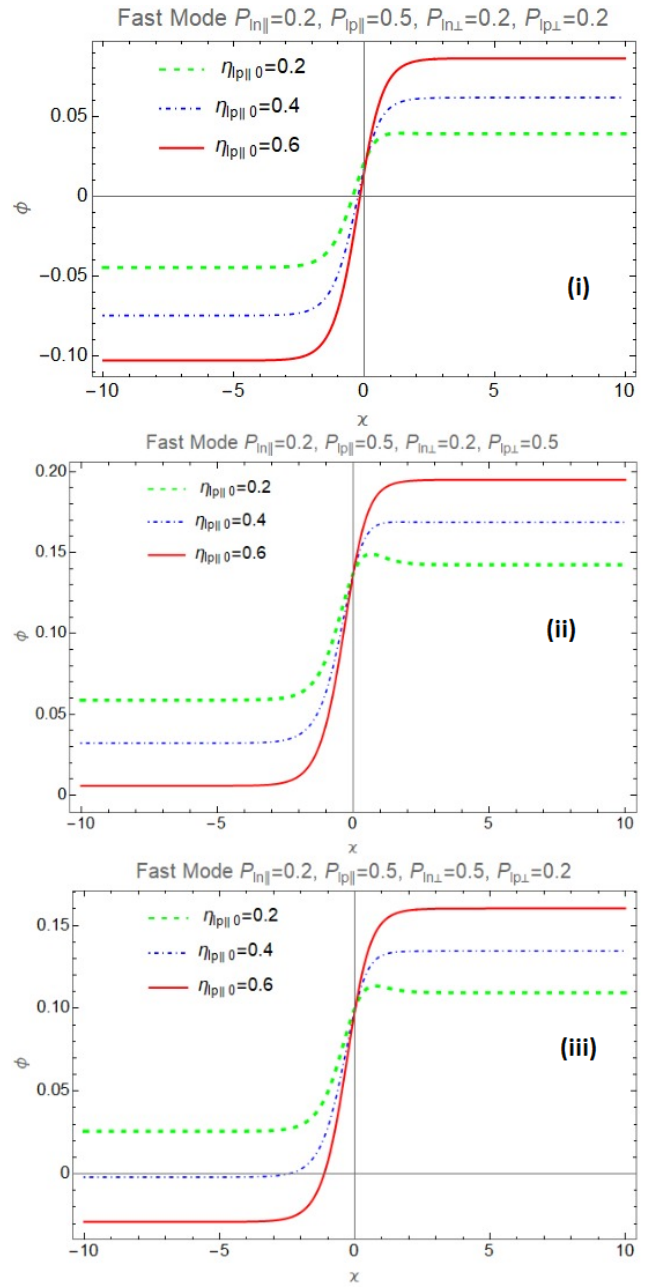


Figure 6. Variation of solitary-shock wave potential profile with different pressure combination of ions for different values of viscosity(parallel) of light positive ions

up above the red curve. Similar but less prominent nature is shown in subfigure (iii) when the perpendicular component of pressure changes but reversed for negative and positive light ions. It is to be also noted that solitary nature is visible only when both the ions are either anisotropy or isotropic(ii) and (iii)).

In Figures 3 and 4 the effects of viscosity due to light negative ions has been studied. Figure 3 shows that for similar values of parallel pressure for light negative and positive ions the left branch of the stationary profile does not show much difference when as the right part shows certain difference in potential values, the only interesting feature is that higher the value of $\eta_{ln\parallel}$, higher is the damping effect due to viscosity. Such a higher energy loss balances the dispersive effects. Such a thing can be witnessed by comparing sub figure(i) with (ii) and (iii) respectively. Likewise in fig4 we see that the solitary nature is almost non existant. The Shock profile shows dependence on viscosity co-efficient. The pressure anisotropy are instrumental in the shifting of the potential profiles. The effect of (parallel)viscosity coefficient for light positive ion is depicted in Figures 5 and 6. In this case also the nature is similar to Figures 3 and 4. The only difference is that the solitary nature is far less prominent which implies to the fact that non linear effects are not much prominent. The other features are similar to these Figures 3 and 4 and therefore no additional explanation required.

5. DYNAMICAL SYSTEM ANALYSIS

Dynamical systems equations and phase portraits play a pivotal role in understanding and analyzing the behavior of plasma in physics. Plasma, often termed as the fourth state of matter, exhibits complex dynamics influenced by electromagnetic fields and particle interactions. Dynamical systems equations provide a mathematical framework to model these intricate dynamics, allowing scientists to predict and interpret the behavior of plasma systems. By formulating differential equations that describe the evolution of plasma parameters such as density, temperature, and velocity, researchers can gain insights into phenomena like plasma instabilities, turbulence, and wave propagation. Phase portraits, a visual representation of dynamical systems, offer a powerful tool to analyze the solutions of these equations. They provide a comprehensive overview of the system's behavior by plotting the trajectories of different plasma states in a multi-dimensional space. By examining the topology and stability of these trajectories, scientists can discern crucial information about the underlying dynamics, identifying equilibrium points, periodic orbits, and attractors.

This understanding is invaluable for optimizing plasma confinement in fusion reactors, developing plasma-based technologies like plasma thrusters for spacecraft propulsion, and advancing our knowledge of fundamental plasma physics phenomena. In essence, dynamical systems equations and phase portraits serve as indispensable tools for unraveling the complexities of plasma physics, driving progress in both theoretical understanding and practical applications.

In order to obtain the dynamical system equation we apply the transformation of the space and variable as $\chi = \xi - U\tau$ and finally obtain the transformed equation as

$$\begin{aligned} \frac{d\phi}{d\chi} &= z_1 \\ \frac{dz_1}{d\chi} &= z_2 \\ \frac{dz_2}{d\chi} &= \frac{Uz_1 - A\phi z_1 + Cz_2 - D\phi}{B} \end{aligned} \tag{16}$$

In the subsequent figure plots the projections of z_1, z_2, ϕ in mutual planes. the horizontal lines are for a given values of perpendicular. In Figure 7 we alter the values of heavy positive ion charge density which varies as 35,50 and 65. The other perpendicular are given as: $\eta_{ln\parallel 0} = 0.2, \eta_{lp\parallel 0} = 0.2, P_{ln\parallel} = 0.5, P_{lp\parallel} = 0.5, P_{ln\perp} = 0.2, P_{lp\perp} = 0.2$

We see that all the $z_1 - \phi, z_2 - \phi, z_1 - z_2$ plots shows the damping effects by the inward spiral motion. Damping here happens due to two factors, viscosity and collision. By thoroughly studying the figures we see that the $\phi - z_2$ plot has an inclined axis with negative slope. It can be interpreted as the spatial division of the electric field has a negative slope which implies that it is asymptotically stable. There is not much change in nature of curve in Figure 8 and Figure 9.

Figure 10 shows that effect of pressure anisotropy of light positive ions in the perpendicular direction. Hence there are great changes with change in parameter $P_{lp\perp}$, the spirality changes. Similar effects shows in Figure 11, when $P_{ln\perp}$ changes, i.e. the perpendicular component of pressure light negative ions changes. The effect of collision is shown in Figure 12. Collision plays an significant role in damping effects as the value of collision parameter increases the spirals are spread out along the axis. Such a nature is due to the dissipation of energy through collision. This is relatable non-radiative dissipation spectroscopy and thermal physics.

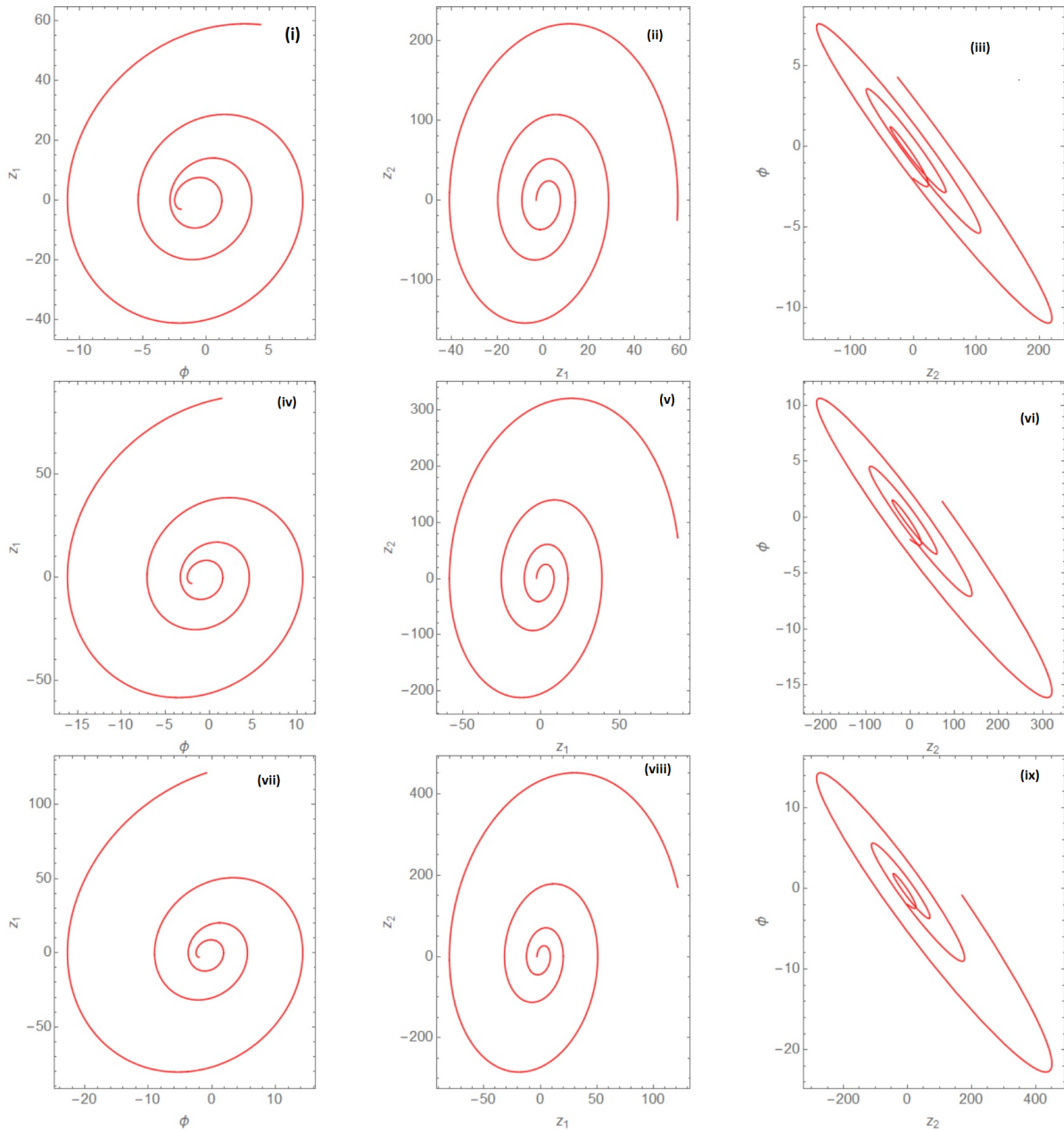


Figure 7. Phase Portrait for system (16) for $\eta_{ln\parallel 0} = 0.2, \eta_{lp\parallel 0} = 0.2, P_{ln\parallel} = 0.5, P_{lp\parallel} = 0.5, P_{ln\perp} = 0.2, P_{lp\perp} = 0.2$ (i),(ii),(iii) $Z_{hp} = 35$ (vi),(v),(vi) $Z_{hp} = 50$,(vii),(viii),(ix) $Z_{hp} = 50$

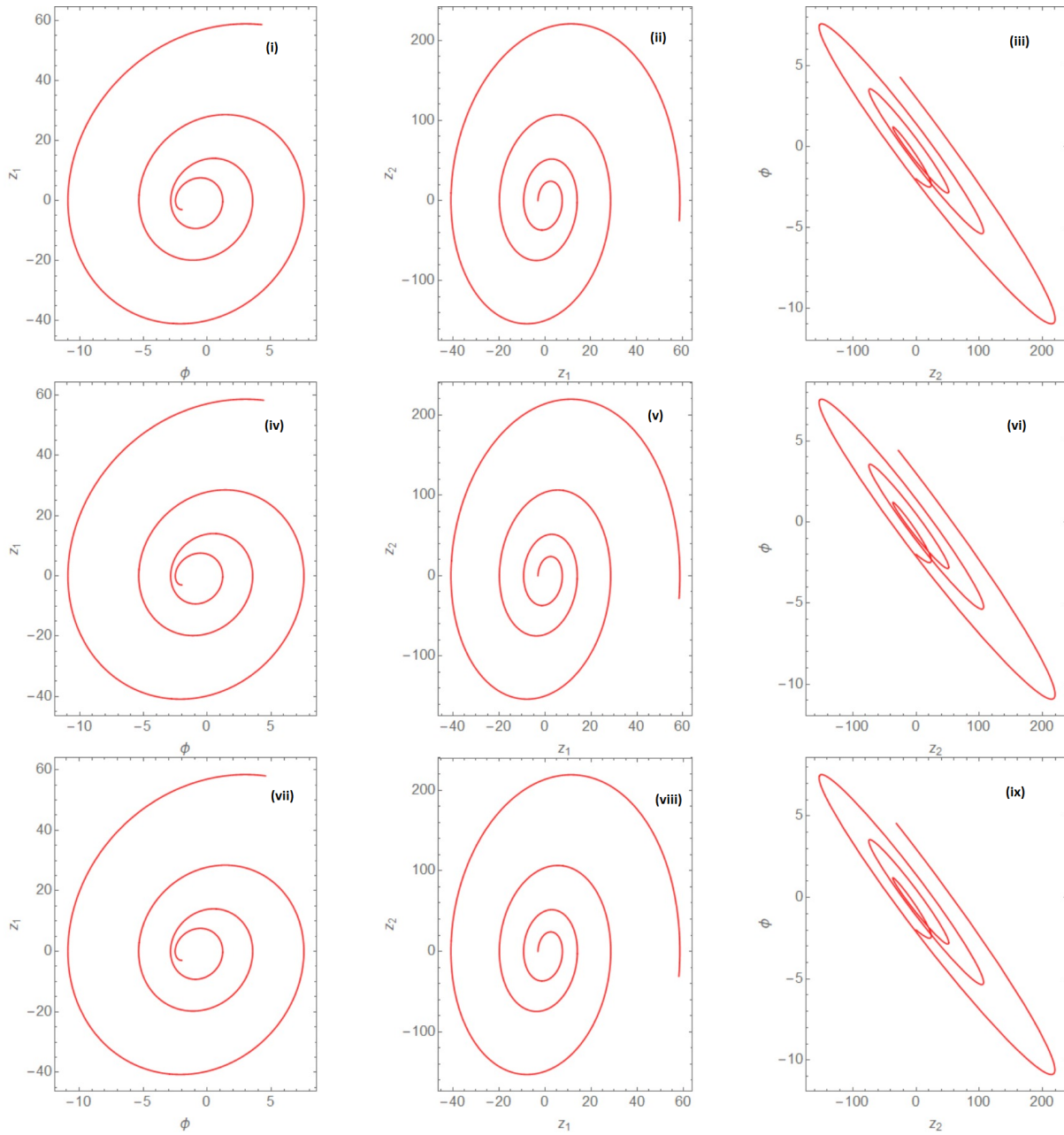


Figure 8. Phase Portrait for system (16) for $Z_{hp} = 35, \eta_{lp||0} = 0.2, P_{ln||} = 0.5, P_{lp||} = 0.5, P_{ln\perp} = 0.2, P_{lp\perp} = 0.2$ (i),(ii),(iii) $\eta_{ln||0} = 0.2$ (vi),(v),(vi) $\eta_{ln||0} = 0.4$,(vii),(viii),(ix) $\eta_{ln||0} = 0.6$

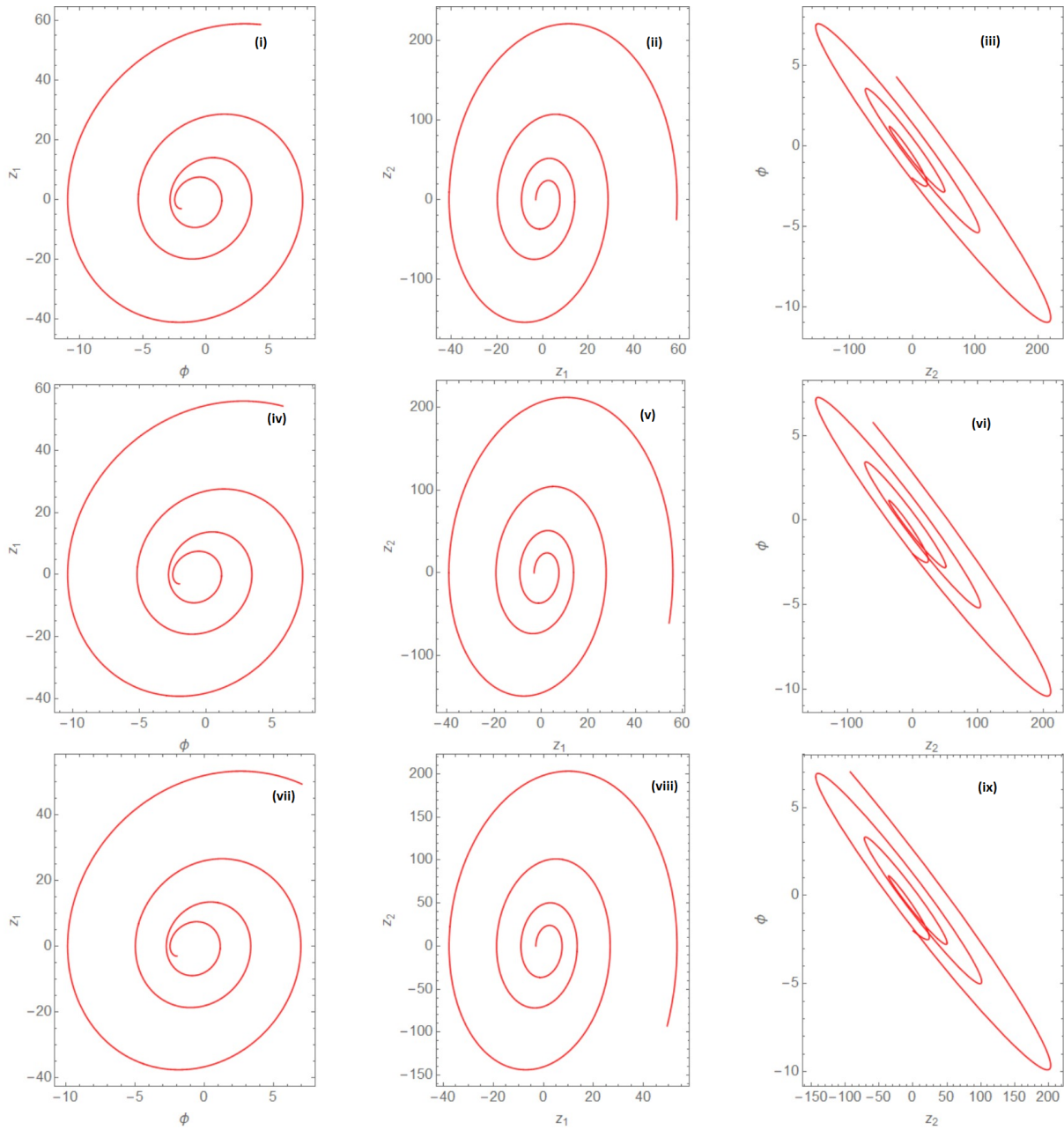


Figure 9. Phase Portrait for system (16) for $Z_{hp} = 35, \eta_{ln\parallel 0} = 0.2, P_{ln\parallel} = 0.5, P_{lp\parallel} = 0.5, P_{ln\perp} = 0.2, P_{lp\perp} = 0.2$ (i),(ii),(iii) $\eta_{lp\parallel 0} = 0.2$ (vi),(v),(vi) $\eta_{lp\parallel 0} = 0.4$,(vii),(viii),(ix) $\eta_{lp\parallel 0} = 0.6$

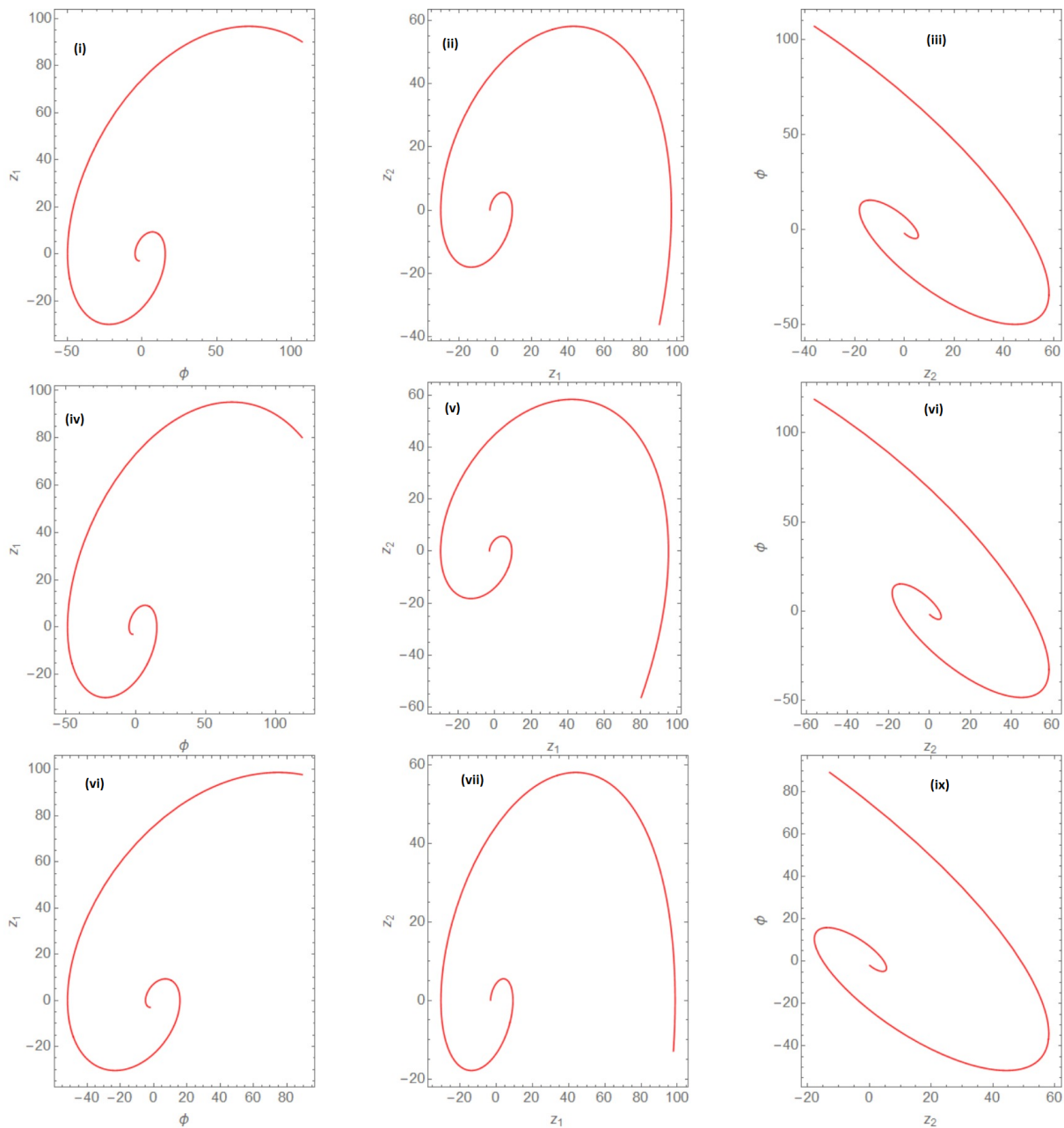


Figure 10. Phase Portrait for system (16) for $Z_{hp} = 35, \eta_{ln\parallel 0} = 0.2, \eta_{lp\parallel 0} = 0.2, P_{ln\parallel} = 0.5, P_{lp\parallel} = 0.5, P_{ln\perp} = 0.2$ (i),(ii),(iii) $P_{lp\perp} = 0.5$ (vi),(v),(vi) $P_{lp\perp} = 0.2$,(vii),(viii),(ix) $P_{lp\perp} = 0.9$

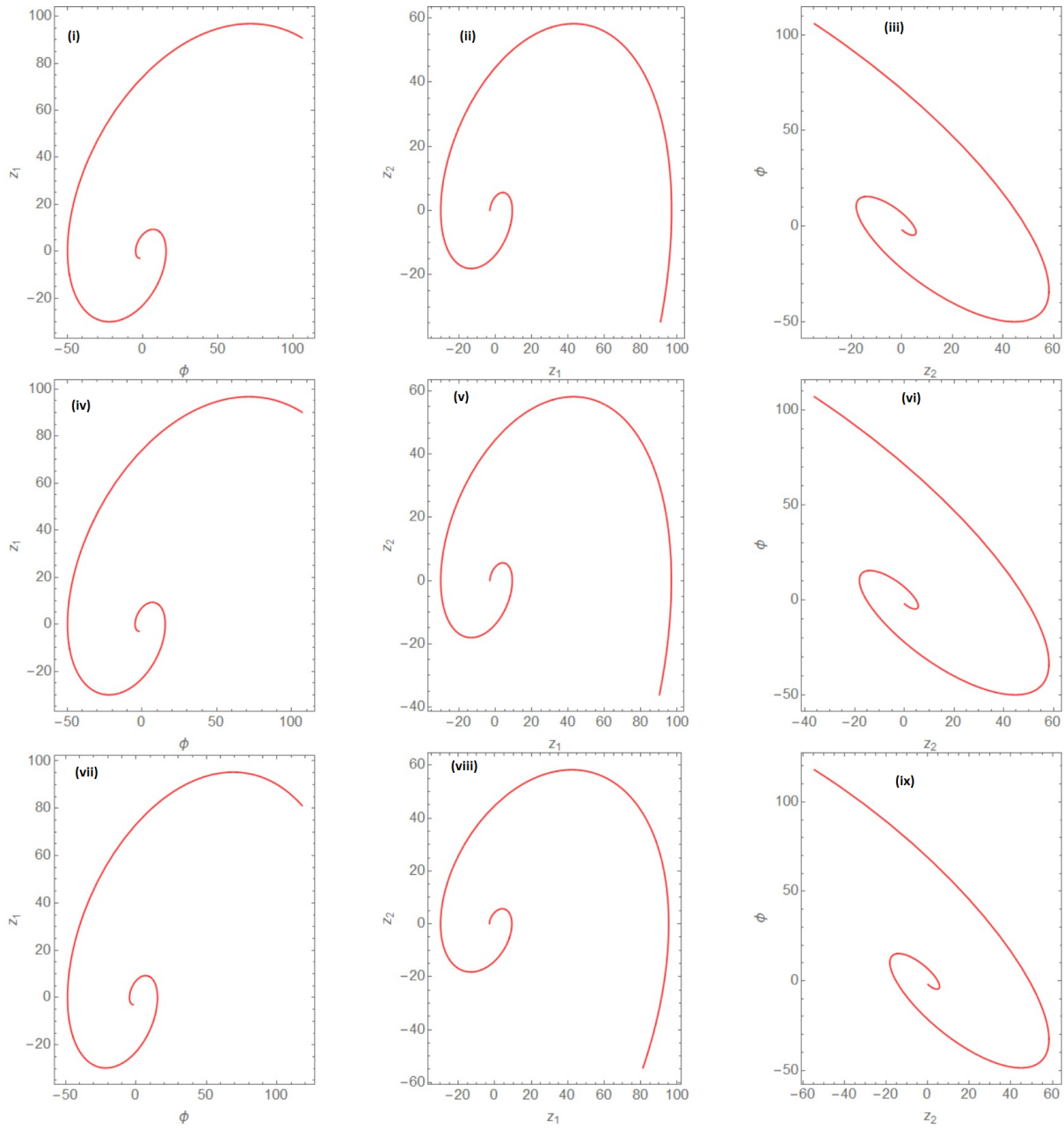


Figure 11. Phase Portrait for system (16) for $Z_{hp} = 35, \eta_{ln\parallel 0} = 0.2, \eta_{lp\parallel 0} = 0.2, P_{ln\parallel} = 0.5, P_{lp\parallel} = 0.5, P_{ln\perp} = 0.2$ (i),(ii),(iii) $P_{ln\perp} = 0.5$ (vi),(v),(vi) for $P_{ln\perp} = 0.2$,(vii),(viii),(ix) $P_{ln\perp} = 0.9$

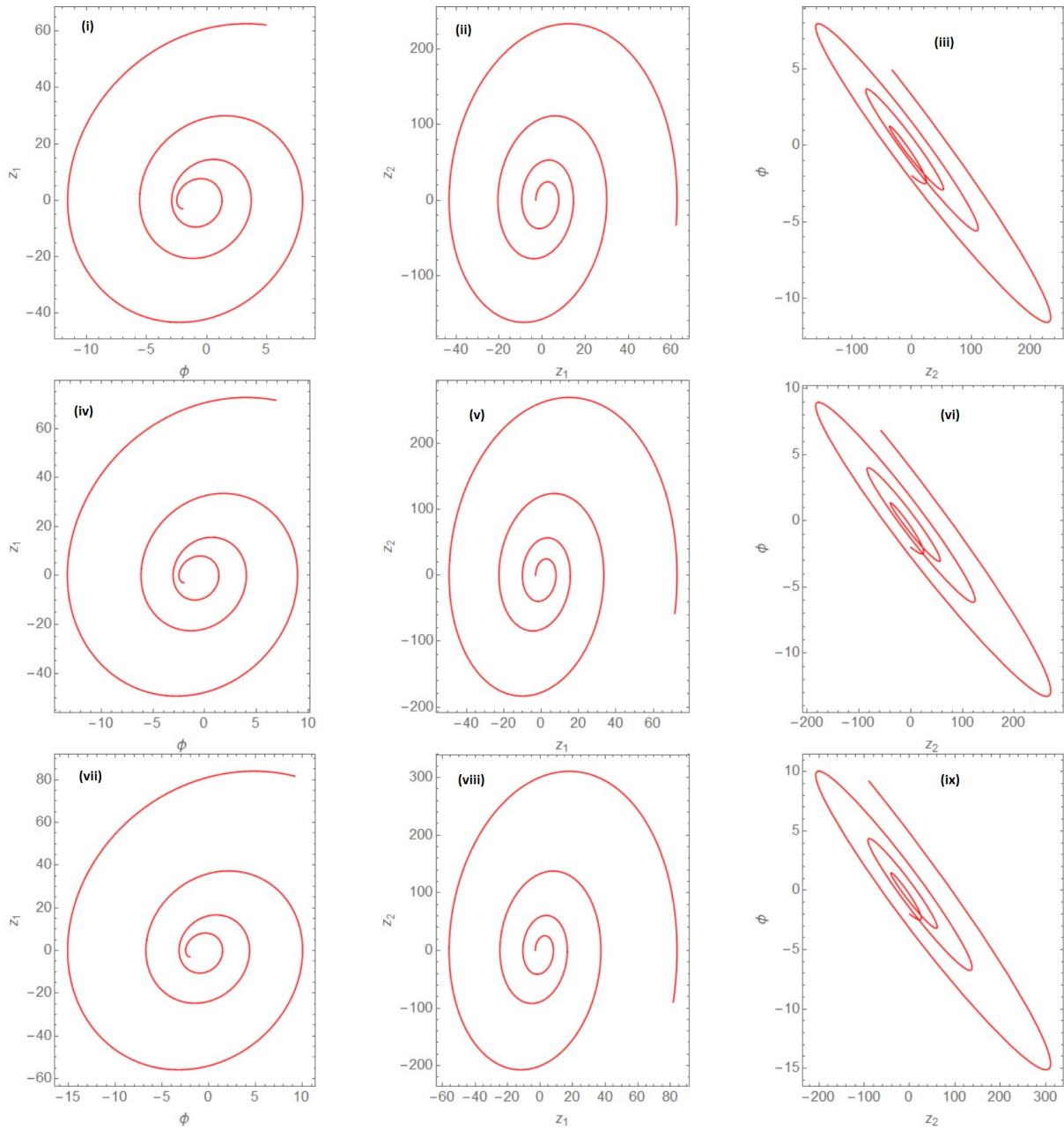


Figure 12. Phase Portrait for system (16) for $\eta_{ln\parallel 0} = 0.2, \eta_{lp\parallel 0} = 0.2, P_{ln\parallel} = 0.5, P_{lp\parallel} = 0.5, P_{ln\perp} = 0.2, P_{lp\perp} = 0.2$ (i),(ii),(iii) $\nu_{ln} = 0.1, \nu_{lp} = 0.1$ (vi),(v),(vi)for $\nu_{ln} = 0.3, \nu_{lp} = 0.3$,(vii),(viii),(ix) $\nu_{ln} = 0.5, \nu_{lp} = 0.5$



6. CONCLUSION

The features of ion-acoustic solitary-shock wave propagating in a collisional plasma under the influence of ionic pressure anisotropy and viscosity is studied with the help of dKdV-B equation and by using standard procedure we obtained the analytic solution. The effect of heavy positive ion, viscosity of light positive ion and light negative ion as well as pressure anisotropy of light positive ion and light negative ion are investigated. Subsequently, we converted our evolutionary equation into a three dimensional dynamical system to perform phase plane analysis. The findings presented here may have implications in both laboratory as well as astrophysical plasma environment

7. ACKNOWLEDGEMENT

D. Mahanta would like to thank Govt. of Assam for providing the Ph.D. Research Scholarship under the Director of Higher Education, Assam, Kahilipara, Guwahati-19. S Chandra also acknowledges the support provided by Institute of Natural Sciences and Applied Technology, Kolkata.

ORCID

 **Deepsikha Mahanta**, <https://orcid.org/0009-0000-5855-2279>;  **Swarniv Chandra**, <https://orcid.org/0000-0001-9410-1619>;  **Jnanjyoti Sarma**, <https://orcid.org/0000-0002-0793-5680>

REFERENCES

- [1] S. Chandrasekhar, "The density of white dwarf stars," *Philosophical magazine letters*, **11**, 592-596 (1982). <https://doi.org/10.1080/14786443109461710>
- [2] S. Chandrasekhar, "The Maximum Mass of Ideal White Dwarfs," *The Astrophysical Journal*, **74**, 81 (1931). <https://doi.org/10.1086/143324>
- [3] H.M. Van Horn, "Dense Astrophysical Plasmas," *Science*, **252**, 384-389 (1991). <https://doi.org/10.1126/science.252.5004.384>
- [4] S. Jahan, E. Booshrat, Sharmin, N.A. Chowdhury, A. Mannan, T.S. Roy and A.A. Mamun, "Electrostatic Ion-Acoustic Shock Waves in a Magnetized Degenerate Quantum Plasma," *Plasma*, **4**, 426-434 (2021). <https://doi.org/10.3390/plasma4030031>
- [5] M.R. Hossen, A.A. Mamun, "Nonplanar shock excitations in a four component degenerate quantum plasma: the effects of various charge states of heavy ions," *Plasma Science and Technology*, **17**, 177 (2015). <https://doi.org/10.1088/1009-0630/17/3/01>
- [6] P. Chaizy, H. Rème, J.A. Sauvaud, C. d'Uston, R.P. Lin, D.E. Larson, D.L. Mitchell, *et al.*, "Negative ions in the coma of comet Halley," *Nature*, **349**, 393-396 (1991). <https://doi.org/10.1038/349393a0>
- [7] H. Massey, *Negative Ions*, (Cambridge University Press, Cambridge, 1976), pp.7.
- [8] M. Bacal, and G.W. Hamilton, " H^- and D^- Production in Plasmas," *Physical Review Letters*, **42**, 1538 (1979). <https://doi.org/10.1103/PhysRevLett.42.1538>
- [9] J. Jacquinet, B.D. McVey, and J.E. Scharer, "Mode conversion of the fast magnetosonic wave in a deuterium-hydrogen tokamak plasma," *Physical Review Letters*, **39**, 88 (1977). <https://doi.org/10.1103/PhysRevLett.39.88>
- [10] R.A. Gottscho, and C.E. Gaebe, "Negative ion kinetics in RF glow discharges," *IEEE transactions on plasma science*, **14**, 92-102 (1986). <https://doi.org/10.1109/TPS.1986.4316511>
- [11] A.A. Mamun, "Degenerate pressure driven self-gravito-acoustic solitary waves in a self-gravitating degenerate quantum plasma system," *Physics of Plasmas*, **25**, 022307 (2018). <https://doi.org/10.1063/1.5013138>
- [12] A.A. Mamun, "Self-gravito-acoustic waves and their instabilities in a self-gravitating degenerate quantum plasma system," *Contributions to Plasma Physics*, **60**, e201900080 (2019). <https://doi.org/10.1002/ctpp.201900080>
- [13] S. Islam, S. Sultana, and A.A. Mamun, "Ultra-low frequency shock dynamics in degenerate relativistic plasmas," *Physics of Plasmas*, **24**, 092308 (2017). <https://doi.org/10.1063/1.4994196>
- [14] S. Islam, S. Sultana, A.A. Mamun, "Envelope solitons in three-component degenerate relativistic quantum plasmas," *Physics of Plasmas*, **24**, 092115 (2017). <https://doi.org/10.1063/1.5001834>
- [15] N. Akhtar, and S. Hussain, "Ion acoustic shock waves in degenerate plasmas," *Physics of Plasmas*, **18**, 072103 (2011). <https://doi.org/10.1063/1.3601768>
- [16] S. Hussain, and N. Akhtar, "Collisional effects in negative ion plasmas in the presence of degenerate electrons," *Physics of Plasmas*, **25**(6), 062109 (2018). <https://doi.org/10.1063/1.5025244>
- [17] T. Mohsenpour, H. Ehsani, and M. Behzadipour, "Ion-acoustic solitons in negative ion plasma with relativistic degenerate electrons and positrons," *Waves in Random and Complex Media*, **34**(2), 845-857 (2024). <https://doi.org/10.1080/17455030.2021.1919338>
- [18] M. Adnan, G. Williams, A. Qamar, S. Mahmood, and I. Kourakis, "Pressure anisotropy effects on nonlinear electrostatic excitations in magnetized electron-positron-ion plasmas," *The European Physical Journal D*, **68**, 1-15 (2014). <https://doi.org/10.1140/EPJD%2FE2014-50384-Y>
- [19] M.K. Deka, D. Mahanta, A.N. Dev, J. Sarma, S.K. Mishra, and E. Saikia, "Propagation of ion beam modes in a spin degenerate quantum magneto plasma in presence of ionic pressure anisotropy," *AIP Conference Proceedings*, **2819**, 070004 (2023). <https://doi.org/10.1063/5.0137748>

- [20] M.K. Deka, D. Mahanta, A.N. Dev, J. Sarma, S.K. Mishra, and E. Saikia, "Features of shock wave in a quantized magneto plasma under the influence of ionic pressure anisotropy and anisotropic viscosity," *AIP Conference Proceedings*, **2819**, 070005 (2023). <https://doi.org/10.1063/5.0137746>
- [21] Almas, Ata-ur-Rahman, N. Faiz, D.M. Khan, W. Emam, and Y. Tashkandy, "Oblique Arbitrary Amplitude Dust Ion Acoustic Solitary Waves in Anisotropic Non-Maxwellian Plasmas with Kappa-Distributed Electrons," *Symmetry*, **15**, 1843 (2023). <https://doi.org/10.3390/sym15101843>
- [22] M. Khalid, A. Kabir, and L.S. Jan, "Qualitative analysis of nonlinear electrostatic excitations in magnetoplasma with pressure anisotropy," *Zeitschrift für Naturforschung A*, **78**, 339–345 (2023). <https://doi.org/10.1515/zna-2022-0312>
- [23] S. Mahmood, S. Hussain, W. Masood, H. Saleem, "Nonlinear electrostatic waves in anisotropic ion pressure plasmas," *Physica Scripta*, **79**, 045501 (2009). <https://doi.org/10.1088/0031-8949/79/04/045501>
- [24] M. Manesh, S. Sijo, V. Anu, G. Sreekal, T.W. Neethu, D.E. Savithri, and C. Venugopal, "Effect of anisotropy of lighter and heavier ions on solitary waves in a multi-ion plasma," *Physics of Plasma*, **24**, 062905 (2017). <https://doi.org/10.1063/1.4986107>
- [25] S.U. Khan, M. Adnan, S. Mahmood, H. Ur-Rehman, and A. Qamar, "Effect of pressure anisotropy on nonlinear periodic waves in a magnetized superthermal electron-positron-ion plasma," *Brazilian Journal of Physics*, **49**, 379–390 (2019). <https://doi.org/10.1007/s13538-019-00653-w>
- [26] M. Khalid, and A. Rahman, "Ion acoustic cnoidal waves in a magnetized plasma in the presence of ion pressure anisotropy," *Astrophysics and Space Science*, **364**, 28 (2019). <https://doi.org/10.1007/s10509-019-3517-0>
- [27] G. Bordbar, and M. Karami, "Anisotropic magnetized neutron star," *The European Physical Journal C*, **82**, 74 (2022). <https://doi.org/10.1140/epjc/s10052-022-10038-0>
- [28] A. Patidar, and P. Sharma, "Magnetohydrodynamic wave modes in relativistic anisotropic quantum plasma," *Physics of Plasmas*, **27**, 042108 (2020). <https://doi.org/10.1063/1.5143764>
- [29] M. Ifran, S. Ali, and A.M. Mirza, "Solitary waves in a degenerate relativistic plasma with ionic pressure anisotropy and electron trapping effects," *Physics of plasmas*, **24**, 052108 (2017). <https://doi.org/10.1063/1.4981932>
- [30] A. Das, P. Ghosh, S. Chandra, and V. Raj, "Electron Acoustic Peregrine Breathers in a Quantum Plasma With 1-D Temperature Anisotropy," *IEEE Transactions on Plasma Science*, **50**(6), 1598-1609 (2022). <https://doi.org/10.1109/TPS.2021.3113727>
- [31] A. Dey, S. Chandra, C. Das, S. Mandal, and T. Das, "Rogue Wave Generation Through Non-Linear Self Interaction Of Electrostatic Waves In Dense Plasma," *IEEE Transactions on Plasma Science*, **50**(6), 1557-1564 (2022). <https://doi.org/10.1109/TPS.2022.3143001>
- [32] S. Chandra, S. Kapoor, D. Nandi, C. Das and D. Bhattacharjee, "Bifurcation Analysis of EAWs in Degenerate Astrophysical Plasma: Chaos and Multistability," *IEEE Transactions on Plasma Science*, **50**(6), 1495-1507 (2022). <https://doi.org/10.1109/TPS.2022.3166694>
- [33] S. Chandra, R. Banerjee, J. Sarkar, S. Zaman, C. Das, S. Samanta, F. Deebea, and B. Dasgupta, "Multistability Studies on Electron-Acoustic Wave in a Magnetized Plasma with Supra-thermal Ions," *Journal of Astrophysics and Astronomy*, **43**, 71 (2022). <https://doi.org/10.1007/s12036-022-09835-6>
- [34] A.R. Seadawy, and K. El-Rashidy, "Classification of multiply travelling wave solutions for coupled Burgers, combined kdV-Modified KdV, and Schrödinger-KdV equations," *Abstract and Applied Analysis*, 369294 (2015). <https://doi.org/10.1155/2015/369294>
- [35] X.Y. Gao, Y.J. Guo, and W.R. Shan, "Shallow water in an open sea or a wide channel: Auto- and non-auto-Bäcklund transformations with solitons for a generalized (2+1)-dimensional dispersive long-wave system," *Chaos, Solitons & Fractals*, **138**, 109950 (2020). <https://doi.org/10.1016/j.chaos.2020.109950>
- [36] C.R. Zhang, B. Tian, Q.X. Qu, L. Liu, and H.Y. Tian, "Vector bright solitons and their interactions of the couple fokas-lenells system in a birefringent optical fiber," *Zeitschrift für angewandte Mathematik und Physik*, **71**, 18 (2020). <https://doi.org/10.1007/s00033-019-1225-9>
- [37] X.Y. Gao, Y.J. Guo, and W.R. Shan, "Water-wave symbolic computation for the Earth, Enceladus and Titan: The higher-order Boussinesq-Burgers system, auto-and non-auto-Bäcklund transformations," *Applied Mathematics Letters*, **104**, 106170 (2020). <https://doi.org/10.1016/j.aml.2019.106170>
- [38] X.X. Du, B. Tian, Q.X. Qu, Y.Q. Yuan, and X.H. Zhao, "Zakharov-Kuznetsov equation in an electron-positron-ion magneto-plasma," *Chaos, Solitons & Fractals*, **134**, 109709 (2020). <https://doi.org/10.1016/j.chaos.2020.109709>
- [39] S.S. Chen, B. Tian, J. Chai, X.Y. Wu, Z. Du, "Lax pair binary Darboux transformations and dark-soliton interaction of a fifth-order defocusing nonlinear Schrödinger equation for the attosecond pulses in the optical fiber communication," *Waves in Random and Complex Media*, **30**, 389-402 (2020). <https://doi.org/10.1080/17455030.2018.1516053>
- [40] X.Y. Gao, Y.J. Guo, and W.R. Shan, "Cosmic dusty plasmas via a (3+1)-dimensional generalized variable-coefficient Kadomtsev-Petviashvili-Burgers-type equation: auto-Bäcklund transformations, solitons and similarity reductions plus observational/experimental supports," *Waves in Random and Complex Media*, **34**(3), 1572-1592 (2021). <https://doi.org/10.1080/17455030.2021.1942308>
- [41] M.R. Hassan, T.I. Rajib, and S. Sultana, "Electron-acoustic solitons in magnetized collisional nonthermal plasmas," *IEEE Transactions on Plasma Science*, **49**, 3749-3758 (2021). <https://doi.org/10.1109/TPS.2021.3129920>
- [42] B.S. Kashkari, and S.A. El-Tantawy, "Homotopy perturbation method for modeling electrostatic structures in collisional plasmas," *The European Physical Journal Plus*, **136**, 121 (2021). <https://doi.org/10.1140/epjp/s13360-021-01120-9>

- [43] M.R. Hassan, and S. Sultana, "Damped dust-ion-acoustic solitons in collisional magnetized nonthermal plasmas," *Contributions to Plasma Physics*, **61**, e202100065 (2021). <https://doi.org/10.1002/ctpp.202100065>
- [44] V. Nosenko, S. Goree, "Shear flows and shear viscosity in a two-dimensional Yukawa system (dusty plasma)," *Physical review letters*, **93**, 155004 (2004). <https://doi.org/10.1103/PhysRevLett.93.155004>
- [45] R.P.H. Chang, and M. Porkolab, "Experimental observation of nonlinear Landau damping of plasma waves in a magnetic field," *Physical review letters*, **25**, 1262 (1970). <https://doi.org/10.1103/PhysRevLett.25.1262>
- [46] M.R. Hassan, S. Biswas, K. Habib, and S. Sultana, "Dust-ion-acoustic waves in a κ - nonthermal magnetized collisional dusty plasma with opposite polarity dust," *Results in Physics*, **33**, 105106 (2022). <https://doi.org/10.1016/j.rinp.2021.105106>
- [47] E.I. El-Awady, and M. Djebli, "Dust acoustic waves in a collisional strongly coupled dusty plasmas," *Astrophysics and Space Science*, **34**, 105–111 (2012). <https://doi.org/10.1007/s10509-012-1159-6>
- [48] J.B. Piper, and J. Goree, "Dispersion of plasma dust acoustic waves in the strong-coupling regime," *Physical review letters*, **77**, 3137 (1996). <https://doi.org/10.1103/PhysRevLett.77.3137>
- [49] B. Pradhan, A. Gowrisankar, A. Abdikian, S. Banerjee, and A. Saha, "Propagation of ion-acoustic wave and its fractal representations in spin polarized electron plasma," *Physica Scripta*, **98**, 065604 (2023). <https://doi.org/10.1088/1402-4896/acd3>
- [50] E.F. El-Shamy, R.C. Al-Chouikh, A. El-Depsy, and N.S. Al-Wadie, "Nonlinear propagation of electrostatic travelling waves in degenerate dense magnetoplasmas," *Physics of Plasmas*, **23**, 122122 (2016). <https://doi.org/10.1063/1.4972817>
- [51] K. Singh, P. Sethi, and N.S. Saini, "Nonlinear excitations in a degenerate relativistic magneto-rotating quantum plasma," *Physics of Plasmas*, **26**, 092104 (2019). <https://doi.org/10.1063/1.5098138>
- [52] W.F. El-Taibany, E.E. Behery, S.K. El-Labany, and A.M. Abdelghany, "Gravito-electrostatic excitations in an opposite polarity complex plasma," *Physics of Plasmas*, **26**, 063701 (2019). <https://doi.org/10.1063/1.5092514>
- [53] P.K. Prasad, and A. Saha, "Bifurcation analysis of ion-acoustic waves for Schrödinger equation in nonextensive Solar wind plasma," *Advances in Space Research*, **67**, 9-19 (2021). <https://doi.org/10.1016/j.asr.2020.07.031>
- [54] A. Saha, B. Pradhan, and S. Banerjee, "Bifurcation analysis of quantum ion-acoustic kink, anti-kink and periodic waves of the Burgers equation in a dense quantum plasma," *The European Physical Journal Plus*, **135**, 216 (2020). <https://doi.org/10.1140/epjp/s13360-020-00235-9>
- [55] M.M. Selim, A. El-Depsy, and E.F. El-Shamy, "Bifurcations of nonlinear ion-acoustic travelling waves in a multicomponent magnetoplasma with superthermal electrons," *Astrophysics and Space Science*, **360**, 66 (2015). <https://doi.org/10.1007/s10509-015-2574-2>
- [56] R.A. Shahein, and A.R. Seadawy, "Bifurcation analysis of KP and modified KP equations in an unmagnetized dust plasma with nonthermal distributed multi-temperatures ions," *Indian Journal of Physics*, **93**, 941-949 (2019). <https://doi.org/10.1007/s12648-018-1357-3>
- [57] P.K. Prasad, and A. Saha, "Dynamical behavior and multistability of ion-acoustic waves in a magnetized Auroral zone plasma," *Journal of Astrophysics and Astronomy*, **42**, 9 (2021). <https://doi.org/10.1007/s12036-021-09721-7>
- [58] M.K. Islam, S. Biswas, N.A. Chowdhury, A. Mannan, et al., "Obliquely propagating ion-acoustic shock waves in a degenerate quantum plasma," *Contributions to Plasma Physics*, **62**, e202100073 (2021). <https://doi.org/10.1002/ctpp.202100073>
- [59] N. Akhtar, and S. Mahmood, "Effect of Ion Temperature Anisotropy on Modulated Electrostatic Waves and Envelope Solitons in a Magnetized Plasma," *IEEE Transactions on Plasma Science*, **50**(10), 3760-3773 (2022). <https://doi.org/10.1109/TPS.2022.3200476>
- [60] J.A. Bittencourt, *Fundamentals of Plasma Physics*, 3rd ed. (Springer, New York, NY, USA, 2004).
- [61] G.F. Chew, M.L. Goldberger, and F.E. Low, "The Boltzmann equation and the one-fluid hydromagnetic equations in the absence of particle collisions," *Mathematical, Physical and Engineering Sciences*, **236**(1204), 112–118 (1956). <https://www.jstor.org/stable/99870>
- [62] M. Irfan, S. Ali, S.A. El-Tantawy, and S.M.E. Ismaeel, "Three dimensional ion-acoustic rogons in quantized anisotropic magnetoplasmas with trapped/untrapped electrons," *Chaos*, **29**, 103133 (2019). <https://doi.org/10.1063/1.5109157>
- [63] W. Baumjohann, and R.A. Treumann, *Basic Space Plasma Physics*, (Imperial College Press, London, 1996).
- [64] E.I. El-Awady, and M. Djebli, "Dust acoustic waves in a collisional strongly coupled dusty plasmas," *Astrophysics and Space Science*, **342**, 105–111 (2012). <http://dx.doi.org/10.1007/s10509-012-1159-6>

ВПЛИВ АНІЗОТРОПІЇ ІОННОГО ТИСКУ В КВАНТОВІЙ КВАНТОВІЙ МАГНІТОПЛАЗМІ З ВАЖКИМИ ТА ЛЕГКИМИ ІОНАМИ

Діпсіха Махант^a, Сварнів Чандра^b, Джнанджоті Сарма^c

^aФакультет математики, Університет Гаухаті, Гувахаті 781014, Індія

^bФакультет фізики, держ. Коледж загального ступеня в Кушиманді, Дакиши Дінаджпур, 733121, Індія;








Інститут природничих наук і прикладних технологій, Колката 700032, Індія

^cФакультет математики, Коледж Радха-Говінда Баруах, Гувахаті 781025, Індія

Ми розглянули вироджену плазму зіткнення, що складається із зарядженого стану важкого позитивного іона та легкого позитивного, а також негативного іона. Використовуючи метод відновних збурень, ми вивели рівняння Кортевега-де Фріза-Бюргерса ($dKdV$ -В) і, використовуючи його стандартне рішення, аналізуємо характеристики профілю одиночного удару за різних параметрів. Крім того, із застосуванням теорії біфуркацій планарних динамічних систем проаналізовано фазові портрети. Цей аналіз динамічної системи дозволив нам отримати важливу інформацію про стабільність цих структур, представлену рівнянням $dKdV$ -В.

Ключові слова: рівняння $dKdV$ -В; квантова плазма; анізотропія тиску; аналіз фазової площини; динамічна система

POSITIVELY CHARGED MICROPARTICLE IN PLASMA WITH HIGH-ENERGY ELECTRON BEAM

 Aleksander A. Bizyukov^a,  Dmitry V. Chibisov^{a*},  Oleksandr D. Chibisov^b,
 Oksana A. Zhernovnykova^b,  Kostyantyn V. Borysenko^b,
 Dmytro Ye. Bobyliev^c,  Oksana H. Shtonda^b

^aV.N. Karazin Kharkiv National University, Svobody Sq., 4, 61022, Kharkiv, Ukraine

^bH.S. Skovoroda Kharkiv National Pedagogical University, Alchevskyyh St., 29, 61002, Kharkiv, Ukraine

^cKryvyi Rih State Pedagogical University, Universytetskyi Ave., 54, 50086, Kryvyi Rih, Ukraine

*Corresponding Author e-mail: dmitriychibisov@karazin.ua

Received June 4, 2024; revised August 5, 2024; accepted August 12, 2024

The processes of recharging, heating and evaporation of a positively charged microparticle (MP) introduced into the plasma with an injected high-energy electron beam are considered. It is assumed that the MP is charged outside the plasma and then introduced into the plasma by an accelerating field, where plasma and beam electrons hitting the MP heat and evaporate it. In addition to introducing the MP into the plasma, the positive MP charge provides an additional source of energy needed to heat and evaporate it. Using the OML theory, the system of current and energy balance equations was numerically solved and the conditions, under which the MP is heated to the boiling point of its substance, resulting in its intense evaporation, were determined. The influence of the energy of the electron beam on the process of MP recharging, as well as on the rate of its heating and evaporation, has been studied. An estimate of the particle entry velocity into the plasma has been made; the distances at which its recharging, heating to the boiling point and complete evaporation occur are determined. The work is carried out in order to creating plasma of a given elemental composition.

Keywords: *Microparticles; Producing plasma; Electron beam; Evaporation of microparticles*

PACS: 52.40.Hf

INTRODUCTION

Currently, a number of methods for producing ion beams and plasma from elements initially in the solid phase are known; the main ones are evaporation from a furnace, cathode sputtering of a solid, evaporation by a vacuum arc or a laser beam [1]. Previously [2,3], we reported one more method for producing plasma from elements in the solid phase, that consists of introducing MPs into a previously created plasma. To introduce the MPs into plasma, we proposed to charge MPs up to a high positive potential and then accelerating them using the method developed in [4, 5] for creating a flow of micrometeorites of micron and submicron size in laboratory conditions. Microparticles introduced into the plasma are heated and evaporated as a result of collisions with plasma and beam electrons; the resulting vapor is then ionized by electrons. The positive charge of the MPs is used to introduce them into the plasma and is also an additional source of energy necessary for heating and evaporation. This method of creating plasma from elements in the solid phase, in addition to producing ion beams, can be used for plasma isotope separation technologies [6-9]. The advantage of this method over traditional methods of creating plasma is its economic efficiency, what is important, for example, when separating rare earth elements [6]. Another important aspect is the higher level of environmental safety compared to evaporation in a furnace, what can be important when separating radioactive elements and their isotopes [7].

In this work, we study the effect of an electron beam injected into the plasma on the processes of recharging, heating and evaporation of a single MP. Previously, the high-energy electron beam was proposed to be used to evaporate micro-droplets of cathode material in plasma generated by a vacuum-arc discharge when coating a substrate [10-12]. The addition of an electron beam to the plasma in this case makes it possible to reduce the positive charge of the MP, which is necessary for its acceleration when they are introduced into the plasma, and also creates additional ability for its heating, evaporation and subsequent ionization. For calculations, we used a previously proposed model [2,3], in which terms, that take into account the electron beam, were added. We also investigated the effect of the electron beam on the evaporation of heated MP and also estimated the distances at which recharging, heating to the boiling point and evaporation of the MP occurs.

MODEL DESCRIPTION

A positively charged MP in plasma with an electron beam absorbs electrons from the plasma and beam, resulting in its recharging and heating. After recharging, the MP also absorbs plasma ions, what is an additional source of its heating. Thermionic and secondary electron emissions also have a significant influence on the MP, which form its equilibrium potential and also determine its temperature. The temperature of the MP is also influenced by thermal

radiation and evaporation of the MP substance. All these processes are taken into account in the system of equations that describe the dynamics of changes in the potential and temperature of a MP in plasma:

$$\begin{cases} I_i^{pl} - I_e^{pl} - I_e^b + I_e^s + I_e^{th} = dQ/dt; \\ P_e^{pl} + P_i^{pl} + P_e^b - P_s - P_r - P_{th} - P_{vap} = mc dT/dt. \end{cases} \quad (1)$$

The first equation of system (1) describes the changing of the MP charge and includes charging processes listed above and denoted as follows: I_i^{pl} and I_e^{pl} are the ion and electron currents from the plasma onto the MP surface, I_e^b is the electron beam current, I_e^s is the secondary electron emission current from the MP surface caused by electron of the plasma and the beam, I_e^{th} is the thermionic electron emission current from the MP surface caused by heating of the MP due to interaction of MP surface with the plasma and the beam MPs. It should be noted, that the secondary electron emission and the thermionic electron emission only take place for negatively charged MPs. Q is the charge, T is the temperature, m is the mass, c is the specific heat capacity of he MP.

Interaction of plasma and electron beam particles with the MP surface is given by the OML theory and particles currents have the form

$$I_\alpha^{pl,b}(\varphi) = e \cdot \Gamma_\alpha,$$

where $\alpha = i, e$ denote the particle species.

$$\Gamma_\alpha = \sqrt{8\pi} a^2 n_0 v_{T\alpha} \left(1 + \frac{|e\varphi|}{kT_\alpha} \right),$$

is the current of particles α in a case of attractive MP potential and

$$\Gamma_\alpha = \sqrt{8\pi} a^2 n_0 v_{T\alpha} \exp\left(-\frac{|e\varphi|}{kT_\alpha}\right),$$

in a case of repulsive MP potential, n_0 is the plasma number density, $v_{T\alpha}$ is the thermal velocity of particles α , a is the initial MP radius, φ_a is the MP potential. Secondary electron emission is described by the relation:

$$I_e^s = \delta I_e,$$

where

$$\delta = \delta_{\max} \frac{|e\varphi|}{E_m} \exp\left(2\left(1 - \sqrt{\frac{|e\varphi|}{E_m}}\right)\right)$$

is the secondary electron emission yield: E_m is the energy of the primary electrons that corresponds to the maximum of secondary emission yield δ_{\max} . Thermionic emission current is described by the Richardson's law

$$I_e^{th} = 4\pi a^2 A T^2 \exp\left(\frac{e\Phi - \Delta W}{k_B T_a}\right),$$

where, $A = \frac{4\pi m_e k_B^2 e}{h^3}$, h is the Planck constant, k_B is the Boltzmann constant, $e\Phi$ is the work function, T_a is the temperature of the MP. $\Delta W = \sqrt{e^3 \varphi_a / a}$ is the decreasing of the electron work function (Schottky effect).

The second equation of the system (1) describes the changing of MP temperature caused by energy flows the following processes: $P_{i(e)}^{pl}$ is the energy flow associated with the absorption plasma particles by the MP; P_e^b is the energy transferred by the electron beam to the MP P_r is the energy radiated from the MP surface, P_{vap} is the cooling of the MP due to evaporation of its substance, P_{th} is the energy flow from the MP surface is transferred by the electrons of thermionic current, P_s is the energy flow due to the secondary electron emission. The values of the respective energy flows are determined by the following relations:

$$P_e^{pl} = \Gamma_e \cdot (2kT_e + e\Phi), \quad P_i^{pl} = \Gamma_i \cdot (2kT_i + e\varphi + I + e\Phi), \quad P_e^b = \Gamma_e \cdot (2kE_b + e\Phi) \quad P_r = \sigma T^4,$$

$$P_{th} = \Gamma_e^{th} \cdot (2k_B T), \quad P_e^s = \Gamma_s \cdot (\varepsilon_s + e\Phi), \quad P_{vap} = \Gamma_a \cdot (2k_B T + p),$$

where I is the ionization energy, $\Gamma_a = n' \sqrt{\frac{k_B T_a}{2\pi m_a}} \exp\left(-\frac{p}{k_B T_a}\right)$ is the atom flow of evaporated MP substance, n' is the concentration of atoms in metal, p is the energy of evaporation an atom, $\Gamma_e^{th} = I_e^{th} / e$, $\Gamma_s = I_s^{e-e} / e$, ε_s is the averaged energy of the secondary electrons, E_b is the energy of electron beam.

By numerically solving the system of equations (1), we determine the change in time of the potential and the temperature of the MP at different values of its initial potential, as well as depending on the energy of the electron beam.

RECHARGING AND HEATING OF THE MP

We consider the positively charged spherical cooper MP with a diameter of 1 micron placed into the plasma, the parameters of which are: number density n_0 is 10^{10} cm^{-3} electron T_e and ion T_i temperatures are 50 eV and 1 eV respectively. Initial MP temperature is $T_0 = 300 \text{ K}$. We suppose that the boiling point of copper is the limiting point for the increase in MP temperature, which is approximately equal to 2800 K, and we also neglect the change in boiling temperature with decreasing pressure of the residual gas. Therefore, the presented calculations represent a qualitative assessment of the processes occurring.

When a positively charged MP is introduced into the plasma with the electron beam, it is recharged due to collisions with electrons. Figure 1a shows the dependence of the MP potential on time for various values of its initial potential φ_0 and electron beam energy $E_b = 20 \text{ keV}$.

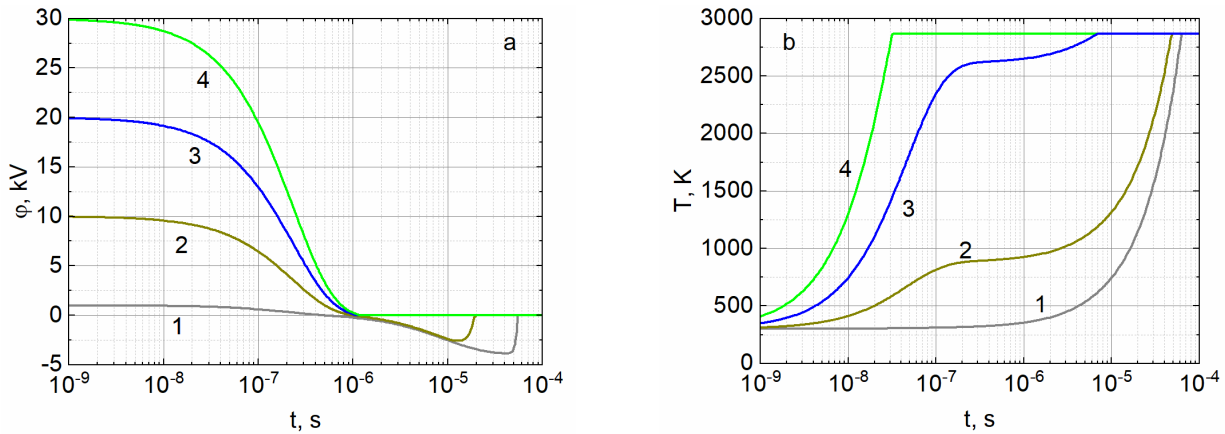


Figure 1. The dependence of MP potential (a) and related temperature of MP (b) on the time at different values of the initial MP potential φ_0 , electron beam energy $E_b = 20 \text{ keV}$: 1 – $\varphi_0 = 1 \text{ kV}$, 2 – $\varphi_0 = 10 \text{ kV}$, 3 – $\varphi_0 = 20 \text{ kV}$, 4 – $\varphi_0 = 30 \text{ kV}$

Here we can see two cases of time dependence of MP potential. In the first case, at the initial values of $\varphi_0 = 1 \text{ kV}$ and $\varphi_0 = 10 \text{ kV}$ (curves 1 and 2), within a time of about 10^{-6} s , the MP potential reaches approximately zero value, which corresponds to the floating potential, due to charging by plasma electrons. A further decrease of the potential to a value of the order of -4 kV is caused by the charging of the MP by beam electrons. In the second case, at the initial potentials $\varphi_0 = 20 \text{ kV}$ and $\varphi_0 = 30 \text{ kV}$ (curves 3 and 4) after recharging, the MP has approximately zero potential, which does not change subsequently. This effect is explained by the fact that as a result of heating the MP by plasma electrons, its temperature reaches a value exceeding the value at which thermionic emission occurs ($\sim 2500 \text{ K}$), compensating for the influx of plasma and beam electrons onto the MP. In the first case, the electrostatic energy of the MP, due to the initial charge, is insufficient to heat to a given temperature. However, due to the beam electrons, the MP continues to heat up and at a time from $2 \cdot 10^{-5} \text{ s}$ to $5 \cdot 10^{-5} \text{ s}$ its temperature reaches the required value, so that thermionic emission becomes possible and the MP potential decreases to a value close to zero.

Figure 1b shows curves of the MP temperature versus time for the same values of the initial MP potential. At the initial potential of the MP $\varphi_0 = 1 \text{ kV}$ (curve 1), the change in the MP temperature as a result of charging by plasma electrons is insignificant. The main contribution to the heating of the MP in this case is made by the electrons of the beam, which in a time of $\sim 5 \cdot 10^{-5} \text{ s}$ increase its temperature to the value when thermionic emission occurs and the MP potential drops to zero (curve 1 in Fig. 1a). Further heating of the MP leads to an increase in its temperature to the boiling point. At the initial potentials of the MP $\varphi_0 = 10 \text{ kV}$ (curve 2) and $\varphi_0 = 20 \text{ kV}$ (curve 3), the heating of the MP by plasma electrons is already significant and ends during the recharging time of the MP ($\sim 10^{-6} \text{ s}$). In the case of $\varphi_0 = 10 \text{ kV}$, its reached temperature ($\sim 800 \text{ K}$) which is lower than the temperature of thermionic emission, and the

potential of the MP decreases to -4 kV (curve 2 in Fig. 1a) due to charging by beam electrons. Simultaneously, the electron beam heats the MP first to the thermionic emission temperature and then to the boiling temperature. At the initial potential $\varphi_0 = 20$ kV the electrostatic energy stored on the MP is sufficient for thermionic emission, but not sufficient for heating to the boiling point. This temperature is achieved due to the beam electrons. At the initial potential of the MP $\varphi_0 = 30$ kV (curve 4), the electrostatic energy of the MP is sufficient to heat it to the boiling point. In this case, the electron beam only maintains a given temperature, compensating for losses due to thermal radiation.

We also investigated the effect of electron beam energy on the change in MP temperature over time for a MP with an initial potential $\varphi_0 = 20$ kV ; the calculation results are shown in Fig. 2.

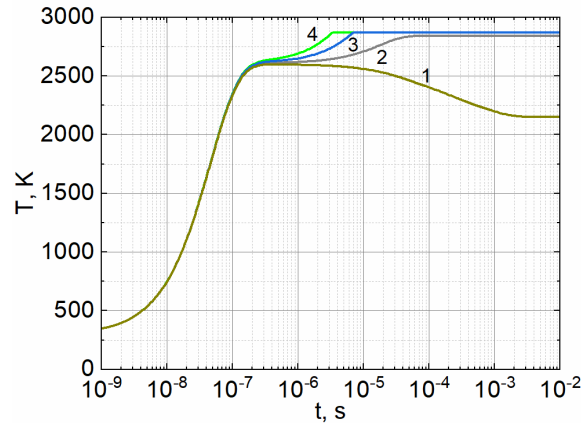


Figure 2. The dependence of the MP temperature on the time at different beam energies:
1 – $E_b = 1$ keV, 2 – $E_b = 10$ keV, 3 – $E_b = 20$ keV, 4 – $E_b = 30$ keV .

As can be seen from the Fig. 2, in a time of about $2 \cdot 10^{-7}$ s, the MP is heated to a temperature of about 2600 K due to plasma electrons during recharging, regardless of the beam energy. With increasing time at the beam energy $E_b = 1$ keV (curve 1), the MP cools down to a certain equilibrium value, which is determined by the equality of the energy coming from the beam and from the plasma, as well as heat losses due to radiation. At beam energies $E_b = 10, 20, 30$ keV (curves 2-4), further heating occurs due to the beam electrons, while the cooling of the MP due to radiation is compensated by the incoming energy from the beam electrons. It also follows from Fig. 2 that an electron beam with an energy exceeding $E_b = 10$ keV heats the MP to the boiling point.

EVAPORATION OF THE MP

We assume that particle evaporation occurs when the boiling point T^b of the substance is reached, neglecting evaporation at lower temperatures. The change in MP mass at the boiling point is described by the equation:

$$4\pi a^2 p_{evpr}(T^b, \varphi^b) \cdot dt = H dm, \quad (2)$$

where $p_{evpr}(T^b, \varphi^b) = \frac{1}{4\pi a^2} (P_e^{pl} + P_e^{pl} + P_i^{pl} - P_s - P_r - P_{th})$ is the power density on the MP surface that is spent to evaporation of the MP substance, H is the specific heat of evaporation, φ^b is the MP potential at $T = T^b$.

Equation (2) gives the relation between specific parameters of MP substance such as density and heat of evaporation and parameters of plasma and electron beam as well as critical MP radius that can be evaporated. Critical means that the obtained parameters separate regions of the parameters where MPs can be evaporated and where is not. Time of complete evaporation of the MP with a radius a is calculated by integrating equality (2):

$$t_{evpr} = \frac{a \rho H}{p_{evpr}(T^b, \varphi^b)}. \quad (3)$$

Dependence of the complete evaporation time of the MP with an initial potential $\varphi_0 = 20$ kV on the energy of the electron beam for different values of the initial MP radius is shown in Fig. 3. As can be seen from Fig. 3, at beam energies $E_b < 3$ keV complete evaporation of the MP does not occur for all considered values of the initial MP radius. This occurs because, that for given plasma parameters the MP is not heated to the boiling point.

It follows from (3) that the dependence of the time of complete evaporation on the initial radius of the particle $t_{evpr}(a)$ is linear. This is also confirmed by Fig. 3. In particular, for a beam energy $E_b = 20$ keV, the time of complete evaporation of a particle with a radius $a = 0.1 \mu\text{m}$ is $t_{evpr} = 6 \cdot 10^{-5}$ s, at $a = 0.5 \mu\text{m}$ we have $t_{evpr} = 3 \cdot 10^{-4}$ s then at

$a = 1 \mu\text{m}$ $t_{\text{evpr}} = 6 \cdot 10^{-4} \text{s}$ and for $a = 5 \mu\text{m}$ the time of complete evaporation is equal $t_{\text{evpr}} = 3 \cdot 10^{-3} \text{s}$. Thus, for a given beam energy we have the relation $t_{\text{evpr}} = 6 \cdot 10^{-4} a$, where a is measured in micrometers.

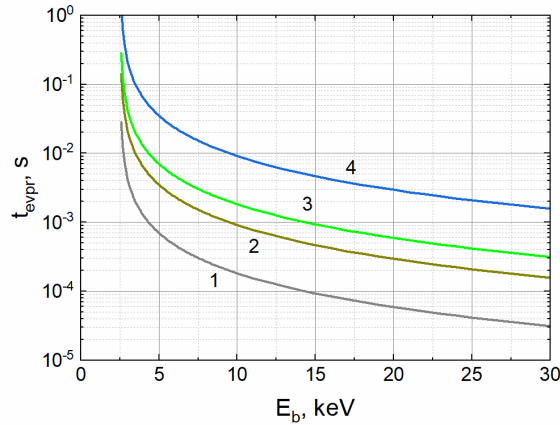


Figure 3. Dependence of the time of complete evaporation of a MP on the energy of the electron beam:
1 – $a = 0.1 \mu\text{m}$, 2 – $a = 0.5 \mu\text{m}$, 3 – $a = 1 \mu\text{m}$, 4 – $a = 5 \mu\text{m}$.

MICROPARTICLE SPEED IN PLASMA

Let us estimate the speed of a charged MP v at the moment of its entry into the plasma, assuming that all the electrostatic energy of MP is converted into its kinetic energy as a result of acceleration by a potential difference equal to the initial potential of the MP φ_0 . From the law of conservation of energy

$$\frac{mv^2}{2} = \frac{C\varphi_0^2}{2},$$

where $C = r$ is the capacity of a spherical MP, m is its mass, we find that the speed is equal to

$$v \approx \frac{\varphi_0}{2r\sqrt{\rho}},$$

where ρ is the density of the substance of the MP. For a copper MP the counting formula is

$$v \approx \frac{0.56\varphi_0}{r},$$

where v measured in cm/s , φ_0 in kV , r in cm . For a MP with a diameter of 1 micron we get

$$v \approx 1.12 \cdot 10^4 \varphi_0.$$

Now we estimate the characteristic distances at which the considered processes occur. For a MP with an initial potential of 20 kV , the speed is $v \approx 2.24 \cdot 10^4 \text{cm/s}$. From the Fig. 1 (curve 3) it follows that the MP recharge occurs over time $t \approx 10^{-6} \text{s}$ and thus the MP completely loses its initial charge at a distance of about 0.02 cm from the point of entry into the plasma. Heating to the boiling point occurs over time $t \approx 7 \cdot 10^{-6} \text{s}$ (Fig. 2, curve 3), which corresponds to the MP passing a distance of 0.16 cm from the point of entry into the plasma. Finally, the time for complete evaporation of the MP, depending on the energy of the electron beam, is equal to $t \approx 10^{-4} - 10^{-3} \text{s}$ (Fig. 3, curve 2). Over this time, the MP travels a distance from 2 to 10 cm . Thus, for complete evaporation in plasma with the stated parameters and for plasma devices of suitable sizes it is desirable that the initial radius of the MP does not exceed 1 micron.

CONCLUSIONS

To obtain plasma of a given elemental composition, the introducing MPs into previously created plasma, followed by their evaporation and ionization is proposed. For more efficient evaporation, as well as ionization, a high-energy electron beam is injected into the plasma. As an example, the evaporation of a copper MP with a diameter of 1 micron is considered. To be introduced into the plasma, the MP is charged to a high positive potential and then accelerated by the created potential difference. It is shown that, regardless of the initial potential, the MP loses charge due to collision with plasma electrons with a density of 10^{10}cm^{-3} in a time of the order of 10^{-6}s . The initial positive potential serves not only to introduce the MP into the plasma, but also as an energy source for heating the MP by plasma electrons. It is shown that a MP with an initial potential of 30 kV can reach the boiling point of copper as a result of heating by

electrons. At the same time, the MP is cooled due to thermal radiation and other processes. To additionally heat the MP and maintain its temperature at the boiling point, when the evaporation rate reaches its maximum, it is proposed to introduce a beam of high-energy electrons into the plasma. It has been shown that the introduction of an electron beam with a density of 10^9 cm^{-3} and an energy of more than 10 keV leads to heating of the MP to the boiling point, regardless of its initial potential. Assuming that the evaporation of the MP substance occurs only at the boiling point, conditions under which complete evaporation of the MP occurs were obtained. The dependence of the time of complete evaporation of a MP on the energy of the electron beam was also obtained. The velocity of introducing of MP into plasma is estimated and the characteristic distances at which the main processes occur with it are determined. It is shown that the MP recharge occurs over time $t \approx 10^{-6} \text{ s}$ and that the MP completely loses its initial charge at a distance of about 0.02 cm from the point of entry into the plasma. Heating to the boiling point occurs in a time $t \approx 7 \cdot 10^{-6} \text{ s}$ corresponding to the passage of the MP at a distance of 0.16 cm from the point of entry into the plasma. Finally, the time for complete evaporation of a MP, depending on the energy of the electron beam, is equal to $t_{\text{evpr}} \approx 10^{-4} - 10^{-3} \text{ s}$.

During this time, the MP passes a distance from 2 to 10 cm. Comparing the time and distance for complete evaporation of MPs of different sizes allows us to conclude that the optimal MP diameter is less than or on the order of 1 micron.

Thus, the possibility of evaporation MP in previously created plasma with the presence of a high-energy electron beam and thereby creating conditions for creating plasma of a given elemental composition is shown. This method of evaporation a substance is an alternative to existing methods such as evaporation from a furnace, cathode sputtering of a solid, evaporation by a vacuum arc.

ORCID

- ©Aleksander A. Bizyukov, <https://orcid.org/0000-0003-0192-5219>; ©Dmitry V. Chibisov, <https://orcid.org/0000-0002-6154-9772>
 ©Oleksandr D. Chibisov, <https://orcid.org/0000-0001-9670-3912>; ©Oksana A. Zhernovnykova, <https://orcid.org/0000-0002-5383-4493>
 ©Kostyantyn V. Borysenko, <https://orcid.org/0000-0002-8172-0215>, ©Dmytro Ye. Bobyliev, <https://orcid.org/0000-0003-1807-4844>
 ©Oksana H. Shtonda, <https://orcid.org/0000-0001-7601-487X>

REFERENCES

- [1] B.H. Wolf, in: *Handbook of ion sources*, edited by B. Wolf (CRC Press Taylor & Francis Group Boca Raton London New York, 1995).
- [2] A.A. Bizyukov, A.D. Chibisov, D.V. Chibisov, O.A. Zhernovnykova, T.I. Deynichenko and N.N. Yunakov, *East European Journal of Physics*, (1), 110 (2022). <https://doi.org/10.26565/2312-4334-2022-1-15>
- [3] D.V. Chibisov, O.D. Chibisov, O.A. Zhernovnykova, G.V. Deynichenko, and V.V. Masych, *Problems of Atomic Science and Technology*, 1(143), 17 (2023). <https://doi.org/10.46813/2023-143-017>
- [4] A. Mocker, S. Bugiel, S. Auer, *et al.*, *Rev. Sci. Instrum.* **82**, 095111 (2011). <https://doi.org/10.1063/1.3637461>
- [5] J.D. Kerby, R.T. Daly, and D.E. Austin, *Earth Planets Space*, **5**, 157 (2013). <http://dx.doi.org/10.5047/eps.2012.08.005>
- [6] S.J. Zweben, R. Gueroult, and N.J. Fisch, *Phys. Plasmas*, **25**, 090901 (2018). <https://doi.org/10.1063/1.5042845>
- [7] R. Gueroult, J.-M. Rax, and N.J. Fisch, *Journal of Cleaner Production*, **182**, 1060 (2018). <https://doi.org/10.1016/j.jclepro.2018.02.066>
- [8] R. Gueroult, D.T. Hobbs, and N.J. Fisch, *J. Hazardous Mater.* **297**, 153 (2015). <https://doi.org/10.1016/j.jhazmat.2015.04.058>
- [9] I.D. Kaganovich, A. Smolyakov, Y. Raitses, E. Ahedo, I.G. Mikellides, *et al.*, *Phys. Plasmas*, **27**, 120601 (2020). <https://doi.org/10.1063/5.0010135>
- [10] A.A. Bizyukov, K.N. Sereda, and A.D. Chibisov, *Problems of atomic science and technology. Series: Plasma Physics*, 1(17), 107 (2011). https://vant.kipt.kharkov.ua/ARTICLE/VANT_2011_1/article_2011_1_107.pdf
- [11] A.A. Goncharov, V.Yu. Bazhenov, A.S. Bugaev, A.M. Dobrovolskiy, V.I. Gushenets, I.V. Litovko, I.V. Naiko, and E.M. Oks, *IEEE transactions on plasma science*, **47**(8), 3594 (2019). <https://doi.org/10.1109/TPS.2019.2915644>
- [12] A.A. Goncharov, V.I. Maslov, I.V. Litovko, and A.V. Ryabtsev, *Problems of Atomic Science and Technology*, 6(142), 89 (2022). <https://doi.org/10.46813/2022-142-089>

ПОЗИТИВНО ЗАРЯДЖЕНА МІКРОЧАСТИНКА В ПЛАЗМІ З ЕЛЕКТРОННИМ ПУЧКОМ ВИСОКОЇ ЕНЕРГІЇ

Олександр Бізюков^а, Дмитро Чібісов^а, Олександр Чібісов^б, Оксана Жерновникова^б,
 Костянтин Борисенко^б, Дмитро Бобилєв^с, Оксана Штонда^б

^аХарківський національний університет імені В.Н. Каразіна 61022, Україна, м. Харків, майдан Свободи, 4

^бХарківський національний педагогічний університет імені Г.С. Сковороди, 61002, Україна, м. Харків, вул. Алчевських, 29

^сКриворізький державний педагогічний університет, 50086, Україна, м. Кривий Ріг, проспект Університетський, 54

Розглянуто процеси зарядки, нагрівання та випаровування позитивно зарядженої мікрочастинки (МЧ), введеної в плазму, що містить пучок електронів високої енергії, з метою створення плазми заданого елементного складу. Передбачається, що МЧ заряджається поза плазмою, а потім вводиться в плазму прискорювальним полем, де плазма та електрони пучка, стикаючись з МЧ, нагрівають і випаровують її. На додаток до введення МЧ у плазму, позитивний заряд МЧ забезпечує додаткове джерело енергії, необхідної для її нагрівання та випаровування. За допомогою теорії OML чисельно розв'язано систему рівнянь балансу струму та енергії та визначено умови, за яких МЧ нагрівається до температури кипіння його матеріалу, що призводить до його інтенсивного випаровування. Досліджено вплив енергії електронного пучка на процес перезарядки МЧ, а також на швидкість його нагрівання та випаровування. Зроблено оцінку швидкості входу частинок у плазму; визначено відстані, на яких відбувається її перезарядка, нагрівання до температури кипіння і повне випаровування.

Ключові слова: мікрочастинки; створення плазми; електронний промінь; випаровування мікрочастинки

METHOD OF DIGITAL PROCESSING OF OPTICAL SPECTRA OF MAGNETRON DISCHARGE PLASMA

 Inna Afanasieva^{a*},  Serhii Afanasiev^b,  Valentin Bobkov^a,  Valentina Gritsyna^a,  Anatoliy Skrypnyk^a

^aV.N. Karazin Kharkiv National University, 4, Svoboda Sq., Kharkiv, 61022, Ukraine

^bNational Science Center “Kharkov Institute of Physics and Technology” 1, Akademicheskaya St., 61108, Kharkiv, Ukraine

*Corresponding Author e-mail: afanimma@i.ua

Received May 25, 2024; revised July 10, 2024; accepted August 07, 2024

To solve the actual problems associated with the development of the theory of magnetron discharge and the expansion of its practical application, a digital method of recording and processing the discharge plasma luminescence spectra is proposed in this work. To obtain the discharge plasma glow spectra, a photographic technique was used, which allowed simultaneous recording of the entire radiation spectrum in the 390.0–700.0 nm region. An additional advantage of this technique is the ability to track spatial changes in the composition and properties of the plasma in the discharge in the selected direction. A Canon EOS 80D digital camera with remote control was used to record the optical signal. A graphical application OSA was created to process digital images of the discharge plasma luminescence spectra. The paper describes the functionality of this application: determination of the wavelength of a spectral line and its belonging to a certain chemical element; measurement of the spatial distribution of the intensity of a spectral line along the selected direction of radiation registration. Determining the wavelength of a spectral line in the application is possible in two modes of operation - automatic and manual. In the first mode, the algorithm developed in this paper determines the wavelength for all spectral lines whose intensity exceeds the background value at a height of 10% of the lower spectral limit. The second mode allows you to independently select a single spectral line or several to determine their wavelengths. The first mode is used for quick analysis, while the second mode allows you to determine the length of the spectral line with greater accuracy. To interpret the spectral lines, the methodology of reference lines from the databases of spectral line tables for various elements is used. The possibility of both full automatic verification, where all elements are sequentially searched, and selective verification, where one or more elements are selected, is provided. The paper shows that the spatial distribution of the intensity of tungsten spectral lines, and thus of excited atoms in a magnetron discharge, is a complex function of the distance from the cathode, which depends on the discharge parameters. The proposed digital methodology makes it possible to significantly speed up the process of obtaining physical information and increase the accuracy in determining the spectrum parameters.

Keywords: optical emission spectrometry, magnetron discharge, plasma emission spectrum, excited particles

PACS: 32.30, 34.35, 34.50, 34.80.Dp, 52.70.Kz, 52.80.Vp

1. INTRODUCTION

Interest in the study of magnetron discharge physics is due to its traditional application for coating. These can be as metal coatings for a wide range of industrial uses [1, 2], bio-coatings used in healthcare products [3] or coatings with high insulating properties [4, 5]. One of the factors that influence on the obtaining of coatings with specified properties is the control of the magnetron discharge plasma. Information about the composition and parameters of the plasma allows monitoring the deposition conditions of the films and regulating the formation of their properties.

It is convenient to control plasma parameters by optical spectroscopy [6, 7]. The main advantage of spectroscopy, in contrast to the probe technique, is the ability to perform plasma analysis without disturbing the plasma itself. An additional advantage is that this method does not require complex equipment: only diagnostic ports that provide direct visibility through the plasma are required. The spectroscopy method is informative and widely used to obtain various parameters of magnetron discharge plasma. For example, the population of excited states of plasma particles can be determined by the intensity of the corresponding spectral lines, and the intensities of the lines of various plasma components make it possible to determine the ion composition [8, 9].

Most often a photoelectric registration system is used in the spectroscopy to obtain physical information, in which the optical signal is converted into an electrical one with the help of a photomultiplier. At that, the integral intensity of a separate spectral line is obtained, which depends on the radiation intensity of the entire investigated area of luminescence along the selected direction. A feature of this registration system is the need to scan radiation spectra to study the selected spectral range. This, firstly, requires some time, and, secondly, when examining a narrow spectral interval, it is not possible to monitor changes in the intensity of spectral lines in the other part of the spectral range. These problems can be solved if a broadband detector, such as a CCD, is used as an optical signal converter [10]. At that, the dispersive element of the spectral device is fixed in a certain position, in which the studied region of the spectrum is projected onto the focal plane. This allows recording optical radiation simultaneously in a fairly wide spectral range, which increases the reliability of

Cite as: I. Afanasieva, S. Afanasiev, V. Bobkov, V. Gritsyna, A. Skrypnyk, East Eur. J. Phys. 3, 166 (2024), <https://doi.org/10.26565/2312-4334-2024-3-16>

© I. Afanasieva, S. Afanasiev, V. Bobkov, V. Gritsyna, A. Skrypnyk, 2024; CC BY 4.0 license

experimental results. An additional advantage of this design is that, in contrast to the photoelectric registration system, it makes it possible to obtain the spatial distribution of the intensity of a separate spectral line, and therefore of the investigated area of fluorescence along the selected direction. In this way, it is possible to monitor the spatial changes in the composition and properties of the discharge plasma in the selected direction.

2. EXPERIMENTAL METHOD

Spectrometers that use CCD as a converter of optical radiation, have high sensitivity and resolution, but are quite expensive, which somewhat limits their wide use in scientific institutions. Also, the software delivering with the device, usually doesn't allow for any modifications or scripts that might be needed while working in a research lab. Therefore, the question arises of creating a high-quality, but affordable CCD-based optical radiation recorder; it can be a digital camera.

The principle scheme of obtaining and digital processing of optical images of radiation spectra was presented in [11, 12]. The researches were carried out on the magnetron sputtering system (MSS) described in [13]. MSS operating conditions were as follows: buffer gas pressure (argon) $p_{Ar} = 10 - 18$ Pa, anode voltage $V_a = 300 - 350$ V, discharge current $I_d = 10 - 160$ mA, magnetic field induction $B = 0.05$ T. The optical radiation of the area of bright glow of the discharge was output through the diagnostic window of the vacuum chamber, focused with an achromatic lens on the input slit of the ISP-51 spectrometer, in which the radiation was dispersed using a triple prism system and focused in the focal plane of the output collimator of the spectrometer. With this geometry, a 4-fold reduced image of the optical spectrum of the magnetron discharge emitting region was projected onto the focal plane ($l = 4h$, where l is the height of the discharge along the axis, h is the height of the spectral line) in the spectral range of $400.0 \div 600.0$ nm.

At the first stage (work [11]), a comparison of physical data obtained by two methods was carried out: i) by the photographic photometry [14] with the photographing of the optical spectrum on photographic film, ii) with the analysis of the corresponding digitized frame. The frames were scanned on a specialized high-resolution slide scanner (size – 5040×3360 pixels) getting black-and-white digital images with the extension *.jpg.

To determine the qualitative and quantitative characteristics of magnetron discharge plasma, the creation of a multi-functional dialog GUI application of Optical Spectrum Analysis (OSA) was started. The OSA application was created in the Python programming language based on the Tkinter graphic library using a set of additional modules: PIL, Numpy, Scipy, Pandas, and Matplotlib [15]. With the the PIL module, the selected digital image of the discharge glow spectrum was converted into a numerical matrix, each element of which has an integer value proportional to the intensity $I[x,y]$ at a given point of the image plane (x and y are integers describing the column number or rows of the matrix, in which this element is placed). The intensity range is from 0 to 255. Mathematical algorithms and procedures implemented in OSA allow to process this matrix and present the results of the processing on the image in the form of graphic objects and text. The Matplotlib library was used as a tool for data visualization with two-dimensional graphics. The graphical application was created within the framework of object-oriented programming (OOP), with the ability to perform a new calculation when a number of parameters were changed and immediately present the obtained data on the image and graphs. In parallel, these results were recorded in an external file.

At the second stage (work [12]), photography of the working area was carried out using a user digital camera with the aim of directly obtaining digital images. Digital images were of better quality than digitized photographic film, and this made it possible to obtain the main characteristics of the magnetron discharge plasma radiation spectrum (wavelength, intensity of spectral lines) with better resolution.

At this stage of research, spectrum registration was carried out using a Canon EOS 80D professional digital camera with a resolution of 7000×5000 pixels, which was controlled remotely via Wi-Fi. Also, along with the improvement of the recording technique, some blocks were improved and new ones were added in the OSA application. The paper will provide a detailed description of the functional capabilities of the OSA application for digital processing of the optical emission spectra of magnetron discharge plasma glow and provide some experimental results.

3. BASIC POSSIBILITIES OF DIGITAL PROCESSING OF OPTICAL SPECTRA

3.1. The zone of the optical spectrum in the image and the spectrogram

The part of the digital image of the radiation spectrum of excited particles of a magnetron discharge in an argon atmosphere with a copper cathode is shown in fig.1. The MSS operating mode was as follows: buffer gas pressure $p_{Ar} = 10$ Pa, anode voltage $V_a = 320$ V, discharge current $I_d = 25$ mA, magnetic field induction $B = 0.05$ T, exposure time $t = 90$ s.

At the first, preliminary stage, the spectrum zone is automatically determined and the primary spectrogram is taken. The spectral lines do not occupy the entire area of the digital photograph, as Fig. 1 shows. It is obvious that the lines along which the pixels corresponding to the spectrum lines are located have a higher intensity compared to other lines. To determine the horizontal boundaries of the spectrum zone of each row, $I^{sum} = \sum_{i=1}^n I_i / n$, was determined, where n is the number of pixels along the row, I_i is the intensity of the i^{th} pixel. Histogram the distribution of I^{sum} depending on the row number is shown in Fig. 2a. The dashed curve shows the results of fitting with a linear function. The coordinates of the intersection of the linear function with the histogram correspond to the lower and upper limits of the spectrum zone and are shown in Fig. 1 with solid horizontal lines. The values of the spectrum boundary coordinates have been used to

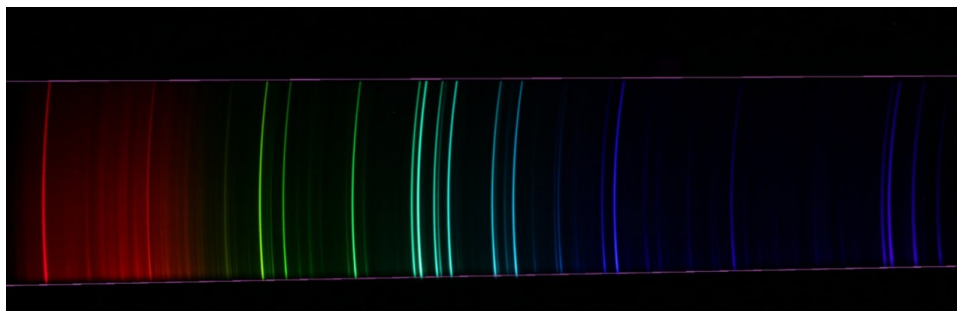


Figure 1. An example of an optical emission spectrum.

construct a spectrogram – dependence of the intensity of each pixel for a conventional line located across the spectrum at a height (difference between the upper and lower boundaries) of 10% from the lower boundary.

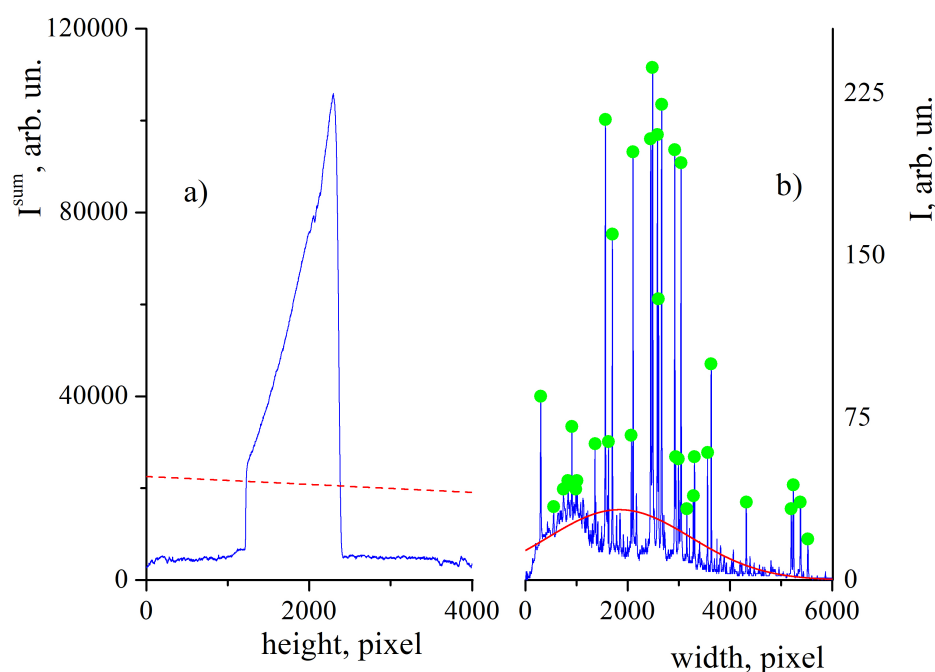


Figure 2. Preliminary estimation of spectrum parameters: a) determination of geometric boundaries, b) determination the coordinates of the most intense lines.

The histogram for the one shown in Fig. 1 spectrum is presented in Fig. 2b. As can be seen from the figure, the most intense spectral lines appear in the form of strong discrete maxima. The background layer is determined by fitting with a Gaussian function (dashed line in Fig. 2b). To automatically determine the position of these maxima, the groupby() function from the Pandas module have been used, which performs grouping by one or more parameters and determines inflection points (extrema). The position of the maxima of the most intense spectral lines in Fig. 2b are indicated by dots.

Thus, a coordinate in pixels along the horizontal axis is automatically determined for each of the intense spectral lines. It is for these lines that the wavelength is determined in the future, that is, the spectrum is deciphered.

3.2. Determination of the wavelength of an arbitrary spectral line and its interpretation

To obtain qualitative and quantitative parameters of the spectrum, it is necessary to bind the digital coordinate system (pixels) to the experimental one. A reference spectrum with known lengths of spectral lines (neon, mercury or hydrogen lamp) is used to obtain a dependence that connects the coordinates of a single pixel along the horizontal direction and the wavelength of a known spectral line.

For the ISP-51 spectrograph, when the radiation is decomposed into a spectrum, nonlinear dispersion [14] is

characteristic, which implies the presence of a nonlinear calibration scale (Fig. 3a), which relates the value of the line position to the wavelength λ in nm. The scale of the values of the digital matrix in pixels is placed along the ordinate axis to the right. In the available range of wavelengths for the reference lines on the abscissa scale, the corresponding values on the ordinate scale (left) in mm are found by interpolation. This allows you to enter a pixel-mm scale factor and automatically determine the wavelength λ for an arbitrary line on a digital image in the pixel coordinate system using reverse interpolation.

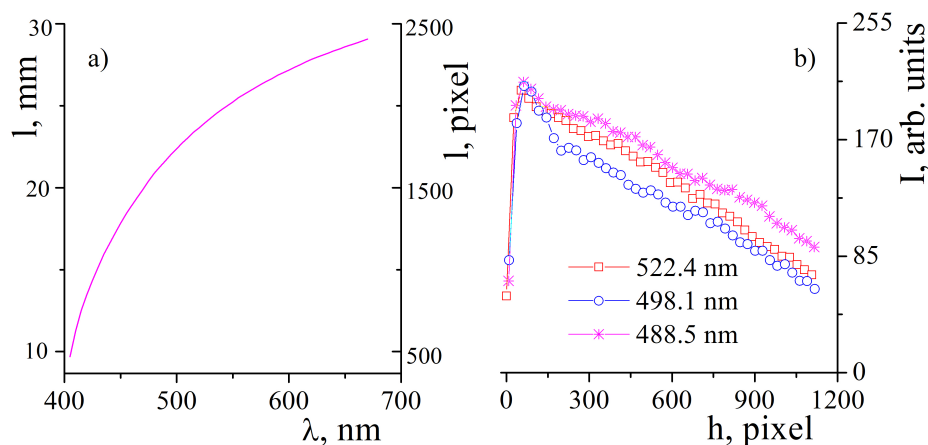


Figure 3. a) calibration function, b) intensity distribution of spectral lines along their height.

In the OSA application, it is possible to use two modes of operation - automatic and manual. In the first mode, for all spectral lines whose intensity at a height of 10% from the lower limit of the spectrum exceeds the background value, the wavelength is determined by the algorithm described above. The second mode allows you to independently choose a separate spectral line or several of the most interesting for determining their wavelengths. The first mode is used for quick analysis, the second allows to determine the length of the spectral line with greater accuracy, thanks to the possibility of using the digital optical zoom function (ZOOM). The value of the wavelength of the spectral lines in nm is displayed on the spectrum and is also recorded in a separate file.

As an example of the manual mode of operation in Fig. 4 shows a fragment of the spectrum, where vertically arranged numbers indicate the wavelength λ for several lines: $\lambda_1^{exp}=522.4$ nm, $\lambda_2^{exp}=498.1$ nm, $\lambda_3^{exp}=488.5$ nm. The wavelengths of a set of spectral lines have been repeatedly measured and the statistical error has been obtained $\delta\lambda$ when determining the wavelength using the OSA application; on average, $\delta\lambda$ is in the range from 0.1 to 0.3 nm.

The most difficult stage in optical spectrometry is the interpretation of the decoded spectrum (that is, determining whether the spectral lines observed in the spectrum belong to certain chemical elements). At the initial stage, it is best to use the method of interpretation based on reference lines - the lines of the studied element, which are the last to disappear from the spectrum of the sample when the concentration of the given element decreases in it. The reference lines of all elements are well known and their parameters (wavelength, excitation energy, intensity, etc.) are given in atlases of spectral lines. For the reliability of element identification, a set of reference lines is always used, with which the lengths of the spectral lines present in the luminescence spectrum of the material under study are compared. In this paper, spectral line databases for various elements were used for the interpretation of spectral lines [16]. In the OSA application, in a separate block, the possibility of both a full automatic check, where a sequential review of all elements takes place, and a selective one (one or several elements) is created.

A simple comparative search fixes the range of values of wavelengths in the table, in which one of the experimental values falls. Of the two limiting values, the one with the lower value of the excitation energy is chosen. In case of equality on this parameter, the third element is used - intensity. Preference is given to the option with the maximum intensity value. Yes, shown in Fig. 4 spectral lines were interpreted as tungsten lines W I - $\lambda_1^{tabl}=522.5$ nm, $\lambda_2^{tabl}=498.3$ nm, $\lambda_3^{tabl}=488.7$ nm.

3.3. Distribution of the intensity of a spectral line along its height

One of the significant advantages of using the photographic method of recording optical spectra is the possibility of obtaining information about the spatial distribution of excited particles along the chosen direction. Since the intensity of the spectral line (I) is an energy quantity and is related to the number of excited particles (n^*) and the quantum energy ($h\nu$) by the ratio $I=n^* \cdot h\nu$, the change in the intensity of the spectral line along the registration direction reflects the change in the number of excited particles, emitting photons at the wavelength of the investigated line. In this work, the registration system was located so that the height of the h lines in the spectrum corresponded to the direction of the ionization zone along the magnetron axis.

In Fig. 4 circles indicate the coordinates of the points where the intensity of the spectral line along its height was fixed. The method of determining the coordinates of points along a line with some curvature was described in [10]. In this work, the optimization of the method is carried out, thanks to which it is possible to determine the distribution for low-intensity lines and a unified form of data output - with the same step for any line. It was also possible to determine the integral intensity of a spectral line by summing the intensity value (I) of all pixels forming this line, taking into account the line width.

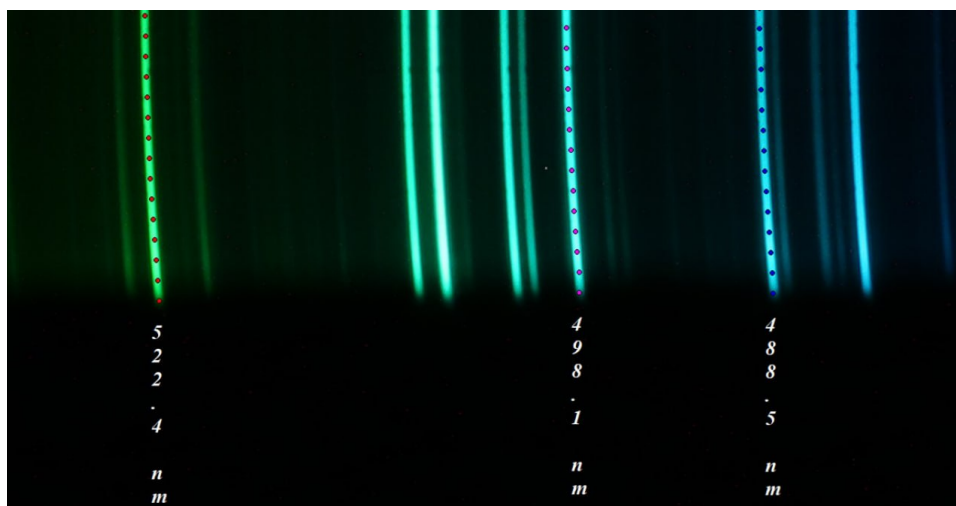


Figure 4. Part of the spectrum with certain values of the wavelengths (vertical inscriptions) of some lines and the distribution of points along these lines.

The distribution of the intensity of three lines belonging to the W I spectrum along their height shows in Fig. 3b as an example. It can be seen from the figure that the spatial distribution of the intensity of the spectral lines, and therefore of the excited tungsten atoms in the magnetron discharge, is a complex function of the distance from the cathode. Moreover, it has been established that depending on the mode of operation of the magnetron, the relative intensity of the studied lines changes significantly. Moreover, this change is different for particles excited into states characterized by different excitation energies. This is probably related to the different efficiency of excitation of the upper state of the studied transition in the tungsten atom by electrons of the ionization zone of the discharge plasma, because excited particles in the magnetron discharge are formed not only by sputtering atoms of the cathode material under the action of incident gas ions, but also by collision particles with a large number of free electrons knocked out of the surface of the cathode in the magnetic field in the ionization (and excitation) zone of the magnetron plasma.






4. CONCLUSIONS

To solve the current problems related to both the development of the theory of the magnetron discharge and the extension of the field of its practical application, a digital method of recording and processing the discharge plasma glow spectra is proposed in the paper. The spectrum was recorded using a Canon EOS 80D digital camera with a resolution of 7000*5000 pixels, which was controlled remotely via Wi-Fi.

For the digital processing of the spectra, a graphic OSA application was created, which made it possible to obtain qualitative and quantitative characteristics (wavelength, interpretation and intensity) of the spectral line of the magnetron discharge plasma radiation. In addition, the use of digital techniques made it possible to obtain an information on the spatial distribution of excited particles along the chosen direction of radiation registration. The OSA application was created in the Python programming language based on the Tkinter graphics library. With the help of the PIL module, access to the matrix of the selected digital image of the glow spectrum of the discharge was obtained. Mathematical algorithms and procedures were developed that allow you to process this digital matrix, visualize the results of the processing on the image, and present the results of the processing in the form of two-dimensional graphics. The graphical application was created within the framework of object-oriented programming, with the ability to make a new calculation when changing a number of parameters and immediately present the output data on images and graphs.

The proposed digital technique made it possible to significantly speed up the process of obtaining physical information and increase the accuracy in determining the parameters of the spectrum. Digitally obtained snapshots of the luminescence spectra of reference objects, supplemented with the data of their processing by the OSA graphic application, made it possible to create a database containing both electronic atlases of the luminescence spectra of various elements and quantitative parameters of these spectra. a data bank containing both atlases of the luminescence spectra of various elements in electronic form, as well as the quantitative parameters of these spectra.

ORCID

 Inna Afanasieva, <https://orcid.org/0000-0002-9523-9780>;  Serhii Afanasiev, <https://orcid.org/0000-0003-1682-4621>;
 Valentin Bobkov, <https://orcid.org/0000-0002-6772-624X>;  Valentina Gritsyna, <https://orcid.org/0009-0004-5284-7382>;  Anatoliy Skrypnyk, <https://orcid.org/0009-0004-6863-6563>

REFERENCES

- [1] Y. Hua, C. Zhou, Y. Li, L. Yang, and Z. Song, *Corrosion Science*, **196**, 110020 (2022). <https://doi.org/10.1016/j.corsci.2021.110020>
- [2] H. Larhlimi, A. Ghailane, M. Makha, and J. Alami, *Vacuum*, **197**, 110853 (2022). <https://doi.org/10.1016/j.vacuum.2021.110853>.
- [3] M. Qadir, Y. Li, and C. Wen, *Acta Biomaterialia*, **89**, 14 (2019). <https://doi.org/10.1016/j.actbio.2019.03.006>
- [4] W.D. Sproul, M.E. Graham, M.S. Wong, S. Lopez, and D. Li, *Journal of Vacuum Science and Technology A: Vacuum, Surfaces and Films*, **13**, 1188 (1995), <https://doi.org/10.1116/1.579859>
- [5] G. Wisz, P. Sawicka-Chudy, A. Wal, P. Potera, M. Bester, D. Ploch, M. Sibiński, *et al.*, *Applied Materials Today*, **29**, 101673 (2022). <https://doi.org/10.1016/j.apmt.2022.101673>
- [6] U. Fantz, *Plasma Sources Sci. Technol.* **15**, S137 (2006). <https://doi.org/10.1088/0963-0252/15/4/S01>
- [7] X.M. Zhu, and Y.K. Pu, *J. Phys. D. Appl. Phys.* **43**, 403001 (2010). <https://doi.org/10.1088/0022-3727/43/40/403001>
- [8] A. Murmantsev, A. Veklich, V. Boretskij, A. Shapovalov, and A. Kalenyuk, *Plasma Physics and Technology*, **6**, 87 (2019). <https://doi.org/10.14311/ppt.2019.1.87>
- [9] H. Mishra, M. Tichý, and P. Kudrna, *Vacuum*, **205**, 111413 (2022). <https://doi.org/10.1016/j.vacuum.2022.111413>
- [10] E. Yokoyama, M. Sanekata, N. Nishimiya, M. Tona, H. Yamamoto, K. Tsukamoto, K. Fuke, *et al.*, *Jpn. J. Appl. Phys.* **62**, SL1008 (2023). <https://doi.org/10.14311/ppt.2019.1.87>
- [11] I.A. Afanasieva, S.N. Afanasiev, N.A. Azarenkov, V.V. Bobkov, V.V. Gritsyna, Yu.E. Logachev, I.I. Okseniuk, *et al.*, *Problems of Atomic Science and Technology*, (2), 164 (2019). https://vant.kipt.kharkov.ua/ARTICLE/VANT_2019_2/article_2019_2_164.pdf
- [12] I.A. Afanasieva, S.N. Afanasiev, V.V. Bobkov, V.V. Gritsyna, D.R. Drozdov, Yu.E. Logachev, A.A. Skrypnyk, and D.I. Shevchenko, *Problems of Atomic Science and Technology*, (4), 35 (2019). https://vant.kipt.kharkov.ua/ARTICLE/VANT_2019_4/article_2019_4_35.pdf
- [13] I.A. Afanasieva, V.V. Bobkov, V.V. Gritsyna, Yu.E. Logachev, I.I. Okseniuk, A.A. Skrypnyk, and D.I. Shevchenko, *Vacuum*, **149**, 124 (2018). <https://doi.org/10.1016/j.vacuum.2017.12.027>
- [14] V.I. Malyshev, *Introduction to experimental spectroscopy*, (Nauka, Moscow, 1979). (in Russian)
- [15] M. Lutz, *Learning Python*, 5th Edition, (“O’Reilly Media”, 2013).
- [16] The National Institute of Standards and Technology, Headquarters, 100 Bureau Drive. Gaithersburg, MD 20899. https://physics.nist.gov/PhysRefData/ASD/lines_form.html

МЕТОДИКА ЦИФРОВОЇ ОБРОБКИ ОПТИЧНИХ СПЕКТРІВ ПЛАЗМИ МАГНЕТРОННОГО РОЗРЯДУ

Інна Афанасьєва^a, Сергій Афанасьєв^b, Валентин Бобков^a, Валентина Грицина^a, Анатолій Скрипник^a

^aХарківський національний університет ім. В.Н. Каразіна, майданСвободи, 4, 61022, Харків, Україна

^bНаціональний Науковий Центр “Харківський Фізико-Технічний Інститут”, вул. Академічна, 1, 61108, Харків, Україна

Для вирішення актуальних задач, пов’язаних з розробкою теорії магнетронного розряду та розширенням області його практичного застосування, в роботі запропонована цифрова методика реєстрації та обробки спектрів світіння плазми розряду. Для отримання спектрів світіння плазми розряду використовувалась фотографічна методика, яка дозволяла одночасно реєструвати весь спектр випромінювання в області 390.0÷700.0 нм. Додатковою перевагою даної методики є можливість відслідковувати просторові зміни складу та властивостей плазми в розряді в обраному напрямку. Для реєстрації оптичного сигналу в роботі використовувалась цифрова камера Canon EOS 80D з віддаленим керуванням. Для обробки цифрових знімків спектрів світіння плазми розряду створено графічний застосунок OSA. В роботі наведено опис функціональних можливостей даного застосунку: визначення довжини хвилі спектральної лінії та її приналежності певному хімічному елементу; вимірювання просторового розподілу інтенсивності спектральної лінії вздовж обраного напрямку реєстрації випромінювання. Визначення довжини хвилі спектральної лінії в застосунку можливо в двох режимах роботи – автоматичному та ручному. В першому режимі за розробленим в роботі алгоритмом визначається довжина хвилі для усіх спектральних ліній, інтенсивність яких на висоті 10% від нижньої межі спектру перевищує фонове значення. Другий режим дозволяє самостійно обрати окрему спектральну лінію або декілька для визначення їх довжин хвиль. Перший режим використовується для швидкого аналізу, другий дозволяє провести визначення довжини спектральної лінії з більшою точністю. Для інтерпретації спектральних ліній в роботі використано методику реперних ліній з баз табличних даних спектральних ліній для різних елементів. Забезпечена можливість як повної автоматичної перевірки, де відбувається послідовний перебір всіх елементів, так і вибіркової – за одним або декількома елементами. В роботі показано, що просторовий розподіл інтенсивності спектральних ліній вольфраму, а, отже, й збуджених атомів в магнетронному розряді, є складною функцією відстані від катоду, яка залежить від параметрів розряду. Запропонована цифрова методика дає можливість істотно прискорити процес отримання фізичної інформації та підвищити точність у визначенні параметрів спектра.

Ключові слова: оптична емісійна спектрометрія, магнетронний розряд, спектр випромінювання плазми, збуджені частинки